INTERVAL VELOCITIES FROM MOVEOUT VELOCITIES OVER A SEISMIC REFLECTION SURVEY AREA

BY

G.F. ALLEN

ABSTRACT

Moveout velocities sampled frequently along seismic horizons on a selection of seismic lines are used to derive interval velocities in an 'inversion' algorithm developed from work published by Hubral. This inversion is based on zero-offset raytrace modelling in a simplistic local ground model. The 'Hubral algorithm' is incorporated into a database which allows spatial smoothing of velocities. The spatial consistency of derived interval velocities can then be assessed by reference to mis-ties at line intersections, while interval velocities from well data can be used to check their validity.

These principles have been used to derive interval velocities both from real data and from 'synthetic' data generated by common mid-point raytracing over schematic ground models. The latter study reveals that the procedure performs well if the local subsurface sampled by the CMP gather conforms approximately to the simplistic ground model assumed by the Hubral algorithm. The method is unsuitable in areas of faulting and interval velocity heterogeneity, and may yield spurious results over fold axes.

Application of the procedure to real data indicates that it is generally desirable to smooth both moveout velocities before inversion and interval velocities after inversion. Comparison with well information shows that interval velocities derived by the Hubral algorithm are consistently higher than those measured from calibrated velocity logs. This observation is disturbing, since the derived interval velocities require a correction if they are to be used for depth conversions, but the discrepancy cannot be explained by ray theoretical considerations. No advantage appears to be gained by the 'layer-by-layer' mode of inversion over the 'direct' inversion, despite the greater potential for error propagation anticipated in the latter. Further work on different data sets is required to justify general use of the layer-by-layer mode of inversion.

INTERVAL VELOCITIES FROM MOVEOUT VELOCITIES OVER A SEISMIC REFLECTION SURVEY AREA

By

G.F. ALLEN

PART ONE

Text

A thesis submitted for the degree of Doctor of Philosophy
at the University of Leicester, April 1985.

CONTENTS

PART ONE

PART TWO

LIST OF TABLES

LIST OF FIGURES

LIST OF ENCLOSURES

ACKNOWLEDGEMENTS

The author wishes to thank both supervisors Dr. Andrew Lucas of BP London and Dr. Peter Maguire of Leicester University for their assistance throughout this project. These thanks are extended to Dr. Peter O'Brien of BP London and Dr. Aftab Khan of Leicester University for their help in initiating the project.

The author also wishes to thank BP Petroleum Development Ltd. for the use of computer, reprographic and typing facilities in the Dyce office.

My sincere gratitude is expressed towards all those who assisted in the final preparation of the thesis. The efforts of Kathy Addison, Lynne Fairbairn and Wilma Lobban in typing the manuscript, and of Gary Leslie in helping with the diagrams, are particularly appreciated.

Acknowledgement is made to BP Petroleum Development of Norway A/S, Conoco Norway Incorporated, Pelican A/S and K/S, and Statoil for granting permission to use and present the real data studied in the project.

This project was funded by a NERC Studentship on Quota Number 51.

INTRODUCTION

Distance equals time multiplied by velocity. This elementary relation demonstrates the significance of the subsurface velocity distribution as the fundamental link between seismic reflection travel times and depths. In view of the increasing need for accuracy in time to depth conversion of seismic reflection data, velocities have assumed an important role in the appraisal of seismic information. There are, however, only two sources of subsurface velocity information - either from wells or from the seismic data itself. It is the latter category with which we are concerned here. This thesis documents a study of the derivation of subsurface velocities from conventional seismic reflection methods currently used in the search for hydrocarbons. The overall aim is to present a logic by which the validity of interval velocities derived from moveout velocities can be judged objectively.

The increasing need for accuracy in time to depth conversion referred to above is a simple consequence of the increase in exploration for hydrocarbons over the last few decades. Except for the few remaining frontier areas, most of the larger and more obvious structures have been drilled. Many of the remaining prospects tend to be either deeper or of a more subtle nature, and it is in this context that the estimation of accurate seismic velocities assumes greater importance. In the case of deeper targets, accurate forecasts of depths to geological formations are critical in the design of a drilling programme, particularly if high pore fluid pressures are expected. In the appraisal of a subtle prospect, the velocities used for depth conversion may have a significant influence on the economic viability of drilling the prospect, while in more extreme cases the very existence of the play may be at stake.

It is generally to wells that we first look for velocity information. The calibrated velocity log provides a reliable measurement of the vertical velocity-depth function local to the well bore, and precise detail of the velocity variation within any chosen interval. However, the spatial distribution of wells is frequently inadequate to constrain the lateral variations of velocity which must be defined over a prospect. Reference to a map of any mature exploration area reveals that wells tend to be concentrated in clusters around hydrocarbon discoveries, with at best a sparse distribution of wells in the intervening 'dry' areas. But the irregularity of well locations is not the only problem. Since hydrocarbons migrate updip and accumulate towards the culmination of the prospect, the locations of wells tend to be biased towards the structural highs. Since few wells are drilled in structural lows, this represents a considerable influence in the sampling of seismic velocities. Structural highs are frequently characterised by anomalously thin or missing geological sections. This, commonly coupled with gross lithological variation from structural highs to lows, serves to make the estimation of seismic velocities away from well control a rather hazardous procedure. In frontier areas there may be no relevant well control at all.

The derivation of velocities from seismic reflection data assumes a particularly attractive aspect in the light of the discussion above. Compared with wells, seismic information is relatively plentiful, and generally provides coverage across both structural highs and lows alike. One need only consult the tabulations at the top of most seismic sections to select stacking velocities and apply the Dix Equation to calculate interval velocities. This procedure will yield reliable estimates of subsurface velocities if the velocity layering, and hence the geological structure, is exactly horizontal - and if the seismic recording and processing system is unbiased. In such a case, the stacking velocity calculated from the moveout of a reflection across the common mid point (CMP) gather is likely to be a reasonable approximation to the root mean square velocity, and the Dix Equation allows an acceptable estimation for interval velocities. However, these conditions are very stringent, and are generally not honoured. Stacking velocities are not generally appropriate for the estimation of true subsurface velocities, and the earth is rarely (if ever) horizontally layered. Indeed, if such an area did exist, it would warrant little geological interest, particularly in the context of hydrocarbon prospectivity. One of the central tenets of this thesis is that while stacking velocities are generally adequate for stacking, they should not be used directly to infer real subsurface velocities for time to depth conversion if accuracy is important.

How, then, should interval velocities be derived from seismic reflection data? The method advocated here is best described at two levels. At the first level, the basic component is similar in concept to the Dix Equation. The Hubral algorithm (Hubral, 1976a, 1976b) is also applied at a surface location to recover interval velocities from two-way times and moveout velocities. However, the method of Hubral accomodates plane reflecting interfaces of arbitrary dip and strike, which can be calculated if the two-way time slopes of each reflection in two orthogonal directions are also specified. As such, the Hubral algorithm allows a three-dimensional solution. At the second level, this algorithm is incorporated into a regional seismic database system. This system accommodates processing of both the data sent to and received from the Hubral algorithm. Specifically, moveout velocities and interval velocities can be smoothed by a variety of filters in order to allow the attenuation of anomalous spatial fluctuations. Several seismic lines can be handled sequentially, and the spatial consistency of derived interval velocities can be assessed both by reference to mis-ties at line intersections and matches with interval velocities at wells. Two further themes are apparent from this discussion. The first is that moveout velocities, and not stacking velocities, should be used for the calculation of interval velocities in the Hubral algorithm. This subtle distinction is important. Moveout velocity pertains strictly to the true moveout of the reflection and not necessarily to the optimum stacking response. The second theme is that moveout velocities are azimuth-dependent since they are controlled principally by the geometry of the CMP gather and its orientation over the subsurface. As such, both moveout velocities and the derived interval velocities should be processed line by line before being combined to form a map.

Following this procedure, interval velocities are estimated using moveout velocities from real seismic data. A study is also made of 'synthetic' data generated over ground models representing typical subsurface features. The seven chapters of this thesis develop the themes introduced above, and ultimately present a general logic for the derivation of interval velocities from moveout velocities.

Chapter One presents a review of the principles of CMP velocity analysis. Since this subject has typically been an area of rather vague and often ambiguous terminology, it has been found necessary to begin with a series of definitions. Each of the commonly used types of seismic velocity have been rigorously defined. Specifically, the distinctions between stacking velocity, moveout velocity, normal moveout velocity and root mean square velocity are highlighted. These distinctions are not common in geophysical literature, but have been used here for greater clarity. The latter part of this chapter consists of a discussion of the various factors affecting CMP velocity analysis. These factors can be classified under two headings, namely those due to acquisition and processing, and those due to the subsurface. It is generally the subsurface factors which have the greater influence on moveout velocity variations over a survey area. The first chapter also discusses the resolution of CMP velocity analysis and the uses of velocities derived from it.

The seismic reflection data used in this project are presented in Chapter Two. These data have been obtained from an offshore concession over a relatively simple geological structure, and are of generally high quality. Seismic data from two surveys were available, together with three well ties. Closely spaced velocity analyses were available for eight lines of the main survey and two lines of a later survey, allowing ties with two of the three wells. Following a discussion of acquisition and processing parameters for both surveys, a basic interpretation of the data is presented. Five seismic horizons have been picked, and interpreted CMP stacked sections for each of the lines with closely spaced velocity analyses are included. Two-way stacked time maps on two of the horizons are also presented. Moveout velocities have then been picked on coherence peaks at, or near to, the interpreted times of each of the five horizons to create a moveout velocity database. Plots of moveout velocity along each horizon for each line are also presented, together with moveout velocity maps for both of the horizons mapped in time. Characteristic associations of moveout velocity with subsurface features are noted and discussed. This chapter concludes by correlating the five seismic horizons to the stratigraphy recorded in each of the wells using calibrated velocity logs and synthetic seismograms. Interval velocities between consecutive seismic horizons have been measured from calibrated velocity logs for their ultimate use in checking interval velocities derived by the Hubral algorithm in Chapter Seven.

Chapter Three presents a statistical analysis of the spatial character of moveout velocities over a survey area. The first part reviews the methods which have been used to study moveout velocities by way of various transforms and smoothing techniques. The second part then discusses their application to the moveout velocities described in the previous chapter. Plots of the semivariance functions, autocorrelation functions and energy spectra for each moveout velocity profile are presented, together with a discussion of the relative merits of each transform. Some persistent spatial frequency components of moveout velocity are observed on the lines. A study of smoothing the moveout velocity profiles with a variety of filters indicates that one of these persistent components may be anomalous.

The fourth chapter documents algorithms based on the work of Hubral (1976a, 1976b) which have been prepared as part of this thesis for the estimation of interval velocities from seismic data. If a ground model is limited locally to consist of uniform velocity layers separated by plane reflecting interfaces of arbitrary dip and strike, the normal moveout velocities, two-way zero-offset times and time slopes in any direction can be calculated without iteration using the equations of Hubral. This simulation of the seismic process is referred to here as the 'forward problem'. Hubral also presents equations to solve the 'inverse problem' by recovering the subsurface parameters of such a limited ground model from the surface seismic measurements. The first section of Chapter Four presents an algorithm for raytracing through the three-dimensional limited ground model. The next section then introduces the concept of wavefront curvature, the vehicle by which the geometry of the zero-offset raypath is used to calculate normal moveout velocities, and which enables the non-iterative inversion of Hubral. Algorithms for forward modelling and inversion of three-dimensional limited local ground models are then presented, while comparisons are made with the results of Hubral for two test models. Chapter Four concludes with a discussion of the practical application of the inversion algorithm to real data. Potential sources of errors are noted, and the need to incorporate the algorithm into a regional seismic database is recognised. Computer programs are included as appendices.

Chapter Five documents the regional seismic database system designed for this project. The first section outlines the requirements of such a system and notes the two 'modes' of inversion introduced briefly in Chapter Four. In the 'direct' inversion, each ground point is processed in turn and the subsurface parameters for each horizon are derived consecutively. Errors generated in shallow layers are likely to propagate downwards during the inversion. The alternative mode of inversion is the 'layer-by-layer' inversion procedure, in which each layer is processed in turn. Following an inversion to derive interval velocities at all ground points for the target layer, the interval velocities are monitored and adjusted as required before raytracing to define the base of the layer and subsequent inversion of the next layer. This procedure should, in principle, allow less scope for the propagation of errors downwards. Further sections present reasoning for the data structure employed and a specification of tasks performed by the system.

Some illustrative examples of interval velocity errors caused by moveout velocity anomalies over typical subsurface features are presented in Chapter Six. Raypaths for CMP gathers over two-dimensional ground models have been traced in order to generate 'synthetic' data sets consisting of moveout velocities, two-way stacked times and time slopes. These data have been used to derive interval velocities in the Hubral inversion algorithm, in order to identify characteristic patterns of interval velocity errors over each subsurface feature. The first section of this chapter describes the raytracing program which was used to generate the synthetic data sets. Subsequent sections then discuss velocity layering, plane reflector dip, velocity gradients, faulting and reflector curvature. The chapter concludes with a study of moveout velocities and derived interval velocities over a model of a typical North Sea structure.

Chapter Seven discusses the application of the Hubral inversion to the real data set described in the second chapter. Moveout velocities, two-way times and time slopes are prepared into a form suitable for the seismic database introduced in Chapter Five. Interval velocity information from wells is then compiled from the second chapter. The 'interval velocity error' is defined here as the difference between the interval velocity derived by the Hubral algorithm and the true interval velocity at the well. Magnitudes of these errors expected as a result of the 'spread length effect' are then calculated by raytracing at two well locations. The following two sections are devoted separately to direct and layer-by-layer inversions of the data set. In both cases a suite of moveout velocity and interval velocity smoothing combinations are tested, and an 'optimal' combination is selected on the basis of maximising the spatial consistency of the derived interval velocities using the minimum of smoothing. The derived interval velocities are finally calibrated using the mean interval velocity error in order to compensate for a systematic biasing influence observed from the well ties. The chapter concludes with a discussion of the results obtained for each mode of inversion. Some important differences, particularly in the calibration of derived interval velocities, are noted and analysed.

These seven chapters therefore cover a wide variety of subjects around the central theme of interval velocities from moveout velocities. Indeed, the diversity of these subjects places a considerable restriction on the logical development of this theme through the early chapters. For this reason, it is important to appreciate the context of each chapter as a necessary foundation for the synthesis of ideas in the last two chapters.

1. VELOCITIES IN SEISMIC REFLECTION PROSPECTING

This chapter reviews the role of velocities in the seismic reflection method, with particular emphasis on the method of CMP velocity analysis and the velocities derived from it.

Problems frequently arise in the discussion of seismic velocities due to ambiguous terminology. The first part of this chapter therefore includes a rigorous definition of the various types of velocity, together with some terms pertinent to CMP velocity analysis. Specific differences in the definitions of stacking velocity, moveout velocity, normal moveout velocity and root mean square velocity are not common in geophysical literature. These differences are highlighted in Section 1.2, and have been introduced here to provide greater clarity in the discussions of interval velocity inversion in subsequent chapters. Uses of velocities obtained from CMP velocity analysis are reviewed briefly in Section 1.3.

The overall purpose of this study is to discuss the derivation of interval velocities from moveout velocities. The fourth section of this chapter presents an outline of the many factors which affect the values of moveout velocities obtained from CMP velocity analysis. These factors can be broadly classified into two categories, namely those due to acquisition and processing, and those due to the subsurface. The resolution of CMP velocity analysis is discussed briefly in Section 1.5.

1.1 DEFINITIONS

The impressive growth of the seismic reflection method has been accompanied by an equally impressive growth of its associated vocabulary. Although most of this new terminology has been necessary to accommodate theoretical advances in the subject, confusion has been introduced into some areas by ambiguous definitions. Nowhere is this confusion more apparent than in the definitions pertaining to the 'Common Mid Point' technique and velocity analysis.

Most of the terms used in this project are defined adequately in Sherriff (1973). The definitions which follow are presented in an attempt to reduce any previous ambiguity, in particular for the suite of velocities related to common mid point velocity analysis. The velocities defined in this section are separate quantities and each have different uses. Although identities may exist for some trivially simple simple ground models, these terms are not interchangeable for a general heterogeneous subsurface.

The objective of this section is to make rigorous definitions which will be fundamental to the understanding of subsequent discussions. The reader is warned, however, that these definitions pertain strictly to this project. Subtle differences in the naming of different types of velocity are not common in geophysical literature, where stacking velocity, moveout velocity, normal moveout velocity and root mean square velocity are often used synonymously.

1.1.1 Seismic Wave Velocity

Seismic wave velocity is the speed of a seismic disturbance propagating through a medium. It is a property of the medium rather than a property of the disturbance.

Dispersion, the dependence of velocity on the frequency of wave propagation, is negligible for homogeneous rock samples subject to seismic disturbances in the frequency range 10-50Hz. The response of velocity to various influencing factors can thus be measured in ultrasonic laboratory experiments and the results then used in the analysis of regional velocity fields implied by seismic data. However, the application of empirical laws derived in the laboratory to real subsurface velocity fields is limited for a number of reasons. Great difficulties are encountered, for instance, in the simulation of temperature and pressure regimes at depth. There is also a vast difference in scale between the samples used in laboratory experiments and the volumes sampled by seismic energy in field velocity measurements. Furthermore, in a heterogeneous medium the seismic wave velocity is affected by wave propogation phenomena including averaging and interference which are influenced by the frequency of wave propagation.

Major direct influences on seismic wave velocity include porosity and jointing, pressure, cementation, interstitial fluids and lithology. It is instructive to consider rock as having both solid and fluid components. The potential of the dry skeleton to hold fluids is determined by its porosity and degree of jointing. The resultant seismic wave velocity then depends on the individual velocities of both the skeletal grains and the fluids and on the elastic properties of the dry skeleton. In general, for any single lithology, the seismic wave velocity increases with the degree of compaction of the rock skeleton.

Increasing pressure generally causes compaction which closes pores and joints and increases seismic wave velocity. Pressures usually increase with depth and can produce irreversible changes in the rock fabric; it is then the maximum depth of burial rather than the current depth of the rock which is of greatest importance in determining its seismic wave velocity. Cementation fills pores and joints by deposition with a resultant overall consolidation of the rock and an increase in seismic wave velocity. Age does not directly affect seismic wave velocity other than by increasing the probability of deeper burial, cementation and consolidation.

In a porous rock with a weak skeleton the interstitial fluids can have a considerable effect on the resultant seismic wave velocity. Since the velocity of oil is lower than that of water but significantly greater than that of gas, water sands often have higher velocities than oil sands and gas sands can have much lower velocities. The fluid pressure of the interstitial fluids reduces the effective pressure, which helps to maintain porosity and keep seismic wave velocities relatively low.

Figure 1.1 shows the seismic wave velocities for different classes of rocks. Each rock type has a wide range of velocities, largely due to porosity variations, and there is significant overlap between different lithologies. Seismic wave velocity cannot be used as a unique indicator of lithology.

Seismic wave velocity generally increases with depth in response to regional pressure gradients. This trend is complicated by local variations of porosity and jointing, pressure, cementation, interstitial fluids and lithology.

1.1.2 Ground Models

A ground model is a simplified representation of the real subsurface and contains only the most significant physical features of the real subsurface within the resolution limits imposed by the surveying technique. In the context of modelling seismic reflection travel times, a ground model is adequately characterised by the subsurface velocity distribution which can be resolved by the surface seismic reflection method.

Observations of surface exposures indicates that the subsurface geology, and hence velocity distribution, of most sedimentary sections is likely to be complex. In addition to heterogeneity within layers of similar material, the interfaces separating the layers are frequently curved and discontinuous due to folding, faulting and unconformity. Further evidence for subsurface complexity derives from well logs, which often show rapid variations of physical properties with depth.

The true velocity distribution can never be fully recovered by the surface seismic reflection method due to practical limitations on the resolution of velocity information which are discussed further in Section 1.5. The aim of seismic reflection interpretation is to recover a 'ground model' from the data which is consistent with the surface measurements and any available well information. The ground model is characterised by the most significant reflection horizons visible in the seismic data, which usually correspond to important lithological boundaries.

The 'forward problem' can now be introduced as the simulation of seismic data from a ground model, and the 'inverse problem' as the recovery of a suitable ground model from seismic data. It is useful in this context to consider types of ground models in which each layer and interface are characterised by a set of parameters. The number of parameters required to define each layer or interface determines the complexity of the ground model and depends largely on the amount and quality of the available data. The accuracy of the inversion then depends both on the applicability of the ground model type to the subsurface and the quality of the data.

Inversion can be performed at individual locations to derive 'local ground models' which are usually quite simple due to the limitations of velocity resolution. In this project the complexity of these local ground models is restricted to uniform velocity layers separated by plane interfaces of arbitrary dip and strike. Local ground models can then be composited together to form a 'regional ground model' which is large enough to represent structural and velocity variations on a regional scale.

The complex velocity distribution of the real earth should always be acknowledged when applying inversion techniques which use implicitly simple ground models.

1.1.3 Common Mid Point and Common Depth Point

A 'common mid point' (CMP) is the common middle point at the surface between each shot-geophone (s-g) pair in a set of seismic traces called a CMP gather. The traces for each CMP gather are selected from different shot records in the original field data tapes.

A 'common depth point' (CDP) exists on a reflector if the raypaths describing wave propagation for each s-g pair in the CMP gather reflect at the same point.

Figure 1.2a shows shots and geophones symmetrically disposed about a CMP over a simple uniform velocity ground model. The separation of the inner s-g pair is the 'near trace offset' of the field data and that of the outer s-g pair is the 'far trace offset'. Raypaths reflected at a single horizontal interface are shown for each s-g pair. The broken line shows the raypath joining a hypothetical coincident s-g pair with 'zero-offset'. The concept of zero-offset is very important in seismic reflection. Although for practical reasons the zero-offset trace cannot be recorded in the field, the output from the CMP stacking process represents the simulated zero-offset trace. For this horizontal reflector model, each raypath reflects at a common depth point which is vertically below the CMP. The zero-offset raypath reflects normally at the interface such that both downgoing and upgoing segments follow the same path; in general the zero-offset raypath is identically the 'normal incidence raypath'.

Figure 1.3a shows the same CMP gather over a uniform velocity model with a single plane dipping reflector. The reflection points are now spread up-dip from the zero-offset raypath reflection point. There is no true common reflection point for a dipping reflector ground model.

In general the s-g raypaths for a CMP gather do not reflect at a common depth point. The spread of reflection points over an interface is controlled by both the depth and shape of the interface and by the velocity distribution in the volume sampled by the CMP gather raypaths.

Although it has been common practise in the literature, the terms CMP and CDP should not be used interchangeably. CMP is a feature of the surface recording geometry alone, and is independent of the subsurface velocity distribution. Confusion arises because this field technique is commonly called CDP. The term CDP should be avoided except when referring specifically to reflection at a common depth point, which can exist in a CMP gather over a horizontally layered ground model or in more advanced data processing schemes.

1.1.4 Moveout Equations

The moveout of a reflection in a CMP gather is the difference in its arrival time at different offsets, defined here as:

$$\Delta t_x = t_x - t_o \tag{1.1}$$

where t_x is the two-way time for the reflection recorded at a geophone offset a distance x from its corresponding shot, t_o is the two-way travel time along the zero-offset raypath and Δt_x is the moveout at offset x.

Figure 1.2b highlights a single s-g raypath from the horizontal reflector model of Figure 1.2a. The vertical depth to the reflector is z and the medium has the uniform velocity V. The two-way time for an s-g raypath with offset x is, by Pythagoras:

$$t_x^2 = (x^2 + 4z^2)/V^2 \tag{1.2}$$

or:

$$t_x^2 = t_o^2 + x^2/V^2 \tag{1.3}$$

where:

$$t_o = 2z/V \tag{1.4}$$

The moveout curve defined by Equation (1.3) is a hyperbola with its apex at zero-offset.

A single raypath is shown in Figure 1.3b from the dipping reflector model of Figure 1.3a. The dip of the reflector is α and the medium again has the uniform velocity V. Point s' is the image of s. Using the triangle sgs' and the sine rule:

$$Vt_x/\sin(90 + \alpha) = x/\sin(90 - \beta)$$

i.e.

$$Vt_x \cos\beta = x \cos\alpha \tag{1.5}$$

and in triangle s'gq:

$$Vt_x \sin\beta = Vt_o \tag{1.6}$$

Adding the squares of both Equations (1.5) and (1.6) to eliminate β :

$$t_x^2 = t_o^2 + x^2 \cos^2\alpha / V^2 \tag{1.7}$$

This moveout relation is also hyperbolic, despite the fact that there is no CDP for a single plane dipping reflector ground model. This result, first documented by Levin (1971), is the basis of the CMP field technique.

1.1.5 Stacking Velocity

Stacking velocity is the velocity used to define a hyperbolic trajectory and apply 'moveout corrections' in order to stack a CMP gather. It is purely a data processing parameter. The CMP stacking process combines the gather traces to produce a single output trace in which the primary reflections have a higher signal to noise ratio.

Stacking a CMP gather with stacking velocity V_s involves summing the gather traces along hyperbolae defined by:

$$t_x^2 = t_o^2 + x^2/V_s^2 \tag{1.8}$$

and projecting the results to zero-offset times. The output trace then simulates the zero-offset trace at the CMP, and the final CMP stacked section ideally represents the zero-offset or normal incidence section.

Stacking velocity generally varies with time in response to the variation of seismic wave velocity with depth. The 'stacking velocity function' (of two-way zero-offset time) is the set of stacking velocities used to stack the CMP gather.

1.1.6 Velocity Analysis

Velocity analysis is the name popularly given to any procedure by which the response of stacking the CMP gather with various stacking velocities or stacking velocity functions can be studied.

The objective of velocity analysis is to provide a display which shows the coherence of the reflected seismic energy on the CMP gather traces at various stacking velocities. From this display the stacking velocities can be selected for the final stack of the section. Velocity analysis can also be the source of information leading to the derivation of interval velocities and ultimately to a final ground model.

Velocity analysis methods can be conveniently grouped into two categories, though both present essentially the same information. The first group shows the actual CMP gather traces after moveout corrections or stacking and the coherence of the reflections for different stacking velocities is assessed 'by eye'. In the second group, a numerical value of coherence is calculated over a series of moveout-corrected time gates and displayed as a function of stacking velocity and two-way zero-offset time.

Included in the first group are the 'constant velocity gather' (CVG) and the 'constant velocity stack' (CVS), which are both described in an information sheet by Prakla-Seismos (1978). These methods are not discussed further here as they are not specifically related to the later chapters.

The second group of velocity analysis methods display the coherence of the stack rather than the seismic data itself. It is these methods which are now usually implied by the term 'velocity analysis'. The technique of velocity analysis has been excellently outlined by Taner and Koehler (1969) and reviewed by both

Montalbetti (1971) and Hubral and Krey (1980). The operation of a standard velocity analysis procedure is summarised briefly below.

A CMP gather (or group of adjacent CMP gathers) is read in by the velocity analysis program and at successive time gates the traces are stacked using a range of stacking velocities. The data are actually stacked along a series of underlying stacking velocity-time functions and the coherence is interpolated onto a rectangular grid. The coherence can then be displayed as a function of stacking velocity and two-way zero-offset time. This two-dimensional function has been referred to as the 'velocity spectrum'. Peaks on this function indicate events with a hyperbolic or near-hyperbolic trajectory, which may be primary reflections, multiple reflections or diffractions.

Different types of coherence measures used in velocity analysis programs are discussed in the references cited previously. The ratio of stacked energy in the time gate to the available energy for stacking in the time gate is inherent in most coherence measures. The coherence measure may be designed to peak for any hyperbolic event, or it may be weighted by amplitude in order to emphasise the stronger hyperbolic events. It is important that the results of a velocity analysis program should be dominated by the seismic data itself, and not by the choice of coherence measure used in the program.

1.1.7 Root Mean Square Velocity

The root mean square (RMS) velocity for a raypath reflecting at the nth interface is:

$$V^2_{rms,\,n} = \sum_{i=1}^{n} V_i^2 \Delta t_i \Big/ \sum_{i=1}^{n} \Delta t_i \qquad (1.9)$$

where V_i and Δt_i are the velocity and two-way transit time in the ith layer, respectively.

For a ground model consisting of a sequence of uniform velocity layers separated by horizontal reflecting interfaces, the moveout relation for the nth reflector is given by Dix (1955) as approximately:

$$t_{x,n}^2 = t_{0,n}^2 + x^2/V_{rms,n}^2 \tag{1.10}$$

where $V_{rms,n}$ is measured along the (vertical) zero-offset raypath. At zero-offset, the equations:

$$t_{o,n} = \sum_{i=1}^{n} \Delta t_i \tag{1.11}$$

and

$$V_{rms,n}^2 = \sum_{i=1}^{n} V_i^2 \Delta t_i / t_{o,n} \tag{1.12}$$

can be rearranged to solve for the velocity of the nth layer in the familiar 'Dix Equation':

$$V_n^2 = \frac{V_{rms,n}^2\, t_{o,n} - V_{rms,n-1}^2\, t_{o,n-1}}{t_{o,n} - t_{o,n-1}} \tag{1.13}$$

It is important to note that use of the Dix Equation strictly implies the knowledge of vertical RMS velocities and vertical two-way times in a horizontally layered ground model.

1.1.8 Moveout Velocity

Moveout velocity is the velocity defining the hyperbolic trajectory which best approximates the moveout of a reflection across the CMP gather. Further reference to moveout velocity implies primary reflection moveout velocity unless otherwise specified.

For realistic ground models including several reflectors with dip and curvature, the moveout is no longer exactly hyperbolic due to raypath refraction at layer interfaces, but the moveout of a reflection can usually be well approximated by the hyperbola:

$$t_x^2 = t_o^2 + x^2/V_{mo}^2 \tag{1.14}$$

where V_{mo} is the moveout velocity defining the hyperbola which is in some sense the best fit to the observed moveout of the reflection.

Some examples of moveout velocities for simple ground models have in fact already been given. The moveout velocity for a CMP over a single horizontal reflector with a uniform velocity layer above is just V, the velocity of the layer, as in Equation (1.3). The moveout velocity for a CMP in a dip line over a single plane dipping reflector with a uniform velocity layer is seen from Equation (1.7) to be $V/\cos\alpha$ where α is the dip angle and V is again the layer velocity. For these simple ground models with a single layer of uniform velocity the reflection moveout is defined precisely by the moveout velocity because all of the CMP offset raypaths are straight. The moveout velocity $V_{rms,n}$ for a horizontal reflector at the base of n uniform velocity horizontal layers in Equation (1.10), however, provides only an approximation to the true moveout curve since the CMP offset raypaths are refracted at layer interfaces and the straight raypaths inherent in the hyperbolic model do not actually exist (except for the trivial case where the velocities of all layers are identical).

When the onset times of a reflection can be picked at each offset in the CMP gather the moveout velocity can be obtained from Equation (1.14) using the 'T^2 - X^2' method, by which a straight line fitted to the t_x^2 - x^2 data (by least squares, for example) yields t_o^2 as the intercept at x=0 and $1/V^2_{mo}$ as the gradient.

Note, however, that if the moveout is not exactly hyperbolic, the extrapolated t_0 described here is only an approximation to the actual two-way time along the hypothetical zero-offset raypath (Al-Chalabi, 1973,1979).

Although the T^2 - X^2 method has been used extensively in the past, moveout velocities are now usually obtained from velocity analyses by picking the peaks of coherence which correspond to primary reflections.

1.1.9 Normal Moveout Velocity

Normal moveout velocity is the velocity defining the hyperbolic trajectory which best approximates the moveout of a reflection in the immediate vicinity of the emerging normal incidence ray. Normal moveout velocity can be thought of as the limiting value of moveout velocity as the spread length tends to zero.

The effect of Equation (1.14) is to replace the layers above the reflector of interest with a medium of uniform velocity V_{mo} which best fits the moveout of the reflection. However, the straight raypaths implied by this model do not account for the refractions at layer interfaces, and as a result the actual moveout times deviate about the best fit hyperbola. In general the moveout velocity depends on the offsets of the traces used in the velocity analysis due to the limitations inherent in the hyperbolic model fitting procedure. For a horizontal reflector beneath horizontal uniform velocity layers, the moveout velocity increases with offset. The difference between the moveout velocity and the normal moveout velocity (equivalent to the root mean square velocity for this simple ground model) has been called the 'spread length bias' (Al-Chalabi, 1974).

At small offsets, the moveout is very small relative to the dominant periods of the seismic data in the CMP gather traces, and the normal moveout velocity is not directly available from velocity analyses of real data. However, normal moveout velocity is important in the context of this work since it can be calculated for some ground models using a relatively simple forward modelling procedure which includes zero-offset raytracing and the concept of wavefront curvature. More significantly, it is possible to perform the inverse computation which allows the recovery of simple ground models from two-way zero-offset times and normal moveout velocities without iterative raytracing.

The curvature of a hypothetical wavefront normal to the zero-offset raypath can be calculated using various laws governing the response of the wavefront to refraction and reflection at layer interfaces and transmission of the zero-offset ray through a layer. On return to the surface, the reflected wavefront describes the 'moveout surface' from which the normal moveout velocity in any direction can be calculated.

Forward modelling formulae and references defining the normal moveout velocity for a selection of ground models consisting of uniform velocity layers and plane reflectors are presented in Table 1.1. Corresponding inversion formulae and references are also included.

Normal moveout velocity can be calculated for ground models including laterally heterogeneous layers and curved interfaces using methods described in Hubral (1980a, 1980b), but no direct inversion procedures have been developed for these complex cases.

1.1.10 Interval Velocity

Interval velocity is the gross average velocity over a depth or time interval. The term is generally referred to an 'interval' between two seismic reflection horizons.

In real data, only a limited number of seismic horizons can generally be recognised confidently, and the velocity distribution within each interval is always heterogeneous to some extent. The exact nature of the interval velocity then depends on the source of the velocity information (Al-Chalabi, 1974). Interval velocities obtained from calibrated velocity logs represent the true average of the velocities in the interval. However, interval velocities derived from root mean square velocities in the Dix Equation (1.13) represent the root mean square of the velocities in the interval. The difference between the true average interval velocity and the root mean square interval velocity increases with the degree of velocity heterogeneity in the interval (Cressman, 1968).

Detailed interval velocity information is obtained in wells from calibrated velocity logs. Sonic transit time, the reciprocal of local velocity, is typically measured every six inches down the well in a sonic logging run and the length of the logging tool generally allows a vertical resolution of around two feet. Calibration of the sonic log by a checkshot survey is generally necessary to calculate integrated travel times and gross interval velocities over large depth intervals in order to avoid cycle skips and other problems inherent in sonic logging. Reasons for differences between the seismic time measured in a checkshot survey and the integrated sonic time to the same depth are discussed in O'Brien and Lucas (1971), Goetz et al (1979) and Dupal et al (1977).

1.1.11 Average Velocity

Average velocity is the distance travelled divided by time. In common usage, the average velocity refers to an implied vertical raypath in a horizontally layered ground model. This parameter can generally only be determined with confidence at wells where a calibrated velocity log is available.

The average velocity to the nth interface is simply:

$$V_{a,n} = 2z_n/t_{o,n} \tag{1.15}$$

where z_n and $t_{o,n}$ are the depth and two-way time to the nth interface, respectively. If Δz_i denotes the thickness of the ith layer, this equation can be rewritten as follows:

$$V_{a,n} = 2\sum_{i=1}^{n} \Delta z_i \Big/ \sum_{i=1}^{n} \Delta t_i \tag{1.16}$$

or:

$$V_{a,n} = \sum_{i=1}^{n} V_i \Delta t_i \Big/ \sum_{i=1}^{n} \Delta t_i \tag{1.17}$$

in order to express the average velocity in terms of interval velocities and two-way transit times.

The most important use of average velocities is in time to depth conversion for a single layer, where the assumption of horizontal velocity layering and vertical raypaths is usually implicit. Time to depth conversion for more complex ground models including laterally variable velocities and reflector structure strictly requires raytracing methods to account for the refraction of seismic energy at layer interfaces and through heterogeneous layers.

1.1.12 Migration Velocity

Migration velocity is the velocity used in a section time migration program. Velocities used within the program for section time migration depend on the algorithm being used. Finite difference methods, for example, require interval velocities, whereas Kirchoff stack migration methods use velocities defining diffraction curves for hypothetical scatterers in the subsurface. Irrespective of these internal differences, velocities for section time migration are generally specified as some average velocity, applied from the datum, called the 'migration velocity'.

Since well control is normally limited, a large proportion of migration velocity information is ultimately derived from velocity analyses of CMP gathers. All the shortcomings of velocity analysis methods should be appreciated when preparing velocities for use in section time migration. There are additional problems in even defining the term 'migration velocity' in complicated ground models; these will not be discussed further. The use of incorrect migration velocities can lead to both loss of coherence and spurious lateral shifting of reflections on the migrated section.

1.2 DIFFERENCES BETWEEN STACKING VELOCITY, MOVEOUT VELOCITY, NORMAL MOVEOUT VELOCITY AND ROOT MEAN SQUARE VELOCITY

In order to completely resolve these velocity definitions, the essential differences between these types of velocity will now be highlighted.

Stacking velocity is a processing parameter, whereas moveout velocity is the property of a reflection event. In the noise-free case the optimum stacking velocity to produce the zero-offset primary reflection would be the moveout velocity of the reflection, but the combined effects of random and coherent noise may require a different stacking velocity to maximise the primary signal to noise ratio. Stacking velocities are sometimes made higher than moveout velocities when the primary reflections are contaminated by multiple energy at the same two-way zero-offset time but with a lower moveout velocity.

Moveout velocity is measured from the CMP gather traces in a velocity analysis and describes the moveout of a reflection across the whole gather. Normal moveout velocity as defined here is a modelling parameter describing the moveout of a reflection in the immediate vicinity of the emerging normal incidence ray; it is the limiting value of moveout velocity as the spread length tends to zero and cannot be obtained directly from real seismic data. Moveout velocity and normal moveout velocity are only equivalent for the refraction-free case of a constant velocity medium. Nevertheless, the difference between moveout velocity and normal moveout velocity is usually less than a few percent unless significant reflector structure or velocity heterogeneity is sampled by the CMP gather.

Root mean square velocity along a vertical raypath is the special case of normal moveout velocity for a ground model consisting of uniform velocity layers separated by horizontal reflectors. The difference between root mean square velocity and normal moveout velocity increases as the ground model departs from horizontal layering and the zero-offset raypath is increasingly distorted from the vertical.

For a CMP gather sampling a heterogeneous velocity distribution, the stacking velocity, moveout velocity, normal moveout velocity and root mean square velocity are generally not mutually equivalent. Furthermore, the vertical root mean square velocity for a CMP over a heterogeneous subsurface with an implied refracted zero-offset raypath is of little use since the horizontal layering condition is not satisfied. The discrepancy between stacking velocity, moveout velocity and normal moveout velocity is liable to increase with the complexity of the subsurface velocity distribution.

1.3 USES OF CMP DERIVED SEISMIC VELOCITIES

Figure 1.4 shows the flow of velocity information from CMP velocity analysis, and the uses of various types of velocity. Two primary paths of information can be identified: both originate at velocity analysis and one path leads to stacking velocities while the other terminates at interval velocities and average velocities.

Stacking velocities are picked from velocity analyses using the criterion of maximising the signal to noise ratio of primary reflections for the final CMP stacked section. These stacking velocities are used both in the final stack of the section and in preliminary section time migration.

It is difficult to define the required accuracy of stacking velocities used for the final stack. CMP stacking is a very robust procedure and differences of a few percent (up to ten percent in some cases) between stacking velocities and true primary reflection moveout velocities do not usually cause a significant loss in primary reflection coherence. Excessive differences between stacking velocities and moveout velocities may, however, lead to attenuation of high frequencies in the stacked zero-offset trace.

The reasoning behind the use of stacking velocities for preliminary section time migration processing lies in the assumption that stacking velocity, root mean square velocity and migration velocity are identical. Since this assumption strictly implies a uniform velocity, migration errors are quite likely in areas where the subsurface includes significant reflector structure or velocity heterogeneity. In practise, due to uncertainties in the use of stacking velocities as migration velocities, a suite of percentage stacking velocity functions (e.g.

95%, 100% and 105% stacking velocities) is often used for preliminary section time migration in order to ascertain the influence of different migration velocities.

Moveout velocities are picked from velocity analyses on the peaks corresponding to primary reflections, which may or may not be the same picks as the stacking velocities used in data processing. The steps including the estimation of normal moveout velocity by reducing the effects of the spread length and the inversion procedure to derive interval velocities are covered in detail in later chapters. In the simplest case, the effects of offset are ignored and horizontal layering is assumed so the Dix Equation can be used directly to obtain interval velocities.

Some of the many potential uses of interval velocity include 'layer-cake' depth conversion, raytracing, detailed section migration, gross lithological and stratigraphic interpretation, estimation of age and maximum depth of burial and the detection of overpressured zones. Some of these potential applications are, however, usually impracticable in real cases.

The precision requirements for interval velocities depend on each individual problem. Obviously the accuracy of interval velocities ultimately derived from moveout velocities depends both on the accuracy of the initial picks and on the validity of the assumptions inherent in the 'inversion' algorithm used.

Errors in moveout velocities are magnified as they are propagated into interval velocity errors. This statement can be appreciated by consideration of a horizontally layered ground model. A cursory glance at the Dix Equation shows that an error in either root mean square velocity must cause a larger percentage error in the derived interval velocity. In general a root mean square velocity error at time T (on one of the horizons bounding the interval) is magnified by the factor T/ ΔT into an error in the interval velocity for the time interval ΔT. Interval velocity errors are thus liable to increase with the depth of the interval and with decreasing interval thickness. In a horizontally layered ground then, a 1% error in root mean square velocity at a two-way time of one second causes a 10% interval velocity error for a layer with a 100 ms two-way time interval. The interval velocity error doubles to 20% for the same layer at two seconds two-way time. Errors in interval velocity increase still further as the root mean square velocity error on the second of the two bounding horizons is considered.

Average velocities are not generally useful in the context of CMP velocity analysis and inversion algorithms as the depths of the reflectors in the ground model must be known for their calculation. Derivation of average velocities at this stage serves little useful purpose except for comparison with other average velocity fields used in alternative depth conversion methods.

1.4 FACTORS AFFECTING CMP VELOCITY ANALYSIS

Both stacking velocities for the final stack and moveout velocities can be measured from velocity analyses, as described in previous sections. The reasons for differences between stacking velocities and moveout velocities have already been discussed, and this section relates specifically to the factors affecting moveout velocities derived from CMP velocity analyses.

Different velocity analysis programs may yield slightly different results from the same seismic data traces due to variations in coherence measures or display types. In this section, however, it is assumed that all velocity analysis programs are identically equivalent to the $T^2 - X^2$ method described in Section 1.8. Any factor affecting either the measured offset or the timing of a reflection therefore directly influences the results of velocity analysis.

The various influences on CMP velocity analysis can be conveniently grouped into two categories; factors in data acquisition and processing, and factors due to the subsurface. The first category consists of errors in acquisition parameters and processes applied to the traces before velocity analysis. The second category includes the distribution of subsurface velocities which influences the volume sampled by the CMP gather and ultimately determines the travel time of the reflected pulse on each trace.

Factors affecting CMP velocity analysis have been reviewed comprehensively by Al-Chalabi (1979). Only a brief summary is presented here; the reader is referred to the original work for greater detail, and to Chapter Six of this project for numerical studies of the more important subsurface factors.

1.4.1 Factors in Data Acquisition and Processing

Errors can be introduced into moveout velocities by errors in the acquisition parameters and by some side-effects of data processing before velocity analysis. These errors, detailed below, are usually greater for marine data because acquisition parameters are more difficult to control at sea. It is possible to make corrections for these effects which can reduce the moveout velocity errors to below two or three percent, but such strict quality control is uncommon in standard data processing practise in view of the robust nature of the CMP stacking process. The factors covered in this section are likely to cause moveout velocity errors for even the simplest of subsurface velocity distributions.

1.4.1.1 Data Acquisition Errors

The most important factors in marine data acquisition which introduce errors into the estimated moveout velocities are streamer feathering, irregular shot spacing and offset errors.

(a) Streamer Feathering

Streamer feathering causes the hydrophones to lie outside of the vertical plane containing the seismic line. The CMP for different s-g pairs then no longer coincides at a point on the line but lies progressively off the line for increasing s-g offset. Moveout velocity errors occur because the strict geometry of the CMP technique is not satisfied, particularly if the moveout velocity varies significantly with azimuth due to dip. In general the effect of streamer feathering is greater on strike lines than on dip lines.

(b) Irregular Shot Spacing

Irregular shot spacing results if the speed of the ship varies or if the spatial shot firing interval is not constant. Moveout velocity errors then occur because velocity analysis assumes a constant shot spacing. Moveout velocity errors due to shot spacing errors are greater for dip lines than for strike lines.

(c) Offset Errors

The most likely type of offset error is a constant error on each trace due to incorrect estimation of the near trace offset. Random offset errors are also possible, particularly in land surveys, but in general are of less significance.

1.4.1.2 Multiplexer Delay

Channels on a digital recording system are not sampled simultaneously. Each channel is sampled consecutively, causing an increasing time delay on each channel. If no correction is made for the multiplexer delay, moveout velocities are biased depending on the channel sampling order. If the near-offset trace is on channel one the moveout velocities are overestimated, whereas if the far-offset trace is on channel one the moveout velocities are underestimated.

1.4.1.3 Noise

Coherent noise, which may be due to cable snatch at sea or traffic on land, generally travels horizontally across the spread and thus has a very slow moveout velocity. As such, it is strongly discriminated against in velocity analysis and does not itself bias moveout velocity estimates. However, the attenuation of coherent noise afforded by wavenumber filtering in the field (the use of arrays) and frequency filtering in processing may lead to other undesirable effects (Sections 1.4.1.4 and 1.4.1.5).

The effect of incoherent (random) ambient noise is to reduce the signal to noise ratio late in the record and so further decrease the resolution of velocity analysis at late times, thus increasing the probability of picking errors, or indeed displacing coherence peaks on the velocity analysis display. However, since the seismic pulse is quite long and the analysis gate usually longer, velocity analysis generally remains a stable process in fairly high incoherent noise levels.

1.4.1.4 Array Length

Each seismic trace is usually composed of the summed output of a linear array of geophones (or hydrophones). The 'offset' is measured to the centre of this array. At longer offsets, or if there is dip, the reflected pulse does not arrive in phase across the array and the output may be reduced in amplitude and high frequencies to produce a weaker, longer recorded pulse. This effect is most severe when the moveout across the array is equal to the predominant period of the reflected pulse. Although the signal to noise ratio may be reduced on the longer offset traces, the effect of the array length does not normally bias the results of velocity analysis.

1.4.1.5 Pre-Processing CMP Gathers

Some preliminary processing is normally necessary before the CMP gather traces are ready for velocity analysis. The most important of these processes in terms of their effect on velocity analysis are filtering, normalisation, datum corrections and common offset stacking.

(a) Filtering

The resolution of velocity analysis increases with the bandwidth of the seismic data. Because velocity analysis is stable in fairly high random noise levels, CMP gather traces should ideally have maximum whitening deconvolution and minimum band-pass filtering applied prior to velocity analysis in order to balance bandwidth and signal to noise requirements.

(b) Normalisation

Amplitudes are often normalised both along each trace and across the CMP gather from trace to trace before velocity analysis. Automatic gain control generally gives better resolution of velocities but is more likely than programmed gain control to enhance spurious low amplitude non-primary events.

(c) Datum Corrections

In the processing of marine data, correction of CMP gather traces to a different datum should not be carried out before velocity analysis as the hyperbolic time-distance relation pertains strictly to the effective datum apparent during acquisition. If datum correction is performed before velocity analysis then the constant time shift on each trace causes systematic moveout velocity errors. For example, if source and streamer are corrected to mean sea level before velocity analysis, moveout velocities are underestimated.

The comments on datum corrections for marine data above do not apply to land data. Since on land the shots and geophone groups generally have different elevations, an initial static correction to a constant local datum is imperative before velocity analysis. High quality static corrections are required for the accurate determination of moveout velocities from land data (see also Section 1.4.2.4).

(d) Common Offset Stacking

Common offset stacking can be useful before velocity analysis since it increases the amount of data analysed and should increase the signal to noise ratio. However, if there is either significant reflector structure or rapid lateral change in reflection character, this process may actually reduce data quality. Common offset stacking in the presence of dip stretches out the reflection pulse and degrades the resolution of velocity analysis in a manner analagous to the effect of a linear array of geophones.

1.4.1.6 Parameters of the Velocity Analysis Program

The most critical parameters of a velocity analysis program (Section 1.1.6) are the length of the analysis gate, the time increment between successive gates in computation and display, and the velocity increment in computation and display. For high resolution, the length of the analysis gate should not be greater than the pulse length, and the time and velocity increments should be very small. The resolution of velocity analysis is discussed further in Section 1.5.

1.4.1.7 Onset Time of the Seismic Pulse

The band-limited nature of seismic data ensures that the reflected signal is not a clean 'spike', but a wavelet of finite duration. The maximum energy in this wavelet is therefore delayed behind the true onset time of the reflection (assuming that deconvolution at this stage has generated minimum phase output). Because the coherence does not reach a maximum until all of the wavelet is within the analysis gate, the coherence peak for any reflection event is usually at too large a time and too low a velocity. This effect is approximately equivalent to a constant time shift of each trace and is very similar to that of the application of datum corrections before velocity analysis.

1.4.2 Factors Due to the Subsurface

The previous section discussed various factors in data acquisition and processing which introduce errors into moveout velocity measurements. The variations of moveout velocity discussed in this section are due to real physical variations in the subsurface and should not be regarded as 'errors' in the conventional sense. If the ideal conditions of error-free acquisition parameters, infinite bandwidth signal, zero noise levels and perfect recording existed, moveout velocities could be measured precisely. These ideal conditions will be assumed throughout this section in order to reduce the problem to one of considering the geometry of offset s-g raypaths travelling through various velocity distributions. Moveout velocity is then obtained from the $t_x^2 - x^2$ data by the optimum linear fit to Equation (1.14).

In general the factors due to the subsurface have a greater effect on moveout velocities than do the factors in data acquisition and processing. Moveout velocities are a function of the reflection moveout over the range of offsets used by CMP velocity analysis and may not be simply related to the velocity distribution vertically below the CMP. Indeed, if structure or layer velocity changes considerably over horizontal distances comparable to the spread length, the lateral variation of moveout velocity may be in the opposite sense to that of the (vertical) root mean square velocity function (Section 1.4.2.4).

The purpose of this section is to present a discussion of the principal subsurface factors which cause the moveout velocity measured in CMP velocity analysis to be different to the root mean square velocity vertically below the CMP. A more detailed quantitative analysis of some of these effects can be found in Chapter Six.

1.4.2.1 Refraction

For a ground model consisting of a series of homogeneous layers of different velocities separated by horizontal interfaces, the moveout relation for the nth reflection is given very accurately by the equation:

$$t_{x,n}^2 = t_{o,n}^2 + x^2/V_{rms,n}^2 + C_{3,n}\ x^4 \tag{1.18}$$

where $C_{3,n}$ is zero or negative and increases in magnitude with the variability of the velocity - time function (Al-Chalabi, 1973).

The T^2 - X^2 method effectively calculates the best-fitting hyperbola from the time and offset data. Because the $C_{3,n}$ term is always less than or equal to zero, velocities derived by this method (and hence moveout velocities estimated from velocity analyses) are always greater than the true vertical root mean square velocity for a horizontally layered ground model. The difference between moveout velocity and root mean square velocity, which increases both with the spread length and the magnitude of the $C_{3,n}$ term, has been referred to previously as the 'spread length bias'.

This bias is due to refraction of seismic energy at the layer interfaces. The hyperbolic relation implies straight raypaths, but if velocity varies from layer to layer the offset raypaths are refracted and the moveout can no longer be exactly modelled by a hyperbola.

It is emphasised that Equation (1.18) is strictly only valid for a horizontally layered ground model. For a more general ground model including reflector structure and velocity heterogeneity within layers, extension of the moveout equation beyond its usual hyperbolic form is very tenuous since the root mean square velocity then loses its significance. Numerical studies suggest that in the case of homogeneous layers separated by plane dipping interfaces of arbitrary dip and strike the difference between moveout velocity and normal velocity are of the same order as in the horizontally layered case (Section 4.3.4), but this generalisation cannot be applied to more complex velocity distributions.

Refraction causes moveout velocity to increase with spread length over a horizontally layered ground model. The magnitude of this effect increases with the amount of velocity variation and is most apparent shallow in the section where the angles of incidence and refraction are greater and the offset raypaths spend relatively more time in the higher velocity layers.

1.4.2.2 Anisotropy

In the context of seismic velocity, a medium is said to be anisotropic if its seismic velocity varies with the direction of wave propagation. Although this phenomenon is likely in most stratified rocks (Cresswell, 1968), it is very difficult to measure and its significance is not yet fully understood.

The anisotropic case of horizontal transverse isotropy (when velocity in the horizontal plane is independent of azimuth but is different to that in the vertical direction) has received some attention because a seismic interval composed of alternating thin isotropic layers of different velocities acts as a transversely isotropic medium for wave propagation with wavelengths which are much greater than the individual layer thicknesses. For a horizontally layered ground model this effect generally results in moveout velocities being greater than the vertical average velocity.

1.4.2.3 Reflector Dip

The effect of reflector dip is to spread the reflection points for all offset s-g raypaths of a CMP gather up-dip from the reflection point of the zero-offset raypath (Section 1.1.3). The variation of moveout velocity with dip and strike for a single plane reflector and a layer of uniform velocity V has been comprehensively covered by Levin (1971) and has been discussed for the 2D case (the dip line) in Sections 1.1.4 and 1.1.8. The moveout velocity of a reflection from a plane with apparent dip α in the direction of the CMP gather is:

$$V_{mo} = V/\cos\alpha \tag{1.19}$$

The apparent dip α is obtained from the formula:

$$\alpha = \tan^{-1}\left(\frac{V_{mo}}{2}\frac{\partial t_o}{\partial x}\right) \tag{1.20}$$

where $\partial t_o / \partial x$ is the 'time slope' of the reflection measured on the CMP stacked section. Moveout velocity therefore assumes its minimum value on a strike line and its maximum value on a dip line. The effect of reflector dip is small, however, for dip angles of less than ten degrees ($\cos 10° = 0.985$).

The more general problem of a ground model consisting of uniform velocity layers separated by plane interfaces of arbitrary dip and strike has been solved analytically by Hubral (1976b) using zero-offset raytracing and wavefront curvature formulae. Hubral showed that for any such limited ground model the variation of normal moveout velocity with azimuth is elliptical. Although these results are strictly only valid for infinitesimal offsets, the spread length bias in the 3D plane layer case appears to be the same as that for horizontal layering (Section 1.4.2.1). The work of Hubral is discussed at length in Chapter Four.

1.4.2.4 Near-Surface Time Delays

Near-surface time delays typically result from uncorrected statics, caused by variations in the thickness of the weathering layer (or the water layer in marine surveys). Their effect is to time-shift segments of the reflection moveout curve such that the moveout velocity estimated from velocity analysis corresponds to the hyperbola which is the best fit to a number of broken reflection segments.

Delays which vary randomly over small distances compared with the spread length do not significantly distort the shape of the best-fit moveout hyperbola. Although the sharpness and resolution of the velocity analysis may be reduced, random near-surface delays generally do not cause significant moveout velocity variations.

In contrast, delays which are correlated over distances of the same order as the spread length systematically distort the moveout curve and result in a spurious best-fit hyperbola. The moveout velocity thus estimated is very strongly dependent on the spread length under these conditions.

To illustrate this point, consider the case of a near-surface step delay in the reflection times from a single horizontal interface (Figure 1.5). The step delay of magnitude T is assumed to originate in a near-surface layer of infinitesimal thickness and the velocity of the medium is V. Where the delay is not sampled by the CMP gather (case A, Figure 1.5), the moveout curve is described exactly by the hyperbola of Equation (1.3):

$$t_x^2 = t_o^2 + x^2/V^2$$

The inclusion of delays in the model introduces two associated hyperbolae:

$$t_x^2 = (t_o + T)^2 + x^2/V^2 \qquad (1.21)$$

where the CMP straddles the step and the geophone samples the delay (case C), and:

$$t_x^2 = (t_o + 2T)^2 + x^2/V^2 \qquad (1.22)$$

where the CMP gather is located entirely over the delay zone and both shot and geophone sample the delay (case E).

The resultant moveout curve for the reflection recorded by a CMP gather in any location over the model is thus composed of hyperbolic segments defined by Equations (1.3), (1.21) and (1.22). The figure also shows the moveout curves and best-fit hyperbolae for CMP gathers in the two intermediate locations B and D, together with the resulting lateral variation of moveout velocity. Note that although the root mean square velocity on the right of the model is less than that on the left, the large swings of moveout velocity are in the opposite sense.

Near-surface time delays can cause moveout velocity variations of over ten percent of the average velocity if they are correlated over distances comparable with the spread length. If the delays are contained wholly within the surface layer, the character of moveout velocity variations along each horizon down through the section may be very similar. However, the amplitude of these moveout velocity variations increases with two-way time as the moveout hyperbolae become increasingly flatter and the near-surface time delay assumes greater significance.

Al-Chalabi (1979) has shown that the moveout velocity responses of different near-surface time delays can be superimposed to produce the 'total' moveout velocity response for a more complex set of time delays. This linearity has been used to 'deconvolve' the observed moveout velocity data in order to obtain a new set of static corrections for the seismic data. Note, however, that the linearity applies not to the moveout velocity itself, but to the factor $1/V_{mo}^2$, the slope of the $t_x^2 - x^2$ graph in Equation (1.14). Although this is a seemingly attractive approach for resolving surface static corrections, considerable errors may be incurred if additional delays are generated deeper in the section by complex subsurface velocity distributions (Section 1.4.2.5).

1.4.2.5 Complex Subsurface Velocity Distributions

Reflection moveout curves over ground models consisting of uniform velocity layers separated by plane reflecting interfaces are generally well approximated by hyperbolae. Refraction at layer interfaces does not seriously distort the shape of the moveout curves and introduces a positive bias into the moveout velocity estimates of a few percent at most.

In the context of this work, a 'complex subsurface velocity distribution' refers to one which includes either layers of variable velocity or non-plane reflecting interfaces, or both. Such conditions may arise due to lithological variation, folding, faulting or unconformity, and are often responsible for much of the moveout velocity variation observed in areas of complex geology.

Velocity variations deeper in the section introduce time delays onto reflection times in a similar manner to the near-surface effects discussed in Section 1.4.2.4. Segments of the reflection moveout curves are time-shifted and the moveout velocity is derived from the trajectory which is the best fit to the broken reflection segments. The effect of these time delays again depends on their distribution over the CMP gather. Time delays which vary systematically over the volume sampled by the CMP gather are again most likely to generate moveout velocity estimation. Convergence of the CMP gather raypaths towards the reflector dictates that the critical lateral wavelength of the time delay variation decreases as the depth of the delays increases (Al-Chalabi, 1979). Only the features giving rise to time delays which vary systematically are considered here. The generation of moveout velocity anomalies is now discussed for the cases of velocity gradients (within layers), reflector curvature and reflector discontinuity (at layer interfaces).

(a) Velocity Gradients

Velocity heterogeneity within layers is generally not a serious factor in velocity analysis if the velocity changes at a fairly constant rate over the volume sampled by the CMP gather. Figure 1.6a shows the zero-offset raypath and an offset raypath for a constant vertical velocity gradient (velocity increasing downwards) in a single layer bounded by a horizontal reflecting interface. Each raypath samples both high and low value regions of the velocity field and the reflection moveout curve is very similar to that which would be observed if the layer were of a constant velocity equal to the average of the velocity function sampled by the CMP gather. Figure 1.6b shows (schematically) the raypaths for a layer with a constant horizontal velocity gradient (velocity increasing from left to right). Here the downgoing raypath segment samples the lower velocity region and the upgoing segment samples the higher velocity region. Although this compensation is not exact, the moveout is again similar to that which would be observed if the layer were of a uniform velocity equal to the average of the velocity function sampled by the CMP gather. Although of limited geological application, the remarks above are valid for constant velocity gradients in any other direction if the reflector is horizontal.

Systematic velocity variation with variable gradients is liable to affect moveout velocities more seriously. Figure 1.7 shows a layer in which the velocity field includes a minimum and a maximum and is bounded by a horizontal reflecting interface. CMP gathers are shown located over both velocity extremals. For the CMP gather at A over the velocity maximum, the proportion of lower velocity sampled increases with offset on both the s and g raypaths (cf. Figure 1.6) and the moveout velocity is less than the maximum value of the velocity field. Similarly the moveout velocity at B, over the velocity minimum, is greater than the minimum value of the velocity field. Between these extremals the rate of change of layer velocity is more gradual; the moveout velocity and vertical root mean square velocity are likely to be similar at C, for example.

Moveout velocities measured from a CMP gather sampling a linear velocity gradient are likely to yield a good estimate of the gross average velocity in the vicinity of the CMP. Irregular (i.e. non-linear) lateral heterogeneity, on the other hand, generally introduces moveout velocity variations which are not easily related to subsurface velocities directly beneath the CMP.

(b) Reflector Curvature

The effects of folding or reflector curvature can be isolated by reference to a ground model where the reflecting interfaces vertically below the CMP are curved and have a horizontal tangent. These conditions exist when the CMP is located directly over the centre of a fold which has a vertical axial plane. Figure 1.8a shows two homogeneous layers folded into an anticline with the velocity increasing downwards. The zero-offset raypath and an offset raypath to the second reflecting interface are shown for a CMP located directly over the fold axis. Any offset raypath encounters relatively more of the upper low velocity layer than it would have done if the first reflecting interface had been a horizontal plane (with zero curvature). Reflection times for all offset s-g pairs are thus greater than the horizontal layering reflection times, and the moveout velocity is accordingly lower than the vertical root mean square velocity at the CMP. This argument is exactly reversed for the synclinal case of Figure 1.8b, where the moveout velocity exceeds the corresponding vertical root mean square velocity. Moveout curves for the anticlinal, synclinal and horizontal cases are shown in Figure 1.8c.

The effects of reflector curvature are obviously intimately related to those of refraction (Section 1.4.2.1). Delays encountered along the raypaths depicted in Figure 1.8 depend not only on the s-g offset and curvature of the interfaces, but on the refraction caused by the velocity contrast at the first interface, since this governs the configuration of the CMP gather raypaths. The effects of reflector curvature can be thought of as the combined effects of velocity replacement (cf. the velocities encountered for horizontal layering) and refraction. However, the geometry of the CMP gather raypaths is rather complex over curved layers and the effects of refraction cannot be isolated as in the case of horizontal layering. Numerical studies (Sections 6.5 and 6.6) indicate that the effects of velocity replacement are generally dominant over refraction where significant reflector curvature exists.

If the velocity increases downwards the moveout velocity is likely to the lower than the vertical root mean square velocity over an anticline, and greater than the vertical root mean square velocity over a syncline. Obviously if the velocity increases upwards the converse is true, but this case is of limited geological application. As formulated here, this argument refers specifically to cases where the average velocity varies monotonically with depth.

For a CMP away from the fold axis, the effects of curvature are combined with those of dip (Section 1.4.2.3). Although moveout velocity is increased by the dip component, the effect of folding is reduced since reflector curvature is less away from the fold axis (Figure 1.9).

(c) Reflector Discontinuity

The mechanism for generating moveout velocity anomalies over faults is very similar to that discussed for near-surface time delays in Section

1.4.2.4. Time delays are introduced by the extra thickness of material on the downthrown side, and the optimum hyperbola is fitted to the broken segments of the reflection moveout curve.

Figure 1.10 shows an idealised fault through two homogeneous layers. Except for a small distance adjacent to the fault on the downthrown side (where the reflection is generally not visible due to critical refraction along the fault plane), the moveout velocity of the upper reflector is everywhere equal to the velocity of the upper layer. The moveout velocity of the lower reflector is more variable because it is affected by the shape of both upper and lower reflectors. Where the CMP gathers are restricted wholly to sampling either the upthrown or downthrown side of the fault, the moveout velocities are equal to the respective vertical root mean square velocities biased slightly by the refraction effect. However, in the region around the fault the offset raypaths are asymmetrical, and the reflection moveout curves are broken. The moveout velocity calculated from best-fit hyperbolae therefore fluctuates around the fault in a similar manner to that observed over a near-surface step time delay. This statement is supported by the similarity of Figures 1.5 and 1.10.

The real subsurface is, of course, much more complex than any of the ideal ground models considered above. Folds, faults and velocity heterogeneity generally exist together in the earth and the reflection moveout curves are much more complicated than a hyperbola. It is the assumption of a hyperbolic model that introduces much of the variation into observed moveout velocities. Moveout velocity is strongly dependent on the amount of fold, fault or velocity heterogeneity sampled by the CMP, again stressing the significance of the spread length. A subsurface feature generating a spurious moveout velocity anomaly for a long spread may yield a genuine moveout velocity variation if sampled by a shorter spread.

1.4.2.6 Associated Seismic Events

The presence of other seismic events in the data should always be acknowledged when estimating the moveout velocity of primary P-wave reflection events. The CMP gather traces may also contain coherent energy derived from diffractions, multiple reflections or mode conversions. In the context of this work, such non-primary P-wave reflection energy may be regarded as coherent noise due to the subsurface.

The effect of these events on the measurement of primary P-wave reflection moveout velocity from velocity analyses is twofold. Firstly, they may be mistaken for primary P-wave reflection energy and interpreted as such to give a false reflection. Secondly, their coherence patterns on the velocity analysis are liable to interfere with the coherence peaks of primary P-wave reflections and may bias the moveout velocity picks.

(a) Diffractions

Diffraction events often give rise to very high moveout velocities (Dinstel, 1971). The moveout velocity of a distant point diffractor located at (x_d, y_d, z_d) in a medium of uniform velocity V is given by the equation:

$$V_{mo,diff} = V/\cos\alpha \qquad (1.23)$$

where α is the angle subtended at the diffraction point between the CMP defining the origin (0,0,0) and the point (x_d, 0,0) in Figure 1.11. This diffraction moveout velocity increases as the CMP moves along the seismic line away from the point diffractor.

For a point diffractor which is not vertically below the CMP, a reflection event at the same zero-offset time as the diffraction originates from deeper in the section. If the velocity increases with depth, as is usually the case, the difference between the reflection moveout velocity and the diffraction moveout velocity at the same zero-offset time is therefore reduced. Indeed, if a point diffractor lies well outside the plane of the section the reflection moveout velocity may be higher than the diffraction moveout velocity.

(b) Multiple Reflections

In the case of horizontal layering, the moveout velocity of a multiple reflection is biased towards the velocities of those layers sampled most frequently by the raypaths. For a vertical (refraction-free) raypath reaching the nth horizontal reflector, the multiple root mean square velocity can be written as:

$$V^2_{rms,mult} = \frac{\sum_{i=1}^{n} M_i V_i^2 \Delta t_i}{\sum_{i=1}^{n} M_i \Delta t_i} \qquad (1.24)$$

where M_i is the number of two-way traverses in the ith layer. The moveout velocity of this multiple is simply the root mean square value biased by the refraction effect. If the velocity increases with depth, the moveout velocity of a primary reflection is usually greater than that of a multiple reflection at the same zero-offset time since the latter has sampled relatively more of the lower velocity layers shallower in the section. Generally this is the case, but if the velocity decreases with depth or if the multiple remains in higher velocity layers, the converse may be true.

Multiple reflections in dipping and curved layers are generally far more complex. Levin (1971) has shown that the moveout velocity of a multiple from a single plane dipping reflector below a homogeneous layer increases rapidly with the order of the multiple. There are no general rules for the behaviour of multiple reflection moveout velocities over folds, faults or velocity heterogeneity.

(c) Shear-Wave Reflections

When a seismic wave is incident on a reflecting interface there is usually some conversion from P-wave to S-wave energy, and vice versa. Mode conversion is zero at normal incidence but increases rapidly with increasing incidence angle. Particularly in land surveys, where a great deal of S-wave energy is generated by surface sources, it is likely that some apparently low velocity events in velocity analyses represent primary reflections which have travelled partly as S-waves. Mode conversion is not generally a serious problem in velocity analysis, since high angles of incidence require large offsets and shallow, steeply dipping reflectors. Serious interpretation of moveout velocities is rarely attempted under such conditions.

It is essential that the CMP gather T-X data display and the stacked section are studied in conjunction with the velocity analysis to prevent any of these associated seismic events being interpreted as a primary P-wave reflection. The redundancy of data provided by diffractions, multiple reflections and mode conversions offers an excellent potential to further constrain inverted ground models, but this power has not yet been fully harnessed.

1.5 RESOLUTION OF CMP VELOCITY ANALYSIS

The complexity of a ground model obtained by inversion is limited by the resolution of reflections both on the CMP stacked section and in the CMP gather. Resolution of reflections on the stacked section allows the measurement of accurate two-way time information, while the resolution of reflection trajectories across the CMP gather traces is essential for the accurate determination of moveout velocities.

Sherriff (1977) has indicated that the resolution of seismic reflection is restricted by the band-limited nature of seismic wave propagation and by noise. The problem is compounded by the fact that an increase in bandwidth is generally only obtained at the expense of increasing random noise, and vice versa. Acquisition and processing controls on resolution can be summarised as follows:

- the duration and shape of the band-limited seismic source pulse;
- non-optimum pulse shaping by the source and receiver arrays;
- loss of high frequencies due to progressive attenuation by the earth;
- CMP stacking increases the signal to noise ratio, but often at the expense of some of the higher frequencies;
- deconvolution increases bandwidth but also increases random noise; and
- band-pass filtering decreases random noise but reduces bandwidth.

The length of the propagating seismic pulse constrains resolution both vertically and laterally. Vertical resolution is limited by the interference effects of closely spaced reflectors, while lateral resolution is explained in terms of reflection of energy not at a point, but over a Fresnel zone which is typically of the order of ten square wavelengths (Woods, 1975).

The resolution of velocity information in CMP velocity analysis is ultimately dependent on the correct definition of reflection moveout trajectories in the CMP gather. To this end, it is essential that the reflections should have a high signal to noise ratio and good bandwidth as described above.

In addition, long offsets are required to fit the hyperbolic moveout models inherent in most velocity analysis procedures, since the most characteristic part of a hyperbola is its far offset region. Reference to Equation (1.3) indicates that:

$$(t_x - t_o)(t_x + t_o) = x^2/V^2 \tag{1.25}$$

or, to a first approximation:

$$\Delta t_x = t_x - t_o \approx \frac{x^2}{2\,t_o V^2} \tag{1.26}$$

with symbols as defined in previous sections. Moveout therefore increases as the square of the offset and inversely as the two-way time and the square of the velocity. The requirement for long spreads becomes more stringent over deeper targets as velocities and times are increased and the curvature of the reflection trajectory is reduced. This argument is easily extended to the case of horizontal velocity layering and root mean square velocities.

However, as offset increases, greater volumes of the subsurface are sampled by the CMP gather. Lateral velocity variations, which appear as local distortions to reflection trajectories, are then effectively smoothed in the hyperbolic model fitting procedure (as described in Sections 1.4.2.4 and 1.4.2.5). At long offsets, although the reflection curve may be well defined, the accompanying velocity information is less well resolved if significant lateral velocity heterogeneity exists.

In conclusion, the resolution of seismic reflections is reduced by seismic noise and poor bandwidth. In the case of horizontal velocity layering, velocity resolution is enhanced by the use of long spreads. However, velocity resolution decreases with offset if lateral velocity heterogeneity exists. Resolution of velocity information generally decreases with two-way time as noise increases, bandwidth decreases and moveout curves become flatter.

1.6 SUMMARY

A new set of velocity definitions has been presented in order to reduce the confusion prevalent in much of the literature relating to seismic reflection velocities.

Stacking velocity, moveout velocity, normal moveout velocity and root mean square velocity are generally not equivalent for a CMP gather sampling a typical heterogeneous subsurface.

Seismic velocities obtained from CMP velocity analyses have many potential uses including time to depth conversion, section migration, raytracing and gross lithological interpretation.

CMP velocity analysis is subject to a number of influencing factors which can be divided into those due to data acquisition and processing, and those due to the subsurface. In general the subsurface has the greater effect on moveout velocities obtained from velocity analysis.

The resolution of CMP velocity analysis is limited by the signal to noise ratio and the bandwidth of the seismic data, and also by the offsets of the traces used in the analysis.

2. REAL DATA

The objective of Chapter Two is to present the seismic reflection data and well information which are used in Chapters Three and Seven. A brief interpretation of the data is included here.

The data have been obtained from an offshore concession with an area of approximately 375 square kilometres. The sea floor is reasonably flat over the area, with an average water depth of 70m. Figure 2.1 presents a schematic location map of the seismic lines and wells which were available for this study.

The seismic data is of two vintages, referred to here as 'Survey A' and 'Survey B'. The former is the source of most of the seismic information. Data from Survey B has been included in order to compare the results of velocity studies from different surveys with contrasting acquisition and processing parameters.

It is noted at the outset that the seismic sections for both surveys were produced completely independently of this project at the BP Processing Centre in London. Only the closely spaced velocity analyses were generated specifically for this project at a later date. Although the author was not directly involved in the processing, some procedures are worthy of comment in view of their potential effect on the two-way time and moveout velocity database presented in this chapter.

Since the inversion method used to derive interval velocities in Chapter Seven requires moveout velocities and two-way zero-offset times, the interpretation here is limited to the CMP stacked sections, as the two-way stacked times are ideally equivalent to the two-way zero-offset times (Section 1.1.5). Migrated sections have only been used to solve problems encountered during the interpretation of CMP stacked sections, and no migrated seismic data are presented here.

Well information was required both to correlate the seismic horizons with local stratigraphy and to obtain accurate interval velocities. Geological composite logs and calibrated velocity logs were studied at four wells for this purpose.

2.1 SURVEY A: DATA ACQUISITION AND PROCESSING

The 38 lines of Survey A used in this project are shown as solid lines in Figure 2.1. These lines form an approximate 1 km square grid over a rectangular area of around 25 x 15 km.

Eight lines (A-103, A-111, A-115, A-120, A-123, A-130, A-132 and A-144) are highlighted by thicker solid lines in the figure. These lines have been selected for a detailed study of moveout velocities and interval velocities, the results of which can be found in Chapters Three and Seven.

2.1.1 Data Acquisition

Table 2.1 lists the principal acquisition parameters for Survey A. The 60 group streamer with a 50m group spacing and 300m near-trace offset provided a spread length (or far-trace offset) of 3250m. Both the shot point and CMP intervals were 25m.

The shot array depth of 6.5m and cable depth of 14m position the mean shot and streamer level some 10.25m below mean sea level for Survey A.

2.1.2 Seismic Sections

Lines A-111 and A-134, which intersect perpendicularly over the culmination of the major structure in the area, were used for parameter testing during the original 'production' processing of these sections. Table 2.2 lists the parameters which were selected by the processing team to produce the final CMP stacked sections for Survey A.

Although the processing was not performed as part of this project, specific comment is warranted on the following steps:

(a) Adjacent Trace Summation

Various configurations of CMP geometry were tested, and a 2-fold adjacent trace sum (with differential NMO correction) followed by a 30-fold CMP stack was found to increase the signal to noise ratio relative to the simple 60-fold CMP stack.

(b) Deconvolution Before Stack (I)

The first deconvolution before stack used a short 80ms operator in order to sharpen the wavelet.

(c) Bulk Static Correction (High-Cut Filter Delay)

This rather unusual procedure was intended to eliminate a forecast 20ms delay introduced by the 62Hz high-cut anti-alias filter.

(d) Normal Moveout Correction

Velocity analysis is described in detail in Section 2.1.3.

(e) Deconvolution Before Stack (II)

The objective of this predictive deconvolution was specifically to attenuate the water-bottom multiple. With an effective water-depth of 60m (from the mean shot and streamer level) and a water velocity of 1480m/s, the two-way time for a bounce in the water layer is 81ms. An operator of total length 140ms was found to be the best to reject such a reverberation.

(f) Deconvolution After Stack

Post-stack whitening deconvolution was performed with a time-variant operator of length 140ms. Three overlapping design gates were used to match corresponding geological zones of differing frequency content. Significantly higher prewhitening was necessary in the deeper zone in order to balance the frequency spectrum before deconvolution.

Display parameters for the sections of Survey A require little discussion. Compressions are shown by white troughs according to the SEG convention. No static corrections for the shot and streamer depths were applied to the sections. The time datum on these sections therefore corresponds to the mean shot and streamer depth of approximately 10m below mean sea level (Section 2.1.1).

2.1.3 Velocity Analysis

As part of the routine processing sequence described in Section 2.1.2, velocity analyses were performed at 1km intervals along each of the lines in Survey A using the BP velocity analysis program 'VLAN'. The operation of such a standard velocity analysis program has been described in Section 1.1.6. In addition, extra velocity analyses were made at 250m intervals along the eight lines highlighted in Figure 2.1 for a more detailed study of seismic velocities.

Since velocity analysis is a pre-stack procedure, the optimum processing parameters for the final CMP stacked sections are not available for pre-processing the CMP gathers. Table 2.3 lists the processing applied to the data before velocity analysis, essentially a crude version of the pre-stack sequence of Table 2.2.

Most of the processing steps are very similar, the major difference being a 2-fold common offset stack which forms a composite CMP gather record from two adjacent gathers. Except for areas of very high dip or where the reflection character changes significantly over one CMP interval (25m), common offset stacking is likely to have improved the signal to noise ratio and hence the quality of the velocity analyses. Figure 2.2 shows two adjacent raw CMP gathers before common offset stacking.

The two deconvolutions were used both to whiten the spectrum (and hence sharpen the wavelet) and to attenuate multiple energy in order to improve the resolution of velocity analysis. However, the random noise left in the wake of these successive deconvolutions made some band-pass filtering necessary, which in turn decreased the bandwidth.

Gain controls were used to balance the energy along each trace. Low amplitude reflections were amplified by the short automatic gain control, while the strong reflections in the time window 1.8-3.2s were reduced in amplitude by the programmed gain control which was linearly interpolated between definition points. Approximate equalisation of reflection amplitudes is desirable before velocity analysis if the stacking velocities and moveout velocities of weaker reflections are to be picked confidently.

Application of the 20ms bulk static correction before velocity analysis was valid since the intention was to eliminate delay introduced by the recording filters, and not to shift the recording datum.

No systematic bias appears to have been introduced into the velocity analyses by the pre-processing sequence.

Within the VLAN program, velocity analyses were performed with 18 user-controlled velocity-time functions. The default analysis gate length (56ms) and gate spacing (28ms) were used throughout, and the coherence values were scaled by an automatic gain control over 250ms to enhance the display.

Figure 2.3 shows the VLAN display for the common offset stacked gathers of Figure 2.2 after pre-processing. A number of well resolved coherence peaks are evident, particularly in the range of 2-3s two-way zero-offset time. Most of the velocity analyses for Survey A are of the same standard, reflecting the relatively high quality of this data set for velocity studies.

2.2 SURVEY B: DATA ACQUISITION AND PROCESSING

Two lines of a more recent survey, Survey B, extend into the grid of Survey A. These lines (B-4 and B-8) were selected for dense velocity sampling along with the eight lines of Survey A, and are shown as broken lines on Figure 2.1.

2.2.1 Data Acquisition

Table 2.4 lists the principal acquisition parameters for Survey B. After channel weighting and summing, the streamer effectively consisted of 119 channels with a 25m group interval. With a near-trace offset of 200m, the resultant spread length was 3150m. The CMP interval for this survey was 12.5m, exactly half that of Survey A.

The mean shot and streamer level for Survey B is 9.75m below mean sea level (cf. 10.25 for Survey A), as the shot array depth and cable depth were 7.5m and 12m, respectively.

2.2.2 Seismic Sections

The parameters selected by the processing team to produce the final CMP stacked sections for Survey B are shown in Table 2.5. The following processing steps deserve further explanation:

(a) Trace Mix

The 119 recorded channels were reduced to 60 traces by a 3-fold trace mix with 1:2:1 weighting and differential NMO corrections. All 60 traces were then used in the pre-stack processing (cf. 30 for Survey A).

(b) Bulk Static Correction (Source Delay)

A correction of 15ms was necessary to eliminate the known source delay introduced by triggering the guns before the recorded time zero.

(c) Low-Cut Filter

The reason for applying the low-cut filter is not certain, but may be related to low-frequency noise generated by the boat.

(d) Deconvolution Before Stack

Pre-stack deconvolution used a time-variant operator of length 140ms in order to whiten the spectrum.

(e) Normal Moveout Correction

Velocity analysis is described in detail in Section 2.2.3.

(f) Trace Equalisation

Trace equalisation was applied before the stack in order to balance the energy across each trace in the CMP gather.

(g) Bulk Static Correction (Shot and Streamer Depth)

The correction of 15ms for shot and streamer depth lifted the datum to mean sea level. A similar correction was not made for the data of Survey A.

(h) Velocity Filter

The rejection of steep dips was intended primarily to reduce non-reflected energy (specifically diffracted energy) on the sections. A time slope of 12ms/trace corresponds to a reflector dip of 27° for an overburden with a constant velocity of 2500m/s.

(i) Deconvolution After Stack

Post-stack deconvolution used a long 300ms operator aimed both at sharpening the wavelet and attenuating residual multiple energy. Existing software demanded that each deconvolution operator be active along the entire length of each trace. The use of 50% prewhitening in the first gate acted virtually as an 'all-pass' filter where no deconvolution was thought necessary.

(j) Band-Pass Filtering

The application of time-variant band-pass filtering followed the structural trends observed on the early 'brute' stacked sections.

The CMP stacked sections of Survey B are displayed with the same polarity as those of Survey A, such that white troughs again represent compressions. The time datum for Survey B is mean sea level.

It is evident that, aside from possible delays introduced by processing filters, Surveys A and B do not share a common time datum as a result of the different acquisition systems and bulk static corrections applied. This discrepancy is discussed further in Section 2.3.1.

2.2.3 Velocity Analyses

Velocity analyses were generated at intervals of 1km during the routine processing of each line in Survey B as described in Section 2.2.2. Additional velocity analyses were performed at 250m intervals along both lines B-4 and B-8. Computation was again made by the VLAN program.

Table 2.6 shows the processing sequence applied to the data before velocity analysis. For the same reasons as in Survey A, pre-processing before velocity analysis differed from the pre-stack processing for the final sections.

Common offset stacking was again used, in this case a 4-fold stack. The composite CMP gathers of Survey B were formed from four adjacent gathers over three CMP intervals (total 37.5m) and were thus slightly more susceptible to rapid lateral changes of structure or reflection character than those of Survey A. In general, common offset stacking was successful in improving the signal to noise ratio for primary reflections.

The deconvolutions, band-pass filtering and automatic gain control were applied for the same reasons as those outlined for Survey A in Section 2.1.3. Figure 2.4 shows a specimen composite CMP gather after pre-processing and before velocity analysis.

The pre-processing sequence is not likely to have introduced a systematic bias into the velocity analyses of Survey B.

Some 30 velocity-time functions were used in the velocity anlayses for Survey B. To maintain consistency with the previous survey, the default analysis gate length (56ms) and gate spacing (28ms) were again used, together with the 250ms automatic gain control on the coherence function.

Figure 2.5 shows the VLAN display for the composite CMP gather record of Figure 2.4. Once again there are many well resolved coherence peaks which allow the stacking velocities and moveout velocities of reflections in the 2-3s two-way zero-offset time range to be picked easily. The velocity analyses of Survey B generally match or exceed the high quality of those of Survey A.

2.3 INTERPRETATION

To conform with previous interpretation in this area, five seismic horizons were chosen for analysis. In order of increasing two-way time, these are referred to here as the Brown, Pink, Yellow, Orange and Red horizons. Correlation of these horizons with local stratigraphy is deferred to Section 2.4.

An interpretation of the two-way times and moveout velocities available from both CMP stacked sections and velocity analysis displays is presented under respective headings below.

2.3.1 Two-Way Times

The Brown, Pink, Yellow, Orange and Red horizons were identified on line A-130 in accordance with a previous interpretation. Each horizon was then followed around the grid of Survey A lines, ensuring that a tie existed at each line intersection. Every available line intersection was then used to lead the horizons onto the two lines of Survey B. Interpreted CMP stacked sections for lines A-103, A-111, A-115, A-123, A-120, A-130, A-132, A-144, B-4 and B-8 are presented in Figures 2.6 through 2.15, respectively.

The most important part of the this project is a study of the eight lines of Survey A and the two lines of Survey B with dense velocity sampling at 250m intervals. Along these lines, the two-way time to each of the five horizons was measured at the surface locations corresponding to the mid-points of CMP gathers selected for velocity analysis. Only the Yellow and Red horizon times were measured on the remainder of the Survey A lines, this time at 1km intervals to coincide with the more sparsely distributed velocity analyses.

Interpretation of the upper three horizons was relatively straightforward. However, complications arose when following the Orange and Red horizons down the flanks of the anticlinal features, especially where the structures were complicated by faults. In general, the lower two horizons are well defined over the major structure in the centre of the grid and interpretation becomes less confident towards the edges of the survey area.

Errors in picked times are generally very small when compared to the absolute value of two-way time, but may become more significant compared to a time interval between two horizons. This is an important consideration if the times are to be used in the calculation of interval velocities (Section 1.3), as indeed will be their destiny in Chapter Seven. Each of the five horizons was picked along a white trough, the pick normally intended to be at the culmination of the trough. Errors resulting from the picking of troughs and measurement of this time on the original work sections at 10cm/second scale using a graduated rule are estimated to be of the order of +/- 10ms. This figure represents maximum errors of 0.33% for a two-way time pick at 3s, 0.5% for a two-way time pick at 2s, 6.7% for a 300ms two-way time interval, and 20% for a 100ms two-way time interval. The RMS two-way time mis-tie for the database consisting of the eight densely sampled lines of Survey A calculated over all five horizons at 16 line intersections is 8ms. This figure is less than the estimated measurement error of +/-10ms and is regarded as being acceptable.

As stated previously (Section 2.2.2), Survey A and Survey B do not share a common time datum. The discrepancy is introduced by a number of component effects, each of which is summarised below:

- differences in acquisition systems should cause time picks on Survey B (DFS V) to be 10ms earlier than on Survey A (DFS IV);
- the processing advance applied to the data of Survey A to eliminate the high-cut filter delay should leave the time picks on Survey B some 20ms later than those on Survey A;

- a shot and streamer depth bulk static correction (to mean sea level datum) was applied only to Survey B, and hence time picks on this survey should be 15ms later than those of Survey A; and
- a source delay correction was made only for Survey B, making time picks for this survey 15ms earlier than those on Survey A.

The net result of these four 'fixed' delays is therefore (theoretically) to make the time picks on Survey B some 10ms later than those on Survey A. However, the unusual processing advance on Survey A and the source delay correction on Survey B are not fully explained and may not adjust the time datum as intended. No source delay correction has been used for the data of Survey A, and it must be assumed that the guns for this survey were perfectly synchronised to time zero in the absence of any other information. In addition, there is likely to be a small time-varying discrepancy in time picks between the two surveys due to differential filter delays in the two processing sequences.

Eight intersections are available where the eight densely sampled lines of Survey A cross the two lines of Survey B; the average and RMS two-way time differences are 20ms (times on Survey B later than times on Survey A) and 22ms respectively, when calculated over all five horizons. Since 10ms can be explained by the combined effects of the systematic differences discussed above, the remaining discrepancy is just within the estimated time measurement errors of +/- 10ms. The two-way times of Survey B have been reduced by 10ms to conform with the Survey A datum which corresponds to the mean shot and streamer level.

Contoured two-way time maps of the Yellow and Red horizons over the 1km grid of Survey A are presented in Figures 2.16 and 2.17 (Enclosures 2.1 and 2.2), respectively. The area is dominated by a large structure in the centre of the seismic grid which reaches its culmination around the intersection of lines A-111 and A-130. This feature is thought to be salt-supported and is surrounded on all sides by a structurally low area which is probably due to salt withdrawal. Part of another salt feature can be seen in the eastern corner of the grid, while a rather less pronounced high structure is observed around the intersection of lines A-105 and A-116.

The Red horizon is cut by many normal faults, which indicate a tensional stress regime. Few of these faults cut the Orange horizon, and hence most of the movement pre-dates the deposition of the stratigraphic boundary corresponding to this horizon. The structure mapped at the Yellow horizon shows that at shallower levels the sediments tend to drape over the fault-controlled structure at depth. Both faults and two-way time contours generally define a northwest-southeast trend.

2.3.2 Moveout Velocities

Two separate moveout velocity 'databases' from Survey A can be identified. The first consists of moveout velocities picked for all five horizons at 250m intervals along the eight densely sampled lines of Survey A, while the second is composed of moveout velocities on the Yellow and Red horizons picked at 1km intervals over the entire grid of Survey A. Additionally, moveout velocities on the five horizons picked at 250m intervals along the two lines of Survey B have been used in conjunction with the first database in order to compare results from two different surveys.

In contrast to the processing geophysicist's criterion of picking stacking velocities for every significant coherence peak on the velocity analysis display, moveout velocities for this study were picked to correspond strictly with the timing of the five horizons interpreted on the CMP stacked sections.

Coherence peaks on the velocity analysis displays are often delayed relative to the picked stacked section times of the horizons. This delay is attributed to the band-limited nature fo the seismic data causing maximum coherence to occur when the analysis gate contains the dominant cycles of the reflected wavelet, which may or may not coicide with the interpreted cycle on the section. In general the coherence peaks were picked either on the cell corresponding to the interpreted time or one cell (28ms) later.

The accuracy of each moveout velocity pick is limited by the elongation of the coherence peak along the velocity axis. A sharp peak may yield a moveout velocity defined by maximum coherence with an uncertainty of only +/- 25m/s (one cell width). However, some coherence peaks are poorly resolved in the velocity dimension and the uncertainty may increase to +/- 100 m/s or more. In general, the smear of coherence increases with two-way time due both to the flattening of moveout curves and the decrease in bandwidth caused by progresssive attenuation of high frequencies by the earth (Section 1.5).

The signal to noise ratio of the reflection is also important, as high noise levels introduce still more smear into the velocity spectrum. Both the Yellow and Red horizons are strong reflections and allow the most confident picks on the velocity analysis displays.

Errors in the picking of an individual moveout velocity are not considered here. Picks were consistently made at the centre of coherence maxima, and it is anticipated that picking errors of a random nature can be at least partially removed by spatial smoothing techniques when they are used to obtain interval velocities (Chapters Three and Seven).

Constant checking with the CMP stacked sections was necessary to identify and omit coherence peaks generated by diffracted energy. It remains a possibility that some of the high moveout velocities observed around faults (especially on the Red horizon) are due either solely to diffractions or to a local reinforcement of reflected energy with diffracted energy.

In some cases no coherence peak was observed on the velocity analysis display around the interpreted time of the horizon and a moveout velocity pick was impossible. Due variously to faulting, rapid lateral changes in reflection character, high noise levels or excessive jitter in the reflection trajectory, these cases accounted for less than 3% of the moveout velocity databases. Since many of the techniques discussed in later chapters require that moveout velocity be sampled at equispaced intervals along the surface, it was necessary to interpolate a value where the pick was impossible. This approach is thought to be valid as the moveout velocity gaps are not due to very complex reflector structure causing a real 'void' on the CMP stacked sections, but to a local signal to noise problem. The method chosen was a simple linear interpolation from adjacent moveout velocity picks. Since no particularly long gaps of moveout velocity existed, the interpolation is not thought to have significantly distorted the overall moveout velocity trends.

A plot of moveout velocity against distance along the seismic line for a single seismic horizon is referred to here as a 'moveout velocity profile'. Moveout velocity profiles for the five horizons along lines A-103, A-111, A-115, A-123, A-120, A-130, A-132, A-144, B-4 and B-8 are presented in Figure 2.18 (Enclosure 2.3).

The RMS moveout velocity mis-tie over all five horizons at the 16 line intersections of Survey A is 44m/s. Since the CMP gathers on each line at the intersection point are not oriented in the same direction, different subsurface volumes and apparent dips are sampled and moveout velocity mis-ties are indeed to be expected. If the subsurface includes any reflector structure, faults, velocity heterogeneity within layers or near-surface time delays, as is likely, the chances of a perfect moveout velocity tie at a line intersection are small. A comprehensive analysis of moveout velocity mis-ties over the survey area is included in Chapter Three.

At the eight intersections of Survey A lines with Survey B lines, the RMS moveout velocity mis-tie is 68m/s. The mean mis-tie of 51m/s indicates that the moveout velocities of Survey B are systematically higher than those of Survey A at the line intersections. The source of this bias is not immediately obvious. Indeed, it cannot be attributed to refraction (Section 1.4.2.1) as the spread length of Survey B is 100m shorter than that of Survey A. Nor is it due to the two surveys having a different time datum. Of the four time delays and corrections discussed in Section 2.3.1, all but the 15ms shot and streamer depth correction on Survey B were applied before velocity analysis, and hence the pre-velocity analysis time datum for Survey B was 5ms earlier than that of Survey A. Inclusion of a time delay in the moveout equation (1.14) indicates that the moveout velocities for Survey B are biased by no more than one-tenth of a percent relative to those of Survey A if a time delay of -5ms, a two-way time of 3 seconds and perfect hyperbolic moveout is assumed. Finally, it must be considered extremely unlikely that this systematic difference is due to a fortuitous selection of line intersection locations. Without a suitable explanation for this difference, and lacking sufficient data from Survey B to establish an empirical relation with Survey A, moveout velocities from both surveys have not been integrated into a single data set.

Moveout velocities on the Yellow and Red horizons have been contoured from the 1km coarse grid of Survey A. The maps are presented in Figures 2.19 and 2.20 (Enclosures 2.4 and 2.5), respectively. The computer gridding program CPS-1 was used as it afforded a relatively objective and unbiased means of contouring these rather noisy data sets. The CPS-1 program, in common with most other computer contouring algorithms, operates by interpolating scattered data onto a rectangular grid through which it can then draw contours. Interpolation at each grid node is made by fitting a local polynomial surface to data points within a specified search area. The moveout velocity maps presented here were obtained by interpolation onto a 2km square grid (rotated to match the orientation of the Survey A seismic grid) using a search radius of 20km. These parameters were chosen as interpolation onto a grid with a smaller cell size tended to generate short wavelength closures or 'bullseyes', while interpolation using a larger cell size was found to smooth the data excessively. Due to the somewhat arbitrary nature of the gridding parameters, the coarse sampling interval and the inconsistencies at line intersections, these maps should not be regarded as being definitive. Rather, they are intended to portray the dominant moveout velocity trends over the survey area. The area of lower moveout velocities over the structure in the centre of the grid is one such trend. Isolated features around the edge of the grid should be viewed with suspicion, as they are most probably edge effects generated by the gridding algorithm where few data points were available.

It is impossible to associate every fluctuation on the moveout velocity profiles with features on the CMP stacked sections. However, it is pertinent to remark on the broader relations between the moveout velocities and time structures observed over the survey area. The most important points to note are:

- At an individual surface location the moveout velocity generally increases with time from a minimum on the Brown horizon to a maximum on the Red horizon.
- Along any one seismic line the moveout velocity profiles generally follow a similar pattern.
- The magnitude of fluctuation in the moveout velocity profiles generally increases with time from a minimum in the Brown horizon to a maximum in the Red horizon.
- Over any individual horizon the moveout velocity has a tendency to increase with two-way time. This is well illustrated by the decrease in moveout velocities over the structure in the centre of the grid.
- Fluctuation in the moveout velocity profiles is increased where the horizon (and more particularly those above it) is broken by faulting or draped over deeper faults. The moveout velocity profiles for the Orange and Red horizons between shot points 250 and 480 on line A-120 are good examples.
- The tendency for the moveout velocities to increase down the flanks of the structure in the centre of the grid (see, for example, lines A-130 and A-132) is probably due both to reflector dip and an increase of average velocity with two-way time (Section 2.4.2).
- High moveout velocities are observed where the reflectors are locally curved concave-upwards. This effect is evident on the Brown, Pink, Yellow and Orange horizons around shot point 150 on line A-130, shot point 140 on line A-132 and shot point 170 on line B-4 where the shallower horizons have draped over a fault on the Red horizon. Although these high moveout velocities may be due in part to reflector dip (on the sides of the syncline) and to a gradual increase of average velocity into the syncline (Section 2.4.2), their correlation with local concave-upward surfaces is thought to be significant (Section 1.4.2.5(b)).

The above comments show that some of the predictions for moveout velocity behaviour made in Section 1.4.2 have been illustrated by this data set.

2.4 INFORMATION FROM WELLS

Three vertical wells and one deviated well have been studied in conjunction with the seismic data from Surveys A and B. Each extends to a total depth below the interface corresponding to the Red horizon. Geological composite logs (including the sonic, gamma ray and lithology logs) and calibrated velocity logs were available for each well.

The three vertical wells are referred to here as wells 'A', 'B' and 'C' (Figure 2.1). Wells A and B are positioned very close to the crest of the structure in the centre of the seismic grid in areas of very shallow dips, while Well C is located on the steep southwestern flank of the structure where dips of up to 10° were encountered at deeper levels. The fourth well, referred to here as well 'CC', was deviated from within the bore of Well C. The deviation kicked off at 1720m (drilled depth) and built up to an angle of approximately 20° to the vertical before terminating some way updip from the bore of Well C.

The reasons for incorporating well information into this project are twofold, namely:

- to correlate seismic reflection horizons with local stratigraphy; and
- to estimate gross average interval velocities between these horizons.

To satisfy the first objective, the calibrated velocity log and density log were used to synthesise a reflection seismogram at Wells A and B. Seismic reflection horizons on the CMP stacked sections were correlated with events on the synthetic seismograms and in turn associated with discontinuities on the logs. Use of the geological composite log enabled the correlation of seismic horizons with local stratigraphy.

Secondly, interval velocities were estimated from the depths and calibrated two-way times of the stratigraphic boundaries corresponding to each of the seismic horizons. These velocities are required primarily for comparison with interval velocities derived by the inversion of moveout velocities in Chapter Seven.

The identification of seismic reflection horizons and estimation of interval velocities are now discussed in turn.

2.4.1 Correlation of Seismic Horizons with Stratigraphy

Synthetic seismograms for Wells A and B are presented in Figures 2.21 and 2.22, respectively. The reader is referred to Appendix 2A for a brief discussion of the method used to calculate these traces.

While a density log has been used in the calculation at Well A, a constant density has been assumed at Well B. The similar character of both density and calibrated velocity logs at Well A (Figure 2.21) indicates that the computation of reflectivity at Well B should not be adversely affected by this assumption. Although sonic and density measurements were recorded every six inches (c. 0.15m) in the wells, the calibrated velocity and density logs have been resampled by linear interpolation to correspond with the 4ms sampling interval of the seismic traces. Finer resolution of the logs is unwarranted for the purposes of matching synthetic seismograms to seismic reflection sections due to the band-limited nature of the seismic method.

The wavelet used for the calculation of synthetic seismograms at Wells A and B had been obtained previously by BP London using an iterative inversion algorithm. Trial seismograms computed from the reflectivity function using different wavelets were repeatedly matched with the (migrated) seismic data at the well locations until an 'optimum' wavelet was found. This wavelet is displayed at the top right corner of both Figures 2.21 and 2.22. It is not a minimum-phase wavelet. Zero-phase elements have been introduced into the wavelet by the effects of filters in the processing sequence, with the result that the wavelet appears to start before zero time.

For both wells, the synthetic seismogram including primaries and internal multiples is a good match with the CMP stacked sections. Since these wells are vertical and are located at the crest of the structure where the layering is near-horizontal, section migration has little effect and the match with the corresponding migrated sections is unlikely to have been significantly better. The match between the total synthetic seismogram (including primaries, internal multiples and surface multiples) and the CMP stacked sections is poor in both cases, indicating that processing has been successful in attenuating surface multiple energy. The synthetic seismograms including primaries only have proved the most useful for the correlation of seismic horizons with stratigraphy.

The procedure outlined in Appendix 2A was used successfully to identify each of the five seismic reflection horizons interpreted in this project. Interpreted correlations between seismic reflection horizons and breaks on calibrated velocity logs at wells A and B are annotated on Figures 2.21 and 2.22.

Figure 2.23 illustrates the spatial correlation for each horizon plotted on the sonic logs for Wells A, B, C and CC. Comparison of the sonic logs for Wells A and B with the calibrated velocity logs in Figures 2.21 and 2.22 shows the filtering effect of the 4ms resampling.

The correlations of each seismic reflection horizon with stratigraphy are summarised in Table 2.7 and discussed in turn below.

The Brown horizon is the least well defined of the five horizons on the calibrated velocity logs. It is not associated with a major lithological or velocity discontinuity, but appears to be generated by a set of thin limestone bands within a thick sequence of clays and mudstones. This horizon is picked on a compression (white trough) and is of reasonably uniform character over the survey area.

The Pink horizon is generated near the top of a thin layer including tuffaceous mudstones and volcanic ash. This horizon is picked on a weak compression (white trough) which changes in character over the structure, indicating that the layer is not deposited uniformly over the area.

The Yellow horizon is generated around the top of a thick carbonate sequence, and is picked on a strong compresion (white trough) caused by the sharp velocity increase at the boundary. The reflection is complicated by the presence of a low velocity mudstone near the top of the carbonates, which varies in thickness from around 30m at Well A to a thin band of less than 10m at Well C. In areas where the mudstone layer is well developed, constructive interference takes place and a broad compresisonal event is observed, the centre of which is delayed relative to the reflection generated at the very top of the carbonates. The character of the Yellow horizon is thus liable to vary considerably over the survey area.

The Orange horizon is generated at the base of the carbonates where a sharp velocity decrease is encountered into shales and mudstones. Although this velocity decrease generates a rarefaction (black peak) as the first cycle of the reflected wavelet, the Orange horizon has been picked in the following white trough. The character is quite uniform over the survey area.

The Red horizon originates at another sharp velocity decrease where a layer of highly organic mudstones with very low velocity is encountered. Again, this horizon has been picked in the white trough following the initial rarefaction (black peak) generated at the velocity decrease. The variation of character of this reflection over the survey area may be due partly to the unconformable nature of this horizon, although in general a strong event is developed.

Having described the nature of the interfaces corresponding to the seismic reflection horizons, it is important to stress that these conclusions can be drawn only from the small area penetrated by the wells. Extrapolation of these results away from the structure is made with the implicit assumption that the overall character of the lithology is consistent over the entire survey area. Evidence from seismic data and from wells drilled in adjoining areas does not suggest otherwise.

The pick time of the reflection horizon on both the synthetic seismogram and the CMP stacked section is generally not coincident with the time of its corresponding break on the calibrated velocity log. As it is desirable to eliminate this 'lag' when the section times are used for interval velocity estimation and depth conversion, the delays for each horizon were estimated at this stage.

The method used here to derive these delays is an empirical one based on the difference between a picked two-way time to an horizon on the section and the two-way time to the supposed causative velocity break measured from the calibrated velocity log. Particular care was given to the two-way time picks on the sections, as any errors will contribute directly to the estimated lags. Since the Survey A sections have a time datum at mean shot and streamer level and the calibrated velocity log times refer to mean sea level datum, the log times have been reduced by 15ms two-way time to conform with the Survey A datum.

The picked section times and corrected calibrated velocity log times to each of the five horizons at wells A and B are presented in Table 2.8. Only Wells A and B were used since the dipping layers around Well C and the deviated well bore of Well CC give rise to non-vertical raypaths in the checkshot survey and caused considerable uncertainty in the calibration of the respective velocity logs (Section 2.4.2). As two lines intersect at Well A and one line passes through Well B, three separate measurements of the lag could be made for each horizon. Table 2.8 also includes the estimated lag for each horizon, which has been obtained simply as the mean of the three individual estimates.

With reference to Table 2.8 and Figures 2.21 and 2.22, the lags for each horizon are discussed briefly below:

- The Brown horizon is picked in the first cycle of the wavelet.
- The Pink horizon is weak over the structure and the correlation on the synthetic seismogram is not at all convincing, as it appears that a black peak has been picked on the section. The reason for this is not known, but may be due to local contamination by multiple energy.
- The Yellow horizon is picked in the third cycle of the wavelet generated at the top of the carbonates. The long lag time is due to this trough being prolonged by interference effects, and the actual pick time being in the centre of the interference trough.
- The Orange horizon is picked in the second cycle of a reverse polarity wavelet.
- The Red horizon is similarly picked in the second cycle of a reverse polarity wavelet.

The magnitude of these lags is rather confusing, as it must be said that a match to mean sea level datum would appear more appropriate. With no evidence to question the Survey A datum, however, it must still be assumed that the datum is at mean shot and streamer level.

Future application of these corrections to the picked two-way times over the survey area assumes that the character of each reflection remains reasonably constant. With no further well control in structurally lower parts of the survey area, this is the best assumption that can be made.

2.4.2 Estimation of Interval Velocities

Estimates of interval velocities from wells are of great importance since they provide the only true check on the validity of interval velocities derived by the inversion of moveout velocities in Chapter Seven. Since the depths and two-way calibrated log times of the interfaces identified from the previous section as generating the five seismic reflection horizons were available, the calculation of interval velocities was straightforward.

Estimated gross average interval velocities at Wells A and B are presented in Tables 2.9 and 2.10, respectively. Vertical wells and horizontal layering were assumed and interval velocities were obtained simply as twice the interval thickness divided by the two-way interval travel time. A velocity of 1480m/s has been assumed for the water layer.

Interval velocities for Wells C and CC had been derived previously by BP London using an iterative raytracing procedure constrained by the checkshot survey results to account for the non-vertical raypaths caused by the dipping reflectors and deviated well bore. Table 2.11 presents the BP London model for the reflector geometry and interval velocities at both Wells C and CC.

Interval velocity - depth functions for the vertical Wells A, B and C are shown in Figure 2.24. In each well the interval velocity reaches a maximum in the carbonate sequence. Each horizon is shallowest at Well A and deepest at Well C.

Variation of velocity for any of the five intervals from well to well is generally small. Around half of the discrepancies are less than 50m/s and in four of the five intervals the differences are less than 200m/s. However, the velocity of the carbonate interval is over 500m/s greater down the flank of the structure at Well C than on the crest at Wells A and B. The implication of a velocity gradient in this layer is further supported by the interval velocity for the carbonate layer in the updip Well CC which is transitional between the interval velocities observed at the crest of the structure and at Well C. If this velocity gradient is widespread over the survey area, the carbonate interval will have higher velocities in the structurally lower areas. Since this interval also tends to thicken into the lower areas (relative to the rather more constant thickness of sediments above the carbonates), the vertical average velocity to the base of the carbonates is bound to show a corresponding increase. This implied increase of average velocity with two-way time may account for much of the moveout velocity variation observed in the Orange and Red horizons (Section 2.3.2).

The quoted interval velocities are the average velocities over the chosen intervals. For comparison, the RMS interval velocities have been calculated from the calibrated velocity logs for Wells A and B and are also included in Tables 2.9 and 2.10. In all cases the RMS interval velocity is less than one percent greater than the average interval velocity, and only in the carbonate interval does the difference approach this level. Inspection of Figure 2.23 confirms that the difference between the average and RMS velocities of the same interval does indeed increase with the degree of velocity variation within the interval (Section 1.1.10).

Vertical interval velocity functions for the intervals defined by the Brown, Pink, Yellow, Orange and Red seismic reflection horizons have been presented for the three vertical wells in the survey area. Although this is the crudest way of representing the velocity distribution within each interval, it is sufficient for the purposes of checking the interval velocities to be derived in Chapter Seven.

2.5 SUMMARY

Two-way times and moveout velocities have been obtained for five seismic reflection horizons from two offshore seismic surveys. Acquisition and processing parameters have been discussed for each survey in the context of their potential effects on velocity analysis.

An interpretation of the seismic information has been made. Interpreted sections and two-way time maps to two of the horizons have been presented, together with corresponding displays of moveout velocities obtained from velocity analyses of CMP gathers. Some correlations between moveout velocity variation and two-way time structures have been observed which conform with the predictions made in Section 1.4.2.

Well information has been used both to correlate seismic reflection horizons with stratigraphy and to estimate the gross interval velocities between horizons. Although limited in extent, this interval velocity information will serve as the only means of checking interval velocities obtained by the inversion of moveout velocities in Chapter Seven.

3. ANALYSIS OF MOVEOUT VELOCITIES OVER A SEISMIC REFLECTION SURVEY AREA

The objective of this chapter is to describe and apply various statistical methods which can be used to estimate both the contribution and significance of different spatial components within moveout velocity profiles.

A moveout velocity profile can be resolved into three components as follows:

- slow variations of moveout velocity caused by reflector structures and/or velocity gradients which vary gradually relative to the spread length and give rise to near-hyperbolic primary reflection moveout trajectories (e.g. dip, linear velocity gradients);
- fluctuations of moveout velocity induced by rapid variations of reflector structure and/or velocity heterogeneity within layers which cause strongly non-hyperbolic moveout of reflections across the CMP gather (e.g. faults, near-surface time delays); and
- errors in the picking of moveout velocities caused by contamination of the CMP gather by non-primary reflected energy which masks the primary reflection trajectories of interest.

Both the first and second components are genuine components of moveout velocity profiles in the sense that they both result from the fitting of an 'optimum' hyperbola to a primary reflection moveout trajectory. However, only in the first case is the resulting moveout velocity likely to be a reasonable estimate of the normal moveout velocity (Section 1.1.9). Only the slowly varying components of moveout velocity profiles should therefore be used in inversion methods which seek to relate inferred normal moveout velocities to zero-offset raypaths through an assumed limited ground model in order to estimate interval velocities. Although the second component can be used in near-ideal conditions to detail near-surface velocity variation (Section 1.4.2.4), the practical application is very limited and is not discussed further here. The distinction between a 'useful' moveout velocity component (in the first category above) and an 'anomalous' moveout velocity component (the second category) is largely dependent on the spread length (Section 1.5), and is ultimately determined by the use to which it is put.

In the context of this project, the first is the only useful component of the three described above since only it can be used confidently to yield valid interval velocities in the inversion method of Hubral described in Chapter Four and used in subsequent chapters. The other two components constitute a 'scatter' on the moveout velocity profiles which is potentially capable of causing very misleading results. In order to use the inversion method successfully, moveout velocity profiles should ideally be free from this scatter. Preliminary processing of moveout velocity profiles is therefore desirable in order to reduce scatter before inversion.

A moveout velocity profile is a one-dimensional (1D) function of distance along the seismic line. The term 'one-dimensional' is significant. The belief that raw (i.e. unsmoothed) moveout velocities should initially be treated as a one-dimensional phenomenon is fundamental to this work. For any CMP over a heterogeneous subsurface the moveout velocity of an horizon generally varies with the orientation of the CMP gather for the reasons outlined in Section 1.4. As the orientation of the CMP gather changes, different subsurface volumes and apparent dips are sampled by the seismic energy and azimuthal variation of moveout velocity is to be expected. It follows that moveout velocities rarely tie exactly at line intersections.

At the initial stage of moveout velocity studies it is generally desirable to consider each line separately and attempt to reduce the scatter on moveout velocity profiles individually. In so doing, it is likely that discrepancies or 'misties' of moveout velocities at line intersections will be reduced and the data can be better combined to form maps in a two-dimensional sense.

The first section of Chapter Three describes various statistical methods for analysing the spatial character of moveout velocity profiles. As velocity analyses were in all cases made at constant spatial sampling intervals, moveout velocity profiles are treated as equispaced data sets throughout. The approach adopted here uses the principles of time-series analysis or communication theory. Each moveout velocity profile is assumed to be an equispaced function of distance (referred to surface CMP locations), much the same as a sampled seismic trace is an equispaced function of time.

The second section then describes the spatial character of the moveout velocity profiles of Chapter Two and presents the method used to reduce their scatter.

3.1 METHODS OF ANALYSIS

This section is restricted to a brief review of the statistical methods used in the latter part of the chapter. Much of the material covered has been discussed at length in many previous texts. Perhaps the most useful single work for reference is that of Bendat and Piersol (1971), where Chapter Nine is of particular relevance.

Some of the methods discussed below are used to ascertain the contribution of different spatial frequencies to the moveout velocity profiles. The autocorrelation, function, semivariance function and energy spectrum are introduced for this purpose. These functions do not change the moveout velocities; they simply 'transform' the data and display it in a different context.

In contrast, the technique of smoothing results in a modification of the moveout velocities as its name suggests. Data can be smoothed by a variety of smoothing operators, each of which can be used to selectively enhance or attenuate different spatial frequency ranges. The contribution and significance of various spatial components within the moveout velocity profiles can then be assessed by reference to the performance of different smoothing operators in reducing discrepancies or mis-ties at line intersections. If a smoothing operator succeeds in drastically reducing moveout velocity mis-ties over a survey area, it is likely (although not certain) that the spatial frequencies attenuated by the smoothing procedure are not representative of real subsurface velocity variations.

The statistical methods to be used in this chapter are now introduced in turn.

3.1.1 Sampling

Let $a(x)$ indicate that the variable a is a continuous function of x (Figure 3.1). This function is then 'sampled' at N points spaced Δx apart, yielding N samples a_i where i takes the values 1 through N. The sample a_i is the value of the function $a(x)$ at $x = x_i$.

The Nyquist frequency f_n (Bendat and Piersol, 1971, p.228) is determined by the sampling interval Δx:

$$f_n = 1/2\,\Delta x \tag{3.1}$$

The function a(x) is sampled adequately if it contains only frequency components in the range:

$$0 \leqslant f \leqslant f_n$$

If the sampling interval is too long, however, sampling causes frequencies higher than the Nyquist to be confused with lower frequencies. The sampled data set a_i is then said to be 'aliased'.

The aliasing problem was the first consideration involved in defining the spatial sampling interval between the CMP gathers used for the velocity analyses described in Chapter Two. It is discussed further in Section 3.2.1.

From hereon it is assumed that the raw data set a_i and all other data sets obtained from it are sampled at the constant sampling interval Δx.

3.1.2 Arithmetic Measures

The sample mean $\bar{a}$ and sample variance S_a^2 of the data set a_i can be defined as below:

$$\bar{a} = \frac{\sum_{i=1}^{N} a_i}{N} \tag{3.2}$$

$$s_a^2 = \frac{\sum_{i=1}^{N} (a_i - \bar{a})^2}{N} \tag{3.3}$$

The sample standard deviation S_a is simply the positive square root of the sample variance.

Bendat and Piersol (1971, p.101) note that the sample variance defined here is a biased estimator of the population variance, and replace the N in Equation (3.3) with N-1. However, such biasing is only significant when very small values of N are used, and the conclusions of this chapter are not likely to be invalidated by the use of Equation (3.3).

In order that moveout velocity profiles be analysed in terms of their spatial frequency components, some functions described in subsequent sections require that the data set be 'stationary'. In its strictest sense, a data set is stationary only if its statistics are constant throughout its length. Indeed, the length of the data set is important, since a short window of an otherwise stationary data set may not be stationary if the window includes a local 'trend'. On inspection, the moveout velocity profiles presented in Chapter Two do not appear to include any significant trends which would distort their analysis in terms of spatial frequency components. It has proved convenient, however, to reduce each of the moveout velocity profiles to a 'zero-mean' data set as their analysis is then limited to the fluctuating components alone. Such a data set b_i can be obtained from a_i by the simple relation:

$$b_i = a_i - \bar{a} \tag{3.4}$$

Reference to Equations (3.2) and (3.3) indicates that for the data set b_i, the following relations apply:

$$\bar{b} = 0 \tag{3.5}$$

and:

$$s_b^2 = \frac{1}{N} \sum_{i=1}^{N} b_i^2 \tag{3.6}$$

The sample variance of a zero-mean data set is thus equal to its mean square.

3.1.3 Transformation to the Lag Domain

Transformation to the lag domain consists of comparing a stationary data set with a copy of itself which is shifted at various offsets along the x-axis (Figure 3.2). The 'lag' is the relative shift between the two identical data sets, and has the dimensions of x. For sampled data, the lag h is always an integer multiple m of the sampling interval Δx:

$$h = m\,\Delta x \tag{3.7}$$

where m takes the values 0 through N-1.

The comparison referred to above is made by a relation which seeks to express the similarity or dissimilarity of the data set at different lags and hence characterises the data set. Such a relation R can be conveniently obtained by calculating the mean value of some function F for all N-m 'sample pairs' b_i and b_{i+m} at lag m Δx:

$$R(h) = R(m\Delta x) = \frac{1}{N-m} \sum_{i=1}^{N-m} F(b_i, b_{i+m}) \tag{3.8}$$

The autocorrelation and semivariance functions are two examples of the relation R, and are now described in turn.

3.1.3.1 The Autocorrelation Function

The autocorrelation function finds application in many branches of geophysics where periodic components within a data set need to be identified.

The autocorrelation function $\phi_b(h)$ of the data set b_i can be defined as:

$$\phi_b(h) = \phi_b(m\Delta x) = \frac{1}{N-m} \sum_{i=1}^{N-m} b_i\ b_{i+m} \tag{3.9}$$

The autocorrelation at lag m Δx is thus equal to the mean product of all sample pairs b_i and b_{i+m} where i takes the values 1 through N-m.

This function may take either positive or negative values. Large positive values occur at lags where the data set is highly correlated, while large negative values indicate lags where the data set is highly correlated but with opposite polarity. Sustained near-zero values indicate lags where the data set is uncorrelated.

At zero lag, Equation (3.9) reduces to:

$$\phi_b(0) = \frac{1}{N} \sum_{i=1}^{N} b_i^2 \tag{3.10}$$

The autocorrelation at zero lag is thus equal to the mean square of the samples. Reference to Equation (3.6) shows that the zero lag autocorrelation of a zero-mean data set is also equal to the sample variance, i.e.

$$\phi_b(0) = S_b^2 \tag{3.11}$$

A plot of autocorrelation against lag is commonly termed an 'autocorrelogram'.

3.1.3.2 The Semivariance Function

The semivariance function is used extensively in mining geology and ore reserve estimation, where it is a fundamental component of the philosophy known as 'geostatistics'. A comprehensive account of semivariance in this context can be found in Clark (1979).

The semivariance function $\gamma_b(h)$ of the data set b_i can be defined as:

$$\gamma_b(h) = \gamma_b(m\,\Delta x) = \frac{1}{2}\,\frac{1}{N-m} \sum_{i=1}^{N-m} (b_i - b_{i+m})^2 \tag{3.12}$$

The semivariance at lag m Δx is thus equal to one half of the mean squared difference between all sample pairs b_i and b_{i+m} where i takes the values 1 through N-m.

This measure ranges from zero at lags where the data set is perfectly correlated with itself to peak values where the data set is highly correlated but with opposite polarity. The squaring in the formula ensures that semivariance can take only positive values, while the factor 1/2 is included in order to simplify the relation between the semivariance and autocorrelation functions (as will become apparent in Section 3.1.3.3).

At zero lag, Equation (3.12) reduces to:

$$\gamma_b(0) = 0 \tag{3.13}$$

A plot of semivariance against lag is known as a 'semivariogram'.

3.1.3.3 The Relation between the Autocorrelation and Semivariance Functions

Since Equations (3.9) and (3.12) take a similar form, it is of interest to investigate the algebraic relation between the autocorrelation and semivariance functions described above.

The semivariance function can be expressed in terms of the autocorrelation function as follows:

$$\gamma_b(m\Delta x) = \frac{1}{2}\,\frac{1}{N-m}\sum_{i=1}^{N-m}(b_i - b_{i+m})^2 \tag{3.12}$$

$$= \frac{1}{2}\,\frac{1}{N-m}\left[\sum_{i=1}^{N-m} b_i^2 + \sum_{i=1}^{N-m} b_{i+m}^2 - 2\sum_{i=1}^{N-m} b_i\, b_{i+m}\right]$$

$$= \frac{1}{2}\,\frac{1}{N-m}\left[\sum_{i=1}^{N-m} b_i^2 + \sum_{i=1}^{N-m} b_{i+m}^2\right] - \frac{1}{N-m}\sum_{i=1}^{N-m} b_i\, b_{i+m}$$

$$= \frac{1}{2} \; \frac{1}{N-m} \left[\sum_{i=1}^{N-m} b_i^2 + \sum_{i=1}^{N-m} b_{i+m}^2 \right] - \phi_b(m\Delta x) \qquad (3.14)$$

For a stationary data set, the following approximations can then be made:

$$\frac{1}{N-m} \sum_{i=1}^{N-m} b_i^2 \approx \phi_b(0) \qquad (3.15)$$

$$\frac{1}{N-m} \sum_{i=1}^{N-m} b_{i+m}^2 \approx \phi_b(0) \qquad (3.16)$$

since both are estimates of the mean square value $\phi_b(0)$ from N-m samples. These approximations become increasingly valid as m approaches zero.

Equation (3.14) then simplifies to:

$$\gamma_b(m\Delta x) \approx \phi_b(0) - \phi_b(m\Delta x) \qquad (3.17)$$

The semivariance function can thus be estimated from the autocorrelation function. Greater accuracy is obtained at small lags.

The semivariance function and autocorrelation function exhibit essentially the same information with opposite polarities.

3.1.4 Transformation to the Frequency Domain

Following the principles of time-series analysis, the continuous function a(x) can be considered as the sum of an infinite number of sinusoidal frequency components of differing phase and amplitude. It is possible to express this function as a continuous function of frequency A(f). The function a(x) is then said to have been transformed to the frequency domain.

This transform can be made by the Fourier Transform (abbreviated FT):

$$a(x) \xrightarrow{\quad FT \quad} A(f)$$

while the inverse procedure is made by the Inverse Fourier Transform (IFT):

$$A(f) \xrightarrow{\quad IFT \quad} a(x)$$

The function A(f) is termed the frequency spectrum and is generally complex-valued. Given a continuous function a(x), it is theoretically possible to recover the frequency spectrum A(f) precisely.

The sampled data set a_i can also be transformed to the frequency domain. However, sampled data differs from continuous data in two important respects:

- the sampling procedure limits the high frequency resolution of the transform as only discrete frequencies up to the Nyquist frequency can be resolved; and
- the length of the sampled data set is finite and the behaviour of the continuous function outside the sampling window is unknown.

Spectral estimation from the sampled data set a_i can therefore only provide an approximation to the true continuous frequency spectrum A(f).

The Fourier Transform is discussed at length in Bendat and Piersol (1971, p.299) and Bath (1974).

3.1.4.1 <u>The Fast Fourier Transform</u>

The Fast Fourier Transform (FFT) is a computationally efficient algorithm used to apply a Fourier Transform to a sampled data set. The algorithm is described in Bendat and Piersol (1971, p.300), while the computer program used for performing the FFT in this project has been adapted from subroutine 'NLOGN' in Robinson (1967).

One limitation of the FFT is that the number of samples in the data set to be processed must be an integer power of two. If the length N of the data set b_i is not a power of two, the data length must be extended to M, which is the next highest integer power of two. This extension is made by 'padding' the data b_{n+1} through b_M with zeros.

From the data set b_i of length M, the FFT calculates the complex-valued frequency spectrum β_j where j takes the values 1 through M/2 + 1. The estimate β_j is made at the discrete frequency f_j, such that there are M/2 + 1 discrete frequencies in the complex frequency spectrum. The spacing between successive frequencies in this spectrum is determined by both the sampling interval and the number of samples in the zero-padded data set (which together define the length of the data set). Specifically, the frequency interval Δf is defined by:

$$\Delta f = 1/M\Delta x \qquad (3.18)$$

with Δx and M as defined previously. The discrete frequency f_j can then be defined as:

$$f_j = (j - 1)\ \Delta f \qquad (3.19)$$

where j takes the values 1 through M/2 + 1. The first frequency f_1 is the zero frequency or 'DC' component, while the last frequency $f_{M/2+1}$ is the Nyquist frequency.

Each complex spectral estimate between zero frequency and the Nyquist consists of a real component and an imaginary component:

$$\beta_j = re(\beta_j) + im(\beta_j) \tag{3.20}$$

The spectrum at zero frequency and at the Nyquist frequency is real-valued, so the total number of independent spectral values is M. It is noted here that if the data set b_i has been zero-padded, the 'extra' spectral values are achieved by interpolation and are not individually independent. Information is conserved, but not added, by the FFT.

3.1.4.2 The Amplitude Spectrum

The real-valued amplitude spectrum B_j is derived from the complex frequency spectrum β_j as follows:

$$B_j = \sqrt{re(\beta_j)^2 + im(\beta_j)^2} \tag{3.21}$$

or alternatively:

$$B_j = \sqrt{\beta_j \, conj\,(\beta_j)} \tag{3.22}$$

where conj (β_j) represents the complex conjugate of β_j.

The term B_j represents the amplitude of a continuous sinusoid at the frequency f_j.

3.1.4.3 The Energy Spectrum

The energy spectrum E_j is also real-valued and is obtained as the square of the amplitude spectrum, i.e.

$$E_j = B_j^2 \tag{3.23}$$

The energy spectrum can be obtained from the complex frequency spectrum with reference to Equations (3.21) and (3.22) as follows:

$$E_j = re(\beta_j)^2 + im(\beta_j)^2 \tag{3.24}$$

or:

$$E_j = \beta_j \, conj\,(\beta_j) \tag{3.25}$$

Alternatively, the energy spectrum can be derived by a Fourier Transform of the autocorrelation function (Bendat and Piersol, 1971, p.312):

$$\emptyset_b(h) \xrightarrow{\quad FT \quad} E_j$$

The term E_j represents the energy contained in the frequency f_j over the data window.

3.1.4.4 Spectral Smoothing

In the spectral analysis of a stationary data set, each spectral estimate is liable to error. It is thus desirable to smooth the raw spectral estimates in some way to reduce their scatter.

Methods of spectral smoothing abound in the literature; Bendat and Piersol (1971, p.318) and Bath (1974) provide good examples. Most of these smoothing methods are based on a convolution in the frequency domain which is equivalent to tapering in the autocorrelation lag window.

The method adopted for smoothing energy spectra in this project entails summing energies over successive groups of L adjacent frequencies. The 'adjacent sum smoothed' energy spectrum E'_k can then be written as:

$$E'_k = \sum_{j=1}^{L} E_{L(k-1)+j} \tag{3.26}$$

where E_j is the raw or unsmoothed energy spectrum, L is the number of adjacent raw spectral estimates to be summed, and k takes the values 1 through (M+2)/2L. The number of frequencies in the raw spectrum is thus reduced by a factor of L in the smoothed spectrum (strictly only if M/2 + 1 is exactly divisible by L). The frequency interval $\Delta f'$ of the smoothed spectrum increases to:

$$\Delta f' = L \ \Delta f \tag{3.27}$$

The length L of the adjacent sum is determined by balancing the resolution and stability requirements of the smoothed spectrum. As L increases, the stability of each smoothed spectral estimate increases but the spectral resolution decreases.

3.1.4.5 A Computational Procedure to obtain the Smoothed Energy Spectrum

In summary, the following procedure is suitable to compute the smoothed energy spectrum:

(a) Sample the Continuous Function a(x)

To obtain the sampled data set a_i where i takes the values 1 through N. The sampling interval is Δx.

(b) Remove Sample Mean

To obtain the zero-mean data set $b_i = a_i - \bar{a}$.

(c) Pad with Zeros

If N is not an integer power of two then set b_{N+1} through b_M to zero where M is the next highest integer power of two greater than N.

(d) Fast Fourier Transform

To obtain the complex frequency spectrum β_j calculated at discrete frequencies f_j where j takes the values 1 through $M/2 + 1$.

(e) Multiply the Complex Frequency Spectrum by its Conjugate

To obtain the energy spectrum E_j.

(f) Adjacent Sum Smoothing

To obtain the smoothed energy spectrum E_k' where k takes the values 1 through $(M+2)/2L$ and L is the length of the adjacent sum.

3.1.5 Spatial Smoothing Techniques

Smoothing is used to reduce scatter on moveout velocity profiles. Analysis of the smoothed data can then lead to conclusions regarding the relative contribution and significance of the various spatial frequency components within raw moveout velocity profiles.

Only smoothing operators of a convolutional type are considered here. Convolutional operators are generally termed 'filters'. Each filter is simply a set of weights which is convolved with the sampled moveout velocity data set. The advantage of this type of smoothing is that the frequency response of each operator can be easily calculated. The frequency response of such a filter is simply the amplitude spectrum derived from the complex frequency spectrum obtained from an FFT of the filter weights.

An alternative approach to smoothing is the 'optimum' fitting of a polynomial by least squares (Davis, 1973, p.192). The frequency response of polynomial smoothing is, however, very poorly defined. Furthermore, it is inconsistent for different data sets as it depends critically on the data length. For these reasons, polynomial smoothing is not considered further in this project.

3.1.5.1 Types of Filters

Two types of filters have been considered, namely the low-pass filter and the boxcar moving average filter.

(a) The Low-Pass Filter

The low-pass filter ideally passes all frequencies up to a specified limit or 'cut-off', and stops all frequencies above. However, when using sampled data, such perfect filtering is impossible due both to the sampled nature of the data and the finite length of the filter. Frequency responses of digital filters differ from the ideal in two important respects:

- the ideal cut-off at a single frequency is modified to a cut-off slope, where the cut-off is transitional over a range of frequencies; and

- the ideal flat responses in the pass band and stop band are contaminated by fluctuation known as 'ripple'.

Low-pass filters are thus specified not by a single cut-off frequency, but by the frequencies at the start and end of the cut-off slope (or by a cut-off frequency and the filter length). For a fixed filter length, increasing the cut-off slope (i.e. sharpening the cut-off) can only be done at the expense of introducing more ripple into both pass and stop bands. The performance of a filter can be assessed by reference to the 'deviation' in the pass and stop bands, which is equal to the maximum difference between the actual filter response and the ideal response (unity in the pass band and zero in the stop band). Filter performance is enhanced by increasing the filter length.

Low-pass filters have been designed using a computer program in Rabiner and Gold (1975, p.187) which calculates low-pass, high-pass, band-pass and band-stop filters using the 'Remez Exchange Algorithm'. One useful feature of this algorithm is the constraint of constant peak ripple amplitude within the pass band and stope band. For the low-pass filter, the following design parameters must be specified:

- the last frequency in the pass band (defining the start of the cut-off slope);
- the first frequency in the stop band (defining the end of the cut-off slope);
- the spacing between successive filter weights (equal to the sampling interval Δx of the data to be filtered); and
- the filter length (defined by the number of weights P in the filter to be derived).

The derived low-pass filter c_j where j takes the values 1 through P is the filter which best fits the desired frequency response. The value P is critical as the filter performance is enhanced significantly by increasing the filter length. The filter is a symmetric, zero-phase operator and is subject to the constraint:

$$\sum_{j=1}^{P} c_j = 1 \tag{3.28}$$

to ensure that the DC is passed unaltered.

Figure 3.3 shows the specified and actual spatial frequency or 'wavenumber' responses for a typical low-pass filter designed by the program. The actual spatial frequency response is also plotted on a logarithmic scale to detail the behaviour of ripple in the stop band.

(b) The Boxcar Moving Average Filter

The second type of filter, the 'boxcar moving average', is simply a set of equally weighted coefficients. Again constrained by Equation (3.28), the filter coefficients c_j are defined by:

$$c_j = 1/P \tag{3.29}$$

where j takes the values 1 through P.

The frequency response of the boxcar moving average is a sinc function (Figure 3.4) which represents a crude low-pass filter. The notches occur at spatial frequencies which are integer multiples of the reciprocal of the boxcar length. The boxcar moving average is again a symmetric, zero-phase operator. Its primary disadvantages are the rather obscure frequency response and the slow cut-off slope down to the first notch. However, this type of filter can be easily tuned to attenuate undesirable frequencies around the first notch, and herein lies its main use in this project.

3.1.5.2 Smoothing End-Effects

Convolution of a data set a_i of length N with a filter c_j of length P results in the filtered data set d_k:

$$d_k = \sum_{j=1}^{P} a_{1+k-j} c_j \tag{3.30}$$

where k takes the values 1 through N+P-1. The smoothing procedure extends the data length by the lead-in and lead-out of the filter at both ends of the original data set. This extension has two principal effects:

- the smoothed data set is delayed relative to the first sample of the unfiltered data set; and
- energy leaks both into and out of the sampling window of the original data set, thus contaminating the filter lead-in and lead-out sections of the smoothed data set.

These are referred to here as 'smoothing end-effects'.

Since the filters discussed here are symmetrical, zero-phase operators of known length, the first effect can be corrected quite simply. The delay introduced by such a filter is simply half the filter length and can therefore be removed by shifting back the smoothed data set by half of the filter length. It is desirable for this reason to use filters with an odd number of weights, say P = 2Q + 1, such that the index k above takes the values 1 through N + 2Q. The delay can then be eliminated by introducing a new data set e_i which omits the first Q and last Q samples of the smoothed data set d_k, i.e.

$$e_i = d_{i+Q} \tag{3.31}$$

where i takes the values 1 through N. In this way the spatial location of the shifted smoothed data set e_i corresponds exactly to that of the original sampled data set a_i.

The effect of energy leakage into and out of the sampling window is rather more serious. Where the filter leads in at the start of the data set and leads out at the end of the data set, it is not wholly contained within the sampling window. The filter elements outside the sampling window are then effectively multiplied by zeros in the convolution. Since the first 2Q and last 2Q samples of the extended data set d_k were affected, the first Q and last Q samples of the shifted data set e_i are contaminated by energy leakage.

Serious distortion at the ends of the smoothed data set may result if discontinuities were introduced by the original windowing of the data set. It is therefore convenient to remove the sample mean of the data set a_i using Equation (3.4), filter the residuals and finally add the sample mean to the residuals. This is equivalent to rewriting Equation (3.30) in the form:

$$d_k = \bar{a} + \sum_{j=1}^{P} b_{1+k-j} c_j \tag{3.32}$$

where b_i represents the residuals about the sample mean $\bar{a}$. The filter delay is then removed using Equation (3.31) as before.

It is stressed that although the procedure outlined above does protect the ends of the data set from gross distortion, the first Q and last Q samples of the smoothed data set are still affected by energy leakage. The ends of smoothed data sets characteristically 'tend to the mean' as a result.

The two aims of optimum filter performance and minimisation of end-effects are thus in direct conflict, since the former requires long filters and the latter demands short filters. For data sets which are very long compared with the dominant wavelengths of the data (seismic traces, for example), this problem becomes almost trivial as the filter length is generally of the same order as the wavelengths of the components to be filtered. However, in smoothing moveout velocity profiles the problem is acute, because the data length is usually quite short compared to the lengths of low-pass filters required for an acceptable frequency response. A suitable balance must be found between filter performance and end-effects in order that the smoothing procedure be effective without invalidating important parts of the moveout velocity profiles.

3.1.5.3 A Smoothing Criterion Applied to Moveout Velocity Profiles

When has a smoothing operator applied to moveout velocity profiles been successful? Which is the 'optimum' filter for the data set? These questions can only be answered by reference to some criterion by which the smoothing can be judged.

One possible criterion is the minimisation of moveout velocity mis-ties over all line intersections. This would indicate that residual errors are comparable with the effects of line azimuth (and subsurface structure) on moveout velocities. A convenient method is to find the smoothing operator for which the root mean square (RMS) moveout velocity mis-tie on each horizon is minimised. The RMS moveout velocity mis-tie can be defined as:

$$\text{RMS mis-tie} = \sqrt{\frac{1}{L}\sum_{\ell=1}^{L} M_\ell^2} \tag{3.33}$$

where there are L line intersections and M_ℓ represents the moveout velocity mis-tie at the ℓth intersection.

Use of this criterion recognises that it is unrealistic to expect a smoothing operator to reduce moveout velocity mis-ties to zero, in accordance with the discussion in the introduction ot this chapter. Acceptance of the 'optimally' smoothed moveout velocity profiles carries the implicit assumption that the moveout velocity components attenuated by the 'optimum' smoothing operator are considered to be anomalous and cannot be directly related to real velocity variations in the subsurface.

Mis-ties calculated at intersections where one or both lines are subject to smoothing end-effects must be treated with caution, and may have to be omitted from further analysis. Conclusions drawn from a suite of mis-ties dominated by end-effects obviously cannot be made with confidence.

3.2 APPLICATION TO REAL MOVEOUT VELOCITIES

The techniques of spatial data analysis described in Section 3.1 are now applied to the moveout velocity profiles described in Chapter Two. The raw moveout velocity profiles presented in Figure 2.18 and Enclosure 2.3 are included here on a reduced scale in Figure 3.5 for reference.

After outlining the reasons for the choice of velocity analysis sampling interval on the densely sampled lines, the dominant spatial components of the moveout velocity profiles are described by way of transforms to the lag domain and the frequency domain. Autocorrelograms, semivariograms and energy spectra of the raw moveout velocity profiles are used for this purpose.

The final part of this section is devoted to smoothing moveout velocity profiles. Problems of filter design in view of the limited length of the moveout velocity profiles are discussed before embarking on the analysis of mis-ties obtained using different smoothing operators. Both the 'optimally' smoothed moveout velocity profiles and the nature of the 'anomalous' moveout velocity components are described.

3.2.1 Choice of Velocity Analysis Spatial Sampling Interval

The velocity analysis spatial sampling interval is 250 m on the densely sampled lines of Survey A and Survey B. Components with wavenumbers higher than 2 km^{-1} are therefore aliased by the sampling procedure.

The choice of this spatial sampling interval was based on the analysis of a test line with a reduced velocity analysis spatial sampling interval. Velocity analyses were made along line A-132 every 50 m and the contribution of wavenumbers up to 10 km^{-1} were then assessed. Energy spectra computed from the moveout velocity profiles along each of the five interpreted horizons showed a general reduction of energy with increasing wavenumber. The decrease was rapid through the 0-1 km^{-1} band, then began to tend asymptotically to an ambient noise level which was attained around 2 km^{-1}. The energy in wavenumbers greater than 2 km^{-1} was around 10 to 15 dB down on the peak energy for each horizon on the test line.

The 250 m velocity analysis spatial sampling interval is therefore not thought to have undersampled the moveout velocity variation in the area. However, the moveout velocities on the coarse grid of Survey A are seriously aliased as the Nyquist spatial frequency in this case is only 0.5 km^{-1}. Conclusions relating to the detailed spatial character of moveout velocity variations should therefore be drawn only from the densely sampled moveout velocity profiles.

3.2.2 Transforms of Moveout Velocity Profiles

Transforms of the moveout velocity profiles to both lag and frequency domains are now presented. The aim of this section is not only to describe the most significant spatial components in the data, but also to assess the relative merits of the autocorrelation function, semivariance function and energy spectrum in this context.

3.2.2.1 Autocorrelograms

Autocorrelograms have been calculated from the moveout velocity profiles for the eight densely sampled lines of Survey A using Equation (3.9). In addition, a 'total' autocorrelation function has been obtained over all eight lines, where the total autocorrelation at lag $m\Delta x$ is defined as the autocorrelation at lag $m\Delta x$ averaged over all eight lines.

Figure 3.6 (Enclosure 3.1) presents autocorrelograms of the moveout velocity profiles for the Brown, Pink, Yellow, Orange and Red horizons. Autocorrelograms for the Brown, Pink and Yellow moveout velocity profiles are presented separately in Figure 3.7 (Enclosure 3.2) on an expanded scale.

Autocorrelation has in each case been calculated up to maximum lag, where the first and last samples constitute the only sample pair. As the number of sample pairs decreases with lag, autocorrelation values at long lags should be treated with caution. Estimates in the total autocorrelation function are generally more stable due to the extra averaging inherent in its derivation.

A study of the autocorrelograms yields the following observations:

- moveout velocity autocorrelation magnitudes generally increase from a minimum on the Brown horizon to a maximum on the Red horizon, indicating an increase of moveout velocity fluctuation with two-way time;
- moveout velocity fluctuation is considerably higher on the Orange and Red horizons than on the three shallower horizons;
- long wavelength fluctuation on lines A-111 and A-132 is probably due to moveout velocity - time trends caused by genuine average velocity - time trends over the structure in the centre of the seismic grid (Section 2.4.2).
- shorter wavelength fluctuation is clearly resolved on line A-103, where high correlation is evident around lags of 3 km and 7km on all five horizons;
- the chaotic and low amplitude autocorrelations on line A-123 are due to the general lack of strong periodic components in the moveout velocity profiles for this line; and
- the mean square moveout velocity variation (i.e. after removal of the sample mean) generally increases from a minimum on the Brown horizon to a maximum on the Red Horizon (note zero-lag autocorrelations).

The most pronounced feature on the total autocorrelogram is the negative autocorrelation lobe centred on a lag of 6 km. This lag corresponds approximately to the width of the structure in the centre of the seismic grid, and is generated principally by the contribution of lines A-111, A-115, A-130 and A-132 which cross the centre of the grid. Negative autocorrelation arises from correlation of lower moveout velocities over the crest of the structure and higher moveout velocities on the flanks of the structure when the lag assumes values of around 6 km.

Moveout velocity autocorrelation functions vary widely between individual seismic lines. The most significant features in the autocorrelograms have been accounted for above.

3.2.2.2 Semivariograms

Semivariograms have been calculated from the moveout velocity profiles for the eight densely sampled lines of Survey A using Equation (3.12). A 'total' semivariogram has been obtained by averaging semivariograms over all eight lines in a similar fashion to the total autocorrelograms described in Section 3.2.2.1.

Semivariograms of the moveout velocity profiles for the Brown, Pink, Yellow, Orange and Red horizons are presented in Figure 3.8 (Enclosure 3.3), while Figure 3.9 (Enclosure 3.4) repeats the semivariograms for the Brown, Pink and Yellow horizons on an expanded scale. Figures 3.6 and 3.8 (Enclosures 3.1 and 3.3) are plotted at the same scale, as are Figures 3.7 and 3.9 (Enclosures 3.2 and 3.4), in order to facilitate the comparison of autocorrelograms and semivariograms calculated from the same data.

Semivariance values at long lags should again be viewed tentatively due to the limited number of sample pairs used in their calculation. Estimates in the total semivariance function are again likely to be more stable.

Although the polarity is inverted, the semivariograms show essentially the same information as the autocorrelograms, as predicted in Section 3.1.3.3. In this case, the semivariograms are rather easier to interpret as on each line the individual semivariograms are better separated than the corresponding autocorrelograms.

Observation of the semivariograms necessarily reveals similar features to those indicated by the autocorrelograms:

- moveout velocity semivariance generally increases from a minimum on the Brown horizon to a maximum on the Red horizon, again inferring an increase of moveout velocity fluctuation with two-way time;
- significantly increased moveout velocity fluctuation on the Orange and Red horizons is again indicated by the semivariograms;
- moveout velocity - time trends over the structure in the centre of the seismic grid are indicated on the semivariograms for lines A-111 and A-132 and on the total semivariogram by a general increase of semivariance up to around 6 km lag followed by a decrease out to maximum lag;
- short wavelength moveout velocity fluctuation on line A-103 is indicated by low semivariance at lags of 3 km and 7 km; and
- low and chaotic semivariance on line A-123 is again caused by the near-random nature of the moveout velocity profiles on this line.

These conclusions mirror those drawn from the corresponding autocorrelograms in Section 3.2.2.1.

3.2.2.3 Energy Spectra

Smoothed energy spectra were obtained from the moveout velocity profiles following the procedure outlined in Section 3.1.4.5. In order to maintain consistency over all eight lines, each moveout velocity profile was zero-padded up to the same length before the FFT. As the longest moveout velocity profile contained 81 samples, each data set was zero-padded up to 128 samples, the next highest power of two. The derived energy spectra then included 65 frequencies out to the Nyquist spatial frequency of 2 km^{-1}. Finally the energy spectra were smoothed by an adjacent sum over groups of four consecutive frequencies to leave 16 spatial frequencies in each spectrum (the last unsmoothed spectral estimate at the Nyquist has been omitted from the plots). The choice of smoothing was determined by balancing the stability and resolution requirements of the derived spectra (Section 3.1.4.4). It is noted here that the effect of zero-padding has been to reduce the independence of adjacent spectral estimates (Section 3.1.4.1), and therefore to reduce the effectiveness of spectral smoothing.

Figure 3.10 (Enclosure 3.5) presents smoothed energy spectra calculated from the moveout velocity profiles for the eight densely sampled lines of Survey A. The spectra are displayed on a logarithmic scale. The figure also presents 'total' energy spectra which have been obtained for each horizon over all eight lines using a Fourier Transform of the total autocorrelation functions described in Section 3.2.2.1. No adjacent sum smoothing has been performed on these total energy spectra as the raw spectral estimates are stable enough for their use here (due to the averaging inherent in the derivation of the total autocorrelation functions). The total energy spectra are displayed on both logarithmic and linear scales.

Energy spectra vary considerably from line to line, as indeed do the autocorrelograms and semivariograms. On each line the energy generally increases from a minimum on the Brown horizon to a maximum on the Red horizon. As for the autocorrelograms and semivariograms, significantly higher moveout velocity fluctuation is evident on the Orange and Red horizons. In each individual spectrum the energy tends to decrease from a maximum at low frequencies to a minimum which is 10-20 dB down on the maximum by the Nyquist spatial frequency.

These observations are also evident in the total energy spectra, where the form of the spectra on each horizon are remarkably similar. Two principal peaks are observed on the total energy spectra. The first, around 0.08 km^{-1} (wavelength 12 km), is again thought to be related to the moveout velocity - time trends over the structure in the centre of the seismic grid. The second peak occurs at 0.3 km^{-1}; the wavelength of this component (3333 m) corresponds very closely to the Survey A spread length of 3250 m.

Although a rather weak component of the total energy spectra, the second peak at 0.3 km^{-1} is an important observation. Its implications are discussed further in the following section.

3.2.2.4 Discussion

This section discusses the relative merits of transforms to the lag and frequency domains, and summarises the results of each which are apparent from this study of moveout velocity profiles.

No advantage has accrued through the use of both autocorrelation and semivariance functions, other than by proving this very point. Similar observations are possible from both transforms, and the choice of either is best left to the individual. The geophysicist will normally choose to use the autocorrelation function out of familiarity, whereas the geostatistician will prefer the semi-variance function due to its further potential in smoothing by kriging (Clark, 1979). However, it is stressed that the use of semivariograms in kriging is critically dependent on a model-fitting procedure whereby the parameters of a model semivariogram are estimated from the measured semivariance. Since the semivariograms presented here bear no resemblance to the form of model semivariograms required for kriging purposes, the adventure into geostatistics originally envisaged for this project was halted prematurely. Although many geostatisticians would argue that this problem can be largely ameliorated by the removal of longer period trends from the data (using polynomials or low-pass filtering) before calculating semivariograms, such an approach is bound to precondition the data and is ultimately liable to distort the important longer wavelength components.

The smoothing problem facing the geophysicist is inherently very different to that confronting a geostatistician. Whereas the assays made in mining geology are often of a near-random nature, most measurements in geophysics are of a deterministic nature and can be smoothed in a manner which is designed to eliminate specific anomalous components. The geophysicist should not normally need to resort to kriging, even when studying moveout velocities!

Energy spectra offer the best way of studying the spatial components within moveout velocity profiles, not least because the concept of spatial frequency, or wavenumber, is both easy to comprehend and physically meaningful. The 'total' energy spectra have been the most successful in defining the two major spatial components in the moveout velocity profiles. Indeed, the 0.3 km^{-1} component is barely discernible on the autocorrelograms and semivariograms without hindsight (except for line A-103 where the longer period structural trend is absent).

The 0.08 km^{-1} and 0.3 km^{-1} spatial components appear to be the most significant in the moveout velocity profiles considered here. However, the statistical analysis presented in this section offers no insight as to the sources of these components. The longer period component, as stated previously, is probably related to the low moveout velocities over the crest of the structure in the centre of the seismic grid and the higher moveout velocities in the surrounding structurally low area. In the sampling windows of the moveout velocity profiles, these low and high moveout velocities generate an apparent fluctuation with a wavelength of approximately 12 km. Although this is a predominantly 'real' moveout velocity component caused by genuine average velocity - time trends over the structure (Section 2.4.2), it is likely that the moveout velocity variation is exaggerated by the combined effects of reflector dip and curvature (Sections 1.4.2.3 and 1.4.2.5).

In contrast, the 0.3 km^{-1} component is likely to be an 'anomalous' fluctuation induced by rapid variation of reflector structure and/or velocity heterogeneity within layers giving rise to strongly non-hyperbolic reflection trajectories across the CMP gather. Without further analysis, however, this statement remains purely conjectural, as there is no observational evidence as yet to deny the validity of any spatial components in the moveout velocity profiles. Some evidence to this effect is presented in the following section.

3.2.3 Smoothing Moveout Velocity Profiles

This section draws on the background of Section 3.1.5 in order to smooth the raw moveout velocity profiles of Chapter Two and hence determine the anomalous spatial components of moveout velocity over the area.

The problems and compromises involved in filter design are discussed before an analysis of moveout velocity mis-ties obtained from different smoothing operators is presented.

3.2.3.1 Filter Design

As stated in Section 3.1.5.2, the two aims of optimum filter performance and minimisation of smoothing end-effects are in direct conflict, as the former requires long filters and the latter demands short filters. In the following discussion it is important to recall that the length of the raw moveout velocity profiles varies from 13 km (the southwest - northeast lines) to 20 km (the northwest - southeast lines) and that the principal periodic components in the moveout velocity profiles have wavelengths of around 3 km and 12 km.

The first choice to be made when smoothing the moveout velocity profiles is the type of filter to be used. Ideally, a low-pass filter should be used since the desired spatial frequency response can be very closely approximated. However, control over the actual spatial frequency response is limited by the length of the filter, which in turn is limited by the extent of the end-effects admissible in the smoothed moveout velocity profiles.

To put this problem in context, a study has been made of the spatial frequency responses of a suite of low-pass filters with a common ideal response. This ideal response is to pass all spatial frequencies up to 0.3 km^{-1} and attenuate all those above. Such a frequency response would be required to eliminate moveout velocity components with wavelengths of less than one spread length (3250 m). This ideal response is impossible for the reasons discussed in Section 3.1.5.1, and the performance of the filter is controlled by the definition of both the cut-off slope and the filter length.

Low-pass filters with desired cut-off slopes of 0.29-0.31 km^{-1}, 0.28-0.32 km^{-1}, 0.25-0.35 km^{-1} and 0.20-0.40 km^{-1} have been calculated for three different filter lengths by the program described in Section 3.1.5.1. Each cut-off slope is centred on 0.30 km^{-1}. The desired response is unity in the pass band, zero in the stop band and transitional on the slope. Spatial frequency responses for each of the four desired cut-off slopes are presented in Figures 3.11, 3.12, and 3.13 for filters of length 3 km, 6 km and 12 km, respectively. Maximum deviations of the actual response from the desired response are listed for each filter in Table 3.1. In each case the filter sampling interval of 250 m corresponds to that of the moveout velocity profiles and the spatial frequency responses are calculated up to the Nyquist spatial frequency of 2 km^{-1}. Observation of these responses yields the following conclusions:

- for each filter, the maximum deviation of the actual response from the desired response is the same in both pass and stop bands;
- when the filter length is held constant, the maximum deviation increases as the cut-off slope is reduced from 0.29-0.31 km^{-1} through to 0.20-0.40 km^{-1};
- when the cut-off slope is held constant, the maximum deviation decreases as the filter length increases from 3 km through to 12 km.

Similar studies with different centre frequencies on the cut-off slope have indicated that the conclusions above are valid for low-pass filters with cut-off slopes centred in the range 0.1 to 1.0 km^{-1}.

The filter with the best performance is obviously the 0.20-0.40 km^{-1} filter of length 12 km which combines the most gradual cut-off slope with the greatest filter length. The 0.25-0.35 km^{-1} filter of the same length and the 0.20-0.40 km^{-1} filter of length 6 km also provide a good approximation to the desired response. However, the remaining filters all have maximum deviations of over ten percent in both pass and stop bands. While this may not be serious in the stop band (as the energy in the moveout velocity profiles tends to decrease with spatial frequency), it is rather disturbing to see such large deviations in the pass band which have the effect of selectively amplifying and attenuating different spatial frequencies within the pass band.

The smoothing end-effects of these zero-phase filters extend for half of the filter length at each end of the smoothed and shifted data set (Section 3.1.5.2). For the eight densely sampled lines of Survey A, the 3 km, 6 km and 12 km low-pass filters have end-effects accounting for 18%, 36% and 72%, respectively, of the total data length of 134 km. An increasing number of line intersections are therefore subjected to uncertainty in mis-tie analysis as the filter length is increased. The use of 12 km filters was rejected on this basis alone. Similar reservations were held about the 6 km filters as over one third of the data length is subject to smoothing end-effects, while none of the 3 km filters were considered to be of use due to considerable differential amplification and attenuation in the pass bands.

In view of the problems associated with the use of low-pass filters, only boxcar moving average filters have been used further in this project. The main advantage of boxcar moving average filters is their basic simplicity, as the length is the only parameter to be specified. Moreover, their main disadvantage of an obscure spatial frequency response becomes rather less significant when compared with the poor spatial frequency response which can be achieved with the short low-pass filters discussed above. The spatial frequency response of a boxcar moving average is a sinc function with notches at integer multiples of the boxcar length, and hence this type of filter can be used effectively to attenuate selected spatial frequencies around the notches, particularly the first notch (Section 3.1.5.1).

3.2.3.2 Analysis of Mis-Ties

Mis-ties calculated at line intersections from smoothed moveout velocity profiles are now used to investigate the anomalous moveout velocity components. The assumption that the effect of smoothing using boxcar moving average filters is dominated by the attenuation of spatial frequency components around the first notch will be inherent in the following discussion.

Moveout velocity profiles along the eight densely sampled lines of Survey A have been smoothed using boxcar moving average filters with lengths of up to 6 km. For each smoothing operator the RMS moveout velocity mis-tie has been calculated separately for each of the five horizons using Equation (3.33). In addition, mis-ties have been calculated for the line mean values, where the fluctuation is removed completely from each moveout velocity profile. This represents the logical limit of smoothing each profile. The results are presented in Table 3.2 and Figure 3.14.

On each horizon, the RMS moveout velocity mis-tie decreases from a maximum for the unsmoothed data (plotted at boxcar length zero) and reaches a minimum when the boxcar length is around the spread length (3250 m). At this point the RMS moveout velocity mis-tie for the Brown, Pink and Yellow horizons appears to reach a limiting value which is similar to that calculated from the line means. In contrast, the Orange and Red RMS moveout velocity mis-ties reach a minimum around the spread length boxcar which is significantly less than that obtained from the line means. Smoothing the moveout velocity profiles with a moving average over a spread length appears to achieve the best reduction in the RMS moveout velocity mis-tie with the minimum of smoothing.

The above results were obtained from the mis-ties at all 16 line intersections. However, mis-ties calculated at line intersections where one or both lines have smoothing end-effects should be treated with caution (Section 3.1.5.3). Mis-ties have been recalculated for these eight lines and all intersections with end-effects have been omitted from subsequent analysis. The results are presented in Table 3.3 and Figure 3.15. The similarity of Figures 3.14 and 3.15 indicates that the conclusions drawn from the study of all 16 line intersections are not invalidated by smoothing end-effects, and that the one spread length boxcar moving average filter still offers a reasonable means of smoothing these moveout velocity profiles.

The harsh attenuation of the one spread length boxcar moving average filter around 0.3 km^{-1} appears to have been effective in reducing the RMS moveout velocity mis-tie to near the minimum for each of the five horizons. This observation can be used to infer that the moveout velocity components recognised in the energy spectra presented in Section 3.2.3.3 around this spatial frequency are 'anomalous' in the sense that they are induced by the spread geometry and are not directly representative of real velocity variations in the subsurface.

Moveout velocity profiles filtered by the one spread length boxcar moving average filter are displayed in Figure 3.16 (Enclosure 3.6). The decrease of moveout velocities over the crest of the structure in the centre of the seismic grid is particularly well illustrated by the smoothed profiles.

It is also of interest to show the effect of spatial smoothing in an alternative 'mathematical space'. Figure 3.17 shows scattergrams of moveout velocity - time pairs obtained from the eight raw moveout velocity profiles and corresponding CMP stacked section times. The graph in the top left corner is a plot of all moveout velocity - time pairs on the same axes, while the data for each of the five horizons is plotted individually in the remaining graphs. The 'quantisation' of moveout velocities at different discrete levels on the graphs is due to the cellular nature of the velocity analysis displays. Each level represents half of one cell width on the VLAN display (a full cell corresponds to 25 m/s). The high degree of scatter for each horizon prevents any realistic moveout velocity - time trends from being established confidently.

Figure 3.18 shows the corresponding scattergrams after the moveout velocity profiles have been smoothed by the one spread length boxcar moving average filter. While the smoothed moveout velocities on the Brown, Pink and Yellow horizons still appear to be largely independent of time, both Orange and Red horizons now show a significant increase of moveout velocity with time. These trends are probably caused by the genuine average velocity - time trends generated as a result of velocity gradients and thickening of the carbonate (Yellow - Orange) interval (Section 2.4.2).

The spatial consistency of moveout velocities over the study area is enhanced considerably by smoothing the moveout velocity profiles. A one spread length boxcar moving average filter is a simple and convenient smoothing operator, albeit with poor overall spatial frequency response, which offers a significant reduction in RMS moveout velocity mis-ties without generating excessive smoothing end-effects.

3.3 SUMMARY

A statistical framework has been established for the purposes of estimating both the contribution and significance of different spatial frequency components within moveout velocity profiles.

The semivariance function can be estimated from the autocorrelation function. Both show essentially the same information in opposite polarities.

The form of the semivariograms obtained from moveout velocity profiles bear little resemblance to the ideal semivariograms envisaged in geostatistical literature. On the basis of this study, geostatistical philosophy would appear to be generally inappropriate for periodic data and smoothing by kriging has therefore not been attempted.

Of the moveout velocity transforms studied, the energy spectrum appears to be the most informative. Significant moveout velocity components with wavelengths of around 3 km and 12 km have been identified on all five seismic horizons.

The moveout velocity profiles available for this study are short data sets compared with the dominant wavelengths of moveout velocity fluctuation.

Mis-ties obtained from smoothed moveout velocity profiles at line intersections can be used to infer the relative significance of the various spatial moveout velocity components.

Simple boxcar moving average filters have been used to smooth moveout velocity profiles as the lengths of low-pass filters required for an acceptable spatial frequency response cause excessive smoothing end-effects. Although the spatial frequency responses of boxcar moving average filters are generally poor, these operators have the advantage of subjecting less of the smoothed data to end-effects and the first notch can be easily adjusted to provide harsh attenuation of selected spatial frequency components.

Filtering the moveout velocity profiles with a one spread length boxcar moving average filter offers a considerable reduction in the RMS moveout velocity mis-tie without generating excessive smoothing end-effects.

While the 12 km wavelength moveout velocity component is thought to be related to real average velocity - time trends over the structure in the centre of the seismic grid, the 3 km wavelength component is probably 'anomalous' in the sense that it does not directly represent real velocity variations in the subsurface.

4. INVERSION OF VELOCITY DATA TO OBTAIN LOCAL THREE-DIMENSIONAL LIMITED GROUND MODELS

Each continuous seismic reflection on a CMP stacked seismic section can generally be characterised at a ground point by the following four 'surface measurements':

- t_o: the two-way zero-offset time;
- V_{mo}: the moveout velocity, picked from a velocity analysis of the CMP gather centred at the ground point;
- S_x: the time slope of the reflection on the section, referred to here as the inline time slope; and
- S_y: the time slope of the reflection measured in the direction perpendicular to that of the section (from the stacked section of an intersecting line), referred to here as the crossline time slope.

If the moveout velocity is assumed to be equal to the theoretical normal moveout velocity (i.e. the limiting value of moveout velocity as the spread length tends to zero), these four parameters can be used to recover a three-dimensional limited ground model in accordance with Hubral (1976a, 1976b). This ground model is limited to layers of constant velocity separated by plane reflectors of arbitrary dip and strike. Each of these reflectors can be characterised by a further four parameters:

- V: the interval velocity of the layer immediately above it;
- D: the vertical depth of the reflector below the ground point;
- ξ: the maximum dip of the plane reflector; and
- θ: the azimuth of maximum dip of the plane reflector.

The recovery of such limited ground models from surface measurements is referred to here as 'inversion'. The objective of this chapter is to present an algorithm for the inversion of three-dimensional limited ground models, and to discuss its practical application to real seismic data.

The method employed in this project to solve the inverse problem uses seismic ray theory, which is an approximation to full seismic wave theory. Ray theory is derived from the principles of geometrical optics, a set of solutions to the elastic wave equation for very high frequency signals. Application of ray theory to the data obtained from seismic reflection surveys is therefore valid if the dominant wavelengths of the propagating seismic pulse are much smaller than the radii of curvature of reflecting horizons, and if spatial changes of density and the Lame parameters are small over the pulse length. In the context of ray theory, seismic travel times are dependent entirely on the velocities of the rocks through which seismic energy passes in travelling from shot to geophone. Conversely, the time-distance relations over various recording geometries can be used to estimate seismic velocities, subject to the validity of some assumptions which limit the complexity of the local velocity distribution.

Seismic theory abounds with methods of processing and interpretation which either explicitly or (more often) implicitly, assume a very simple subsurface velocity model. One common assumption is that the subsurface locally consists of a series of homogeneous layers of different velocities separated by horizontal reflecting interfaces. Perhaps the best known inversion method incorporating this 'horizontal layering assumption' is that of Dix (1955). In the case of horizontal velocity layering, Dix showed that the moveout velocity was approximately equal to the root mean square of the vertical velocity-depth function. The velocity of any layer could therefore be expressed in terms of the two-way times and moveout velocities at the base and the top of the layer (Section 1.1.7).

The inversion technique used in this project is conceptually an extension of the Dix Equation to three dimensions. The normal moveout velocity of a horizon can be obtained from the curvature of a hypothetical wavefront which has propagated along the zero-offset ray from the normal incidence point to the surface. The curvature of this wavefront is in turn determined solely by the properties of the zero-offset raypath. Inversion is achieved by reversing the propagation of the wavefront back from the surface towards the normal incidence point, which allows the interval velocity to be derived in the target layer above the normal incidence point. The concept of wavefront curvature was introduced by Shah (1973b) for a two-dimensional limited ground model, while Hubral (1976a, 1976b) and Hubral and Krey (1980) document the extension to three dimensions. The methods of both Dix and Shah can be shown to be special cases of the Hubral solution where the ground model is reduced to one and two dimensions, respectively.

An algorithm for the calculation of raypaths through a ground model limited to layers of constant velocity separated by plane reflectors of arbitrary dip and strike is presented in Section 4.1.

The curvature of the hypothetical wavefront is calculated using various laws governing the response of the wavefront to refraction and reflection of the zero-offset ray at a boundary and transmission through a layer. The laws of wavefront curvature in the 3D limited ground model are reviewed in Section 4.2.

The calculation of normal moveout velocities, two-way zero-offset times and time slopes for a specified ground model is referred to here as 'forward modelling'. Section 4.3 presents a forward modelling algorithm for the simulation of these surface measurements above the 3D limited ground model.

An inversion algorithm to recover the 3D limited ground model from normal moveout velocities, two-way zero-offset times and time slopes is then presented in Section 4.4.

These four theoretical sections are then set in context by Section 4.5, which discusses the practical application of the local inversion technique to real seismic data. Specific attention is given to the many sources of error inherent in the inversion, together with some options for increasing the accuracy of inversion.

FORTRAN subroutines implementing the raytracing, forward modelling and inversion algorithms are included as appendices.

4.1 RAYTRACING IN A THREE-DIMENSIONAL LIMITED GROUND MODEL

In order to implement Hubral's forward modelling and inversion procedures, it is first necessary to develop an algorithm for tracing a zero-offset ray (or equivalently, normal incidence ray) in a 3D ground model consisting of uniform velocity layers separated by plane interfaces. The familiar tools of vector algebra and Snell's Law are sufficient for this purpose.

The first requirement for the 3D raytracing algorithm is that the plane interfaces be specified in mathematical notation. This is covered in the first part of this section. The second part defines the nature of the 3D raytracing problem while the solution is provided in the third. This solution pertains to any raypath in the limited ground model; it is not restricted to the normal incidence ray.

A FORTRAN implementation of the algorithm (Subroutine RAYTR3D) is included in Appendix 4A.

4.1.1. Definition of the Limited Ground Model

A 3D ground model consisting of uniform velocity layers separated by plane reflecting interfaces of arbitrary dip and strike can be described by the interval velocity in each layer, together with the vertical depth, maximum dip and azimuth of maximum dip for each interface. Implementation of a raytracing algorithm is facilitated by defining each interface as an equation of the form $\phi(x,y,z) = 0$. It is first necessary to define the coordinate system.

The coordinate system is right-handed with +z pointing vertically upwards. The x-axis lies along the seismic line (and hence along the CMP gather) with +x pointing in the direction of increasing shot point numbers. Increasing depth implies positive dip and increasing time implies positive time slope. The surface is defined by the horizontal plane z=0. In addition to this 'global' coordinate system, a 'local' coordinate system which travels along the raypath is used in order to calculate rotation angles at layer interfaces. This concept is introduced in Section 4.1.3.

Each plane reflecting interface can now be expressed in the form:

$$(n_1\ n_2\ n_3)\begin{pmatrix} x \\ y \\ z \end{pmatrix} + \rho = 0 \tag{4.1}$$

where $(n_1\ n_2\ n_3)$ is the transpose of the interface normal vector $\underline{n}$ and ρ is the distance measured perpendicularly (i.e. along the interface normal) from the interface to the origin (0,0,0). Specifically, for each interface:

$$\underline{n} = \begin{pmatrix} n_1 \\ n_2 \\ n_3 \end{pmatrix} = \begin{pmatrix} \sin\xi\ \cos\theta \\ \sin\xi\ \sin\theta \\ \cos\xi \end{pmatrix} \tag{4.2}$$

and

$$\rho = D\cos\xi \tag{4.3}$$

with ξ, θ and D defined as in Section 4. Interface normal vectors point upwards.

4.1.2 The 3D Raytracing Problem

Tracing a ray through a system of plane reflecting interfaces of arbitrary dip and strike can be broken down to a simple mathematical problem by considering the ray segment in each layer in turn.

Consider a ray starting at a point O (Figure 4.1). The point O has coordinates (x_O, y_O, z_O) and represents either a source or a point on a previous reflector. The ray direction is specified by the unit vector $\underline{r}^I$. The next plane reflecting interface is defined by its unit normal vector $\underline{n}$ and perpendicular distance ρ to the origin (Section 4.1.1).

In the context of this work, the requirement is to obtain the following:

P:	the point with coordinates (x_P, y_P, z_P) where the ray is incident on the next interface;
s :	the length of the ray segment (the distance from O to **P**);
α:	the angle of incidence at **P**;
β:	the angle of refraction at **P**;
δ:	the 3D rotation angle (Hubral, 1976a) at **P**; and
$\underline{r}^T$:	the unit normal vector of the refracted ray in the next layer.

The problem is then restated as **P** and $\underline{r}^T$ become O and $\underline{r}^I$ for the next layer.

The solution to this problem (Section 4.1.3) allows any ray to be traced through the specified ground model. Only the initial starting point and direction of the raypath need be defined.

4.1.3 A 3D Raytracing Algorithm

Solutions to the general 3D raytracing problem including curved reflectors separating layers of uniform velocity can be found in Shah (1973a) and Hubral and Krey (1980, p.44). The solution to the 3D plane reflector raytracing problem presented here is a simplification of the above works for the case of zero curvature.

In addition to the 'global' coordinate system (x,y,z), it is useful also to consider a 'local' coordinate system $(\bar{x},\bar{y},\bar{z})$ defined at O (Figure 4.1) as follows:

- the local z-axis $\bar{z}$ points along the direction of the ray (and is therefore equivalent to the ray direction unit vector $\underline{r}^I$);
- the local x-axis $\bar{x}$ lies in the plane of incidence at **P** on the next interface; and
- the local y-axis $\bar{y}$ is selected in order to ensure that the local coordinate system is right-handed.

Unit vectors along the $\bar{x}$-, $\bar{y}$- and $\bar{z}$-axes at O are denoted by $\underline{e}_x^I$, $\underline{e}_y^I$ and $\underline{e}_z^I$, respectively.

The local $\bar{x}$- and $\bar{y}$-axes need only be defined in the first layer used in the raytracing, as both are updated by rotation at subsequent interfaces. In the first layer, since both $\underline{e}_x^I$ and $\underline{e}_z^I$ lie in the plane of incidence at **P**:

$$\underline{e}_y^I = \underline{e}_z^I \times \underline{n} \tag{4.4}$$

where **x** denotes the vector cross product. The unit vector along the $\bar{x}$-axis is then defined by:

$$\underline{e}_x^I = \underline{e}_y^I \times \underline{e}_z^I \tag{4.5}$$

The solution to the raytracing problem now proceeds as follows:

(a) Angle of Incidence at **P**

The angle of incidence α at **P** is simply:

$$\cos\alpha = \underline{e}_Z^I \bullet \underline{n} \qquad (4.6)$$

where $\bullet$ denotes the vector dot product.

(b) Length of the Ray Segment From **O** to **P**

The length s of the ray segment from **O** to **P** is available from Equation (4) of Shah, (1973a) as:

$$s = -(\underline{n} \bullet \underline{O}' + \rho) / \cos\alpha \qquad (4.7)$$

where $\underline{O}$ is the position vector of the point **O** and ' denotes the matrix transpose. The perpendicular distance ρ has been defined in Equation (4.3).

(c) Coordinates of Point **P**

The position vector $\underline{P}$ of point **P** is obtained from:

$$\underline{P}' = \underline{O}' + \underline{e}_Z^I s \qquad (4.8)$$

(d) Angle of Refraction at **P**

The angle of refraction β at **P** is given by Snell's Law as:

$$\sin\alpha / V^I = \sin\beta / V^T \qquad (4.9)$$

where V^I and V^T are the layer velocities on the incident and transmitted sides of the interface, respectively.

(e) Angle of Rotation at **P**

The angle of rotation δ at **P** is defined by Hubral and Krey (1980, p.51). If the interface normal $\underline{n}$ at **P** is expressed in the local $(\bar{x},\bar{y},\bar{z})$ system, the rotation angle can be obtained from:

$$\tan\delta = \left(\frac{\underline{e}_y^I \bullet \underline{n}}{\underline{e}_x^I \bullet \underline{n}}\right) \qquad (4.10)$$

(f) Refracted Raypath

The unit vector $\underline{e}_Z^T$ along the refracted raypath is obtained from Equation (9c) of Shah (1973a) as:

$$\underline{e}_z^T = \frac{V^T}{V^I}\underline{e}_z^I - \left(\frac{V^T}{V^I}\cos\alpha - \cos\beta\right)\underline{n} \tag{4.11}$$

(g) Local Coordinate System After Refraction

The refracted $\bar{z}$-axis is defined by the unit vector $\underline{e}_Z^T$. The refracted $\bar{x}$-axis can be obtained by rotating the incident $\bar{x}$-axis $\underline{e}_X^I$ using Equations (4.7) and (4.28) of Hubral and Krey (1980):

$$\underline{e}_x^T = \cos\sigma\left(\cos\delta\,\underline{e}_x^I + \sin\delta\,\underline{e}_y^I\right) + \sin\sigma\,\underline{e}_z^I \tag{4.12}$$

where σ is the angle $\alpha - \beta$.

The solution to the 3D plane reflector raytracing problem is complete; the required parameters are available from the equations above. The refracted ray now becomes the incident ray on the next interface and the ray is traced through the ground model until parameters have been obtained for each layer.

4.2 WAVEFRONT CURVATURE

The concept of wavefront curvature allows the normal moveout velocity of a reflector to be related to parameters obtained by tracing a zero-offset ray to that reflector. This relation can be used either in the 'forward modelling' or 'inverse' sense. The purpose of this section is to introduce the formulae which can be used to calculate the curvature of a hypothetical wavefront associated with the zero-offset ray.

Hubral (1976b) and Hubral and Krey (1980) present laws governing the response of the wavefront to refraction or reflection at a layer interface and propagation through a layer. A 3D ground model consisting of uniform velocity layers separated by plane reflecting interfaces of arbitrary dip and strike is assumed. These laws are logical extensions of those presented by Shah (1973b) for a 2D ground model.

The most convenient measure of curvature is the radius of curvature of the wavefront. In a 2D ground model Shah was able to represent this parameter by a single number. However, in a 3D ground model the radius of curvature must be characterised by the 2x2 radius matrix $\underline{R}$:

$$\underline{R} = \begin{pmatrix} R_{11} & R_{12} \\ R_{21} & R_{22} \end{pmatrix} \tag{4.13}$$

This matrix is defined in the local coordinate system following the raypath, and changes in accordance with the laws of wavefront curvature discussed below. At the initial starting point of the ray the radius matrix is zero.

The three laws for wavefront curvature in a 3D ground model with plane reflecting interfaces are taken directly from Hubral (1976b), and are reviewed below:

(a) Propagation Law

The change of radius matrix due to expansion of the wavefront propagating through a uniform velocity layer is described by:

$$\underline{R}_{t+\Delta t} = \underline{R}_t + V_i \Delta t \, \underline{I} \tag{4.14}$$

where $\underline{R}_t$ is the radius matrix at time t;

Δt is some time increment;

V_i is the layer velocity; and

$\underline{I}$ is the 2x2 identity matrix:

$$\underline{I} = \begin{pmatrix} 1 & 0 \\ 0 & 1 \end{pmatrix} \tag{4.15}$$

(b) Refraction Law

The radius matrix $\underline{R}_T$ after refraction through a plane interface is:

$$\underline{R}_T = \frac{V^T}{V^I} \underline{D}^{-1} \underline{S} \, \underline{R}_I \, \underline{S} \, \underline{D} \tag{4.16}$$

with

$$\underline{S} = \begin{pmatrix} \cos\beta/\cos\alpha & 0 \\ 0 & 1 \end{pmatrix} \tag{4.17}$$

and

$$\underline{D} = \begin{pmatrix} \cos\delta & -\sin\delta \\ \sin\delta & \cos\delta \end{pmatrix} \tag{4.18}$$

where $\underline{R}_I$ is the radius matrix on the incident side of the interface;

V^I is the velocity of the layer on the incident side of the interface;

V^T is the velocity of the layer on the transmitted side of the interface;

α is the angle of incidence;

β is the angle of refraction; and

δ is the 3D rotation angle.

The diagonal matrix $V^I/V^T \; \underline{S} \; \underline{S}$ describes the change in radius matrix due to Snell's Law refraction at the interface, while the orthogonal matrix $\underline{D}$ rotates the matrix $\underline{S} \; \underline{R_I} \; \underline{S}$ by the angle δ onto the new local coordinate system on the transmitted side of the interface.

(c) Reflection Law

The radius matrix $\underline{R_R}$ after reflection at a plane interface is:

$$\underline{R_R} = \underline{I_R} \; \underline{R_I} \; \underline{I_R} \tag{4.19}$$

where $\underline{R_I}$ is the radius matrix on the incident side of the interface; and

$\underline{I_R}$ is the 2 x 2 matrix:

$$\underline{I_R} = \begin{pmatrix} -1 & 0 \\ 0 & 1 \end{pmatrix} \tag{4.20}$$

These three laws are sufficient to determine the radius matrix along any raypath in a 3D ground model consisting of uniform velocity layers separated by plane interfaces. All of the parameters required by these laws are immediately available from the 3D raytracing algorithm described in Section 4.1.3.

When referred to the zero-offset ray, the 3D raytracing algorithm and wavefront curvature laws provide the basic components of Hubral's forward modelling and inversion procedures. Algorithms for the solutions to both are presented in the following sections.

4.3 FORWARD MODELLING OVER A THREE-DIMENSIONAL LIMITED GROUND MODEL

The 3D forward modelling algorithm presented in this section is developed principally from Hubral (1976a, 1976b). It has been found desirable to combine aspects of both papers in order to achieve maximum compatibility with the inversion algorithm desribed in Section 4.4. Hubral and Krey (1980) has also been used, particularly for the definition of 3D 'rotation angles' (Section 4.1.3 (e)). Zero-offset raytracing is performed by the algorithm described in Section 4.1.

It is stressed that the forward modelling procedure outlined here is only one possible combination of Hubral's equations. The exact form of the algorithm has not been 'prescribed' by Hubral.

This section is subdivided into four parts. The first defines the nature of the 3D forward modelling problem, while the solution is presented in the second part. The third part compares the results obtained from the algorithm with those of Hubral (1976a) and notes one discrepancy in the normal moveout velocities. The performance of the algorithm is validated by a simple CMP raytracing exercise in the final part.

A FORTRAN implementation of the 3D forward modelling algorithm (Subroutine HUBRALF) is presented in Appendix 4B.

4.3.1 The 3D Forward Modelling Problem

The forward modelling problem for the 3D limited ground model is posed as follows. Given a surface origin (x_O, y_O, 0) and a limited ground model consisting of n layers, each defined by the four parameters:

V_i: the uniform velocity of the ith layer;

D_i: the depth of the ith interface vertically below the origin;

ξ_i: the maximum dip angle of the ith interface; and

θ_i: the azimuth of maximum dip of the ith interface,

where i takes the values 1 through n, it is required to obtain the following four surface measurements for horizon n:

$t_{o,n}$: the two-way zero-offset time;

$V_{nmo,n,x}$: the normal moveout velocity measured along the seismic line;

$S_{x,n}$: the time slope $\partial t_{o,n}/\partial x$ along the seismic line; and

$S_{y,n}$: the time slope $\partial t_{o,n}/\partial y$ across the seismic line.

4.3.2 A 3D Forward Modelling Algorithm

This section presents the fundamental steps required for the solution of the 3D forward modelling problem outlined in the previous section.
The algorithm proceeds as follows:

(a) Express Plane Reflectors in Mathematical Notation

The depths D_i, maximum dip angles ξ_i and azimuths of maximum dip θ_i for reflectors 1 through n are expressed as interface normals and perpendicular distances (Section 4.1.1) using Equations (4.2) and (4.3).

(b) Direction of the Surface Downgoing Ray Which is Incident Normally at Horizon n

Use is made of the fact that all zero-offset rays to horizon n follow parallel paths through each layer in the limited ground model. A normal incidence ray is traced upwards from horizon n to the surface using the algorithm described in Section 4.1.3. The direction of the surface downgoing ray which is incident normally on horizon n is then the reverse of the direction of the upgoing zero-offset ray segment in the first layer.

(c) Parameters Along the Zero-Offset Ray

The zero-offset ray is now traced downwards from the surface origin $(x_o, y_o, 0)$ to horizon n, again using the algorithm described in Section 4.1.3. The angles of incidence α_i, refraction β_i and rotation δ_i are thus immediately available for the refractions at horizons 1 through n-1, together with the two-way transit time Δt_i in layers 1 through n.

(d) Two-Way Zero-Offset Time

The two-way zero-offset time $t_{o,n}$ to horizon n is simply:

$$t_{o,n} = \sum_{i=1}^{n} \Delta t_i \tag{4.21}$$

(e) Radius Matrix

The 2x2 radius matrix $\underline{R}$ describing the radius of curvature of the hypothetical wavefront associated with the normal incidence ray from the surface origin to horizon n is defined in Equation (26) of Hubral (1976b) as follows;

$$\underline{R} = \frac{1}{V_1} \sum_{i=1}^{n} V_i^2 \Delta t_i \underline{I} \prod_{k=1}^{i-1} \underline{D}_k^{-1} \underline{S}_k^{-1} \prod_{k=1}^{i-1} \underline{S}_{i-k}^{-1} \underline{D}_{i-k} \tag{4.22}$$

where

$$\underline{D}_k = \begin{pmatrix} \cos\delta_k & -\sin\delta_k \\ \sin\delta_k & \cos\delta_k \end{pmatrix} \tag{4.23}$$

and

$$\underline{S}_k = \begin{pmatrix} \cos\beta_k/\cos\alpha_k & 0 \\ 0 & 1 \end{pmatrix} \tag{4.24}$$

pertain to refraction at horizon k as described in Section 4.2.

(f) Ray Emergence Angles at Surface

The zero-offset ray emergence direction at the surface is defined uniquely by the projection of the emerging ray into the surface plane and its inclination to the vertical. A further coordinate system (x_n, y_n) in the surface is now defined (Hubral, 1976a) which is specific to the zero-offset ray to horizon n. This coordinate system has the same origin as the previously defined (x,y,z) system and is a rotation of the latter such that $+x_n$ points along the projection of the emerging zero-offset ray (Figure 4.2). The direction cosines of the downward zero-offset ray segment in the first layer can now be defined from Equation (14) of Hubral (1976a) as:

$$\underline{e}_z = \begin{pmatrix} -\cos\phi_n \sin\beta_0 \\ \sin\phi_n \sin\beta_0 \\ -\cos\beta_0 \end{pmatrix} \tag{4.25}$$

where ϕ_n is the angle between the profile (+x) and the surface projection of the zero-offset ray ($+x_n$), measured away from the latter; and

β_0 is the angle between the emerging zero-offset ray and the surface normal.

(g) Time Slopes

If zero-offset rays are traced from all points (x,y,0) on the surface to horizon n, the two-way zero-offset times $t_{o,n}$ (x,y) fall into the common time plane described by:

$$t_{o,n}'(x,y) = t_{o,n}(0,0) + S_{x,n}x + S_{y,n}y \tag{4.26}$$

The direction of maximum gradient of this time plane is along the x_n-axis and the time slope in this direction is designated $S_{-\phi_n}$, available from Equation (13) of Hubral (1976a) as follows:

$$S_{-\phi_n} = 2 \sin \beta_o / V_1 \tag{4.27}$$

The inline time slope $S_{x,n}$ and crossline time slope $S_{y,n}$ are then:

$$S_{x,n} = S_{-\phi_n} \cos \phi_n \tag{4.28}$$

and

$$S_{y,n} = S_{-\phi_n} \sin \phi_n \tag{4.29}$$

(h) <u>Normal Moveout Velocity Ellipse</u>

The azimuthal variation of normal moveout velocity to horizon n is defined by Equation (10) of Hubral (1976a):

$$\frac{1}{V^2_{nmo,n,\phi}\, t_{o,n}} = \frac{d_n \cos^2\phi}{2} + e_n \cos\phi \sin\phi + \frac{f_n \sin^2\phi}{2} \tag{4.30}$$

where ϕ is the angle between the azimuth of measurement and $+x_n$;

d_n, e_n and f_n are parameters associated with the radius matrix $\underline{R}$; and

$V_{nmo,n,\phi}$ is the normal moveout velocity measured in the azimuth ϕ.

The form of Equation (4.30) indicates that the azimuthal variation of normal moveout velocity is exactly elliptical. The parameters d_n, e_n and f_n can be obtained by reference to both Equation (8) of Hubral (1976a) and Equation (4.22), which can be combined to form:

$$\underline{R}^{-1} = \begin{pmatrix} d_n/\cos^2\beta_0 & e_n/\cos\beta_0 \\ e_n/\cos\beta_0 & f_n \end{pmatrix} \tag{4.31}$$

Since both V_1 and $\underline{R}$ are known, the parameters d_n, e_n and f_n are immediately available.

The azimuth of an axis of the normal moveout velocity ellipse can now be found by locating a turning point ϕ_t on the function defined by the right hand side of Equation (4.30), i.e.

$$\partial/\partial\phi\ (d_n\cos^2\phi/2 + e_n\cos\phi\sin\phi + f_n\sin^2\phi/2) = 0$$

$$e_n(\cos^2\phi_t - \sin^2\phi_t) - (d_n - f_n)\cos\phi_t\sin\phi_t = 0$$

$$(d_n - f_n)\cos\phi_t\sin\phi_t = e_n(\cos^2\phi_t - \sin^2\phi_t)$$

$$\frac{d_n - f_n}{e_n} = \frac{1}{\tan\phi_t} - \tan\phi_t = \frac{2}{\tan 2\phi_t}$$

$$\phi_t = \frac{1}{2}\tan^{-1}\left(\frac{2e_n}{d_n - f_n}\right) \tag{4.32}$$

The angle ϕ_t defines either the major axis or the minor axis of the ellipse and is measured away from the x_n-axis. Since both major and minor axes are perpendicular, the angles ϕ_t and $\phi_t + \pi/2$ can be substituted into Equation (4.30) to determine the extremal normal moveout velocities. Minimum and maximum normal moveout velocities $V_{nmo,n,min}$ and $V_{nmo,n,max}$, together with the azimuth of the major axis ϕ_{max}, are then selected as appropriate (Figure 4.2).

The normal moveout velocity $V_{nmo,n,\phi}$ is then available in any azimuth ϕ from the ellipse using the formula:

$$\frac{1}{V^2_{nmo,n,\phi}} = \frac{\cos^2(\phi_{max} - \phi)}{V^2_{nmo,n,max}} + \frac{\sin^2(\phi_{max} - \phi)}{V^2_{nmo,n,min}} \tag{4.33}$$

(i) Inline and Crossline Normal Moveout Velocities

The inline and crossline normal velocities $V_{nmo,n,x}$ and $V_{nmo,n,y}$ are obtained from Equation (4.33) as follows:

$$\frac{1}{V^2_{nmo,n,x}} = \frac{\cos^2(\phi_{max} - \phi_n)}{V^2_{nmo,n,max}} + \frac{\sin^2(\phi_{max} - \phi_n)}{V^2_{nmo,n,min}} \qquad (4.34)$$

and

$$\frac{1}{V^2_{nmo,n,y}} = \frac{\sin^2(\phi_{max} - \phi_n)}{V^2_{nmo,n,max}} + \frac{\cos^2(\phi_{max} - \phi_n)}{V^2_{nmo,n,min}} \qquad (4.35)$$

4.3.3 Comparison with the Results of Hubral

Hubral (1976a, Tables 1 and 2) presents surface measurements obtained from two different limited ground models. These are referred to here as Ground Models 1 and 2, respectively. The data for both models have been processed by the algorithm described in Section 4.3.2 (Subroutine HUBRALF) in order to simulate surface measurements to compare with those of Hubral. The results are presented in Tables 4.1 and 4.2.

The data generated by the HUBRALF algorithm are in general agreement with Hubral, except for two discrepancies:

- for horizon 3 of Ground Model 1 Hubral quotes a crossline normal moveout velocity of 7898 ft/s, whereas the HUBRALF algorithm indicates 7847 ft/s; and
- the signs of the x- and y- normal incidence point coordinates are reversed between Table 2 of Hubral and Table 4.2.

It would appear that the second problem is caused by an inconsistency between dip angles and normal incidence point coordinates in Table 2 of Hubral. The first problem, however, could not easily be accounted for, and a simple finite-offset raytracing exercise was performed over both models in order to confirm the normal moveout velocities generated by the HUBRALF algorithm.

4.3.4 Comparison with CMP Moveout Velocities

Finite-offset CMP raypaths were traced through both models using a computer program provided by Geophysics Research Branch, BP London. The program allowed the generation of a CMP ray family for a spread orientated in any direction over the three-dimensional limited ground model.

For each model, finite-offset rays were traced for spreads of various lengths orientated along both x- and y-axes. Moveout velocities for each spread length could then be estimated from the offsets and two-way times by the T^2 - X^2 method (Section 1.1.8) and extrapolated towards the normal moveout velocity at zero-offset.

Raytracing was performed for five shot-geophone pairs s_1 - g_1 through s_5 - g_5 (see Figure 1.2a) for each spread. A tolerance of +/- 0.1 ft was specified for the surface outlet of the raypath with respect to the required geophone location. The near-offset s_1g_1 and the offset increment (s_2g_2-s_1g_1) were reduced in steps of 100 ft from 600 ft to 300 ft to simulate four spread lengths of 3000, 2500, 2000 and 1500 ft. Four independent estimates of moveout velocity for different spread lengths were thus available along both x- and y-axes for each horizon.

These spread lengths are small compared to the vertical depth of the deepest reflector (around 10000 ft in both models). Indeed, a much longer spread would be required to resolve the moveout velocity of a real reflection from this depth in order to highlight the reflection trajectory in the background noise. However, small spread lengths have been chosen not to compare with 'real' spread lengths, but to examine the behaviour of moveout velocity as the spread length is reduced towards zero. The smallest spread length of 1500 ft appears to represent the limiting spread length for the calculation of meaningful moveout velocities for these ground models. At shorter spread lengths the results are dominated by numerical inaccuracy caused by scatter of the T-X pairs about a nearly flat hyperbolic trajectory. Moveout velocities can therefore only be extrapolated towards the normal moveout velocity in an approximate sense.

The moveout velocities calculated for each spread length, together with the HUBRALF normal moveout velocities, are presented in Tables 4.3 and 4.4 and in Figures 4.3 and 4.4 for Ground Models 1 and 2 respectively.

Although each value is subject to numerical inaccuracy in the T^2-X^2 calculation, there are two particularly anomalous moveout velocities in the results. The crossline moveout velocity for horizon 3 of Ground Model 1 obtained from the 2500 ft spread is in error due to the inclusion of a 'rogue' raypath (outside the prescribed 0.1 ft tolerance). Although the T^2-X^2 procedure uses the actual offset rather than the nominal offset, this rogue raypath is thought to have taken a sufficiently different route for the resulting two-way time to have distorted the least-squares analysis. The inline moveout velocity for horizon 3 of Ground Model 2 using a spread length of 1500 ft also appears to be in error. As no obvious source of error can be detected, it is likely that the 1500 ft spread length is too short to derive an accurate moveout velocity for this reflection. These anomalous data points are indicated by a question mark on Figures 4.3 and 4.4.

Moveout velocities for the first horizon in each model do not vary with spread length, as the uniform velocity in the first layer allows straight ray segments between the surface and reflector. However, for the second and third horizons the CMP raypaths are refracted at layer interfaces and the moveout velocity increases with spread length (Section 1.1.9). The data points plotted on Figures 4.3 and 4.4 define concave-upward curves, although the 'true' curves may not pass exactly through each data point due to the numerical inaccuracy discussed previously. That the curves are concave-upward, and not straight lines, is to be expected by analogy with moveout velocity behaviour over a model with horizontal velocity layering. The graphs in Figures 4.3 and 4.4 indicate that the normal moveout velocities calculated by the HUBRALF algorithm are in each case a realistic approximation to the limiting values of moveout velocity at zero-offset. Specifically, the HUBRALF crossline normal moveout velocity of 7847 ft/s for Horizon 3 of Ground Model 1 is vindicated.

4.4 INVERSION OF A THREE-DIMENSIONAL LIMITED GROUND MODEL

The 3D inversion algorithm described in this section follows the method outlined in Hubral (1976a). Hubral and Krey (1980) has also been used. Zero-offset raytracing is again performed by the algorithm described in Section 4.1.

This section is subdivided to three parts. The 3D inversion problem is stated in the first part while the solution is presented in the second part. The integrity of the algorithm is demonstrated in the final part by reference to its performance in exactly inverting the forward modelled data presented in the last section.

A FORTRAN implementation of the 3D inversion algorithm (Subroutine HUBRALI) is presented in Appendix 4C.

4.4.1 The 3D Inversion Problem

The inversion problem for a 3D limited local ground model can be posed as follows. Given a surface origin $(x_o,y_o,0)$ and a horizon n characterised by the four surface measurements:

$t_{o,n}$: the two-way zero-offset time;

$V_{nmo,n,x}$: the normal moveout velocity measured along the seismic line;

$S_{x,n}$: the time slope $\partial t_{o,n}/\partial x$ along the seismic line; and

$S_{y,n}$: the time slope $\partial t_{o,n}/\partial y$ across the seismic line,

it is required to derive the following:

V_n: the interval velocity in layer n;

D_n: the vertical depth of the nth plane interface below the origin;

ξ_n: the maximum dip angle of the nth plane interface; and

θ_n: the azimuth of maximum dip of the nth plane interface.

When inverting at layer n the limited local ground model must be known down to and including layer n-1 and interface n-1.

Layer n is referred to here as the 'target' layer, while the known ground model down to interface n-1 is termed the 'overburden'.

4.4.2 A 3D Inversion Algorithm

This section presents the fundamental steps required for the solution of the 3D inversion problem stated in the previous section.

The algorithm proceeds as follows for the inversion of layer/interface n:

(a) If n = 1: Interval Velocity of First Layer

The interval velocity of the first layer V_1 can be related to the inline normal moveout velocity $V_{nmo,1,x}$ and ray emergence angles β_o and ϕ_1 by rewriting Equation (5) of Levin (1971) as:

$$V_1^2 = V^2_{nmo,1,x}(1-\sin^2 \beta_o \cos^2 \phi_1) \tag{4.36}$$

The ray emergence angles can then be substituted by the inline time slope $S_{x,1}$ using Equations (4.27) and (4.28). Equation (4.36) then becomes:

$$V_1^2 = V^2_{nmo,1,x}(1 - V_1^2 S^2_{x,1}/4) \tag{4.37}$$

or

$$\frac{1}{V_1^2} = \frac{1}{V^2_{nmo,1,x}} + \frac{S^2_{x,1}}{4} \tag{4.38}$$

(b) If n > 1: Express Plane Reflectors in Mathematical Notation

The depths D_i, maximum dip angles ξ_i and azimuths of maximum dip θ_i for reflectors 1 through n-1 of the known ground model are expressed as interface normals and perpendicular distances using Equations (4.2) and (4.3).

(c) Ray Emergence Angles at Surface

The ray emergence angles ϕ_n and β_o can be derived from Equations (4.27), (4.28) and (4.29) as:

$$\tan \phi_n = - S_{y,n}/S_{x,n} \tag{4.39}$$

and

$$\sin \beta_o = V_1 S_{-\phi_n}/2 \tag{4.40}$$

where

$$S_{-\phi_n} = S_{x,n} \cos \phi_n - S_{y,n} \sin \phi_n \tag{4.41}$$

(d) Direction of the Surface Downgoing Ray Which is Incident Normally at Horizon n

The direction cosines of the downgoing zero-offset ray segment in the first layer are given by Equation (4.25).

(e) Parameters Along the Zero-Offset Ray Down to Horizon n-1

The zero-offset ray is now traced downwards from the surface origin $(x_o,y_o,0)$ to horizon n-1 using the algorithm described in Section 4.1.3. All parameters α_i, β_i, δ_i and Δt_i are thus obtained down to horizon n-1. The angle of refraction β_{n-1} (into layer n) is not yet defined.

(f) Interval Velocity in Layer n

The solution for the interval velocity in layer n is taken from Hubral

(1976a, p.238). The core of the solution is the expression of d_n, e_n and f_n as functions of V_n:

$$d_n = d_n(V_n) = \cos^2 \beta_o \, w(V_n)/p(V_n) \tag{4.42}$$

$$e_n = e_n(V_n) = -\cos \beta_o \, q(V_n)/p(V_n) \tag{4.43}$$

$$f_n = f_n(V_n) = h(V_n)/p(V_n) \tag{4.44}$$

which correspond to Equations (18), (19) and (20) of Hubral. The reader is referred to the original work for the precise form of the 'subsidiary' functions w,q,h and p. These equations are then used in conjunction with Equation (4.30) to provide a direct association between the normal moveout velocity V_{nmo,n,ϕ_n}, the wavefront curvature down to horizon n-1 and the required interval velocity V_n.

The expression of V_{nmo,n,ϕ_n}, as a function of V_n in Equations (4.30), (4.42), (4.43) and (4.44) is appropriate for solution via a Newton-Raphson iteration of the general form:

$$V_{n,k+1} = V_{n,k} - \frac{f(V_{n,k})}{f'(V_{n,k})} \tag{4.45}$$

where $V_{n,k}$ is the kth estimation of V_n in the iteration procedure;

f is the function of V_n such that $f(V_n) = 0$; and

f' is the first derivative of f with respect to V_n.

The function f is formulated by rewriting Equation (4.30) with $\phi = \phi_n$ as follows:

$$f(V_{n,k}) = \frac{d_{n,k}\cos^2\phi_n}{2} + e_{n,k}\cos\phi_n \sin\phi_n + \frac{f_{n,k}\sin^2\phi_n}{2} - \frac{1}{V_{nmo,n,\phi_n} t_{o,n}} = 0 \tag{4.46}$$

where k again denotes the trial value assumed during the kth iteration. The derivative f' can be conveniently obtained numerically as:

$$f'(V_{n,k}) = \frac{f(V_{n,k} + \Delta V_{n,k}) - f(V_{n,k})}{\Delta V_{n,k}} \qquad (4.47)$$

where $\Delta V_{n,k}$ is a small perturbation of $V_{n,k}$ ($\Delta V_{n,k} = V_{n,k}/100$ is used in the HUBRALI algorithm).

Equations (4.45), (4.46) and (4.47) are sufficient for the derivation of V_n. The first estimate $V_{n,1}$ can be provided by the 'Dix Estimate' (Section 1.1.7):

$$V_{n,1}^2 = \frac{V_{nmo,n,x}^2 t_{0,n} - V_{nmo,n-1,x}^2 t_{0,n-1}}{t_{0,n} - t_{0,n-1}} \qquad (4.48)$$

Occasionally this estimate may be impossible or may yield absurd velocities (say outside the range $1000 < V_n < 10000$ m/s) where the subsurface is complex and the time interval is small. An alternative first estimate is then required, for example:

$$V_{n,1} = V_{nmo,1,x} \qquad (4.49)$$

The iteration continues until consecutive estimates $V_{n,k}$ and $V_{n,k+1}$ differ by less than a specified tolerance. Convergence to within 0.001% is typically achieved after three or four iterations, which is quite sufficient for the purposes of the algorithm in view of the magnitude of inaccuracies introduced by errors inherent in the method itself (see Section 4.5).

(g) Normal Moveout Velocity Ellipse

Although not strictly part of the inversion procedure, it is noted that d_n, e_n and f_n are available from the successful iteration step and can be substituted into Equations (4.32) and (4.33) to determine the parameters of the normal moveout velocity ellipse.

(h) Ray Segment in Layer n

The geometry of the refracted ray segment in layer n can now be obtained using parts of the algorithm described in Section 4.1.3. The angle of refraction β_{n-1} is given by Snell's Law in Equation (4.9) and the direction cosines $\underline{r}$ of the refracted ray segment are defined by Equation (4.11). The normal incidence point coordinates (x_n,y_n,z_n) are available from Equation (4.8) with the length of the ray segment s defined by:

$$s = V_n \ \Delta t_n/2 \tag{4.50}$$

where

$$\Delta t_n = t_{0,n} - \sum_{i=1}^{n-1} \Delta t_i \tag{4.51}$$

(i) Parameters of the nth Plane Interface

Since the downward ray segment in layer n is incident normally on interface n, the interface normal $\underline{n}$ is given simply by:

$$\underline{n} = -\underline{r} \tag{4.52}$$

The angle of maximum dip ξ_n and azimuth of maximum dip θ_n of interface n are then immediately available from Equation (4.2). The perpendicular distance ρ (Section 4.1.1) is given by the vector dot product:

$$\rho = \underline{r} \bullet \begin{pmatrix} x_n - x_o \\ y_n - y_o \\ z_n \end{pmatrix} \qquad (4.53)$$

and the vertical depth D_n to interface n is obtained from Equation (4.3).

4.4.3 Comparison with the Results of Hubral

The data presented by Hubral (1976a, Tables 1 and 2) and discussed in Section 4.3.3 have been used to test the algorithm described in the previous section. The two-way zero-offset times, normal moveout velocities and time slopes generated by HUBRALF (Tables 4.1 and 4.2) were processed by HUBRALI and both limited local ground models were recovered exactly, thus confirming the integrity of the algorithm.

4.5 PRACTICAL APPLICATION OF THE LOCAL INVERSION TECHNIQUE TO REAL DATA

The theory reviewed in the previous sections has thus culminated in the presentation of an algorithm for the 'inversion' of 3D limited local ground models from two-way zero-offset times, normal moveout velocities and time slopes. It is now prudent to escape from the realms of theory and discuss the practical application of Hubral's inversion to real seismic data.

The limited ground model can be recovered exactly if, and only if, the following conditions are satisfied:

- the two-way zero-offset times, normal moveout velocities and time slopes are known precisely; and
- The assumption limiting the local ground model to constant velocity layers separated by plane reflectors is valid.

These are severe restrictions. Indeed, these ideal conditions are not likely to exist in seismic data which has sampled a real subsurface plagued by geological phenomena. The sources of error in the application of Hubral's inversion to real data are reviewed in Section 4.5.1, while their magnitudes are discussed briefly in Section 4.5.2.

Since a correct inversion for layer n requires correct raytracing through the 'overburden' down to horizon n-1, it follows that errors in the overburden are effectively propagated downwards into the results for the target layer n. In order to control errors introduced by the overburden, it is generally desirable to inspect the ground models after each inversion step. Use of the inversion technique in two alternative operational 'modes' is discussed in Section 4.5.3. Finally, the case for processing these data in a spatial context is presented in Section 4.5.4.

4.5.1 Sources of Error

The inversion of real data using the local inversion technique is subject to a number of problems which introduce errors into the derived ground model. The sources of error fall broadly into two categories, which are discussed under separate headings below.

4.5.1.1 Errors in Surface Measurements

The two-way zero-offset time, normal moveout velocity and time slopes are required for each horizon in the Hubral inversion. In general the times and time slopes can be specified very accurately compared with the errors inherent in the definition of normal moveout velocity.

It is generally assumed that the CMP stacked section is equivalent to the zero-offset section which could be obtained using a single coincident s-g pair (Section 1.1.3). Each reflection on a stacked trace is then considered to represent energy which has travelled along a zero-offset raypath to and from its reflector of origin (or at least in so far as ray theory is applicable). CMP stacking is a remarkably robust procedure and this assumption is generally valid for all but the most complex subsurface velocity configurations.

Two-way times picked from a CMP stacked section are therefore a good approximation to the required zero-offset times. However, small errors may be introduced through uncertainties in the datum and the timing of the wavelet. Datum errors may be caused by incorrect bulk shifts to account for gun depth, streamer depth, gun delays or very occasionally rather more abstract corrections including filter delays. The time is ideally picked at the onset of the wavelet.

However, seismic horizons are usually picked at the culmination of a strong cycle which is delayed relative to the true onset. Both datum and picking errors are small relative to absolute two-way times. Datum errors are constant over all horizons but are not apparent in time intervals (i.e. between two horizons). Picking errors are constant over any one horizon (if the wavelet is invariant) but may affect time intervals if the delay varies from horizon to horizon. Both can be largely eliminated if the seismic data can be tied to calibrated velocity logs at nearby wells. Synthetic seismograms are particularly useful in this respect.

While inline time slopes are generally measured from the CMP stacked section, crossline time slopes are ideally obtained from maps of two-way zero-offset times. If such maps are unavailable, the crossline time slopes can be carefully interpolated between known values at line intersections. Time slopes are generally not subject to the datum and picking errors discussed above since they are purely relative measurements along the time surface. Significant errors are only likely to occur if the data quality is poor or if the wavelet is not constant.

Normal moveout velocities present an altogether different problem. The non-equivalence of normal moveout velocity, moveout velocity and stacking velocity has been discussed at length in Sections 1.1 and 1.2 and is stressed again at this point.

Normal moveout velocity is a modelling parameter which describes the optimum hyperbolic moveout of a reflection in the immediate vicinity of the emerging zero-offset ray. It cannot be obtained directly from real seismic data.

Moveout velocity describes the optimum hyperbolic moveout of a reflection trajectory across the traces of a CMP gather. It can be obtained from velocity analyses of real data.

Stacking velocity is a processing parameter.

Moveout velocities can therefore only be used as an estimate of the normal moveout velocities required by the inversion algorithm. Errors then accrue both through errors in picking the moveout velocities and the non-equivalence of normal moveout velocity and moveout velocity.

The term 'error in moveout velocity' as used here is restricted to the difference between the picked moveout velocity and that defining the optimum hyperbolic trajectory. Errors in moveout velocities are imposed by the resolution of CMP velocity analysis and generally increase with two-way time as noise increases, seismic bandwidth decreases and moveout curves become flatter (Section 1.5). The use of stacking velocities listed at the top of seismic sections (without reference to velocity analyses) to estimate normal moveout velocities is particularly undesirable and should be used only at the last resort. Moveout velocities should always be picked from velocity analyses if the latter are available.

The non-equivalence of normal moveout velocity and moveout velocity is principally due to complexities in the subsurface velocity distribution (Section 1.4.2). The effects of refraction, near-surface time delays, velocity heterogeneity within layers, reflector curvature and faulting are liable to render the moveout velocity a poor approximation to the normal moveout velocity. The difference between normal moveout velocity and moveout velocity is likely to increase with the complexity of the subsurface. However, since the inversion technique is strictly limited to constant velocity units separated by plane reflectors, its performance is drastically reduced anyway in these circumstances. The difference between normal moveout velocity and moveout velocity can be viewed as an expression of an underlying problem of greater significance, namely failure of the assumptions about the ground model. This problem is addressed in the next section.

4.5.1.2 Errors Introduced by Ground Model Assumptions

If the real subsurface does not conform to the assumptions inherent in the inversion procedure, errors are introduced into the derived ground model. That is, if the subsurface does not consist of constant velocity layers and plane reflectors, then the derived constant velocities and plane reflectors will be in error.

The most obvious problem introduced by a more complex subsurface is the unsuitability of the wavefront curvature formulae presented in Section 4.2. If reflector curvature exists, the 'Refraction Law' in Equation (4.16) is no longer applicable as the curvature of the reflector should also then be included (Hubral and Krey, 1980). If significant velocity heterogeneity exists within layers, the 'Propagation Law' in Equation (4.14) may only provide a poor approximation to the true expansion of the wavefront, which should then strictly be derived using complex formulae presented in Hubral (1980a, 1980b). In extreme cases curved raypaths are implied and the raytracing algorithm of Section 4.1 may be inappropriate.

A further problem is introduced by the raytracing algorithm if considerable reflector curvature exists. Plane reflectors generated during the inversion procedure are defined at their normal incidence points. Although desirable for positioning the plane when it is the target horizon, it may not be the optimal definition of the reflector when it becomes part of the overburden for a deeper target. Indeed, if a curved reflector exists in the subsurface, raytracing to deeper reflectors will be incorrect since the original plane reflector is assumed.

In practice the subsurface never exactly conforms to the constant layer velocity and plane reflector assumptions. As a general rule, errors can be minimised by restricting usage of the inversion to areas where the assumptions are most valid, or at least by assigning more weight to the results obtained from these areas. The problem is least when the different horizons are nearly parallel and worst when there is a wide divergence of dips.

4.5.2 The Magnitude of Inversion Errors

A correct inversion for layer n and reflector n is possible only if the surface measurements are free from errors and the assumptions of constant layer velocities and plane reflectors are valid. Errors must therefore be expected in the inversion of real seismic data.

It would be dangerous, however, to prescribe the magnitude of errors likely in a Hubral 3D inversion for some 'general' ground model. Each case should be studied on its own merits, preferably by raytrace modelling followed by a suite of inversions using test data corrupted over realistic ranges of errors. The effects of errors in the surface measurements or in the ground model assumptions can then be assessed independently.

Nevertheless, two important observations should be made. Inversion errors are likely to increase both as two-way time increases and as the target interval reduces in thickness. This potential magnification of errors is in accordance with that expected for the derivation of interval velocities using the Dix Equation (Section 1.3) and is due to the inherent similarity of the two algorithms.

4.5.3 Alternative Modes of Inversion

Inversion errors assume an added significance since errors in the upper layers 1 through n-1 cause incorrect raytracing to interface n-1 and hence generate greater inversion errors in the inversion for layer n. in this way the inversion errors tend to propagate downwards through the ground model.

An inversion where all horizons are inverted in turn at a single ground point is referred to here as a 'direct' inversion. Downward error propagation is inevitable when the algorithm is applied in this sense as the ground model cannot be monitored and adjusted during the inversion.

It is obviously desirable to control the ground model as it extends downwards. The chances of a successful inversion at layer n are greatly increased if the ground model is defined accurately down to interface n-1. the 'layer-by-layer' mode of inversion allows one layer to be processed at a time over a range of ground points. After a set of inversions to the target layer, the derived interval velocities can be checked and adjusted by reference to well ties or mis-ties at line intersections. Only when the interval velocity variation in the target layer is accepted does the inversion proceed to the definition of the structure at the base of that layer. The ground model can then be extended to the next layer with less risk of error propagation from above. This procedure is repeated until the last layer and reflector have been processed.

Downward error propagation by raytracing, also apparent in the 2D inversion of Shah, is absent in the Dix Equation where only trivial (refraction-free) raytracing is required. Reference to Equation (1.13) shows that a Dix inversion for the interval velocity and thickness of layer n is dependent only on the two-way times and RMS velocities to the top and base of that layer. It is important to note, however, that absolute depths derived by repeated application of the Dix Equation are indeed subject to errors in layer thicknesses in all the layers above.

This is not to advocate inversion by the Dix Equation in preference to the Hubral 3D algorithm. If the subsurface comforms approximately to the constant layer velocity and plane reflector assumptions the latter will always provide a better estimate of the ground model as the effects of reflector dip can be taken into account. The point to be made is that careful quality control via the layer-by-layer inversion can restrict downward error propagation and allow still greater accuracy in the derived ground model.

Both direct and layer-by-layer modes of inversion are accomodated in the HUBRALI algorithm presented in Appendix 4C.

4.5.4 The Need for Spatial Processing

An isolated inversion at a single ground point is subject to a multiplicity of errors. It is therefore preferable to process a number of ground points in sequence, as the spatial continuity of both the surface measurements and the derived data can then be evaluated and attended to if necessary.

From the preceding discussions it will be apparent that the definition of normal moveout velocity is generally the largest single source of error. When moveout velocities are sampled frequently along a seismic line, the moveout velocity profiles typically show considerable lateral variation (Section 2.3.2). Moreover, much of this variation is introduced by the limited lateral resolution of the velocity analysis technique. Since these fluctuations are inevitably fed through into the derived interval velocities, conclusions drawn from an isolated inversion may be grossly inaccurate.

It is therefore recommended that the Hubral 3D inversion should, wherever possible, be used in conjunction with information at adjacent ground points. Two significant opportunities then emerge to improve the accuracy of the derived ground models.

In the first place, moveout velocity profiles can be processed before the inversion in order to provide a better estimate of the normal moveout velocities. Although no analytical methods exist to transform moveout velocities directly to normal moveout velocities, it is possible to make a better estimate of the latter by smoothing the moveout velocity profiles. Methods have been presented in Section 3.1.5 to reduce rapid lateral fluctuations of moveout velocity in order to leave the more slowly varying components which are thought to be a more faithful representation of the theoretical normal moveout velocities. Smoothing techniques, albeit based on somewhat empirical criteria, do yield significantly more consistent moveout velocity data volumes when judged by the criterion of mis-ties of moveout velocity at line intersections (Section 3.2.3).

Spatial processing also allows the derived interval velocities to be fully evaluated. This approach is highly desirable as spatial variations of interval velocities can be interpreted with respect to lithological variation, porosity variation and compaction, for example. Interval velocity trends implied by the inversions can then be accepted or rejected as appropriate. Furthermore, over the gross intervals used in the inversion, lateral variations of velocity are likely to be gradual. It is therefore reasonable to reduce the scatter in derived interval velocities by further smoothing. Reference to interval velocity mis-ties at line intersections can then be used to indicate the spatial consistency of the data set. In contrast to moveout velocities, which are generally azimuth-dependent, interval velocities should theoretically tie at line intersections as the zero-offset ray through the ground model is independent of azimuth. If well information is available, the derived interval velocities can be further constrained by data from calibrated velocity logs.

Operation of the Hubral 3D inversion within a spatial database system offers considerable scope for the improvement of derived ground models. Lateral variations of moveout velocity can be evaluated and processed before inversion to provide better estimates of normal moveout velocities, while the derived interval velocities can be interpreted and processed after inversion. Application of the inversion in the 'layer-by-layer' mode (Section 4.5.3) is particularly appropriate in this context as the adjusted interval velocities and reflector depths are used for the inversion of subsequent layers. The incorporation of this local inversion technique into a regional moveout velocity database system is described in Chapter Five.

4.6 SUMMARY

Normal moveout velocity is a modelling parameter which can be derived from the curvature of a hypothetical wavefront travelling along the zero-offset ray. The calculation of normal moveout velocities, two-way zero-offset times and time slopes from a specified ground model is referred to here as 'forward modelling'. If the ground model is limited to layers of constant velocity separated by plane reflectors of arbitrary dip and strike, the calculation can be performed in reverse to derive the ground model from the surface measurements. This reverse calculation, termed the 'inversion', can be performed without iterative raytracing by collapsing the wavefront back along the zero-offset ray to the normal incidence point.

Formulae for raytracing and wavefront curvature in the 3D limited ground model have been reviewed in the first two sections of the chapter.

Hubral (1976a, 1976b) has documented methods for forward modelling and inversion over a three-dimensional limited ground model. Algorithms implementing these methods have been presented.

Finally, the problems of applying the Hubral 3D inversion to real data have been addressed. Errors are likely to accrue both through inaccuracies in the surface measurements and violations of the ground model assumptions. The real subsurface rarely, if ever, conforms to these assumptions, and it is always preferable to perform the inversion in a spatial context. The 'layer-by-layer' mode of inversion offers the greatest scope for monitoring the accuracy of inversion.

5. INCORPORATION OF THE LOCAL INVERSION TECHNIQUE INTO A REGIONAL MOVEOUT VELOCITY DATABASE SYSTEM

Previous chapters have presented methods for the analysis of moveout velocities over a seismic reflection survey area (Chapter Three) and algorithms for both forward modelling and inversion of simple local ground models from CMP stacked seismic data using the geometry of the zero-offset raypath (Chapter Four). This chapter describes the synthesis of these ideas into the regional moveout velocity database system 'KRUNCH'.

The reader is reminded immediately of the important distinction between moveout velocities measured from seismic data and theoretical normal moveout velocities calculated from wavefront curvature formulae (Chapters One and Four). The role of KRUNCH as an interface between real moveout velocities and zero-offset modelling is discussed in Section 5.1.

The choice of data structure for a regional moveout velocity database is important. The KRUNCH data structure, together with the critical factors influencing this choice, is described in Section 5.2.

The various processes which are applied to the times and velocity information within the database are referred to here as 'tasks'. Section 5.3 discusses the many tasks that such a database system should perform. All are implemented in the KRUNCH program.

Brief examples showing how KRUNCH might be used to process a typical moveout velocity database are included in Section 5.4.

Although notoriously difficult when describing a computer program or system, all effort has been made to avoid specific computer terminology. The aim has been to restrict the discussion in the text to the 'concepts', thus isolating 'jargon' to the appendices.

5.1 HUBRAL 3D MODELLING IN A REGIONAL CONTEXT

It is stressed at the outset that KRUNCH has no magical powers with which to transform the moveout velocities measured from real seismic data to the theoretical normal moveout velocities required for Hubral 3D inversion. Nor can KRUNCH control the forces of nature; the limited local ground model implied by Hubral 3D modelling, consisting of uniform velocity layers separated by plane reflectors, is not likely to occur in the real subsurface. Handling data in bulk can never alleviate these problems.

The net result is that errors are certain to occur when using moveout velocities to derive interval velocities in the Hubral 3D algorithm. The role of KRUNCH is to provide a means by which these errors can be reduced to a level where the data can be confidently accepted or rejected. This is achieved through selective analysis, manipulation and processing of the data both before and after inversion.

Many of the tasks available for use in KRUNCH will not be unfamiliar to the reader. Methods for the spatial analysis of moveout velocities were described comprehensively in Section 3.1, while Hubral 3D forward modelling and inversion are performed using the algorithms described in Chapter Four. Indeed, much of the analysis in Section 3.2 (notably the spectral analysis, filtering and calculation of mis-ties) was performed by KRUNCH.

A typical scheme for the derivation of interval velocities from a regional moveout velocity database might be expressed as:

(a) assess the spectral content of the moveout velocity profiles on each line by transforming to the spatial frequency/wavenumber domain;

(b) determine the 'optimum' moveout velocity smoothing filter by calculating mis-ties derived from a suite of moveout velocity profiles smoothed by trial filters (remembering that a genuine inherent moveout velocity mis-tie will exist for two lines sampling different apparent dips at the line intersection);

(c) smooth moveout velocities using this 'optimum' filter in an attempt to attenuate offset-induced moveout velocity fluctuations;

(d) reduce moveout velocities for each horizon by a factor designed to eliminate offset-induced refraction bias;

(e) Hubral 3D inversion; and

(f) smooth and/or adjust derived interval velocities in order to match information at line intersections and tie to available wells.

If a 'layer-by-layer' inversion is used, steps (e) and (f) are repeated alternately from the first layer downwards until the ground model has been extended to the last layer and reflector (Section 4.5.3). Each of the six steps above (and many others) can be performed by KRUNCH using either a single instruction or a short sequence of instructions for each line.

A final step could be added to those above. The derived interval velocities can be accepted or rejected on the basis of comparing surface observations of two-way times and moveout velocities to those calculated by tracing finite-offset CMP raypaths through the proposed regional velocity-depth model. This is beyond the scope of KRUNCH however, as such a raytracing algorithm generally requires a rather more complex data structure.

KRUNCH can be viewed as a line-orientated piecewise velocity inversion system. It is 'line-orientated' (as opposed to map-orientated) in that information for each seismic line is processed separately; data from one line is never related to that on another line except in the case of mis-tie calculation. It is 'piecewise' in that each inversion takes place referred to a simple limited local ground model; data from one ground point is never related to that from another ground point during the inversion (except for the implicit inter-dependence of adjacent moveout velocities introduced by smoothing). For all its simplicity, however, KRUNCH provides a remarkably robust and functional interpretation system which quickly yields a considerable amount of information from a regional moveout velocity database.

5.2 DATA STRUCTURE

Each seismic database has its own criteria for determining its optimum data structure. The most important factor is how the data structure is to be searched in order to retrieve information required for tasks. In addition, the choice of data structure is influenced by the size of computer memory, the amount of information which needs to be in memory simultaneously, and the types of files available on the local operating system.

The information to be handled by KRUNCH consists essentially of the eight parameters associated with Hubral 3D modelling (Chapter Four). Each continuous seismic reflection horizon on a CMP stacked seismic section can be characterised at a ground point by the following four parameters:

1. the two-way zero-offset time;
2. the moveout velocity, picked from a velocity analysis of the CMP gather centred at the ground point;
3. the time slope of the reflection on the section, referred to here as the inline time slope; and
4. the time slope of the reflection measured in the direction perpendicular to that of the stacked section, referred to here as the crossline time slope.

Each plane reflector in the derived limited local ground model can then be characterised at the ground point by a further four parameters:

5. the interval velocity of the layer immediately above it;
6. the vertical depth of the reflector below the ground point;
7. the maximum dip of the plane reflector; and
8. the azimuth of maximum dip of the plane reflector.

The data structure must accomodate these eight parameters for each horizon at each ground point along the seismic line. Each 'parameter value' in the data structure needs to be associated with a parameter, horizon and ground point.

The principal tasks of KRUNCH which affect the choice of data structure are smoothing and Hubral 3D inversions. This is unfortunate, since there is a conflict of interest in the 'searching direction'. Smoothing requires a 'horizontal' search as a string of parameter values for consecutive ground points are retrieved for a single parameter along a single horizon. However, Hubral 3D inversion requires a search in the 'vertical' sense as parameter values at consecutive horizons are retrieved at a single ground point. The problem arises because FORTRAN has a preferred sequence of access to an array, which will correspond to one searching direction above. The second search is made by a slower and less efficient access sequence.

In order to provide flexibility, KRUNCH uses a three-dimensional matrix to store parameter values indexed uniquely by parameter, horizon and ground point (Figure 5.1). This data structure is defined in the computer by a 3D array with subscripts:

(GROUND POINT, HORIZON, PARAMETER)

By standard FORTRAN convention, parameter values for one parameter along one horizon are thus stored in continguous memory locations in the computer. Each such string of parameter values is referred to henceforth as a 'horizon/parameter vector'. Priority has therefore been given to the 'horizontal' search direction, since these horizon/parameter vectors can be accessed most rapidly from the data structure.

The 3D matrix used by KRUNCH pertains to one seismic line only. Data stored in this matrix is termed the 'current data set'. Further seismic lines can be handled by processing sequentially; data sets are read into the matrix from file and written to file as appropriate.

The KRUNCH 3D matrix data structure has two principal limitations, namely:

- in order to avoid handling individual ground point location information, the ground points are assumed to be equispaced; and
- each horizon must extend along the entire line from the first ground point to the last.

The first limitation requires that moveout velocities are available at regular intervals (time and time slope information is available in continuous form from seismic sections and maps). This is not likely to be a problem, as detailed velocity studies will generally include equispaced velocity analyses. Furthermore, equispaced moveout velocity data are necessary for conventional filtering and spectral analysis. The second limitation is likely to cause difficulty if a horizon terminates (eg. by onlap or subcrop) within the line. In these cases KRUNCH needs to generate a 'dummy' horizon immediately below the last valid horizon, which ensures that all horizons extend over each ground point. The dummy horizon is generated some 0.001 distance units (metres or feet) below the last valid horizon above and the corresponding two-way interval transit time is calculated using the interval velocity above the same horizon. All other parameters for the dummy horizon are taken directly from the last valid horizon. The inclusion of such a thin dummy layer has no apparent affect either on the results obtained for inversion to deeper layers or on the ability of the raytracing algorithm to trace rays through it (since it acts effectively as an extension of the layer above it with the same velocity).

5.3 SPECIFICATION OF TASKS

Having defined the KRUNCH data structure, it is now necessary to specify the tasks which are required to manipulate and process the data available for regional velocity studies.

KRUNCH has been written in the guise of a 'high-level' programming language. Each task is initiated by a separate instruction, which consists of a mnemonic and several data fields. The mnemonic selects the task while the data fields qualify how the task is to be performed. This allows considerable flexibility in running the program, as the tasks can be run in any order within reason.

The tasks performed by KRUNCH fall into three distinct categories, namely:

- 'scientific' tasks e.g. filtering, Hubral 3D inversion;
- 'data transfer' tasks i.e. transferring data between files and the KRUNCH matrix; and
- user facilities to aid in running the program.

Each category of tasks is now discussed in turn. Within each category, tasks are listed in alphabetic order of their mnemonics, although this order is not intended to indicate their relative importance. Full documentation for each task can be found in Appendix 5A.

5.3.1 Scientific Tasks

KRUNCH supports the following 'scientific' tasks:

(a) Compute inline time slopes for specified horizons from zero-offset two-way times in the current data set: "CDTDX".

The inline time slope $dt/dx_{m,n}$ on horizon m at ground point n is estimated by the formula:

$$dt/dx_{m,n} = (t_{m,n+1} - t_{m,n-1})/2 \; \Delta x \qquad (5.1)$$

where $t_{m,n}$ is the normal incidence time to horizon m at ground point n and Δx is the distance between adjacent ground points as defined in LINDEF (see below).

(b) Scale or shift parameter values in a specified horizon/parameter vector by a constant: "CONST".

(c) Compute mis-ties of parameters from parameter values at line intersections: "CROSS" and MISTIE".

Calculation of mis-ties is a two-stage process. CROSS is used to specify the intersection points of all crossing lines with the current line and interpolates parameter values from the current data set onto a temporary work file. One CROSS instruction is required for each line.

The second stage is performed by MISTIE and involves sorting through the interpolated parameter values after all CROSS instructions have been processed. The mean mis-tie and RMS mis-tie (Section 3.1.5.3) for each parameter are calculated separately for each horizon.

(d) Generate a dummy horizon over a specified range of ground points: "DUMMY".

This task is necessary to maintain integrity of the data structure if a horizon terminates within the line (eg. by onlap or subcrop) for the reason outlined in Section 5.1.

(e) Update or inspect a single parameter value in the current data set: "EDIT".

(f) Design a set of filter coefficients to become the current filter: "FDESN".

One of three types of filter can be designed:

- rectangular boxcar moving average (Section 3.1.5.1);
- zero-phase bandpass/bandstop filter defined in the wave-number domain (Section 3.1.5.1); or
- user-defined filter coefficients.

An option allows the amplitude response of the filter to be calculated and plotted.

(g) Filter specified horizon/parameter vectors with the current filter: "FILTER".

The delay imposed by the convolution is removed by shifting the output vector back by one half of the filter length, which is valid for zero-phase filters (Section 3.1.5.2).

A trend is removed from the vectors before filtering and added back afterwards. By default the DC component (zero wavenumber component or arithmetic mean) is removed. If the moveout velocity is being filtered, however, the trend can be defined as a linear function of time.

Real normal moveout velocity 'jumps' introduced by time discontinuities (i.e. faults) can thus be 'protected' from the convolution. Application of the null (single zero) filter can be used to eliminate the residuals and leave the trend.

Further options allow either the residuals (raw - filtered) or both raw and filtered data to be plotted.

(h) Plot graphs of specified horizon/parameter vectors: "GRAPH".

Options allow symbols (associated with each horizon) and plotting window to be specified.

(i) Perform Hubral 3D forward modelling for specified horizons over a range of ground points: "HFORWRD".

This task uses the algorithm described in Section 4.3. Forward modelling may be impossible in some locations in cases where extreme layer velocity contrasts or divergences of reflector dip have been specified. Although of little value, missing parameter values must be interpolated from adjacent ground points in order to maintain integrity of the data structure.

(j) Perform Hubral 3D inversion for specified horizons over a range of ground points: "HINVERT".

This task uses the algorithm described in Section 4.4. Either 'direct' or 'layer-by-layer' inversions can be performed.

Layer-by-layer inversions can be used in conjunction with pre-set interval velcoities for conventional zero-offset raytrace migrations using limited local ground models.

Normal incidence point co-ordinates and interval velocities can be written to file for subsequent plotting if required.

Inversion may be impossible at some locations, in which case missing parameter values must be interpolated from adjacent ground points in order to maintain integrity of the data structure.

(k) Define a new line: "LINDEF".

This task sets the invariants used to process the next current line. The following naming convention is adopted:

- a 'ground point' is here defined as a location at which velocity analysis results are available;
- the 'CMP number' (or shot point number) is an index of position along the seismic line used for annotation; and
- ground points are assumed to occur at a constant increment of CMP number.

LINDEF sets the following data (Figure 5.2):

- the (integer) line number;
- the number of ground points on the line;
- the number of horizons to be processed;
- the CMP number of the first ground point;
- the number of CMPs between adjacent ground points;
- the distance between adjacent ground points; and

- the orientation of the line.

The number of ground points and number of horizons (together with the number of parameters, which is fixed at eight) define the limits of the KRUNCH matrix occupied by the current data set. The length of each horizon/parameter vector is equal to the number of ground points on the line.

(l) Calculate and display energy spectra for specified horizon/parameter vectors: "PSPEC".

Options allow the length of the complex spectrum and degree of spectral smoothing to be specified. Smoothing is performed by the method of 'adjacent sum' smoothing described in Section 3.1.4.4 (Equation 3.26). Energies can be transformed to decibels if required.

Further options allow symbols (associated with each horizon) and plotting window to be specified.

(m) Resample a new data set from within the current data set: "SELECT".

This task can be used to reduce the amount of information in a data set. The required range of equispaced ground points are selected from the current data set using an integer multiple of the old ground point spacing.

(n) Design a smooth curve and sample equispaced parameter values for a single horizon/parameter vector: "SPLINE".

Parameter values are sampled at each ground point from a smooth curve composed of a series of local cubic splines. The curve is constrained to pass through data points which are either existing parameter values at selected ground points or new parameter values at spcified CMP numbers.

It is important to note that SPLINE is merely another 'housekeeping' operation to ensure that the data conforms to the KRUNCH data structure. No extra information is provided by the sampling, and if SPLINE is used to smooth existing data the original wavenumber content may be severely distorted.

5.3.2 Data Transfer Tasks

The following tasks are necessary to transfer data between files and the KRUNCH matrix:

(a) Read the new current data set into the KRUNCH matrix from a direct access file: "DREAD".

The data set is addressed via a 'keyword' (written by a DWRITE instruction, see below) and its contents are defined by the last LINDEF instruction.

(b) Write the current data set from the KRUNCH matrix to a direct access file: "DWRITE".

The data set is assigned a user-specified 'keyword' by which it is identified for future addresses by DREAD.

(c) Read a horizon/parameter vector into the KRUNCH matrix from a formatted file: "INPUT".

This task is used in the creation of a data set from data on different files in varied formats. Parameter values for specified ground points are read from the required file in a user-defined FORTRAN format. The file can be rewound and card images skipped over as necessary.

INPUT also allows a horizon/parameter vector in an existing data set to be overwritten.

(d) Open a file for subsequent read/write operations: "OPENF".

Both formatted and direct access files can be opened.

(e) Write specified horizon/parameter vectors from the KRUNCH matrix to a formatted file: "OUTPUT".

This task allows parameter values for specified ground points to be written to a file in a user-defined FORTRAN format.

5.3.3 User Facilities

These tasks have been implemented in order to aid the user while running KRUNCH:

(a) List the specification of a KRUNCH instruction: "HELP".

The relevant part of the KRUNCH documentation file (Appendix 5A) is directed to the current output device.

(b) Create a list of pre-set instructions which can subsequently be invoked repeatedly: "MACRO".

This task is particularly useful when a standard set of instructions is required for each seismic line in a runstream processing several lines.

(c) Reset current input or print file: "RESET".

This task allows standard runstreams to be read from different files and directs required parts of printout to different files.

(d) Stop the program: "STOP".

A log of all instructions processed in the run is automatically appended to the current print file.

(e) List details of the current version of KRUNCH to the current print file: "VERSION".

This task lists the restrictions imposed by FORTRAN array sizes eg. maximum number of horizons and maximum number of ground points in the KRUNCH matrix, maximum length of the complex spectrum used in PSPEC and maximum number of files which can be opened to the run.

5.4 EXAMPLES

Some typical task sequences are included here to show the varied uses of KRUNCH. The sequences below are merely intended to illustrate the logic used by KRUNCH; the actual instructions necessary to run the program are included in Appendix 5B.

Example 1. INITIAL KRUNCH RUN:

To read in times, moveout velocities and crossline time slopes; calculate inline time slopes; plot graphs of each parameter and store the current data set on a new direct access file. The indented sequence can be repeated for successive lines:

```
START
OPEN TIME FILE
OPEN MOVEOUT VELOCITY FILE
OPEN CROSSLINE TIME SLOPE FILE
OPEN NEW DIRECT ACCESS FILE
        DEFINE LINE
        READ TIMES
        READ MOVEOUT VELOCITIES
        READ CROSSLINE TIME SLOPES
        CALCULATE INLINE TIME SLOPES
        PLOT GRAPHS OF INPUT DATA
        WRITE CURRENT DATA SET TO DIRECT ACCESS FILE
STOP
```

Example 2. SMOOTHING MOVEOUT VELOCITIES AND CALCULATION OF MIS-TIES:

To design a smoothing filter; read in the current data set; filter moveout velocities and interpolate filtered moveout velocities at intersections of crossing lines with the current line. The indented sequence is repeated for each line and mis-ties are calculated from the intersection data at the end of the run:

START

OPEN OLD DIRECT ACCESS FILE

DESIGN FILTER

> DEFINE LINE
>
> READ CURRENT DATA SET FROM OLD DIRECT ACCESS FILE
>
> FILTER MOVEOUT VELOCITIES
>
> INTERPOLATE FILTERED MOVEOUT VELOCITIES AT LINE INTERSECTIONS

CALCULATE MOVEOUT VELOCITY MIS-TIES

STOP

Example 3. HUBRAL 3D INVERSION:

To design the 'optimum' smoothing filter (based on previous tests); read in the current data set; filter moveout velocities; perform Hubral 3D inversion at each ground point; plot graphs of derived interval velocities and write the updated current data set to a new file. The indented sequence can again be repeated for successive lines:

START

OPEN OLD DIRECT ACCESS FILE

OPEN NEW DIRECT ACCESS FILE

DESIGN FILTER

DEFINE LINE

READ CURRENT DATA SET FROM OLD DIRECT ACCESS FILE

FILTER MOVEOUT VELOCITIES

HUBRAL 3D INVERSION

PLOT GRAPHS OF DERIVED INTERVAL VELOCITIES

WRITE UPDATED CURRENT DATA SET TO NEW DIRECT ACCESS FILE

STOP

5.5 SUMMARY

A computer program has been written to handle a database consisting of two-way zero-offset times, moveout velocities and time slopes with the primary objective of allowing regional Hubral 3D inversions. The database system KRUNCH allows extensive processing of the data both before and after inversion.

KRUNCH is a line-orientated piecewise velocity inversion system. Each inversion takes place at a single ground point and is very largely independent of the surrounding data.

The KRUNCH database was used to process much of the information presented in Chapter Three, and is used extensively in Chapters Six and Seven.

6. APPLICATION OF THE LOCAL INVERSION TECHNIQUE TO SYNTHETIC DATA OBTAINED BY MODELLING OVER COMPLICATED GROUND MODELS

This chapter presents the results of applying the local inversion technique to 'synthetic' data obtained by raytracing over various ground models. CMP raypaths have been traced to calculate two-way stack times and moveout velocities, which have then been processed by KRUNCH (Chapter Five) to derive interval velocities and depths. Comparison with the original ground models then allows the performance of the local inversion technique to be assessed over different subsurface features.

The scope of this chapter is limited to an illustration of characteristic anomalies which are liable to occur over a selection of typical subsurface features. In view of the large number of variables involved, it is neither feasible nor desirable to generate a suite of 'characteristic moveout velocity curves' in the same way as is done for magnetic or electrical resistivity interpretation. Consider, for example, the number of permutations of depths, dips, layer thicknesses, fault throws, interval velocities and spread geometries for a simple two layer fault model! Rather, the intention is to provide examples of systematic interval velocity errors which can be caused by typical subsurface configurations.

It is important at this stage to stress the terms of reference for this study. The objective is to assess the accuracy of interval velocities derived by the local inversion technique. This approach is not equivalent to that of Blackburn (1980), where the difference between moveout velocity and true vertical average velocity was used to indicate the 'accuracy' of moveout velocity. The latter approach carries the implicit assumption that velocity derivation and depth conversion is constrained to one dimension (the vertical). This, of course, is not necessary if Hubral's 3D inversion method (Chapter Four) is to be used, and the correct philosophy should be to monitor the derived interval velocities.

All CMP raytracing was performed by the BP London Raytracing Program. Relevant details of the program are discussed briefly in Section 6.1.

The following four sections are then devoted to a study of the performance of the local inversion technique in the presence of reflector dip, velocity gradients, faulting and reflector curvature.

Section 6.6 presents CMP modelling and Hubral inversion of a typical North Sea salt dome model. The use of 'direct' and 'layer-by-layer' inversions in conjunction with smoothing is discussed.

6.1 THE BP RAYTRACING PROGRAM

The BP London 2D raytracing program was used to generate two-way stacked times and moveout velocities over the ground models studied in this chapter. The program can handle 2D ground models including curved and discontinuous reflectors bounding layers of either constant or variable interval velocity. Two 'modes' of raytracing are pertinent to the examples shown in the following sections, namely zero-offset raytracing and CMP gather raytracing.

Zero-offset raytracing is commonly used to simulate the times observed on CMP stacked sections, each trace of which ideally represents the energy arriving at zero-offset (Section 1.1.3). Zero-offset raypaths are shown for some of the ground models in this chapter as they provide a guide to the approximate position of the CMP gather raypaths, and hence an indication of the subsurface sampling.

CMP gather raytracing has been used to calculate two-way stacked times and moveout velocities over each of the ground models. The gather is defined by:

- the number of traces, n_t;
- the near offset, x_1; and
- the offset increment (or trace spacing), δx.

The spread length is then simply $x_1 + (n_t-1) \delta x$. In order to trace the CMP gather raypaths to a reflector, the program starts by tracing the zero-offset raypath. The near offset raypath is then calculated using the emergence angle and RMS velocity along the zero-offset raypath in a complicated iteration procedure. Subsequent offset raypaths are then calculated iteratively using the knowledge gained from tracing the preceding offset. When all offset raypaths have been traced, the two-way stacked time and moveout velocity are calculated from the (zero-offset) intercept and gradient of the least squares line through the $T^2 - X^2$ data (Section 1.1.8).

An implicit assumption throughout most of this chapter is that the ray theoretical approach outlined here is an adequate representation of the full wave theoretical response of the ground model to seismic reflection processes. Attention is drawn to the cases where this assumption is suspect. Raytracing is not a perfect simulation of seismic reflection processes, and the moveout velocities calculated here should only be regarded as representative of the data one would expect to obtain over comparable subsurface features using real seismic recording and processing methods. Similarly the stacked time, simulated from the intercept time in the T^2 - X^2 fit rather than the actual zero-offset normal incidence time, is an approximation.

6.2 REFLECTOR DIP AND MULTILAYERED MODELS

The material in this brief section has been covered previously but is included here for emphasis. Chapter Four showed that Hubral's inversion algorithm can be used to derive a ground model consisting of layers of uniform velocity separated by plane reflecting interfaces of arbitrary dip and strike if the normal moveout velocities, two-way times and orthogonal time slopes are known. Since the moveout velocity over such a simple model is known to be a slightly biased overestimate of the normal moveout velocity (Section 4.3.4), it can be adjusted accordingly to allow a very accurate inversion. Such an adjustment can be made simply by CMP raytracing over an approximate ground model, which is likely to yield a sufficiently accurate estimate of the 'spread length bias'.

If the Hubral algorithm is used, the extension to three dimensions causes no errors in the inversion if the subsurface conforms to the ground model assumed. Reflector dip and multilayering need cause few problems in the derivation of interval velocities if the Hubral algorithm is used.

6.3 VELOCITY GRADIENTS

The effect of linear velocity gradients on moveout velocities was discussed qualitatively in Section 1.4.2.5(a). Two models have been used in this section to generate two-way stacked times and moveout velocities, which in turn have been used in the Hubral algorithm to derive interval velocities. Both models incorporate three layers separated by parallel dipping reflectors inclined at 5° to the horizontal.

Model 1A (Figure 6.1a) has a vertical velocity gradient of 0.4 s^{-1} in the second layer defining a velocity function of:

$$V_2(z) = 2000 + 0.4z \text{ m/s}$$

Model 1B (Figure 6.1b) has a horizontal velocity gradient of 0.035 s^{-1} in the same layer, defining the velocity function:

$$V_2(x) = 2200 + 0.035x \text{ m/s}$$

In both cases, it is noted that the gross (vertical average) interval velocity of the second layer increases from 2200 m/s at x=0 to 2550 m/s at x=10000m.

CMP raypaths were then traced using the following spread geometry:

- number of traces: 10
- near offset: 300m
- offset increment: 300m
- spread length: 3000m

with a surface CMP interval of 1000m. The resulting two-way stacked times and moveout velocities are listed in Table 6.1 for three representative locations.

The first layer presents no problems for the inversion (Section 6.2) and has not been included in the table.

These data were then processed using KRUNCH. Time slopes were calculated from the two-way stacked times using Equation (5.1) and the Hubral inversion was used to derive interval velocities and depths vertically beneath the CMP locations. Table 6.1 presents the results of inversion, together with the actual model values for comparison. The velocity values in parentheses for layer 2 indicate the gross (vertical average) interval velocity of the layer vertically below the surface CMP location.

Results of the Hubral inversion are seen to be quite favourable. In each case the interval velocity is slightly overestimated as a consequence of the spread length bias in the moveout velocities. Note that as the depth of the second layer increases, there is more scope for the bending of CMP raypaths by refraction and the inversion error increases accordingly. The increasing accuracy of the derived interval velocity in layer 3 is probably fortuitous as a result of the compensation of inversion errors in this layer and the layer above.

From the discussion above, it is evident that interval velocities derived by the Hubral algorithm are not likely to be seriously corrupted by linear velocity gradients in isolation. The technique has been shown to be robust in the presence of reflector dip, both for a layer with a velocity gradient and a layer beneath it. The reason for this follows a 'swings and roundabouts' argument, as in a linear velocity gradient each CMP raypath must sample both a lower and higher velocity region. The moveout velocity then tends to that which would be observed for a constant velocity equal to the average of the local velocity distribution sampled by the CMP gather raypaths. The derived interval velocity is therefore a good approximation to the local average velocity of the interval.

One further point is worthy of note in this example. Although the inversion detects the presence of a velocity gradient quite accurately, it is impossible to determine the precise nature of the gradient if the layer is dipping. Specifically, from the two-way stacked times and moveout velocities in this example the direction of the gradient is unresolved, since near-identical surface measurements are obtained for both the vertical and horizontal gradients. However, if the layer is horizontal, the vertical velocity gradient has no effect and the lateral velocity gradient can be isolated.

6.4 FAULTING

The effects of subsurface faulting have been discussed qualitatively in Section 1.4.2.5(c). Figure 6.2 shows a CMP gather passing over Model 2, which consists of two horizontal layers cut by a vertical fault. CMP raypaths have been traced using the following spread geometry:

- number of traces: 10
- near offset: 300m
- offset increment: 300m
- spread length: 3000m

with a surface CMP interval of 50m.

Figures 6.3a and 6.3b show the two-way stacked times and moveout velocities obtained from the raytracing exercise. As the first reflector is horizontal on either side of the fault and has a constant moveout velocity of 2000 m/s, the first layer presents no problems for the inversion. Data are therefore presented only for horizon 2 in the lower part of Figure 6.3.

The fault is sampled by CMP gathers between 4400m and 5650m. In this zone, both two-way stacked times and moveout velocities exhibit variations which are summarised in Table 6.2. Whereas the differences between two-way stacked and zero-offset times are small (maximum 12 ms), the differences between moveout velocities and vertical RMS velocities (the corresponding zero-offset parameter in this example) are considerable. In addition, the swing in moveout velocity is in the opposite sense to that of the real velocity distribution as measured by the vertical average or RMS velocity.

Interval velocities and depths estimated by the Hubral algorithm are presented in Figures 6.3c and 6.3d, respectively. Each interval velocity is plotted at the corresponding normal incidence point location since this is more representative of the zone sampled by the CMP gather than a vertical projection below the surface location. Similarly, depths are plotted as normal incidence points rather than depths on the plane reflector extrapolated to below the surface CMP location. The actual interval velocities and depths of the model are included as solid lines.

Both interval velocities and depths are overestimated away from the fault. This is a direct consequence of the spread length bias, the magnitude of which is slightly greater to the left of the fault where the reflectors are shallower and the refraction of offset raypaths is greater. In the vicinity of the fault, however, the derived interval velocities and depths are seriously in error. Both are underestimated to the left of the fault and overestimated to the right of the fault in accordance with the anomalous moveout velocity fluctuation on the second horizon. The interval velocity errors of around 20% on both sides of the fault are generated wholly by two-way stacked time and moveout velocity variations on horizon 2, since the inversion is accurate down to the first horizon (see above).

The apparent focussing of derived normal incidence points to the left of the fault and defocussing to the right of the fault (Figures 6.3c and 6.3d) is caused by variations in the two-way stacked time around the fault. Close observation of Figure 6.3a shows that on both sides of the fault there is a small component of time dip (time increasing to the right) in the two-way stacked times to horizon 2 caused by the asymmetry of offset raypaths in the CMP gather crossing the fault. Additional fluctuation in two-way stacked times is caused by a reduction of raypaths available for the T^2 - X^2 calculation at CMP locations where the raytracing algorithm fails at one or more offsets. The extent to which the latter effect is a true representation of reflected energy on the CMP stacked section is uncertain, but the element of time dip is thought to be likely to occur on a stacked section. For this model, however, there would be no such time dip on a true zero-offset section. This time dip leads to a non-vertical zero-offset ray being traced by the inversion algorithm and a consequent migration of normal incidence points 'updip' to the left. A cursory interpretation of Figure 6.3d would erroneously position the fault around 4750m with additional faults around 4500m and 5500m.

Since faults rarely occur in isolation in nature, and indeed rarely in the simple configuration discussed above, real moveout velocity profiles are generally a complicated superposition of the simple type of moveout velocity anomaly presented here. Attempts to estimate interval velocities and depths using the Hubral algorithm in faulted areas should therefore be avoided where possible.

6.5 REFLECTOR CURVATURE

Reflector curvature can have a significant influence on moveout velocities and the derived interval velocities. In the context of interval velocity derivation by the Hubral algorithm, this is a composite effect manifest both in curvature of the reflector at the base of the 'target' layer and in the curvature of 'intermediate' reflectors above the target layer. If, as is generally the case, the reflector includes components of both curvature and dip, the first effect causes a spread of reflection points for the CMP gather raypaths which is different to that caused by the dip component alone. The effect of reflector curvature at the base of the target layer can be best demonstrated by reference to the variation of moveout velocities and derived interval velocities at the base of a single uniform velocity layer. The effect of curvature of intermediate reflectors was introduced in Section 1.4.2.5(b) as a 'velocity replacement' effect and can be isolated by reference to a symmetrically folded sequence with vertical fold axes, which includes a uniform velocity target layer beneath a layer of different velocity. In this way the CMP gather raypaths have a true 'common reflection point' for CMPs vertically above the fold axes, and reflector curvature at the base of the target layer has no effect. This section presents an example to illustrate the nature of both effects, neither of which can be correctly accomodated by the Hubral inversion algorithm.

Model 3 (Figure 6.4) includes two layers which have been folded to form a syncline between two anticlines. Both reflectors are in fact described by sinusoids of amplitude 200m and wavelength 4000m. The folding is therefore parallel.

Figure 6.4 shows zero-offset raypaths and CMP raypaths to both reflectors. The zero-offset raypaths were traced using a constant normal incidence point spacing of 100m along the reflectors and indicate the subsurface sampling pattern. Note particularly that horizon 2 has a surface focus directly over the syncline (Figure 6.4c). CMP raypaths were traced using a spread defined by:

- number of traces: 10
- near offset: 300m
- offset increment: 300m
- spread length: 3000m

with a surface CMP interval of 250m. For the sake of clarity, only the gathers for CMPs at 3000m, 4000m and 5000m have been displayed. The lack of symmetry in the CMP raypaths to horizon 2 over the synclinal axis is due to the surface focus, as many different raypaths are possible at each offset. The raypaths shown in the figure represent just one solution.

Two-way stacked times and moveout velocities obtained during the CMP raytracing are illustrated in Figure 6.5 and summarised in Table 6.3. Moveout velocity variations on the first horizon are less than 5%, being controlled largely by dip and curvature at the base of the layer. In contrast, the moveout velocity swing from anticline to syncline for the second horizon is around 25%. This considerable variation is attributed largely to distortion of the raypaths by refraction at the first horizon as predicted in Section 1.4.2.5(b) (note the similarity of Figures 1.8 and 6.4e).

It is important to note that the moveout velocity profiles in Figure 6.5b provide a rather simplified picture of the true moveout velocity variation over the syncline. Asymmetry in the moveout velocity profile for horizon 2 (different moveout velocities for CMPs at 4750m and 5250m) is indeed symptomatic of the fact that the true moveout velocity variation is multivalued in the vicinity of the surface focus. The iteration algorithm in the raytracing program has chosen different CMP ray families on either side of the synclinal axis. Moveout velocities in this zone are therefore not single precise values, but samples drawn from a multivalued population. However, the moveout velocities are thought to be representative of the general trend as the discrepancy noted above is small compared to the total variation of moveout velocity on horizon 2 (Figure 6.4b).

The two-way stacked times and moveout velocities were then processed in KRUNCH. Having calculated the inline time slopes, a 'direct' inversion (Section 4.5.3) was used to derive interval velocities and depths (Figures 6.5c and 6.5d) which are again plotted at normal incidence point locations. The actual interval velocities and depths of the model are included as solid lines.

Derived interval velocities for the first layer are generally accurate, with extremal values of 1979 m/s for CMPs at 2000m, 4000m, 6000m and 8000m and 2043 m/s for CMPs at 4750m and 5250m. These errors occur because the CMP raypath reflection points are dispersed over a curved reflector at the base of the target layer and not the linear reflector assumed by the Hubral algorithm. The dip correction (multiplication by a cosine) inherent in Equation (4.36) then tends to overcorrect on convex-upward surfaces (near the anticlinal axis) and under-correct on concave-upward surfaces (near the synclinal axis). The interval velocity is obtained precisely on the fold axes since the dip is zero and there is no spread of reflection points.

Interval velocities in the second layer are adversely affected by the anomalous fluctuations of moveout velocity on horizon 2 which were in turn caused by the curvature of the first reflector. Table 6.3 shows that interval velocities derived over the crest of the anticlinal axis are over 10% too low, while those directly over the synclinal axis are over 30% too high. These errors are due to the second effect of reflector curvature discussed above, namely the curvature of an intermediate reflector. Since the extremal interval velocity errors for layer 2 occur over the fold axes (where the effect of curvature at the base of the target layer is zero), it must be concluded that of the two effects of reflector curvature introduced at the start of the section, the effect of curvature of intermediate reflectors is dominant for this model.

The implications of these interval velocity errors are readily apparent in the depth conversion shown in Figure 6.5d. The structure on reflector 2 is exaggerated by the depth conversion as the depth estimates to the anticline and syncline are too shallow and too deep respectively. Note that this effect is not equivalent to 'velocity pull-up' in the traditional sense (as observed on time sections), but a consequence of using the wrong interval velocity for depth conversion.

It is now timely to remark upon an interesting and significant paradox. While the moveout velocity on horizon 2 increases considerably from anticline to syncline, both vertical average and RMS velocities decrease as the lower velocity first layer thickens towards the synclinal axis (Table 6.3). A velocity - time crossplot (Figure 6.5e) shows that care should be exercised in the inference of average velocity - time trends from moveout velocity - time trends if significant reflector curvature exists.

6.6 A NORTH SEA STRUCTURE

As a further demonstration of the effects of reflector curvature, a more realistic model has been studied which is typical of the salt structures in the southern part of the North Sea. Model 4 is taken from an example in Taner, Cook and Neidell (1970) and is shown in Figure 6.6a. Since the structure is symmetrical, only one side is shown in the figures accompanying this section.

The main feature in the model is the Zechstein salt dome which rests on horizontal Rotliegendes sands. The salt dome was formed by withdrawal of salt from what now appears as a rim syncline which developed during the Triassic, and to a lesser extent during the Jurassic. The sequence is then completed by Cretaceous and Tertiary sediments which drape over the Zechstein high and thicken downflank. A water depth of 160 ft and water velocity of 5000 ft/s have been assumed. Except for the velocity inversion at the base of the Cretaceous chalk, the layer velocities increase progressively with depth down to the base of the salt.

Zero-offset raypaths to each of the five geological boundaries are shown in Figure 6.6. Rays have been traced at intervals of 250ft along the reflectors. The buried focus over the rim syncline at the base of the Triassic is particularly striking, and note also that this syncline focusses the zero-offset rays down to the base of the salt.

CMP raypaths have been traced over the model using the following spread geometry:

- number of traces: 12
- near offset: 500 ft
- offset increment: 500 ft

- spread length: 6000 ft

with a surface CMP interval of 500 ft. Additional CMP gathers were raytraced over the buried focus at the base of the Triassic in order to cover each of the three reflection segments in the zone of triplication. Both times and moveout velocities are multivalued in this zone. The resulting two-way stacked times and moveout velocities are presented in Figure 6.7. Note the high moveout velocities for the base of the Triassic over the buried focus and the oscillatory character of the moveout velocities on the base of the salt. It is important to note here that the raytracing program does not include the treatment of phase variations associated with buried focii in the simulation of moveout velocities.

These data have been processed using KRUNCH, where the buried focus causes an immediate problem. The KRUNCH data structure requires that the time and moveout velocity profiles be single-valued, and hence only part of the triplication can be used. For this reason, the minimum time values and associated moveout velocities have been used in KRUNCH (highlighted by the solid lines in Figure 6.7) since these correspond to the data which can be generally be most easily recognised in real data.

These data have been inverted in four different ways, using the alternative modes of inversion discussed in Section 4.5.3 and combinations of smoothing the moveout velocities and interval velocities. Smoothing has been performed by a one spread length boxcar moving average filter, on the somewhat arbitrary basis that such an operator has previously been successful in reducing anomalous components of moveout velocity (Section 3.2.3). This basis is, however, sufficient for the purposes of testing the alternative styles of inversion. The derived interval velocities are presented in Figure 6.8, while the resulting depth conversions are shown in Figure 6.9. For each inversion, the derived interval velocities and depths are displayed as symbols, together with the actual model values as solid lines.

In the direct inversions, the local model is recovered completely at each ground point in turn using in the first case the raw moveout velocities and in the second case the moveout velocities smoothed by the spread length boxcar filter. As expected, the action of smoothing moveout velocities causes a reduction in the scatter of the derived interval velocities. In both cases the interval velocities tend to be too low over the anticline and too high over the syncline, giving rise to the characteristic depth conversion errors discussed in Section 6.5.

The layer-by-layer inversions show a further improvement in the estimation of interval velocities. Raw and smoothed moveout velocities have been used in these inversions, and in both cases the interval velocities have been smoothed by the spread length boxcar filter before inversion of the next layer. Note that the interval velocities are filtered as an equispaced data set in the KRUNCH matrix, and not exactly as the interval velocity variation appears on the figure. The last inversion, using both smoothed moveout velocities and interval velocities offers the greatest accuracy of the four inversions. However, the interval velocity errors over both anticline and syncline persist.

Layer-by-layer inversion in conjunction with smoothing both moveout velocities and interval velocities have therefore been successful in considerably improving interval velocity estimates over a realistic structure. However, these techniques cannot eliminate the characteristic interval velocity errors associated with long wavelength reflector curvature. The false structure consequently generated at the base of the salt dome should be noted.

6.7 SUMMARY

CMP raypaths have been traced through a purely illustrative range of models in order to calculate synthetic two-way stacked times and moveout velocities. This information should not be regarded as exact since raytracing is not a perfect simulation of seismic reflection processes over a complex subsurface. These data have then been used to estimate interval velocities and migrated depths using the Hubral algorithm in the KRUNCH program.

Reflector dip and multilayering cause few problems in the derivation of interval velocities if the Hubral algorithm is used.

Interval velocities derived by the Hubral algorithm are not likely to be corrupted by linear velocity gradients in isolation. However, the precise nature of the velocity gradient may not be resolved.

Faulting causes large fluctuations in both moveout velocities and derived interval velocities. Faulted zones should be avoided wherever possible for the purposes of interval velocity estimation.

Curvature both of the reflector at the base of the target layer and of intermediate reflectors above the target layer can have a significant influence on moveout velocities and the derived interval velocities. Of the two, curvature of intermediate reflectors may be the dominant effect and typically causes interval velocities to be underestimated over anticlines and overestimated over synclines if the layer velocities increase with depth. Care should be taken in the inference of average velocity - time trends from moveout velocity - time trends if significant reflector curvature is known to exist.

Layer-by-layer inversion in conjunction with smoothing both moveout velocities and interval velocities allows considerable improvement in interval velocity estimates. However, the characteristic interval velocity errors induced by reflector curvature cannot be eliminated and are liable to cause serious depth conversion errors.

Although no attempt has been made to create generalisations from these models, some characteristic patterns of interval velocity errors have been recognised. Knowledge gained from this study, albeit on a rather qualitative basis, will allow a more confident evaluation of interval velocities derived from real seismic data.

7. APPLICATION OF THE LOCAL INVERSION TECHNIQUE TO REAL DATA

This, the last chapter, documents the practical application of the Hubral inversion algorithm to derive interval velocities from a real moveout velocity database. The overall aim is to present a logic which can be used to obtain an optimal interval velocity solution based on objective criteria. It is accepted that this solution may require further 'tidying up' before its ultimate use in time to depth conversion. However, the procedure presented here does allow a far more objective approach than is typical of current practice.

The first two sections review the real data used in this project which was introduced in Chapter Two. Seismic parameters are prepared for the KRUNCH database, and then interval velocities at wells are compiled in a form suitable for checking interval velocities derived by the Hubral algorithm.

The following two sections present the results of direct and layer-by-layer inversion of the moveout velocity database. A suite of possible interval velocity solutions are generated by various moveout velocity and interval velocity smoothing combinations. Optimal solutions are then chosen by reference both to the internal consistency of derived interval velocities at line intersections and to their comparison with well interval velocities. A calibration is necessary in each case to scale down interval velocities derived by the Hubral algorithm to fit those available from well information. A further section is included to discuss the relative merits of direct and layer-by-layer inversion.

7.1 PREPARATION OF DATA FOR INVERSION

In view of the numerous Hubral inversions to be performed on the data of Chapter Two, it was convenient to first prepare a separate KRUNCH matrix (Section 5.2) for each of the eight lines of Survey A. Each such matrix could then be accessed easily in order to retrieve the required data for smoothing and Hubral inversions described in subsequent sections of this chapter.

The preparation of two-way times, moveout velocities, inline time slopes and crossline time slopes are discussed in turn below. The inclusion of a water layer of constant thickness is also noted.

7.1.1 Two-Way Times

The two-way times available from the CMP stacked sections of Chapter Two are assumed to correspond to the two-way zero-offset times required for Hubral inversions. As the subsurface geometry of the area is relatively simple, the errors incurred by this assumption will be small by analogy with the differences between zero-offset times and stacked times observed over the ground models studied in Chapter Six.

It is desirable to remove the 'lags' from seismic times before inversion. Two-way times corrected in this way should provide a better estimate of the two-way zero-offset time, as the delay imposed by the band-limited seismic wavelet is then removed. The following lags (estimated in Section 2.4.1) were removed from the CMP stacked section times for each horizon:

BROWN	21 ms
PINK	36 ms

YELLOW	55 ms
ORANGE	29 ms
RED	35 ms

in order to make this correction.

7.1.2 Moveout Velocities

As discussed in Chapters Four and Five, the Hubral inversion algorithm ideally requires normal moveout velocities (as distinct from moveout velocities) for the accurate derivation of interval velocities. Unfortunately, this parameter is not immediately available from real data, and the observed moveout velocities must be used as the best and most convenient alternative. One obvious source of error introduced by this substitution is the spread length effect. This is discussed further in Section 7.2.3.

These moveout velocities are subject to the factors discussed in Section 1.4, but since none of these effects are likely to be constant over the survey area, the moveout velocity profiles of Chapter Two have been used without modification.

7.1.3 Inline Time Slopes

Inline time slopes were calculated as the derivative of the two-way stacked times with respect to distance along the seismic line using the CDTDX instruction in KRUNCH (Section 5.3.1(a)). The calculation was performed along continuous segments of a horizon between faults in order to avoid the generation of spurious time slope values across discontinuities.

The direction of +x is defined as the direction of increasing shot point number for each line, and hence a positive inline time slope indicates that two-way times increase with shot point number.

Inline time slopes are independent of the lag corrections described in Section 7.1.1.

7.1.4 Crossline Time Slopes

Crossline time slopes are best estimated from two-way stacked time maps for each horizon. However, such maps were only prepared for the Yellow and Red horizons, and in order to maintain consistency for all five horizons a different method was used.

Since the seismic data of Survey A were collected on a rectangular grid, the crossline time slope at a line intersection can be measured directly from the inline time slope of the horizon on the intersecting line. For each line the direction of +y is determined by the previously defined +x and +z (vertically up) axes. A crossline time slope was estimated for each horizon at each intersection point, giving control at intervals of approximately 1 km along each line. The required equispaced crossline time slopes were then linearly interpolated along each horizon from these control points. Care was again taken to restrict this interpolation to continuous time segments between faults in order to avoid spurious time slope values. Although in areas of very complex structure this procedure may be suspect, reference to the two-way time maps in Chapter Two (Figures 2.16 and 2.17) indicates that the structure is in this case simple enough to allow linear interpolation of crossline time slopes between intervals of 1 km.

Crossline time slopes are again independent of lag corrections.

7.1.5 Water Layer

A water layer has been introduced into the data before inversion by including a horizon at the seabed. Constant values of two-way zero-offset time (81 ms) and moveout velocity (1480 m/s) have been set for this horizon, corresponding to an effective water depth of 60 m (measured from the Survey A datum, Section 2.1.1), with a water velocity of 1480 m/s. Both inline and crossline time slopes are zero as the assumed seabed is horizontal. This inclusion merely subdivides the uppermost Surface - Brown seismic interval in order to separate the water layer from the Seabed - Brown lithological interval.

7.2 SUMMARY OF WELL INFORMATION

Comparison with interval velocities at wells provides the ultimate test of the validity of interval velocities derived by the Hubral algorithm. In view of the importance of well velocities, the three vertical wells and one deviated well available for this study (Chapter Two) are seen to be a sparse database. Moreover, it is reduced still further since no detailed velocity analyses were performed for seismic line A-136 which ties to Well B, and hence this well cannot be used for the purposes of checking interval velocities derived from moveout velocities. Wells A and C (together with the deviated well CC) therefore provide the only opportunities for this crucial comparison.

7.2.1 Interval Velocities at Wells

The well interval velocities which have been used for checking the derived interval velocities are those which best correspond to the velocities sampled along the hypothetical zero-offset raypaths which are calculated by the Hubral algorithm. This approach is generally not equivalent to checking derived interval velocities against the precise interval velocities encountered along each well bore (except for the simple case of a vertical well and horizontal layering). This latter approach has not been adopted since in this case the interval velocities do not correspond to zero-offset raypaths. The estimation of interval velocities for ground points at the surface locations of Wells A and C is discussed below.

Since Well A lies very near to the crest of the structure and the reflectors are locally near-horizontal, the zero-offset raypaths calculated in the Hubral algorithm are near-vertical. As Well A is vertical, the zero-offset raypaths sample the velocity distribution of the rocks close to the well bore and the interval velocities derived by the Hubral algorithm can be compared directly with those obtained from the calibrated velocity log at the well. These interval velocities have been presented previously in Chapter Two (Table 2.9) and are summarised below:

WELL A:	SEABED	
		1969 m/s
	BROWN	
		2104 m/s
	PINK	
		2414 m/s
	YELLOW	
		4038 m/s
	ORANGE	
		3086 m/s
	RED	

Two seismic ties are available at Well A, namely line A-111 at shot point 600 and line A-132 at shot point 240.

The comparison of interval velocities at Wells C and CC is less straightforward. As these wells were drilled on the flank of the structure where reflectors are dipping and velocity gradients have been observed (Section 2.4.2), the zero-offset raypaths calculated by the Hubral algorithm for a ground point at the surface location of the well are not vertical. Interval velocities derived by the Hubral algorithm therefore cannot strictly be checked directly against those obtained from the calibrated velocity logs for the vertical Well C or the deviated well CC, as the zero-offset energy is not travelling along either of the well bores. Since the deviated well CC kicked off from the vertical above the depth corresponding to the Brown horizon, all seismic intervals are affected.

In order to estimate the appropriate interval velocities at a fixed surface location, the BP raytracing program (Section 6.1) was used. A zero-offset raypath was traced to each reflector of the ground model defined by the depths, dips and interval velocities for Wells C and CC in Table 2.11. Linear velocity gradients were assumed in each layer. As the deviation was drilled within one or two degrees of the true dip direction, the ground model has been assumed to be two-dimensional. The required interval velocity for a layer was then available as the interval velocity encountered in the model along the deepest segment of the zero-offset raypath to the reflector at the base of that layer. The following interval velocities were obtained:

WELL C/CC:	SEABED	
		1971 m/s
	BROWN	
		2131 m/s
	PINK	
		2523 m/s
	YELLOW	
		4340 m/s
	ORANGE	
		3071 m/s
	RED	

These interval velocities represent those which would ideally be encountered along a zero-offset raypath calculated by the Hubral algorithm. Although the modelling involved in this approach does introduce further uncertainty into the checking procedure, the paucity of well information requires that the data for Wells C and CC must be used in some way. The interval velocities above are subsequently referred to as those of Well C unless otherwise stated.

A further two seismic ties are available for Well C, as lines A-115 (shot point 838) and A-130 (shot point 312) intersect at the surface well location.

7.2.2 Quantification of Interval Velocity Error

For each horizon, four ties are available to compare interval velocities derived by the Hubral algorithm with the well interval velocities presented above. In the context of this project, the 'error' is defined as:

ERROR = HUBRAL INTERVAL VELOCITY - WELL INTERVAL VELOCITY (7.1)

It is then possible to quantify the error by calculating two statistics for each horizon, namely the sample mean and sample standard deviation of the four errors.

7.2.3 Expected Error due to the Spread Length Effect

Interval velocities derived by the Hubral algorithm are subject to the great variety of factors influencing moveout velocities described in Section 1.4. The magnitude of one of the significant subsurface effects can be estimated at this stage, namely that due to the spread length. This effect is manifest in interval velocity estimates since the normal moveout velocities (pertaining to zero spread length) are not available from real data and must be approximated by moveout velocities which generally contain a positive bias (Section 1.4.2.1). Variations of this bias between the horizons at the top and base of an interval are likely to cause a systematic error in the derived interval velocities.

The magnitudes of such interval velocity errors have been estimated for each layer by CMP raytracing over the ground models defined previously for Wells A and C (Tables 2.9 and 2.11), followed by Hubral inversion of the modelled two-way stacked times, moveout velocities and time slopes. CMP raytracing was performed by the BP raytracing program using the following CMP geometry:

- number of traces: 10
- near offset: 300 m
- offset increment: 300 m
- spread length: 3000 m

which is an adequate representation of the actual Survey A geometry for this purpose. Two-way stacked times and moveout velocities were calculated for each horizon using CMP gathers centred at the surface locations of the wells. In addition, the two-way stacked times were also calculated for a CMP gather centred 100 m distant from the surface location of Well C in order to estimate the inline time slopes for the dipping reflections observed over this model. Since this ground model is two-dimensional (Section 7.2.1) the crossline time slopes are zero, as are both inline and crossline time slopes for the horizontally layered ground model at Well A. The two-way stacked times, moveout velocities and time slopes obtained by CMP raytracing are presented in Table 7.1.

These data were then used to derive interval velocities in the Hubral algorithm. The results of inversion, together with the magnitudes of the errors (as defined in Section 7.2.2) are also included in Table 7.1. Note that the zero-value inline and crossline time slopes for the ground model at Well A imply a 'Dix' (1D) inversion, while the zero-value crossline time slopes for the ground model at Well C imply a 'Shah' (2D) inversion.

The error does not reach a significant level at depths shallower than the Yellow-Orange (carbonate) interval. The spread length effect within the shallower section is therefore small. Indeed, errors of less than 5 m/s are probably dominated by numerical inaccuracy. In contrast, the error for the Yellow-Orange interval reaches a value of around six per cent at both wells. This is due largely to the differential moveout velocity bias between the Yellow and Orange horizons. Table 7.2 lists the moveout velocity bias for each of the horizons in the ground model for Well A obtained by comparing the moveout velocities of Table 7.1 with the normal moveout velocities obtained by the Hubral forward modelling algorithm (which are in this 'one-dimensional' case simply the vertical RMS velocities). A similar study has not been attempted for the ground model at Well C as the interval velocity gradients are not handled correctly by the forward modelling algorithm. The greater bias in moveout velocities on the Orange horizon is caused by the strong velocity contrast encountered at the top of the carbonate interval, and the interval velocities derived by the Hubral algorithm are exaggerated accordingly.

Errors for the Orange-Red interval are reduced in magnitude down to below two per cent, but are negative values. The reason for this change in sign is partly that the moveout velocity bias is actually smaller on the Red horizon than on the Orange horizon (Table 7.2). The Orange-Red interval velocity is then underestimated in order to compensate the effect of the overestimated Yellow-Orange interval velocity.

As the lithology, and hence the interval velocity, of each layer is thought to remain reasonably uniform over the survey area, expected errors due to the spread length effect are not likely to vary significantly from those presented above. While these errors are generally small for the shallower three intervals, interval velocities in the Yellow-Orange interval are likely to be overestimated by 5-6% and those in the Orange-Red interval may be underestimated by 1-2%. The compensation of errors observed in the Orange-Red interval provides a striking example of a case where layer-by-layer inversion would appear to be preferable, allowing an attempt to correct systematic errors in one interval before proceeding to invert the next.

7.3 DIRECT INVERSIONS

The 'direct' inversion procedure is the simplest method for obtaining interval velocities using the Hubral algorithm in KRUNCH. The inversion is performed just once at each location in order to derive the limited local ground model down to the deepest reflector (Section 4.5.3). The objective of this section is to present the results of the direct inversion obtained by various combinations of smoothing moveout velocities before inversion, and smoothing interval velocities after inversion.

In line with the reasoning presented in Section 3.2.3.1 for the preference of boxcar moving average filters over conventional low-pass filters applied to moveout velocity profiles, only simple boxcar filters have been used in this chapter. Four filters were used which can be applied to both moveout velocities and interval velocities. In addition to boxcar moving averages of lengths 1.5, 3.0, 4.5 and 6.0 km, the logical limits of smoothing are represented by the raw data and the line means (Section 3.2.3.2).

There are thus 36 possible combinations of smoothing moveout velocities and interval velocities in the direct inversion procedure outlined here. Any of the six cases can be applied to moveout velocities before inversion, and either can then be applied to the interval velocities after inversion. Since the ground model is not monitored or adjusted during direct inversion at a single ground point, it is convenient to perform moveout velocity smoothing on all horizons before inversion and interval velocity smoothing for all intervals after inversion.

Interval velocity profiles for a direct inversion with no smoothing applied to either moveout velocities or interval velocities are shown in Figure 7.1. Interval velocities are plotted at normal incidence point locations since this is the best representation of the zone sampled by the CMP gather. The high degree of scatter evident in the interval velocity profiles is very pertinent to the discussion in this section. This scatter tends to increase downwards from a minimum in the Seabed-Brown interval to a maximum in the Orange-Red interval and includes many interval velocities outside the 'expected' range of 1900-5000 m/s (from the well velocities reviewed in Section 7.2.1).

Normal incidence point locations are described above as the best representation of the zone sampled by the CMP gather. However, the smoothing of interval velocities in KRUNCH acts along slightly different interval velocity profiles, where the spatial location of each interval velocity estimate is referred to the ground point at the origin of the zero-offset raypath. These are equispaced because the original velocity analyses were equispaced. Figure 7.2 presents the same interval velocities plotted in this manner. The interval velocity profiles are generally similar in both Figures 7.1 and 7.2, except for a slight focussing of data over the anticlinal features and defocussing over synclinal features in Figure 7.1. The similarity of the two figures is advanced in support of smoothing along the equispaced profiles being valid in a spatial sense, though one could indeed argue that use of the profiles in Figure 7.1 (by resampling, for example) would strictly be more 'correct'. Errors incurred by this simplification are, however, not likely to dominate the results of inversion, and this course is not pursued further here.

Appraisal of the various smoothing combinations is now made by reference both to the consistency of the derived interval velocities at line intersections and to the comparison of Hubral interval velocities with interval velocities at wells.

7.3.1 Spatial Consistency of Derived Interval Velocities

When the direct inversion for one of the 36 smoothing combinations is complete, the RMS interval velocity mis-tie can be calculated from interval velocities interpolated at the 16 line intersections. The RMS interval velocity mis-tie is defined in an identical manner to the RMS moveout velocity mis-tie of Section 3.1.5.3, i.e.

$$\text{RMS Mis-tie} = \sqrt{\frac{1}{L}\sum_{\ell=1}^{L} M_\ell^2} \tag{3.33}$$

where there are L line intersections and M_ℓ now represents the interval velocity mis-tie at the ℓth intersection.

Graphs of the RMS interval velocity mis-ties calculated for each of the 36 smoothing combinations are plotted separately for each of the five intervals in Figure 7.3. Each graph consists of six curves which represent the six moveout velocity operators. Each curve is connected through six points which represent the six interval velocity operators. In each graph, mis-ties derived for the raw data are plotted at zero boxcar length, while those derived for the line mean interval velocities are plotted at a nominal distance to the right of the mis-ties from the boxcar filters.

The data are presented in this way as each curve then represents the variation of RMS interval velocity mis-ties with interval velocity operator from a common moveout velocity database for a different moveout velocity operator. It is then possible to ascertain the relative effects of smoothing either moveout velocities or interval velocities.

Whereas there are sound reasons for expecting mis-ties of moveout velocities at line intersections (both moveout velocities and normal moveout velocities vary with azimuth in the presence of reflector dip), interval velocities derived by the Hubral algorithm should ideally tie at line intersections. The Hubral algorithm seeks to account for the dip component of normal moveout velocities, and if the surface data are consistent, an identical zero-offset raypath should ideally be derived for the ground points on both lines at the intersection. Use of the word 'ideally' is significant, however, as real moveout velocities contain many other components than those due to dip alone (Section 1.4). A perfect interval velocity tie at an intersection is therefore unlikely, even if the ground model were limited to layers of constant velocity separated by plane dipping interfaces. Nevertheless, there is more reason to expect interval velocities to tie at line intersections than there is to expect a similar consistency of moveout velocities. The spatial consistency of interval velocities is assessed in this section by reference to the performance of each smoothing combination in reducing the RMS interval velocity mis-tie.

One general point should be made before proceeding to specific observations from the mis-tie curves in Figure 7.3. RMS interval velocity mis-ties tend to decrease as the degree of smoothing increases. This decrease is generally rapid in going from the raw data to short filters but is much less marked where combinations of longer filters (and line means) are used. On each graph the RMS interval velocity mis-ties decrease to a level beyond which further smoothing is of no apparent benefit. The shape of the curves is controlled by the interaction of the reduction of random errors and the destruction of genuine spatially-consistent variation as the filter length increases. The point at which the curve begins to flatten marks the onset of the destruction of genuine spatial components, or 'oversmoothing'.

It is suggested here that on the basis of RMS interval velocity mis-ties alone, the optimum smoothing combination should be selected as that which offers the greatest reduction of RMS interval velocity mis-ties without oversmoothing, and with the minimum smoothing of both moveout velocities and interval velocities. This statement constitutes what is referred to here as the 'minimum smoothing criterion'.

Analysis of the RMS interval velocity mis-ties presented in Figure 7.3 allows the following observations:

(a) The magnitude of RMS interval velocity mis-ties for different intervals tends to increase progressively downwards from the Seabed-Brown interval to the Orange-Red interval. The effect is due largely to the increase of moveout velocity fluctuation with depth (Section 2.3.2). This causes a corresponding downwards increase of RMS moveout velocity mis-ties (Section 3.2.3.2) and gives rise to the observed increase of RMS interval velocity mis-ties. Interval velocity fluctuations, and hence RMS interval velocity mis-ties, tend to be rather higher (relative to this general trend) in the thinner Pink-Yellow and Orange-Red intervals due to the magnification of errors in a thin interval. The particularly low RMS interval velocity mis-ties in the Seabed-Brown interval are due partly to the thickness of this interval, but more significantly to the constant moveout velocity assumed for the seabed at the top of the interval (Section 7.1.5). RMS interval velocity mis-ties in the four lower intervals are, of course, subject to moveout velocity fluctuation at both the top and base of the intervals.

(b) For each moveout velocity filter, the RMS interval velocity mis-tie generally reduces as the length of the interval velocity filter is increased. This effect is most apparent for the shorter moveout velocity filters.

(c) For each interval velocity filter, the RMS interval velocity mis-tie generally reduces as the length of the moveout velocity filter is increased. This effect is most apparent for the shorter interval velocity filters.

(d) For each interval, a region can be identified on the graph where the RMS interval velocity mis-tie curves tend to converge and flatten as described above. The convergence indicates that further smoothing of moveout velocity profiles has little effect on the mis-ties, while the flattening indicates oversmoothing.

(e) In four out of the five intervals the line mean moveout velocity filter appears to offer the greatest reduction of RMS interval velocity mis-ties for any one interval velocity filter. In contrast, the RMS interval velocity mis-ties derived from line mean moveout velocities in the Yellow-Orange interval are significantly greater than those derived from the alternative moveout velocity filters, including the raw moveout velocities. This observation is explained by the presence of significant velocity gradients in the carbonate interval (Section 2.4.2), the effects of which are grossly distorted by the line mean moveout velocity filter.

(f) Similarly, the line mean interval velocity operator offers little advantage. Only in the shallowest two intervals are the RMS interval velocity mis-ties reduced by the application of this operator, and here the reduction is small. In the deeper intervals, RMS interval velocity mis-ties are generally increased by the line mean interval velocity filter, which indicates a gross distortion of the real interval velocity variation.

On the basis of RMS interval velocity mis-ties alone, there is no obvious unique choice of smoothing combination for each interval. Moreover, the treatment above is far from exhaustive as only a limited selection of filter lengths of a single filter type have been used in the analysis. Nevertheless, the reduction of RMS interval velocity mis-ties afforded by these rather crude filters is quite significant when compared to the magnitude of mis-ties generated by the raw data, and selection of a smoothing combination to effect such a reduction is possible, albeit with an element of subjectivity.

Using the minimum smoothing criterion outlined above, the smoothing combinations selected for direct inversion are listed in Table 7.3 and are highlighted on the graphs in Figure 7.3. The choice of raw moveout velocities for the shallower three intervals may appear rather provocative. However, on the basis of RMS mis-ties, the anomalous variation is better removed from the interval velocity profiles. This decision may be partly related to the limited number of filters to choose from - a short boxcar of, say, 0.5 km may be more appropriate in general. The moveout velocity smoothing required for the two deepest intervals is attributed to the need to reduce the increased moveout velocity fluctuation observed on the Orange and Red horizons (Section 3.2.2). In each case, the 3 km boxcar filter is preferred for interval velocity smoothing, indicating a tendency for anomalous interval velocity components to occur with wavelengths around the spread length.

Although the downward increase of RMS interval velocity mis-ties has previously been attributed to a corresponding increase of moveout velocity fluctuation in (a) above, it is possible that this observation is also due in part to an inherent limitation of the direct inversion procedure itself. As explained in Section 4.5.3, the direct inversion procedure is subject to downward error propagation. Inversion errors in the shallower layers persist as the ground model is extended downwards at each ground point, giving scope for increased errors in the deeper target layers and ultimately to an increase in RMS interval velocity mis-ties.

7.3.2 Comparison with Interval Velocities at Wells

When the direct inversion of one of the 36 smoothing combinations is complete, the resulting interval velocities can be compared with the interval velocities at Wells A and C described in Section 7.2.1. This comparison is made by calculating the mean and standard deviation of the four errors as defined in Section 7.2.2.

The resulting means and standard deviations have then been presented in a similar format to that adopted for the RMS interval velocity mis-ties in the last section. Figures 7.4 and 7.5 present the variation of means and standard deviations of the four interval velocity errors with different smoothing combinations. The data are again plotted against interval velocity boxcar length, and each curve once more represents a common moveout velocity operator. The smoothing combinations selected in Section 7.3.1 using the minimum smoothing criterion are highlighted on both figures.

Examination of the curves presented in Figures 7.4 and 7.5 has enabled the following observations to be made:

(a) The mean error is positive in nearly every case, indicating that interval velocities derived by the Hubral algorithm are generally higher than those obtained from well information.

(b) The magnitude of both mean and standard deviation of the errors shows a general increase downwards from the Seabed-Brown interval to the Orange-Red interval. This trend, which was also observed in the RMS interval velocity mis-ties, is again related to the increasing fluctuation of moveout velocity with depth.

(c) For each interval, the mean error generally increases as the length of both moveout velocity and interval velocity filters is increased. This observation should not be used to infer that the raw data gives a better estimate at the well which is damaged by filtering. Rather, a significant error exists in all cases, and the mean error curves are a poor indicator of the optimum smoothing combination. The curve for the line mean moveout velocity operator is in each case considerably separated from the curves for the boxcar filters, indicating that line means are generally inappropriate. Similarly, for each of the moveout velocity cases, application of the line mean interval velocity operator after inversion causes a considerable increase in the mean error.

(d) For each interval, the standard deviation of the error generally decreases as the length of both moveout velocity and interval velocity filters is increased. The most obvious exception to this general trend is the relatively high standard deviation for the line mean moveout velocities in the Yellow-Orange interval, which is thought to be due to gross distortion of valid moveout velocity trends in accordance with a similar observation in Section 7.3.1(e).

The relation of the mean interval velocity error curves to the expected errors due to spread length effects (Section 7.2.3) is not straightforward. Mean errors for the smoothing combination selected by the minimum smoothing criterion are listed in Table 7.3, and it is immediately apparent that the observed interval velocity errors cannot be attributed simply to this effect. The mean interval velocity error is also quoted as a percentage which is the average of the mean error expressed as a percentage of the actual interval velocity at Wells A and C.

In the three shallower intervals, the expected interval velocity error (Table 7.1) is in all cases less than 0.5% at Wells A and C. However, the observed mean errors are consistently an order of magnitude higher over these three intervals. In contrast, the expected errors for the Yellow-Orange and Orange-Red interval velocities do at least fall into the range of observed mean errors. Nevertheless, in view of the discrepancies observed for the three shallower intervals, selection of a smoothing combination on the basis of expected errors due to the spread length effect is clearly not desirable. The role of the mean interval velocity error in direct inversion procedures is discussed further in Section 7.3.3.

In common with the RMS interval velocity mis-ties in Section 7.3.1, the mean interval velocity error is also subject to downward error propagation during direct inversion. Moreover, since the mean error represents a systematic bias, interval velocity estimates in deeper target layers are liable to be corrupted in a systematic fashion by inversion errors in the layers above. Although the expected interval velocity errors due to the spread length effect are not supported by the observed mean errors, the case for layer-by-layer inversion made in the concluding paragraph of Section 7.2.3 is still valid.

7.3.3 A Strategy for Direct Inversion

While a formidable quantity of data has been processed and displayed in order to judge smoothing combinations in conjunction with the direct inversion procedure, interpretation of the results does not yield an immediate solution. Comparison of the smoothed derived interval velocities with measurements at wells has not proved useful in determining an 'optimal' smoothing combination, while the choice made on the basis of RMS interval velocity mis-ties is not conclusive.

It is suggested here that the choice of a smoothing combination for direct inversion should be dominated by the need to reduce RMS interval velocity misties with reference to the minimum smoothing criterion introduced in Section 7.3.1. Such a choice allows a balance to be made between the need to obtain a spatially consistent data set and the need to avoid distortion of the data set by oversmoothing. The resulting smoothed interval velocities can then be scaled or 'calibrated' by reference to the mean interval velocity error observed for the selected smoothing combination. In this way the derived interval velocities can be adjusted to conform (approximately) to the well interval velocities, albeit in a rather empirical manner.

Interval velocities derived using the selected smoothing combination have been calibrated by reference to the percentage mean interval velocity errors presented in Table 7.3. These calibration factors have been determined from the relation:

$$\text{CALIBRATION FACTOR} = \frac{100}{(100 + \%\ \text{MEAN INTERVAL VELOCITY ERROR})} \qquad (7.2)$$

and are also listed in Table 7.3. The resulting interval velocities (obtained by direct inversion using the selected smoothing combination and these calibration factors) are presented in Figure 7.6. Calibration in this way therefore performs a reduction of interval velocities over the entire survey area, as the percentage mean interval velocity error is positive for each seismic interval studied here. These data are discussed further in Section 7.5.

7.4 LAYER-BY-LAYER INVERSIONS

The theoretical case for preference of layer-by-layer inversion over direct inversion has been presented in Section 4.5.3. In summary, the layer-by-layer inversion procedure allows one layer to be inverted at a time, thus accomodating adjustment of interval velocities in the ground model before proceeding to the next layer. This case has been supported by the study of 'synthetic' data over a typical North Sea structure in Section 6.6, and the purpose of this section is to investigate the interval velocities derived by layer-by-layer inversion from real seismic data.

The logic and criteria used in this section to judge the validity of derived interval velocities are very similar to those used for the direct inversion in Section 7.3. The same six procedures have been used to smooth moveout velocities before inversion and interval velocities after inversion, yielding the same 36 possible smoothing combinations. The difference lies in the order in which the data are processed.

Following a trivial direct inversion to the assumed seabed, each of the five seismic intervals were inverted in turn. In each case, all ground points were used over the eight seismic lines to perform moveout velocity smoothing, followed by Hubral 3D inversion for interval velocities, and then interval velocity smoothing in the target layer. The results of each of the 36 smoothing combinations can then be assessed by reference to the interval velocity statistics used in Section 7.3 (i.e. RMS interval velocity mis-ties and the mean and standard deviation of interval velocity errors at wells). This procedure allows the selected smoothing combination and interval velocity 'calibration factor' (Section 7.3.3) to be applied in order to define interval velocities in the target layer. Each layer is then inverted in turn.

One important feature of layer-by-layer inversions is worthy of comment at this stage. Interval velocities derived during layer-by-layer inversion are generally (for this data set) greater than those derived by direct inversion. This is due both to the calibration of interval velocities in the ground model and to the nature of the Hubral inversion algorithm itself. In the direct inversions, interval velocities derived by the Hubral algorithm were consistently greater than those observed at the wells, and calibration was used to reduce the derived interval velocities by a constant scale factor. This same observation is made for each interval during layer-by-layer inversion. However, whereas in the direct mode all calibrations are made after inversion, the layer-by-layer mode requires inversion of the target layer through an overburden which has already been calibrated. The wavefront curvature calculated through this calibrated overburden to the reflector defining the top of the target layer represents a zero-offset parameter. In contrast, the moveout velocity (used as an estimate of normal moveout velocity) of the horizon defining the base of the target layer is subject to the effects of non-zero spread length. The spread length effect is therefore concentrated into the target interval. These circumstances are radically different to those of direct inversion, where moveout velocities of horizons at both the top and base of the target layer are subject to spread length effects. The spread length effect is accordingly magnified in the layer-by-layer inversion relative to the direct inversion, and increases as the target layer decreases in thickness. It is this magnification which causes the calibration factors presented below to depart significantly from unity. The resulting calibrated interval velocities are, however, still constrained by the well interval velocities, and should therefore assume similar absolute values to the calibrated interval velocities from direct inversion.

Inversion statistics for the layer-by-layer inversion are now discussed. Graphs of RMS interval velocity mis-ties, and of means and standard deviations of interval velocity errors at wells, are presented in Figures 7.7 through 7.11 for each interval. These graphs take the same form as those for the direct inversions in Section 7.3, and have been used to select smoothing combinations and calibration factors in a similar manner. These selections are summarised for each interval in Table 7.4. The exaggeration of interval velocities derived by layer-by-layer inversion (discussed above) is apparent in each of the three interval velocity statistics.

(a) Surface-Seabed Interval (Water Layer)

Since a dummy layer of constant thickness and interval velocity was included at the top of the model (Section 7.1.5), a simple direct inversion to the seabed was employed to derive the parameters of the first layer and the first depth interface. This inversion is, of course, free from error since the nature of this layer implies vertical zero-offset raypaths through a constant velocity medium.

(b) Seabed-Brown Interval (Figure 7.7)

As no errors are generated by inversion of the water layer, layer-by-layer inversion for velocities in the Seabed-Brown interval yields identical results to those obtained during the direct inversions of Section 7.3. The graphs of interval velocity statistics presented in Figure 7.7 are therefore identical to the corresponding graphs of Figures 7.3, 7.4 and 7.5, respectively. The selected smoothing combination and calibration factor are accordingly the same as the choice made for direct inversion.

(c) Brown-Pink Interval (Figure 7.8)

The shape of the RMS mis-tie curves is very similar to that for the direct inversion of the Brown-Pink interval, due largely to the use of the same smoothing combination for the overlying interval in both the direct and layer-by-layer inversion procedures. There is an important difference, however, in the magnitude of RMS mis-ties derived for each mode of inversion. This difference is also observed in the mean interval velocity errors at wells, and is due to the derived interval velocities being significantly greater for the layer-by-layer mode of inversion (as described above).

On the basis of the minimum smoothing criterion and the calibration procedure described above, interval velocities derived from raw moveout velocities have been smoothed by a 3 km boxcar filter and scaled by the calibration factor 0.735.

(d) Pink-Yellow Interval (Figure 7.9)

For each moveout velocity operator, the RMS interval velocity mis-tie curves reach a minimum at the 1.5 km interval velocity boxcar length. The spatial consistency of Pink-Yellow interval velocities is therefore improved by the application of this filter. On the basis of the minimum smoothing criterion, a 1.5 km moveout velocity boxcar filter has been chosen to complete the smoothing combination. The increase of RMS interval velocity mis-ties for longer interval velocity boxcars indicates that the data have been 'oversmoothed', resulting in a distortion of real spatial components of interval velocity.

As for the overlying interval, calibration of the ground model to the top of the target layer has resulted in the exaggeration of derived interval velocities indicated by the mean error curves. The high magnitude of the mean errors is explained by the greater influence of the spread length effect on the Yellow horizon in this generally thin interval (the Pink-Yellow time interval is of the order of one-quarter of the Brown-Pink interval). Pink-Yellow interval velocities have been scaled by the factor 0.539.

(e) <u>Yellow-Orange Interval (Figure 7.10)</u>

RMS interval velocity mis-ties for this layer show a considerable reduction at the 3 km interval velocity boxcar with no further improvement for longer filters. The increase of RMS mis-ties for line mean interval velocities again indicates oversmoothing. The 1.5 km moveout velocity boxcar has been selected to complete the smoothing combination in view of its marginal reduction of RMS interval velocity mis-ties relative to the raw interval velocities.

As expected, the derived interval velocities are again exaggerated by the calibration of the overlying ground model. Yellow-Orange interval velocities have been scaled by 0.831.

(f) <u>Orange-Red (Figure 7.11)</u>

The form of the RMS interval velocity mis-tie curves again illustrates a minimum at the 3 km interval velocity boxcar with oversmoothing for longer filters. A smoothing combination of the 1.5 km moveout velocity boxcar and the 3 km interval velocity boxcar has been selected for the Orange-Red interval.

The large magnitude of both RMS interval velocity mis-ties and mean interval velocity errors is attributed to the very thin nature of the interval. A calibration factor of 0.655 has been used for the Orange-Red interval velocities.

Interval velocities derived in this manner are displayed for each line in Figures 7.12 and 7.13. Interval velocities are plotted at normal incidence point locations in Figure 7.12 and at ground point locations in Figure 7.13. In common with raw interval velocities from the direct inversion (Figures 7.1 and 7.2), no serious discrepancies are observed between these two methods of plotting the data. As in the previous case, the only significant difference in the appearance of the plots is the slight focussing of data over the anticlinal features and defocussing over synclinal features observed in the normal incidence point plots.

A comparison of interval velocities derived by layer-by-layer inversion with those derived using the direct procedure is made in the following section.

7.5 DISCUSSION

Interval velocities have thus been derived for the eight lines of Survey A using the Hubral 3D inversion algorithm. Raw interval velocities and the 'optimal' solutions for both direct and layer-by-layer inversions have been presented. These solutions are optimal in the sense that they represent the interval velocities which most closely satisfy the demands of maximum spatial consistency with the minimum of smoothing. This section presents a brief discussion of the selected interval velocity profiles.

The high degree of scatter in the raw interval velocities shown in Figure 7.1 and 7.2 has been noted in Section 7.3. The scatter tends to increase downwards from the Seabed-Brown interval to the Orange-Red interval in accordance with similar trends of moveout velocity fluctuation. Superimposed on this general observation, however, is an increased scatter in both the Pink-Yellow and Orange-Red intervals. Reference to the interpreted seismic sections in Chapter Two (Figures 2.6 through 2.15) reveals that of the five seismic intervals, the Pink-Yellow and Orange-Red intervals are considerably thinner than the remaining three intervals, and are therefore less stable for interval velocity inversion by this method (Sections 1.3 and 4.5.2).

The increased variation of Pink-Yellow and Orange-Red interval velocities is retained through smoothing and is apparent in the optimal solutions for both the direct and layer-by-layer inversion procedures. This variation is particularly marked for the Orange-Red layer. While a considerable variation of interval velocities is to be expected in this onlapping interval of varying thickness, it is unlikely that interval velocities in excess of 5000 m/s are realistic. Indeed, the highest and most suspect Orange-Red interval velocities are observed where the interval is at its thinnest (the whole of line A-123, shot points 390-520 on line

A-130 and shot points 380-520 on line A-132, for example) and where the derivation of interval velocities from moveout velocities is at its most fallible.

A feature common to the optimal solutions for both direct and layer-by-layer inversions is extensive use of the 3 km boxcar filter in the selected smoothing combinations. Improvements in the spatial consistency of interval velocities obtained through the use of the 3 km boxcar filter are probably due to the harsh attenuation of anomalous spatial wavelengths around the spread length afforded by this filter. The need for attenuation of these spatial wavelengths derives from the anomalous components of moveout velocity profiles which are thought to be induced by the geometry of the CMP gather (Section 3.2.3.2).

It is difficult to resolve features in the derived interval velocity profiles which correspond precisely to individual components of the ground model. The effects of interval velocity gradients, reflector curvature, faulting and other time-delays are compounded in the moveout velocity profiles and remain that way in the derived interval velocities (see the illustrations in Chapter Six, for example).

Much of the scatter in the raw interval velocity profiles is attributed to the effects of faulting and other time-delays along offset CMP raypaths. However, it is probably largely attenuated by the smoothing of both moveout velocities and interval velocities and is not likely to be dominant in the 'optimal' interval velocity profiles.

The effects of reflector curvature in generating spurious interval velocity gradients are particularly hard to determine. Indeed, the apparent decrease of Orange-Red interval velocities and Yellow-Orange interval velocities over the anticlinal feature and increase downflank (see lines A-130 and A-132) was characteristic of anticlinal features with constant interval velocities (Sections

6.5 and 6.6). Nevertheless, that there is an interval velocity gradient, at least in the Yellow-Orange layer, is beyond doubt since such a gradient is indicated by the interval velocities at Wells A and C. Even for the valid gradients apparent in the interval velocity profiles, it is difficult to define the precise nature of the gradient (Section 6.3). The relative influence of compaction and lateral variations of lithology therefore cannot be estimated confidently.

These uncertainties should not be taken to infer that the lessons learnt in Chapter Six cannot be applied to the interpretation of interval velocities derived from moveout velocities over a survey area. Rather, it is preferable that subjective judgements based on these lessons are applied after what could be described as the more objective phase of interval velocity estimation presented here.

Interval velocities derived by the Hubral algorithm are consistently higher than those measured at wells. Calibration factors of less than unity have therefore been used to correct the derived interval velocities. The nature of this positive bias cannot be explained easily, since its magnitude is considerably greater than that predicted by raytracing CMP gathers through ground models at the well locations. Moreover, since both Wells A and C are situated towards the crest of the main structure, the bias not only exceeds that expected for non-zero spread length, but also outweighs the negative bias forecast over anticlines in Section 6.5.

The data set presented here is not unusual in exhibiting this discrepancy. The positive bias in interval velocities derived by 'wavefront curvature' inversion methods (Hubral, Shah or Dix) can rarely be attributed entirely to the spread length effect. At least one further process must be active in order to account for the magnitude of the bias. The rôle of velocity anisotropy (Section 1.4.2.2) in this context may be important. Banik (1984) has recently presented an interpretation of bias in RMS velocity - time curves in terms of velocity anisotropy for several wells in the North Sea. Although the treatment is simplistic, the dominant contribution of the effect from shaly intervals (which are likely to be the most anisotropic) is significant.

Differences between interval velocities resulting from the optimal direct and layer-by-layer inversions are generally not of a fundamental nature. This is due largely to the fact that similar smoothing combinations have been used in corresponding intervals for both modes of inversion. It is acknowledged that considerable differences exist between the calibration factors used in the two modes of inversion. This phenomenon has been discussed in Section 7.4, and is due to a concentration of the spread length effect into the target layer for layer-by-layer inversions following a calibration of interval velocities in the overburden. However, since calibration in both modes of inversion is constrained by the same well interval velocities, the resulting calibrated interval velocities are of a similar magnitude. The most obvious discrepancies are in the thinner Pink-Yellow and Orange-Red intervals, once more displaying their inherent instability for inversion. While plotting the interval velocities on a larger scale would, no doubt, reveal more subtle differences between the two solutions, the plots presented here show that the overall trends for the more stable Seabed-Brown, Brown-Pink and Yellow-Orange interval velocities are retained in the solutions chosen for both modes of inversion.

One might therefore be tempted to argue that no advantage is gained as a result of the additional work required to monitor the ground model as it is extended downwards in a layer-by-layer inversion, and that the results obtained from the direct inversion are equally valid. Furthermore, the departure of layer-by-layer calibration factors from unity casts serious doubts on the validity of this approach. Unfortunately, in the absence of further well information there is no way of discriminating between these two solutions. This uncertainty also precludes recommendation of either inversion procedure for different data sets.

The optimal interval velocity profiles presented in Sections 7.3 and 7.4 may be thought of as the limit of objective judgement on interval velocities derived from moveout velocities, since they are based on the criteria of minimising RMS interval velocity mis-ties with minimum smoothing. This statement must be immediately qualified by acknowledging that the treatment presented here is clearly not purely objective. The choice of seismic lines, the choice of seismic intervals and the choice of the boxcar moving average filter, for example, all influence the results presented here.

The important point, however, is that a general logic for judging the worth of interval velocities has been established, which is essentially independent of the seismic lines, seismic intervals and the type of filters used. The optimal interval velocity solution should be chosen from a suite of possible solutions derived by smoothing moveout velocity profiles before Hubral 3D inversion and smoothing interval velocity profiles after inversion. The optimal solution is then defined by the smoothing combination which offers the maximum spatial consistency with the minimum of smoothing. The use to which these interval velocities are ultimately put may necessitate 'editing' of a rather more subjective nature based, for example, on the lessons learnt from Chapter Six or on geological constraints. One particularly useful geological constraint would be the definition of upper and lower bounds for the velocity within each seismic interval. However, this treatment is inherently unique to the problem in hand, and is not discussed further here.

The logical framework presented in this chapter should provide a useful foundation for determining interval velocities from moveout velocities by reference to objective criteria.

7.6 SUMMARY

Two-way times, moveout velocities and both inline and crossline time slopes have been prepared in a separate KRUNCH matrix for each of the eight lines of Survey A. Lags have been removed from the two-way times and a water layer has been included.

Well control is available only at Wells A and C (and CC). Interval velocities pertaining to zero-offset raypaths for ground points at the surface locations of the wells have been compiled from the data presented in Chapter Two. Expected errors due to the spread length effect have been calculated for each horizon by raytracing.

Optimal interval velocity profiles have been determined for the direct inversion procedure on the basis of maximising their spatial consistency with the minimum of smoothing. Interval velocities have been calibrated by reference to the well interval velocities.

Using similar criteria, optimal interval velocity profiles have been presented for the layer-by-layer inversion procedure. In this case the ground model is monitored as it extends downwards, allowing smoothing and calibration of derived interval velocities before inversion of the next layer.

Optimal solutions for both direct and layer-by-layer inversion procedures employ very similar smoothing filters and generally show the same interval velocity trends. Although the interval velocity calibration factors are significantly higher for the layer-by-layer mode of inversion, the resulting calibrated interval velocities are of a similar magnitude in each case. Dissimilarity is most evident in the thinner Pink-Yellow and Orange-Red intervals, which are less stable for inversion. The 3 km boxcar filter is common in the selected smoothing combinations for both modes of inversion, due largely to its role in attenuating the effects of anomalous components of moveout velocity with wavelengths around the spread length.

The interval velocity profiles presented here represent the limit of objective judgement on the validity of interval velocities derived from moveout velocities. Further adjustments may be necessary before these interval velocities are used for time to depth conversion.

Contrary to expectations, the layer-by-layer inversion procedure has not allowed an interval velocity solution to be selected with any more confidence than that available from the direct inversion procedure. Moreover, the drastic calibration required to correct the derived interval velocities to well information (and extra effort required to process each layer separately) may render the layer-by-layer approach a less attractive option than direct inversion. Further studies using different data sets will be required to make a strong case for the general use of layer-by-layer inversion.

CONCLUSIONS

This thesis has presented a study of the derivation of interval velocities from moveout velocities. It is not suggested that such an exercise be attempted for all time to depth conversions. If there is a specific requirement, however, the exercise can be undertaken in a much more rigorous manner than is typical in current practise.

A method has been proposed for the 'inversion' of interval velocities from moveout velocities using a procedure which is a logical extension of the Dix Equation to three dimensions. An algorithm developed from the work of Hubral (1976a, 1976b) allows the derivation of interval velocities in a three-dimensional ground model limited to layers of uniform velocity separated by plane reflecting interfaces of arbitrary dip and strike. This algorithm has been incorporated within a database system which allows the spatial processing of both moveout velocities before inversion and interval velocities after inversion. The rôle of smoothing is particularly important, as it allows the attenuation of selected moveout velocity and interval velocity spatial fluctuations. Use of a range of smoothing operators then allows the contribution and validity of the attenuated components to be assessed by reference to the spatial consistency of the smoothed data.

Most of the conclusions of this project can be made within the context of the real data case study presented in Chapter Seven. Some important points arising from previous chapters are summarised in the list of guidelines towards the end of this section. It is first appropriate to review the objectives and scope of the project.

Optimal interval velocities have been obtained from moveout velocities over a seismic reflection survey area. These interval velocities are optimal in the sense that they have been selected from a suite of alternative solutions on the basis of objective criteria. The aim has been to maximise the spatial consistency of the derived interval velocities, while employing the minimum smoothing of both moveout velocities and interval velocities. The derived interval velocities have then been 'calibrated' to fit the absolute values of interval velocities measured from calibrated velocity logs at wells.

It is unlikely that these optimal interval velocities will be immediately useful for depth conversion. In the first place, as interval velocity mis-ties have been minimised rather than eliminated, some discrepancies still exist at line intersections. Furthermore, the simple nature of the calibration leaves some residual differences between the final interval velocities and those measured from calibrated velocity logs at wells. In addition, some unrealistic trends persist in the interval velocity profiles which require editing, particularly in the two thinner seismic intervals. A hiatus has been reached in the processing of these data, beyond which objective judgement must be relaxed and other lines of reasoning brought into play. Interval velocities can then be edited to exclude unrealistic values, and can be adjusted to tie both at line intersections and with well information. This final 'tidying-up' operation is necessary for accurate and consistent time to depth conversions over a survey area.

It is at this hiatus that the case study has been closed. These final adjustments may take the form of contouring time or depth residuals, or of absorbing these discrepancies with the velocities into an all-encompassing conversion factor (often called 'pseudo-velocity'). Such adjustments are, however, subjective in nature. The final method chosen depends on the degree of velocity variation, the amount of well control, the quality and density of velocity information from seismic data and, perhaps more significantly, on the tastes and prejudices of the geophysicist.

There has been no intention to embark upon such a tidying-up operation here. It is unlikely that any conclusions gained from the exercise would be directly applicable outside the context of this case study, whereas the methods advocated up to this point can be usefully administered to most other moveout velocity data sets.

The strength of this thesis therefore lies in the methods proposed for the selection of suitable interval velocities from a two-way time and moveout velocity data set. Conversely, its weakness is apparent in the very singularity of this data set. The results presented during the course of this thesis, particularly the choice of moveout velocity and interval velocity smoothing filters, pertain strictly to this data set alone. The case study has allowed characteristic moveout velocity and interval velocity periodicities to be detected. These appear to be correlated both to the spread length and to the spatial wavelength of subsurface structures and velocity variations. It has not, however, been the intention to prescribe specific smoothing filters for general use elsewhere.

Raw interval velocities derived from raw moveout velocities exhibit a considerable degree of scatter. This tends to increase both as the interval thickness reduces and as the depth of the interval increases (in accordance with a corresponding increase of moveout velocity fluctuation). The need for adequate spatial sampling is immediately apparent from these raw interval velocity profiles, as spatial aliasing is likely to occur if values are obtained at widely spaced ground points.

Both direct and layer-by-layer inversion procedures have been used to estimate optimal interval velocities from the data set. In both cases, moveout velocity and interval velocity smoothing combinations have been selected for each interval by maximising the spatial consistency of interval velocities with the minimum of smoothing. The spatial consistency is judged by reference to the root mean square interval velocity mis-tie calculated from all line intersections. Moveout velocities should not be expected to tie at line intersections if structure exists due to their inherent azimuthal variation. However, interval velocities at a line intersection pertain strictly to the same zero-offset raypath and should therefore tie precisely in the ideal case. Such a perfect tie is unlikely in the inversion of real data, but the contention that smoothing parameters should be determined by reference to mis-ties of interval velocity (in preference to mis-ties of moveout velocity) remains a valid one.

Optimal interval velocity solutions for the direct and layer-by-layer inversion procedures generally preserve the same major trends, due largely to the similarity of the smoothing combination selected for each interval. The 3 km boxcar moving average filter is prevalent in the smoothing combinations, indicating that an important moveout velocity component with a wavelength around that of the spread length is anomalous. The major difference between the two modes of inversion is in the magnitudes of calibration factors required to scale derived interval velocities to the values measured from calibrated velocity logs at wells. The considerably more severe calibration required for layer-by-layer inversion is due to previous calibration of interval velocities in the overlying ground model. However, the resulting calibrated interval velocity profiles are of very similar absolute magnitude for both modes of inversion, since both calibrations are constrained by the same well velocities. Although the layer-by-layer procedure may be conceptually preferable there is therefore little evidence from this data set to propose its general use in favour over the direct procedure. In both modes of inversion, the calibration factors are considerably greater than those predicted for the spread length effect by raytracing. This discrepancy, which may be due to the effects of velocity anisotropy, is disturbing since it precludes a confident deterministic calibration of interval velocities.

And so to the inevitable question: can accurate interval velocities be derived from moveout velocities? This is difficult to answer conclusively on the basis of evidence presented to this point. However, theoretical considerations and the results obtained from the 'synthetic' data study in Chapter Six and the real data case study in Chapter Seven indicate that if the answer is to be yes, the following guidelines should be adhered to:

(a) The subsurface should be of limited complexity; stacked seismic data and velocity analyses are unlikely to be of sufficient quality for velocity studies if the subsurface is dominated by buried focii and faults.

(b) Seismic data should ideally be of very high quality, with good signal to noise ratio and bandwidth.

(c) Velocity analyses should be made at closely spaced intervals along the seismic lines selected for velocity studies. The real data case study here suggests that a lateral spacing of around 250m between velocity analyses may be necessary to prevent spatial aliasing of moveout velocities. Where possible, lines should be selected which are approximately perpendicular to the dominant known (or expected) spatial velocity trends. Each of these lines should ideally be as long as possible in order to reduce end-effects resulting from the spatial smoothing of both moveout velocities and interval velocities. In addition, the lines should form a grid which provides sufficient intersections to allow a statistical analysis of mis-ties, and which ties to all available wells.

(d) The choice of seismic horizons should allow the subsurface to be subdivided into the major velocity units. It is particularly important that velocity units which vary significantly in thickness are defined. Very thin intervals should be avoided, particularly deeper in the section, since measurement of their lateral velocity variation will generally be beyond the resolution of seismic data.

(e) Moveout velocities should be picked at (or very near to) horizon times measured from stacked sections. Moveout velocity picks from adjacent velocity analyses then relate consistently to the same seismic horizons.

(f) The Hubral 3D inversion algorithm should be used to derive interval velocities if significant 3D structure is thought to exist. It is acknowledged that moveout velocities measured from real data are only an approximation to the (zero-offset) normal moveout velocities which are strictly required for a correct inversion. Nevertheless, this method can accommodate plane reflector dip in three dimensions and is clearly preferable to the Dix Equation if the structure is complex. The Hubral algorithm should be incorporated into a spatial database system which allows both direct and layer-by-layer modes of inversion in conjunction with spatial smoothing of velocities.

(g) Spatial smoothing should generally be applied both to moveout velocities before inversion and to the derived interval velocities after inversion. The spatial frequency response of the filter is limited by the length of the filter. However, smoothing end-effects are increased as the filter length increases. The type of filters selected will therefore be constrained by the length of seismic lines available for velocity studies.

(h) Selection of the optimal smoothing combination should be based on the need to improve the spatial consistency of interval velocities without excessive smoothing. The root mean square interval velocity mis-tie at line intersections has been used as a measure of the spatial consistency. Spatial consistency is improved as the root mean square interval velocity mis-tie is reduced by smoothing. The interval velocity solution should ideally be chosen from a suite of possible solutions, each generated by a different smoothing combination.

(i) Calibration of interval velocities should be performed to scale the derived interval velocities to the level of those measured from calibrated velocity logs at wells. This scaling is generally likely to take the form of a reduction of the derived interval velocities to match well velocities.

(j) Editing should then be undertaken to allow final adjustments of interval velocities at line intersections and well locations. Additional adjustments may be necessary if the derived interval velocities assume unrealistic values outside designated upper and lower bounds.

If accurate interval velocities are to be obtained from moveout velocities, the data must be given a chance. Sufficient time and effort must be spent to prepare a suitable data set and evaluate the results of inversion in response to various smoothing combinations. Only then can an optimal interval velocity solution be obtained.

Considerable damage has been done in the past, and continues to be done, by the flagrant abuse of seismic velocity data - particularly by mis-use of the Dix Equation. Interval velocities should be obtained from moveout velocities, and not from the stacking velocities selected by processing staff. Nor should they be obtained from widely spaced velocity analyses if the moveout velocity fluctuation is likely to be spatially aliased. They should not be obtained using the Dix Equation if structure is known to exist. Finally, they should not be judged by arbitrary smoothing methods without reference to their spatial consistency at line intersections.

The aim of this thesis has been to demonstrate that far superior and more objective methods are available for obtaining interval velocities without recourse to sophisticated and time-consuming modelling techniques. It is hoped that these methods can now be employed on a wider variety of moveout velocity data sets in order to determine their potential use in future interval velocity solutions.

It is perhaps appropriate to conclude with a modification of a familiar maxim. If a velocity problem is known to exist - it is worth solving properly.

RECOMMENDATIONS

The following points are recommended for further study:

(a) Application of the methods described in Chapter Seven to different data sets. Observations and conclusions made thus far relate specifically to the single data set studied for this project. Further data sets need to be analysed in order to make general statements on the subject of interval velocity inversion by the Hubral algorithm, particularly on the question of direct versus layer-by-layer inversion.

(b) Extension of the synthetic data study presented in Chapter Six to include 3D raytracing in a 3D ground model. The logic of Chapter Seven could then be used to obtain an interval velocity solution with reference to misties of derived interval velocities at line intersections.

(c) A study of interval velocities measured from calibrated velocity logs at wells should be made over selected areas with abundant well velocity information. Such a study would provide illustrations of the complexity of interval velocity fields occurring naturally in the subsurface (albeit rather sparsely sampled).

(d) The compromises made in Chapters Three and Seven to balance the conflicting requirements of optimising the spatial frequency response of filters and minimisation of smoothing end-effects can clearly be imroved upon. An attempt should be made to design short low-pass filters with an improved spatial frequency response in future work.

(e) Interval velocities derived by the Hubral algorithm are generally greater than those measured from calibrated velocity logs at wells. This systematic difference has been demonstrated in Chapter Seven, and cannot be attributed simply to 'spread length' effects. Further work should be undertaken to investigate possible causes of this problem. The rôle of velocity anisotropy may be important in this context. A better understanding of this characteristic discrepancy will be necessary to allow a more stringent 'calibration' of interval velocities derived by the Hubral algorithm.

INTERVAL VELOCITIES FROM MOVEOUT VELOCITIES OVER A SEISMIC REFLECTION SURVEY AREA

By

G.F. ALLEN

PART TWO

Tables, Diagrams and Appendices

A thesis submitted for the degree of Doctor of Philosophy
at the University of Leicester, April 1985.

CONTENTS

PART TWO

LIST OF TABLES

LIST OF FIGURES

LIST OF ENCLOSURES

	GROUND MODEL	FORWARD COMPUTATION	INVERSION
1D	Single layer with velocity V overlying horizontal plane reflector	$V_{mo} = V_{nmo} = V$	$V = V_{nmo} = V_{mo}$
1D	n layers of velocity V_i separated by horizontal plane reflectors	$V^2_{nmo,n} = V^2_{rms,n} = \frac{\sum_{i=1}^{n} V_i^2 \Delta t_i}{t_{o,n}}$ Dix (1955)	$V_n^2 = \frac{V^2_{rms,n} t_{o,n} - V^2_{rms,n-1} t_{o,n-1}}{t_{o,n} - t_{o,n-1}}$ Dix (1955)
2D	Single layer with velocity V overlying plane reflector with dip ξ in recording direction (dip line)	$V_{mo} = V_{nmo} = V/\cos\xi$ Levin (1971)	$V = V_{nmo}\cos\xi = V_{mo}\cos\xi$ $\left[\xi = \tan^{-1}\left(\frac{V_{nmo}}{2}\frac{dt_o}{dx}\right)\right]$ Levin (1971)
2D	n layers of velocity V_i separated by parallel plane reflectors with dip ξ in recording direction (dip line)	$V^2_{nmo,n} = \frac{V^2_{rms,n}}{\cos^2\xi} = \frac{1}{\cos^2\xi}\frac{\sum_{i=1}^{n} V_i^2 \Delta t_i}{t_{o,n}}$ Shah (1973b)	$V_n^2 = \cos^2\xi \frac{V^2_{rms,n} t_{o,n} - V^2_{rms,n-1} t_{o,n-1}}{t_{o,n} - t_{o,n-1}}$ Shah (1973b)
2D	n layers of velocity V_i separated by plane reflectors with arbitrary dip ξ_i in recording direction (dip line)	$V^2_{nmo,n} = \frac{1}{t_{o,n}\cos^2\beta_o}\sum_{i=1}^{n}\prod_{k=0}^{i-1}\frac{\cos^2\alpha_k}{\cos^2\beta_k} V_i^2 \Delta t_i$ Shah (1973b)	Not documented in open literature
3D	n layers of velocity V_i separated by plane reflectors of arbitrary dip ξ_i and strike θ_i	Hubral (1976b) Section 4.3 (q.v.)	Hubral (1976a) Section 4.4 (q.v.)

Key to Symbols Used:

- $V_{mo,n}$ is the moveout velocity at horizon n
- $V_{nmo,n}$ is the normal moveout velocity at horizon n
- $V_{rms,n}$ is the RMS velocity at horizon n
- V_i is the interval velocity of layer i
- $t_{o,n}$ is the two-way zero-offset reflection time to horizon n
- Δt_i is the two-way transit time in layer i
- α_k is the angle of incidence at horizon k
- β_k is the angle of refraction at horizon k
- β_o is the angle of emergence of the zero-offset ray

TABLE 1.1 Normal Moveout Velocity Formulae for Plane Layer Models

INSTRUMENTS	Texas Instruments DFS IV record length 6.0s; sample period 4ms filters: low-cut 8Hz, slope 18dB/octave high-cut 62Hz, slope 72dB/octave
SPREAD	60 group streamer (12 group HSSH + 48 group HSSG) HSSH streamer 64 phones over 47m tapered array HSSG streamer 32 phones over 91.2m linear array (overlapping arrays) group interval 50m reported near-trace offset 300m; cable depth 14m
SOURCE	airgun array (24 guns) depth of array 6.5m pop and shot point interval 25m
COVERAGE	60-fold; 60 trace CMP interval 25m near-trace 60, far-trace 1

TABLE 2.1 Survey A: Acquisition Parameters

1.	Adjacent trace summation	with differential NMO correction (2-fold) output 30 traces at 100m effective group interval
2.	Amplitude recovery	formula for curve $te^{0.00125t}$
3.	Deconvolution	operator 80ms (tapered autocorrelation) prewhitening 5% near-trace design gate 0.67 - 4.5s far-trace design gate 2.83 - 4.5s
4.	Early mutes	
5.	Bulk static correction	-20ms for 'high-cut filter delay'
6.	Normal moveout correction	velocities analysed using cross-correlation method (VLAN) every 1km
7.	Deconvolution	operator 2 x 100ms; prediction time 40ms near-trace design gates 0.64 - 2.88s 2.80 - 5.50s far-trace design gates 2.53 - 3.72s 2.80 - 5.50s
8.	Common mid point stack	30-fold
9.	Deconvolution	operator 3 x 140ms (tapered autocorrelation) prewhitening 5%, 5%, 20% design gates 0.5 - 2.6s 2.2 - 4.3s 3.8 - 5.8s
10.	Band-pass filter	time-variant operator 200ms time 0 - 1.3s filter 10,14 -50,60Hz 1.3 - 3.5s 6,10 -40,50Hz 3.5 - 4.1s 4,8 -35,45Hz 4.1 - 4.6s 3,7 -30,40Hz 4.6 - 6.0s 3,7 -24,32Hz
11.	Dynamic equalisation	initial time 0s initial gate length 250ms final gate length 1.0s

TABLE 2.2 Survey A: Processing Parameters for Final CMP Stacked Sections

1.	Adjacent trace summation	with differential NMO correction (2-fold) output 30 traces at 100m effective group interval
2.	Amplitude recovery	formula for curve $te^{0.00125t}$
3.	Common offset stack of adjacent CMP gathers	2-fold
4.	Deconvolution	operator 80ms (tapered autocorrelation) prewhitening 5% near-trace design gate 0.70 - 4.5s far-trace design gate 2.79 - 4.5s
5.	Deconvolution	operator 100ms; prediction time 40ms near-trace design gate 0.70 - 5.0s far-trace design gate 2.79 - 5.0s
6.	Early mutes	
7.	Band-pass filter	time-variant operator 200ms time 0 - 1.55s filter 10,14 - 50,60Hz 1.05 - 3.75s 6,10 - 40,50Hz 3.25 - 6.00s 3,7 - 30,40Hz
8.	Automatic gain control	gate length 100ms
9.	Programmed gain control	time 0s gain 80% 1.8s 25% 3.2s 25% 6.0s 80%
10.	Bulk static correction	-20ms for 'high-cut filter delay'

TABLE 2.3 Survey A: Processing Before Velocity Analysis

INSTRUMENTS	Texas instruments DFS V record length 6.0s; sample period 4ms filters: low-cut 3.5Hz, slope 18dB/octave high-cut 90Hz, slope 72dB/octave
SPREAD	240 channel cable; group interval 12.5m weighted and summed to 119 channels at 25m interval reported near-trace offset 200m; cable depth 12m
SOURCE	airgun array (14 guns) depth of array 7.5m pop and shot point interval 25m
COVERAGE	59/60-fold (119 trace) CMP interval 12.5m near-trace 1, far-trace 119

TABLE 2.4 Survey B: Acquisition Parameters

1.	Amplitude recovery	formula for curve $te^{0.3t}$ static correction for multiplexor delay
2.	Trace mix	3-fold with differential NMO correction weighting 1:2:1 output 60 traces at 50m effective group interval
3.	Bulk static correction	-15ms for source delay
4.	Low-cut filter	operator 500ms; 5,8Hz
5.	Deconvolution	operator 2 x 140ms prewhitening 2%, 2% near-trace design gates 0.88 - 2.85s 1.98 - 5.00s far-trace design gates 3.30 - 4.37s 3.30 - 5.00s
6.	Normal moveout correction	velocities analysed using cross-correlation method (VLAN) every 1km
7.	Early mutes	
8.	Trace equalisation	near-trace design gate 1.98 - 5.0s far-trace design gate 3.30 - 5.0s
9.	Common midpoint stack	60-fold
10.	Bulk static correction	15ms for shot and streamer depth
11.	Velocity filter	70% rejection of dips greater than +/- 12ms/trace
12.	Deconvolution	operator 2 x 300ms prewhitening 50%, 2% design gates 0.6 - 2.8s 0.2 - 5.0s
13.	Band-pass filter	time-variant operator 200ms application gates follow gross structural trends eg. time 0 - 0.90s filter 10,15 - 55, 65Hz 0.70 - 1.34s 7,12 - 50,60Hz 1.04 - 2.45s 5,10 - 45,55Hz 2.25 - 4.75s 5,8 - 40,50Hz 4.45 - 5.60s 5,8 - 35,45Hz 5.40 - 6.00s 5,8 - 30,40Hz
14.	Dynamic equalisation	initial time 0s initial gate length 250ms final gate length 1.5s

TABLE 2.5 Survey B: Processing Parameters for Final CMP Stacked Sections

1.	Amplitude recovery	formula for curve $te^{0.3t}$ static correction for multiplexor delay
2.	Trace mix	3-fold with differential NMO correction weighting 1:2:1 output 60 traces at 50m effective group interval
3.	Common offset stack of adjacent CMP gathers	4-fold
4.	Bulk static correction	-15ms for source delay
5.	Early mutes	
6.	Deconvolution	operator 140ms prewhitening 2% near-trace design gate 0.8 - 5.0s far-trace design gate 3.3 - 5.0s
7.	Band-pass filter	time-variant operator 200ms time 0 - 2.5s filter 5,10 -55,65Hz 1.5 - 6.0s 5,10 -40,50Hz
8.	Automatic gain control	gate length 100ms

TABLE 2.6 Survey B: Processing Before Velocity Analysis

Horizon	Polarity of first break	Stratigraphic boundary
BROWN	+	Limestone stringers over a 40m depth interval
PINK	+	Velocity increase at the top of a layer of tuffaceous mudstones and volcanic ash
YELLOW	+	Velocity increase at the top of a carbonate sequence
ORANGE	-	Velocity decrease at the base of the carbonate sequence
RED	-	Velocity decrease at the top of a layer of highly organic mudstones

Note that '+' implies compression, and
'-' implies rarefaction

(Each of the five seismic horizons was picked on a white trough)

TABLE 2.7 Correlation of Seismic Reflection Horizons with Stratigraphy

Well	Line SP	Horizon	Calibrated velocity log time ms t_l	Corrected log time ms t_l-15	Section time ms t_s	Delay ms $t_s-(t_l-15)$
A	A-111 SP 600	Brown	2167	2152	2170	18
		Pink	2512	2497	2530	33
		Yellow	2630	2615	2665	50
		Orange	2821	2806	2835	29
		Red	2974	2959	2995	36
A	A-132 SP 238	Brown	2167	2152	2170	18
		Pink	2512	2497	2535	38
		Yellow	2630	2615	2670	55
		Orange	2821	2806	2835	29
		Red	2974	2959	2995	36
B	A-136 SP 487	Brown	2228	2213	2240	27
		Pink	2592	2577	2615	38
		Yellow	2710	2695	2755	60
		Orange	2912	2897	2925	28
		Red	3041	3026	3060	34

Estimated Lags:

Brown	21ms
Pink	36ms
Yellow	55ms
Orange	29ms
Red	35ms

TABLE 2.8 Estimation of Lag for Each Horizon

WELL A

Rotary Table Elevation 25m
Water Depth 71m

Horizon	Depth BRT m	Depth Subsea m	Calibrated Two-way Time ms	Layer Thickness Δz m	Two-way Interval Time Δt ms	Average Interval Velocity V_i^a m/s	RMS Interval Velocity V_i^{rms} m/s	$\frac{V_i^{rms} - V_i^a}{V_i^a} \times 100\%$
MSL	25	0	0.0					
				71	95.9	1480	1480	0.0
SEABED	96	71	95.9					
				2039	2070.7	1969	1973	0.2
BROWN	2135	2110	2166.6					
				363	345.0	2104	2109	0.2
PINK	2498	2473	2511.6					
				143	118.5	2414	2416	0.2
YELLOW	2641	2616	2630.1					
				386	191.2	4038	4072	0.9
ORANGE	3027	3002	2821.3					
				235	152.3	3086	3095	0.3
RED	3262	3237	2973.6					

TABLE 2.9 Interval Velocities from Well A

WELL B

Rotary Table Elevation 25m
Water Depth 70m

Horizon	Depth BRT m	Depth Subsea m	Calibrated Two-way Time ms	Layer Thickness Δz m	Two-way Interval Time Δt ms	Average Interval Velocity V_i^a m/s	RMS Interval Velocity V_i^{rms} m/s	$\frac{V_i^{rms} - V_i^a}{V_i^a} \times 100\%$
MSL	25	0	0.0					
SEABED	95	70	94.6	70	94.6	1480	1480	0.0
BROWN	2190	2165	2227.9	2095	2133.3	1964	1968	0.2
PINK	2583	2558	2591.6	393	363.7	2161	2163	0.1
YELLOW	2737	2712	2710.0	154	118.4	2601	2609	0.4
ORANGE	3145	3120	2911.9	408	201.9	4042	4078	0.9
RED	3350	3325	3041.0	205	129.1	3176	3185	0.3

TABLE 2.10 Interval Velocities from Well B

WELLS C AND CC

Rotary Table Elevation 25m
Water Depth 71m

Horizon	Dip Degrees	WELL C Depth BRT m	WELL C Depth Subsea m	WELL C Interval Velocity m/s	WELL CC Depth* BRT m	WELL CC Depth* Subsea m	WELL CC Interval Velocity m/s
MSL		25	0		25	0	
				1480			1480
SEABED	0.0	96	71		96	71	
				1971			1971
BROWN	0.0	2215	2190		2247	2222	
				2137			2131
PINK	5.7	2632	2607		2655	2630	
				2544			2511
YELLOW	5.6	2792	2767		2827	2802	
				4544			4181
ORANGE	10.3	3255	3230		3262	3237	
				3093			3043
RED	9.3	3498	3473		3514	3489	

* Well CC was deviated from Well C at 1720m BRT. These data are drilled depths and have not been corrected to the vertical.

TABLE 2.11 Interval Velocities from Wells C and CC

Filter Length km	End of Pass Band km^{-1}	Start of Stop Band km^{-1}	Deviation	Deviation dB
3	0.29	0.31	0.447	-7.00
3	0.28	0.32	0.400	-7.97
3	0.25	0.35	0.287	-10.85
3	0.20	0.40	0.163	-15.74
6	0.29	0.31	0.382	-8.36
6	0.28	0.32	0.296	-10.59
6	0.25	0.35	0.143	-16.91
6	0.20	0.40	0.044	-27.17
12	0.29	0.31	0.279	-11.09
12	0.28	0.32	0.164	-15.72
12	0.25	0.35	0.038	-28.35
12	0.20	0.40	0.004	-47.63

TABLE 3.1

Performance of Low-pass Filters Designed by the Remez Exchange Algorithm

Length of Boxcar Moving Average km	RMS Moveout Velocity Mis-tie m/s				
	Brown	Pink	Yellow	Orange	Red
Raw Data	32.9	35.1	22.2	65.5	52.4
0.5	23.3	21.9	16.3	54.2	39.7
1.0	18.4	15.7	16.0	51.4	43.0
1.5	16.8	13.8	14.8	46.9	39.6
2.0	13.5	12.1	12.8	40.7	33.4
2.5	11.8	8.9	10.6	37.5	28.8
3.0	10.9	7.4	9.1	38.3	29.2
4.0	11.4	8.9	9.2	39.7	33.3
5.0	11.0	9.5	8.6	40.1	36.8
6.0	9.9	10.6	8.8	37.9	34.6
Line Means	7.4	4.9	10.6	50.7	54.8

TABLE 3.2

Variation of RMS Moveout Velocity Mis-tie with Length of Moving Average

(Including Line Intersections with Smoothing End-effects)

Length of Boxcar Moving Average km	Number of Valid Mis-ties	RMS Moveout Velocity Mis-tie m/s				
		Brown	Pink	Yellow	Orange	Red
Raw Data	16	32.9	35.1	22.2	65.5	52.4
0.5	16	23.3	21.9	16.3	54.2	39.7
1.0	16	18.4	15.7	16.0	51.4	43.0
1.5	16	16.8	13.8	14.8	46.9	36.9
2.0	16	13.5	12.1	12.8	40.7	33.4
2.5	8	15.0	10.1	11.8	32.1	35.4
3.0	8	14.2	8.5	9.7	38.0	35.3
4.0	8	14.4	9.8	8.7	48.0	42.1
5.0	6	15.2	12.1	8.9	45.3	39.8
6.0	6	13.0	13.7	11.0	46.3	35.3
Line Means	16	7.4	4.9	10.6	50.7	54.8

TABLE 3.3

Variation of RMS Moveout Velocity Mis-tie with Length of Moving Average

(Excluding Line Intersections with Smoothing End-effects)

GROUND MODEL I

Horizon	Vertical Depth ft	Maximum Dip		Interval Velocity ft/s
		Angle	Azimuth	
				5000
1	1038	21.4	45.0	6783
2	4873	15.7	-156.5	9748
3	9760	25.1	-11.4	

SIMULATED SURFACE MEASUREMENTS

Horizon	Two-Way Time s	Normal Incidence Point			Emergence Angles		Time Slopes ms/ft		Normal Moveout Velocity ft/s				Major Axis
		x_n	y_n	z_n	β_o	ϕ_n	$S_{x,n}$	$S_{y,n}$	x-axis	y-axis	Max	Min	$\phi_{max}-\phi_n$
1	0.386	-250	-250	-899	21.4	45.0	.1035	.1035	5176	5176	5372	5000	45.0
2	1.502	1011	391	-4570	5.9	-179.9	-.0414	0	6742	6520	6965	6336	-145.4
3	2.416	-2623	724	-8489	12.7	0.0	.0877	0	8473	7847	8483	7839	6.8

TABLE 4.1 Surface Measurements Obtained from the HUBRALF Algorithm for Ground Model I (Hubral, 1976a; Table I)

GROUND MODEL 2

Horizon	Vertical Depth ft	Maximum Dip		Interval Velocity ft/s
		Angle	Azimuth	
1	1000	25.0	90.0	5000
2	5000	25.0	180.0	8000
3	10000	20.0	90.0	12000

SIMULATED SURFACE MEASUREMENTS

Horizon	Two-Way Time s	Normal Incidence Point			Emergence Angles		Time Slopes ms/ft		Normal Moveout Velocity ft/s				Major Axis
		x_n	y_n	z_n	β_o	ϕ_n	$S_{x,n}$	$S_{y,n}$	x-axis	y-axis	Max	Min	$\phi_{max}-\phi_n$
1	0.363	0	-383	-821	25.0	90.0	0	.1691	5000	5517	5517	5000	90.0
2	1.285	1773	-173	-4173	18.6	146.0	.1057	.0712	7914	7773	8110	7599	37.0
3	2.123	707	-2756	-8997	18.6	107.8	-.0390	.1217	9755	10082	10203	9649	63.2

TABLE 4.2 Surface Measurements Obtained from the HUBRALF Algorithm for Ground Model 2 (Hubral, 1976a; Table 2)

Horizon	Normal Moveout Velocity ft/s		Spread Length ft	Moveout Velocity ft/s		$V_{mo} - V_{nmo}$ ft/s	
	x-axis	y-axis		x-axis	y-axis	x-axis	y-axis
1	5176	5176	(0)				
			1500	5176	5176	0	0
			2000	5176	5176	0	0
			2500	5176	5176	0	0
			3000	5176	5176	0	0
2	6742	6520	(0)				
			1500	6747	6525	5	5
			2000	6751	6528	9	8
			2500	6757	6532	15	12
			3000	6763	6537	21	17
3	8473	7847	(0)				
			1500	8478	7850	5	3
			2000	8482	7852	9	5
			2500	8486	?7866	13	?19
			3000	8494	7857	21	10

TABLE 4.3 Variation of Moveout Velocity with Spread Length for Ground Model 1 (Hubral, 1976a; Table 1)

Horizon	Normal Moveout Velocity ft/s		Spread Length ft	Moveout Velocity ft/s		$V_{mo} - V_{nmo}$ ft/s	
	x-axis	y-axis		x-axis	y-axis	x-axis	y-axis
1	5000	5517	(0)				
			1500	5000	5517	0	0
			2000	5000	5517	0	0
			2500	5000	5517	0	0
			3000	5000	5517	0	0
2	7914	7773	(0)				
			1500	7917	7784	3	11
			2000	7919	7791	5	18
			2500	7922	7802	8	25
			3000	7925	7815	11	42
3	9755	10082	(0)				
			1500	9757	10086	2	4
			2000	9765	10088	10	6
			2500	9771	10094	16	12
			3000	9776	10098	21	16

TABLE 4.4 Variation of Moveout Velocity with Spread Length for Ground Model 2 (Hubral, 1976a; Table 2)

			FORWARD MODELLING		INVERSION	
HORIZON	CMP	MODEL	TWO-WAY STACKED TIME (ms)	MOVEOUT VELOCITY (m/s)	INTERVAL VELOCITY (m/s)	DEPTH (m)
2	2000	1A	1075	2204	2276	1180
		1B	1073	2202	2274	1177
		ACTUAL			(2270)	1175
	5000	1A	1327	2200	2391	1447
		1B	1325	2199	2390	1444
		ACTUAL			(2375)	1438
	8000	1A	1582	2194	2504	1712
		1B	1580	2194	2504	1710
		ACTUAL			(2480)	1700
3	2000	1A	1739	2550	3018	2185
		1B	1737	2551	3023	2183
		ACTUAL			3000	2175
	5000	1A	1991	2503	3008	2448
		1B	1989	2504	3012	2447
		ACTUAL			3000	2438
	8000	1A	2246	2464	3001	2711
		1B	2244	2464	3003	2710
		ACTUAL			3000	2700

TABLE 6.1 Forward Modelling and Hubral Inversion Over Models 1A and 1B

PARAMETER (horizon/layer 2)	LEFT	RIGHT
Two-way zero-offset time (ms)	1833	2033
Two-way stacked time away from fault (ms)	1835	2034
Range of two-way stacked times (ms)	1826-1845	2022-2041
Vertical average velocity (m/s)	2182	2164
Vertical RMS velocity (m/s)	2216	2195
Moveout velocity away from fault (m/s)	2240	2214
Ditto as % vertical average velocity	102.7%	102.3%
Extremal moveout velocity (m/s)	2103	2385
Ditto as % vertical average velocity	96.4%	110.2%
Ditto as % vertical RMS velocity	94.9%	108.7%
Ditto as % moveout velocity away from fault	93.9%	107.7%
Actual interval velocity (m/s)	3000	3000
Derived interval velocity away from fault (m/s)	3094	3083
Ditto as % actual	103.1%	102.8%
Extremal derived interval velocity (m/s)	2465	3739
Ditto as % actual	82.2%	124.6%

TABLE 6.2

Summary of Data Obtained During CMP Raytracing and Hubral Inversion over Model 2

PARAMETER (horizon/layer 2)	ANTICLINE	SYNCLINE
Two-way zero-offset time (ms)	1467	1867
Two-way stacked time (ms)	1466	1873
Vertical average velocity (m/s)	2454	2357
Vertical RMS velocity (m/s)	2505	2405
Moveout velocity (m/s)	2325	2871
Ditto as % vertical average velocity	94.7%	121.8%
Ditto as % vertical RMS velocity	92.8%	119.4%
Actual interval velocity (m/s)	3000	3000
Derived interval velocity (m/s)	2664	3975
Ditto as % actual	88.8%	132.5%

TABLE 6.3

Summary of Data Obtained During CMP Raytracing and Hubral Inversion Over Model 3

Well	Horizon	CMP Raytracing			Hubral Interval Velocity m/s	Well Interval Velocity m/s	Expected Error	
		Two-Way Stacked Time ms	Moveout Velocity m/s	Inline Time Slope s/m			m/s	% of Well Interval Velocity
A	SEABED	96	1480	0				
					1970	1969	1	0.05
	BROWN	2167	1951	0				
					2106	2104	2	0.10
	PINK	2512	1973	0				
					2413	2414	-1	-0.05
	YELLOW	2631	1995	0				
					4264	4038	226	5.60
	ORANGE	2823	2224	0				
					3028	3086	-58	-1.88
	RED	2975	2272	0				
C	SEABED	96	1480	0				
					1972	1971	1	0.05
	BROWN	2246	1953	0				
					2133	2131	2	0.09
	PINK	2626	1988	-0.000093				
					2535	2523	12	0.48
	YELLOW	2752	2016	-0.000087				
					4612	4340	272	6.27
	ORANGE	2954	2293	-0.000092				
					3023	3071	-48	-1.56
	RED	3113	2334	-0.000076				

TABLE 7.1 Expected Interval Velocity Errors Due to the Spread Length Effect

Horizon	Moveout Velocity m/s	Normal Moveout Velocity m/s	Bias	
			m/s	%
SEABED	1480	1480	0	0
BROWN	1951	1950	1	0.05
PINK	1973	1972	1	0.05
YELLOW	1995	1994	1	0.05
ORANGE	2224	2193	31	1.41
RED	2272	2248	24	1.07

TABLE 7.2 Moveout Velocity Bias at Well A

Horizon	Selected Smoothing Combination		Mean Interval Velocity Error[1]		Calibration Factor[3]
	Moveout Velocities	Interval Velocities	m/s	%[2]	
SEABED					
	RAW	3 km BOXCAR	110	5.6	0.947
BROWN					
	RAW	3 km BOXCAR	264	12.5	0.889
PINK					
	RAW	3 km BOXCAR	178	7.2	0.933
YELLOW					
	1.5 km BOXCAR	3 km BOXCAR	107	2.6	0.975
ORANGE					
	1.5 km BOXCAR	3 km BOXCAR	133	4.3	0.959
RED					

1 Mean interval velocity error determined at Wells A and C from four seismic ties using Equation (7.1).
2 The average of the mean interval velocity error expressed as percentages at Wells A and C.
3 From Equation (7.2)

TABLE 7.3 Selected Smoothing Combinations, Mean Interval Velocity Errors and Calibration Factors for the Direct Inversion

Horizon	Selected Smoothing Combination		Mean Interval Velocity Error[1]		Calibration Factor[3]
	Moveout Velocities	Interval Velocities	m/s	%[2]	
SEABED					
	RAW	3 km BOXCAR	110	5.6	0.947
BROWN					
	RAW	3 km BOXCAR	765	36.1	0.735
PINK					
	1.5 km BOXCAR	1.5 km BOXCAR	2108	85.4	0.539
YELLOW					
	1.5 km BOXCAR	3 km BOXCAR	850	20.3	0.831
ORANGE					
	1.5 km BOXCAR	3 km BOXCAR	1624	52.8	0.655
RED					

1 Mean interval velocity error determined at Wells A and C from four seismic ties using Equation (7.1)
2 The average of the mean interval velocity error expressed as percentages at Wells A and C.
3 From Equation (7.2)

TABLE 7.4 Selected Smoothing Combinations, Mean Interval Velocity Errors and Calibration Factors for the Layer-by-Layer Inversion

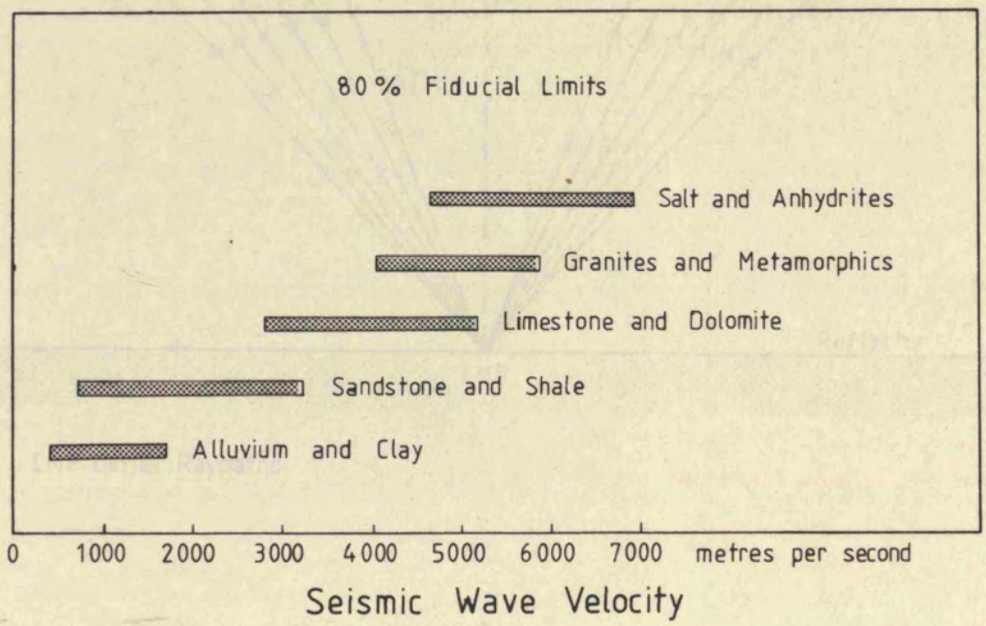

Figure 1.1 Variation of Seismic Wave Velocity with Lithology (after Birch, 1942)

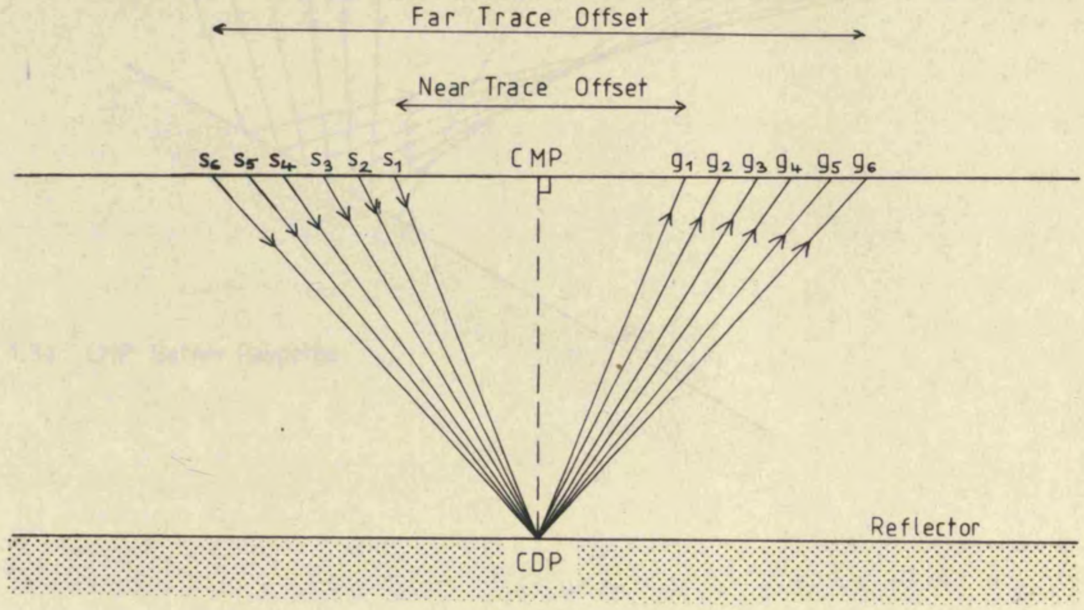

1.2a CMP Gather Raypaths

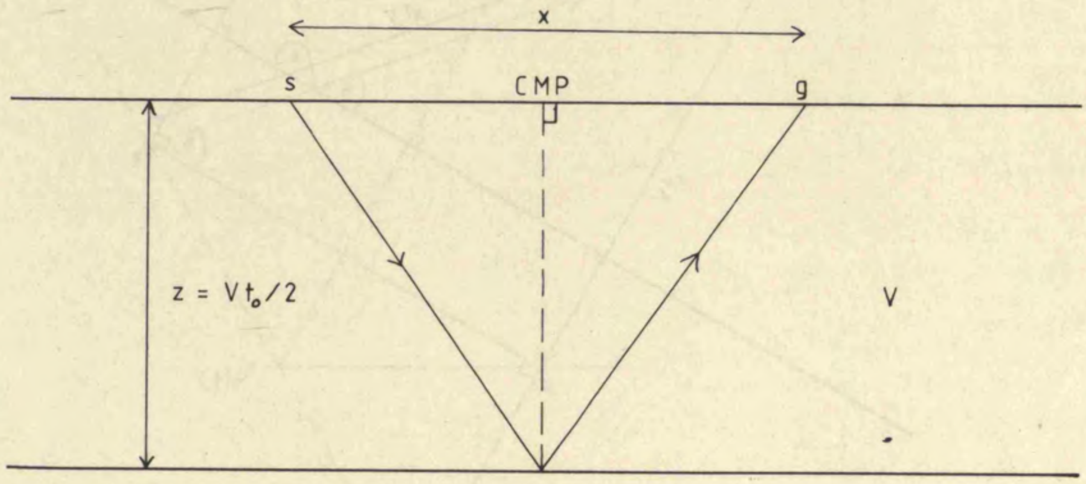

1.2b Single Offset Raypath

Figure 1.2 CMP Geometry for a Uniform Velocity, Single Horizontal Reflector Depth Model

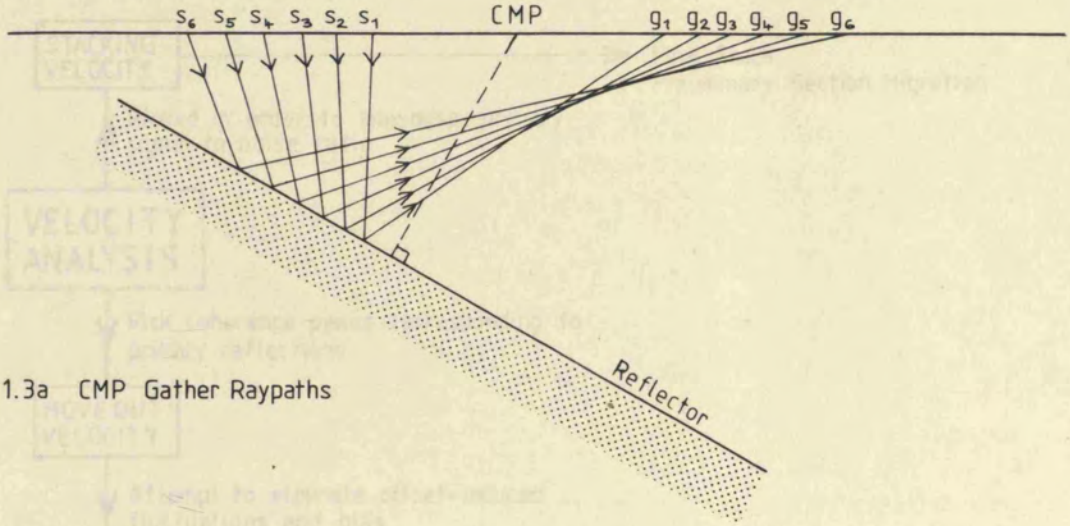

1.3a CMP Gather Raypaths

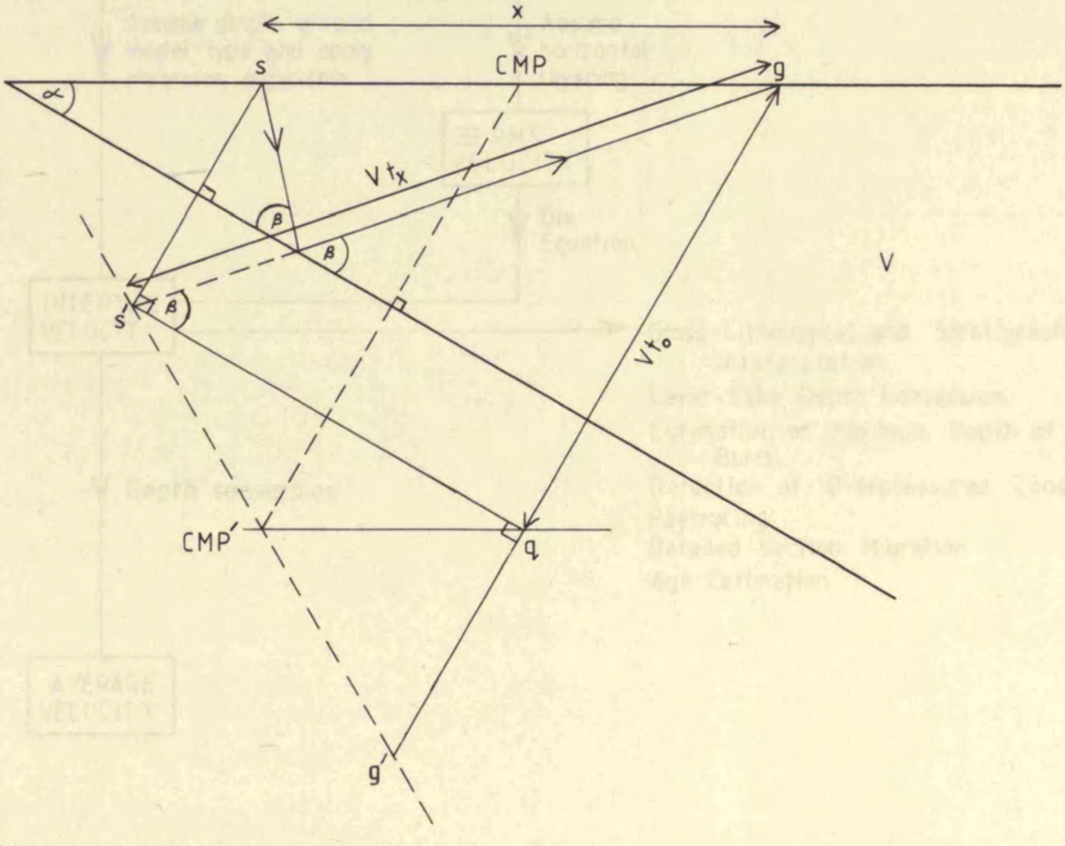

1.3b Single Offset Raypath

Figure 1.3 CMP Geometry for a Uniform Velocity, Single Plane Dipping Reflector Depth Model

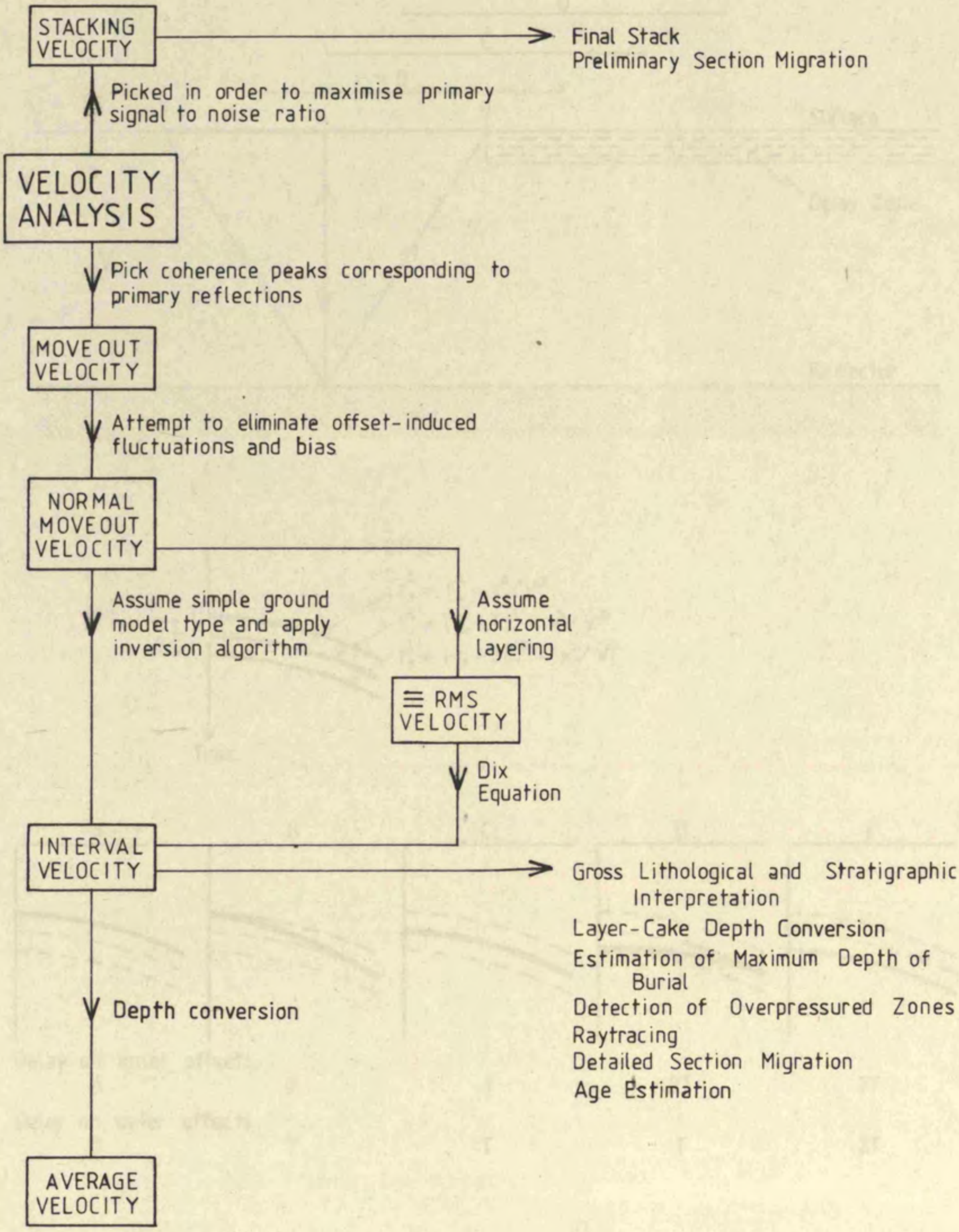

Figure 1.4 Uses of Velocities Obtained from CMP Velocity Analysis

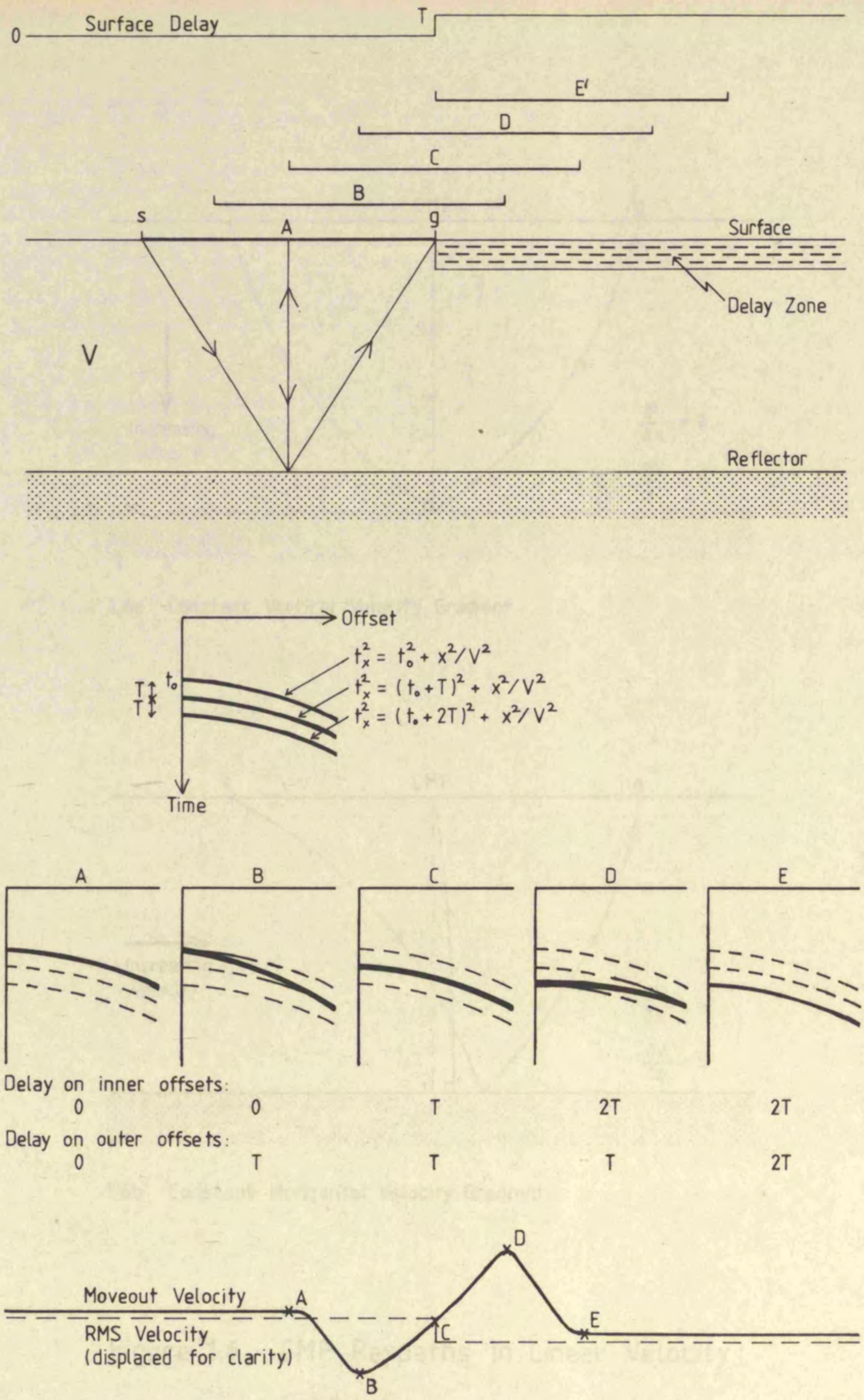

Figure 1.5 Moveout Velocity Variation over a Near-Surface Step Time Delay

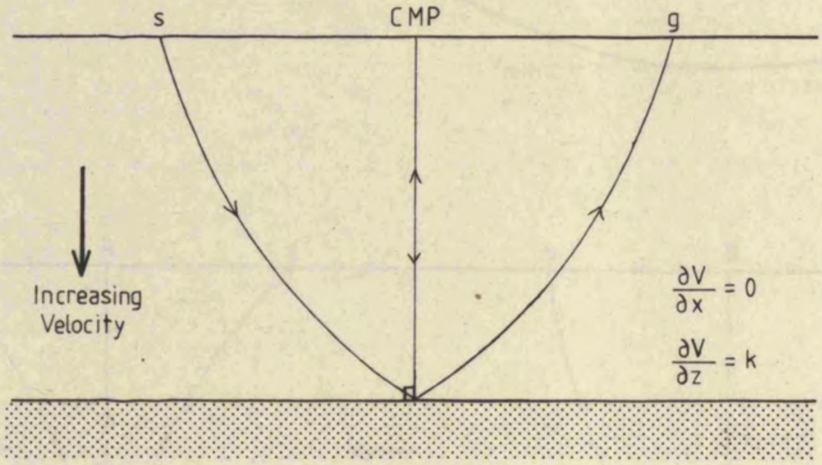

1.6a Constant Vertical Velocity Gradient

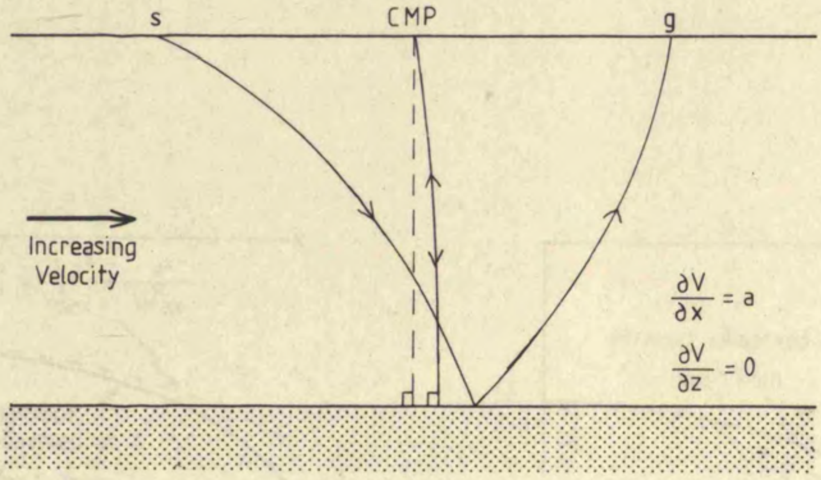

1.6b Constant Horizontal Velocity Gradient

Figure 1.6 CMP Raypaths in Linear Velocity Gradients

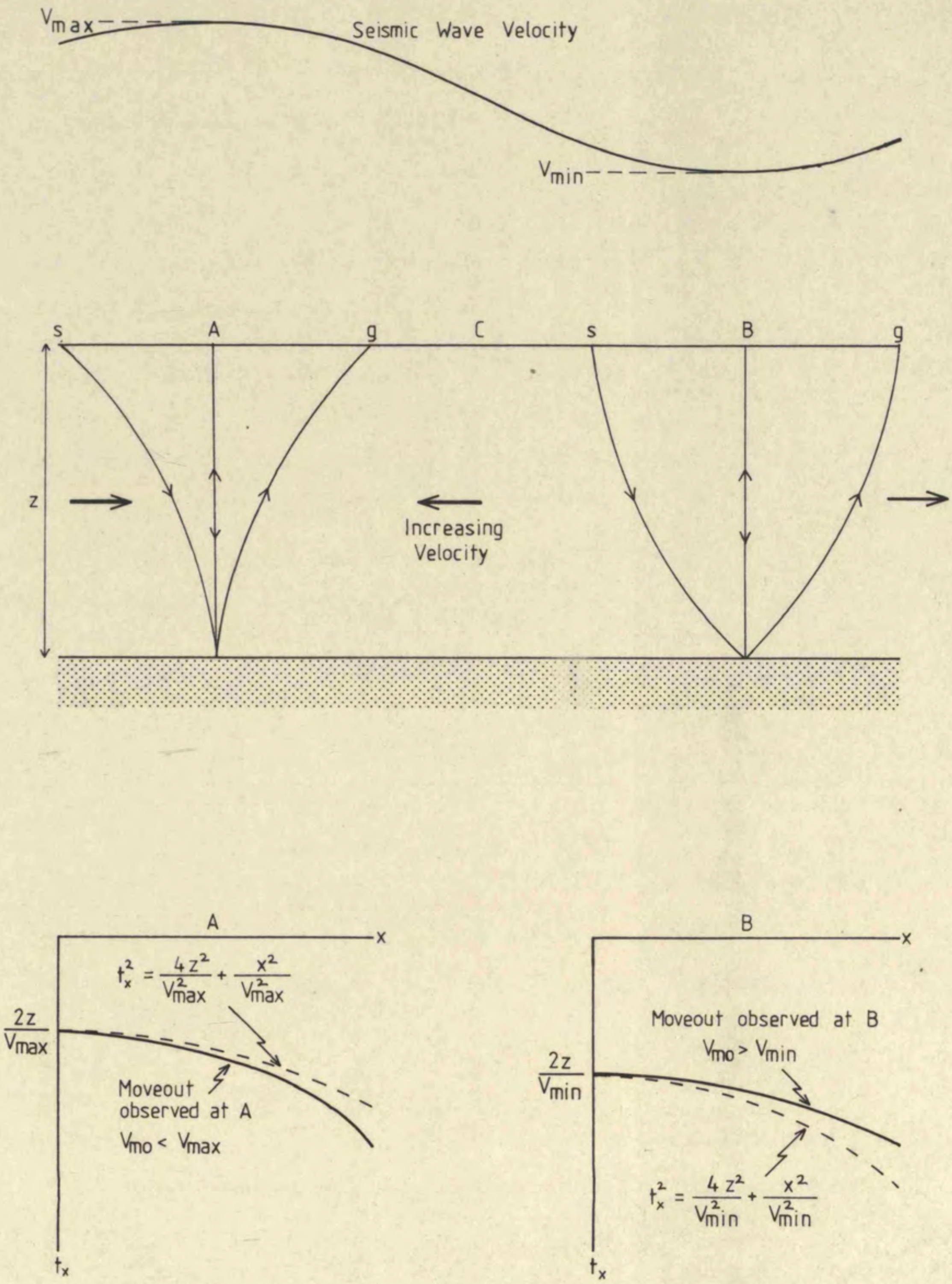

Figure 1.7 CMP Raypaths in a Layer with Variable Velocity Gradients

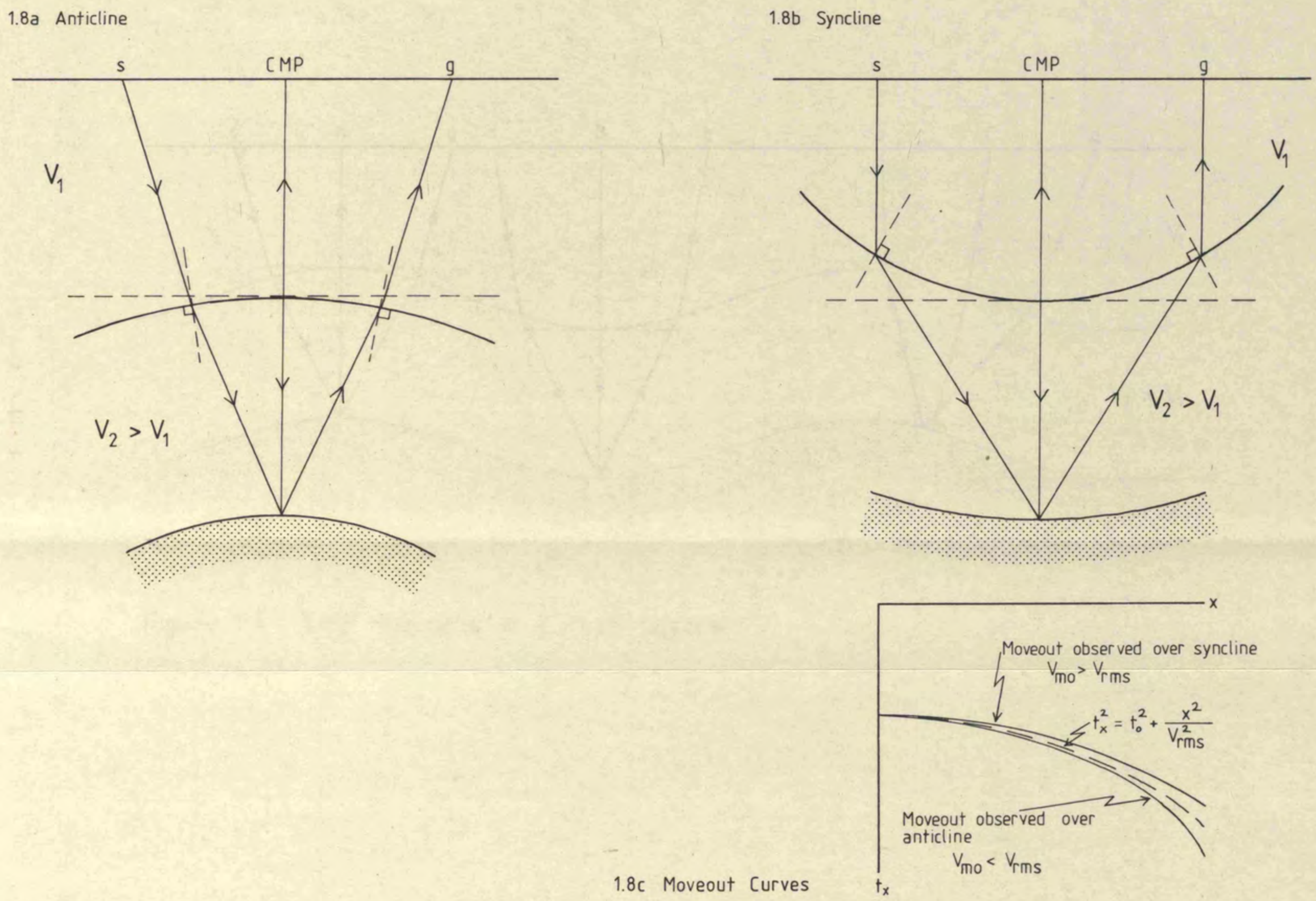

Figure 1.8 CMP Raypaths over Fold Axes

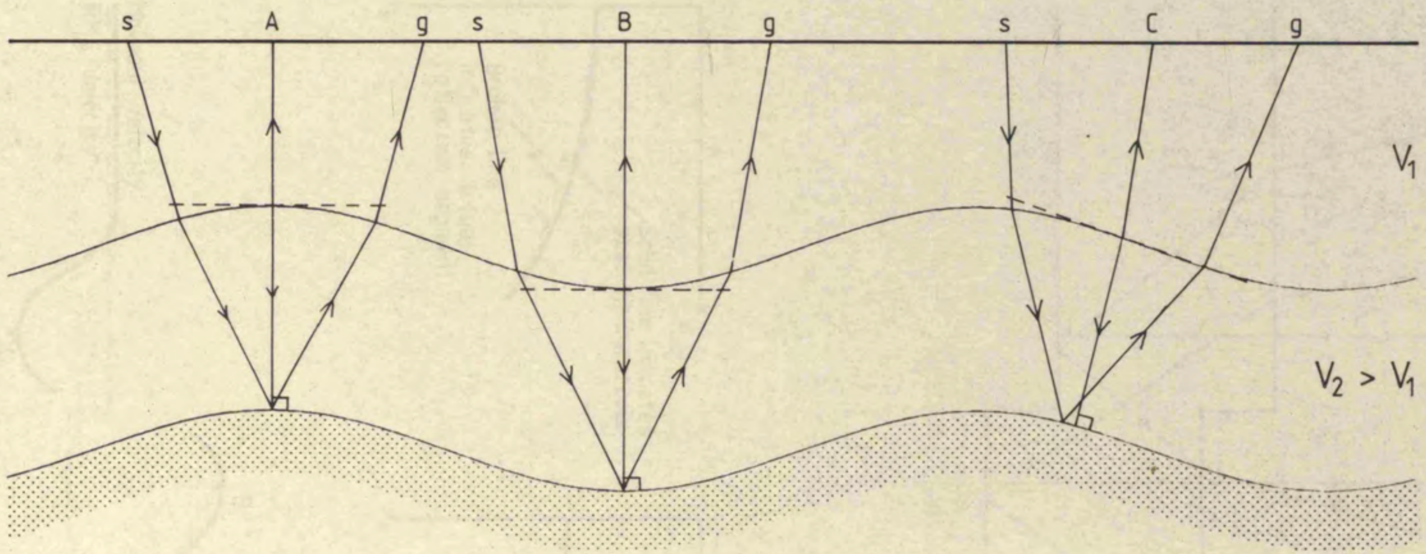

Figure 1.9 CMP Raypaths in Curved Layers

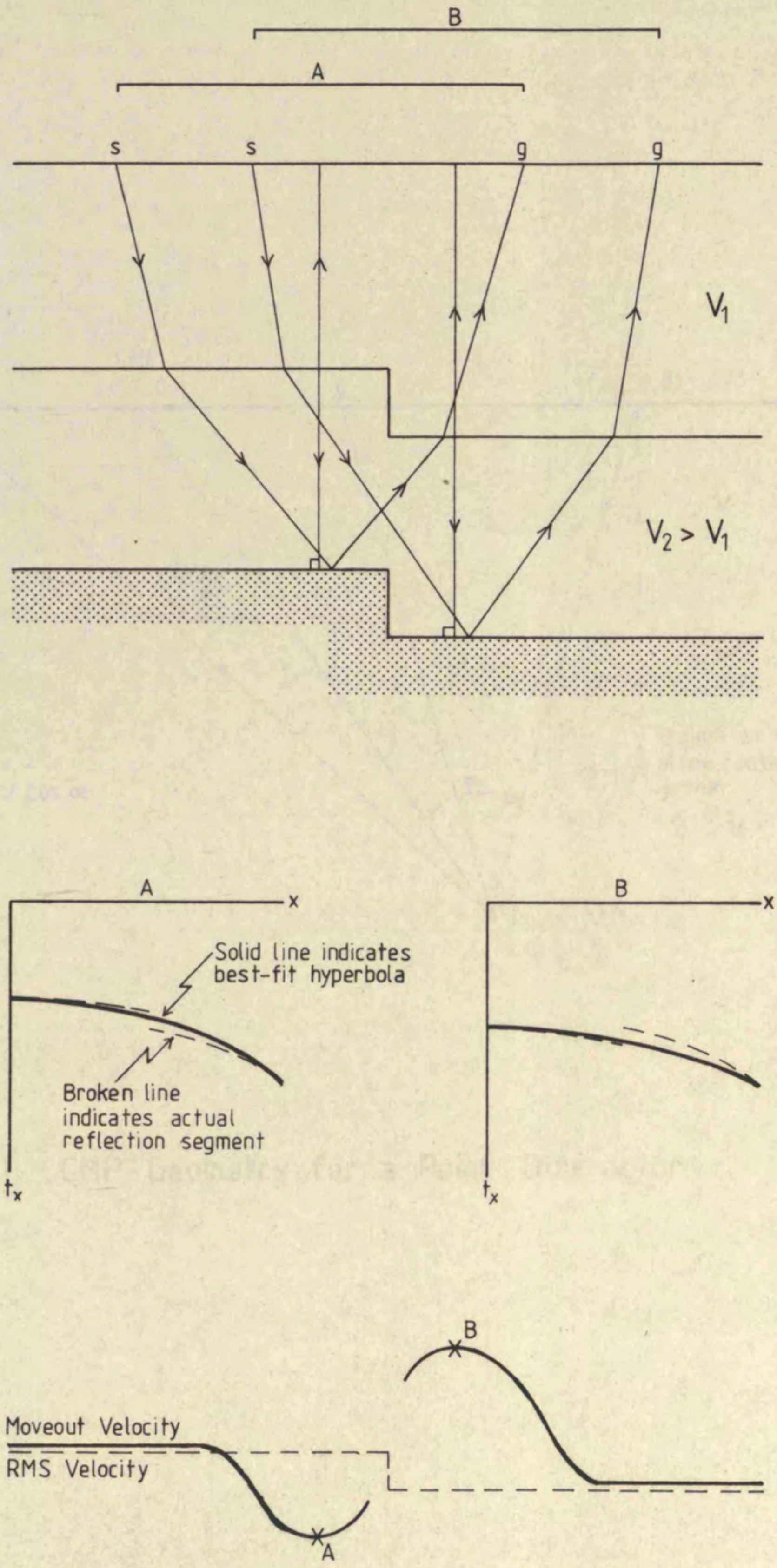

Figure 1.10 Moveout Velocity Variation over a Fault

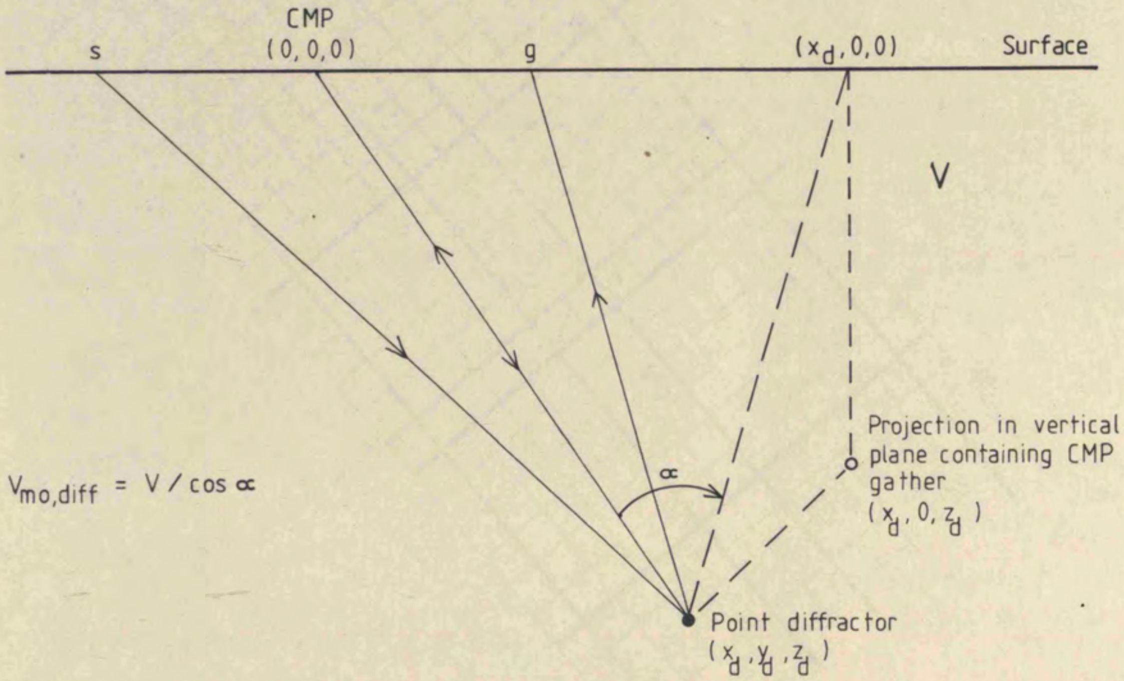

Figure 1.11 CMP Geometry for a Point Diffractor

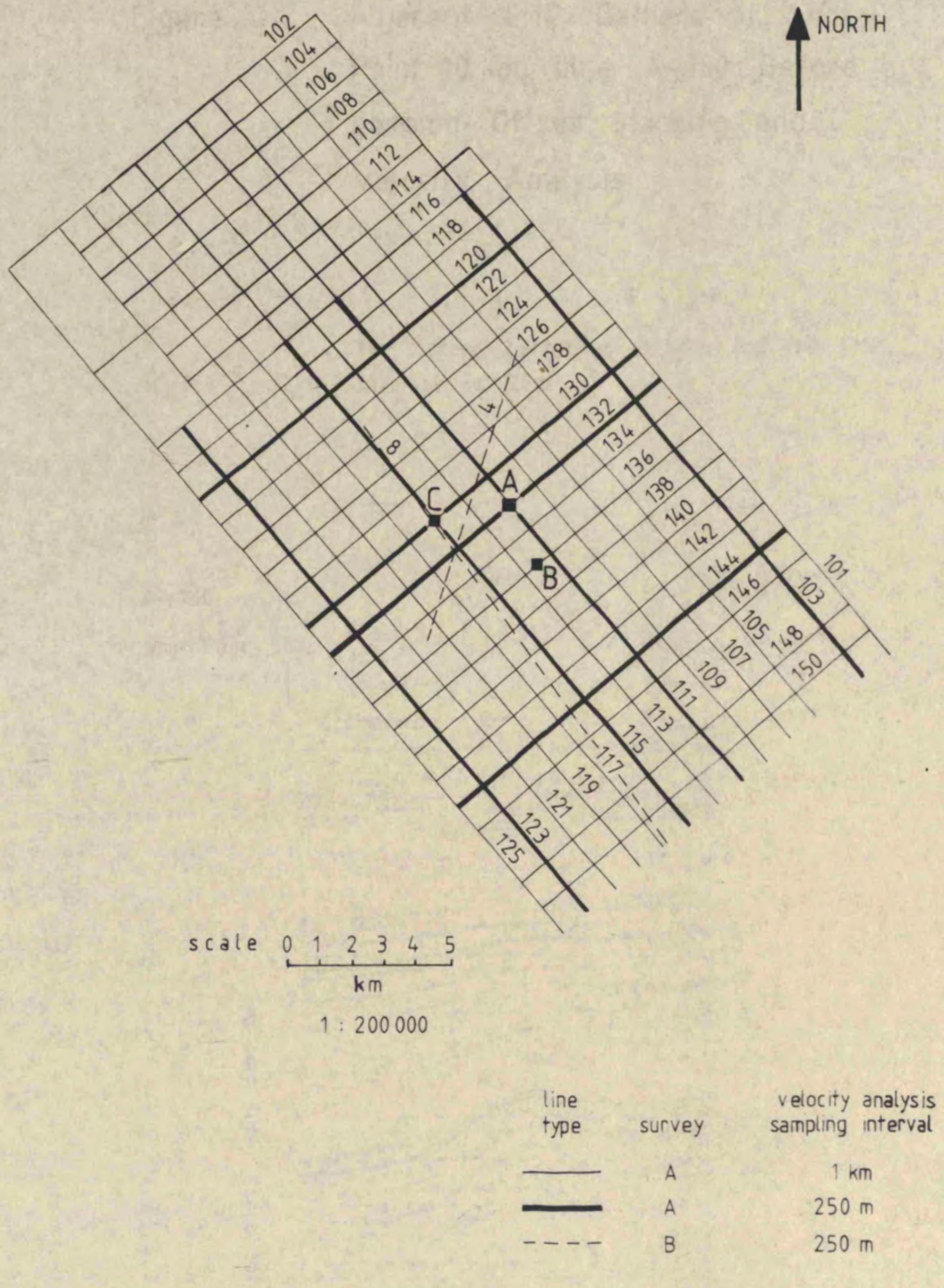

Figure 2.1 Schematic Location Map

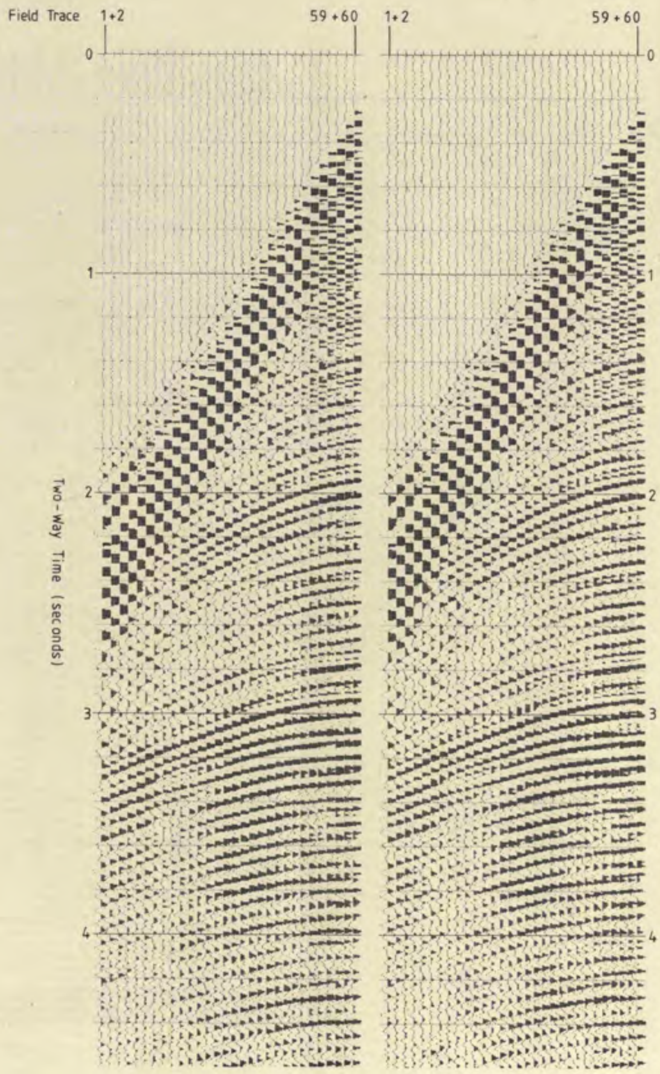

Figure 2.2 Adjacent CMP Gathers at Shot Point 10 on Line A-130 Before Common Offset Stacking and Velocity Analysis

The Spread Length is 3250m and the CMP Interval is 25m

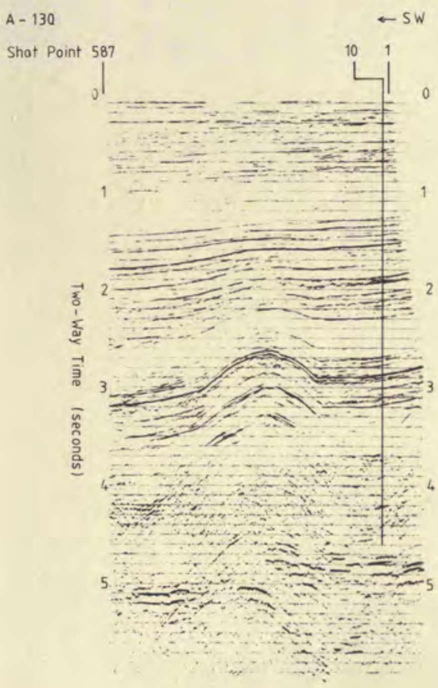

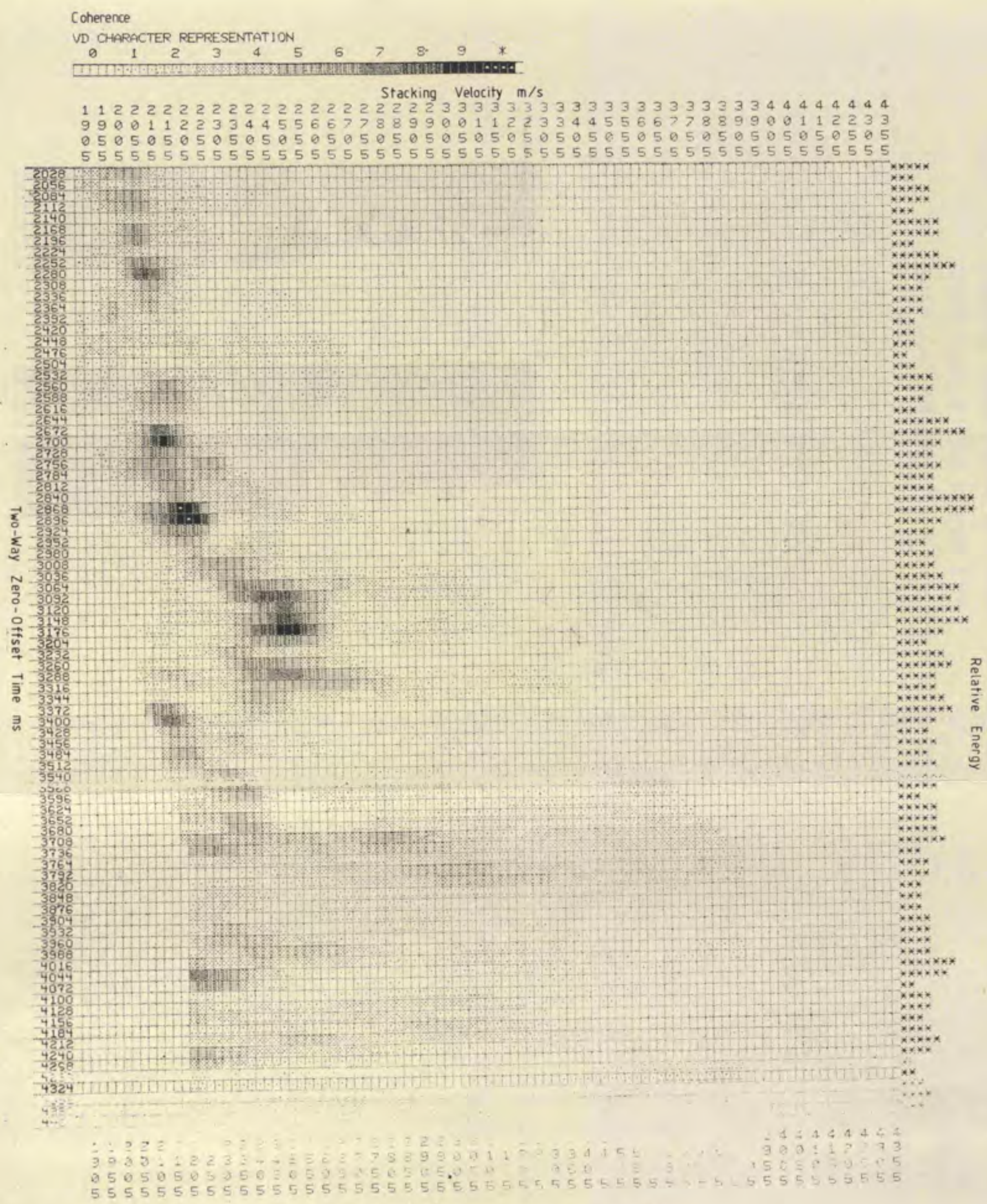

Figure 2.3 Velocity Analysis at Shot Point 10 on Line A-130

From the Data of Figure 2.2
Analysis and Display by VLAN

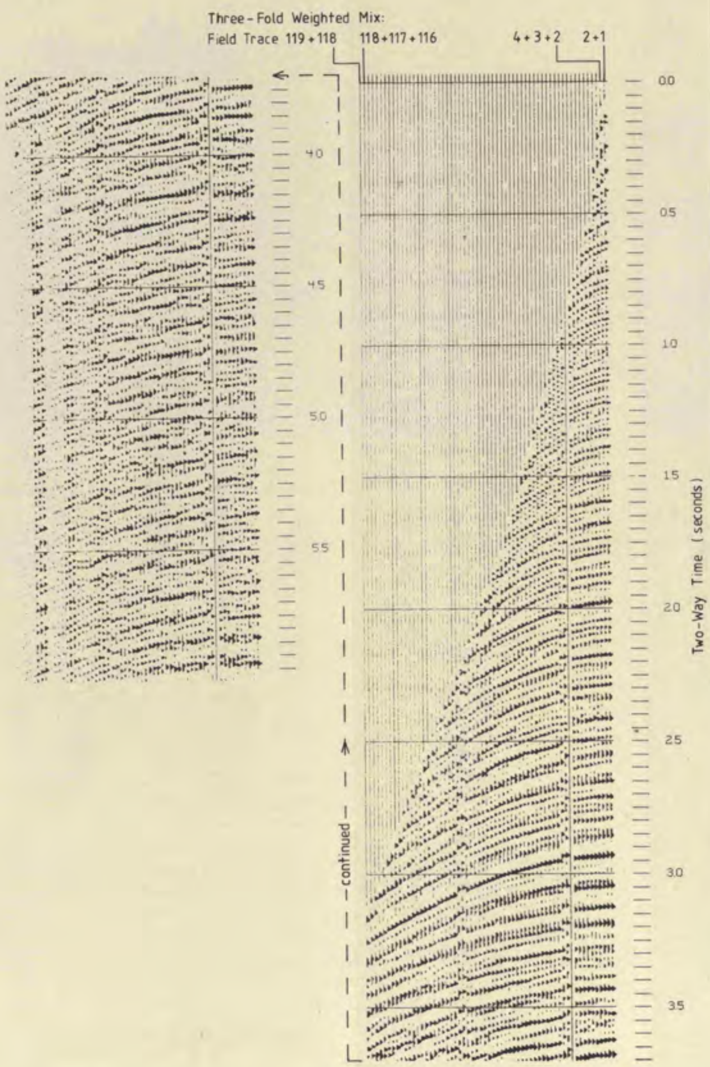

Figure 2.4 Composite Gather Formed by Common Offset Stack of Four Adjacent CMP Gathers at Shot Point 108 on Line B-4

The Spread Length is 3150 m and the CMP Interval is 12.5 m

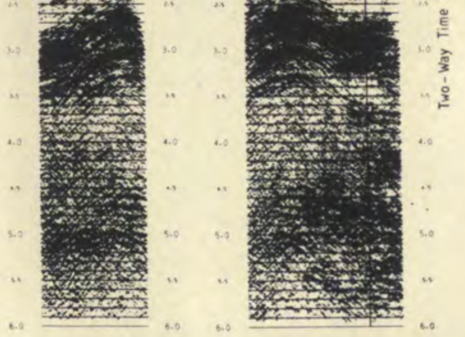

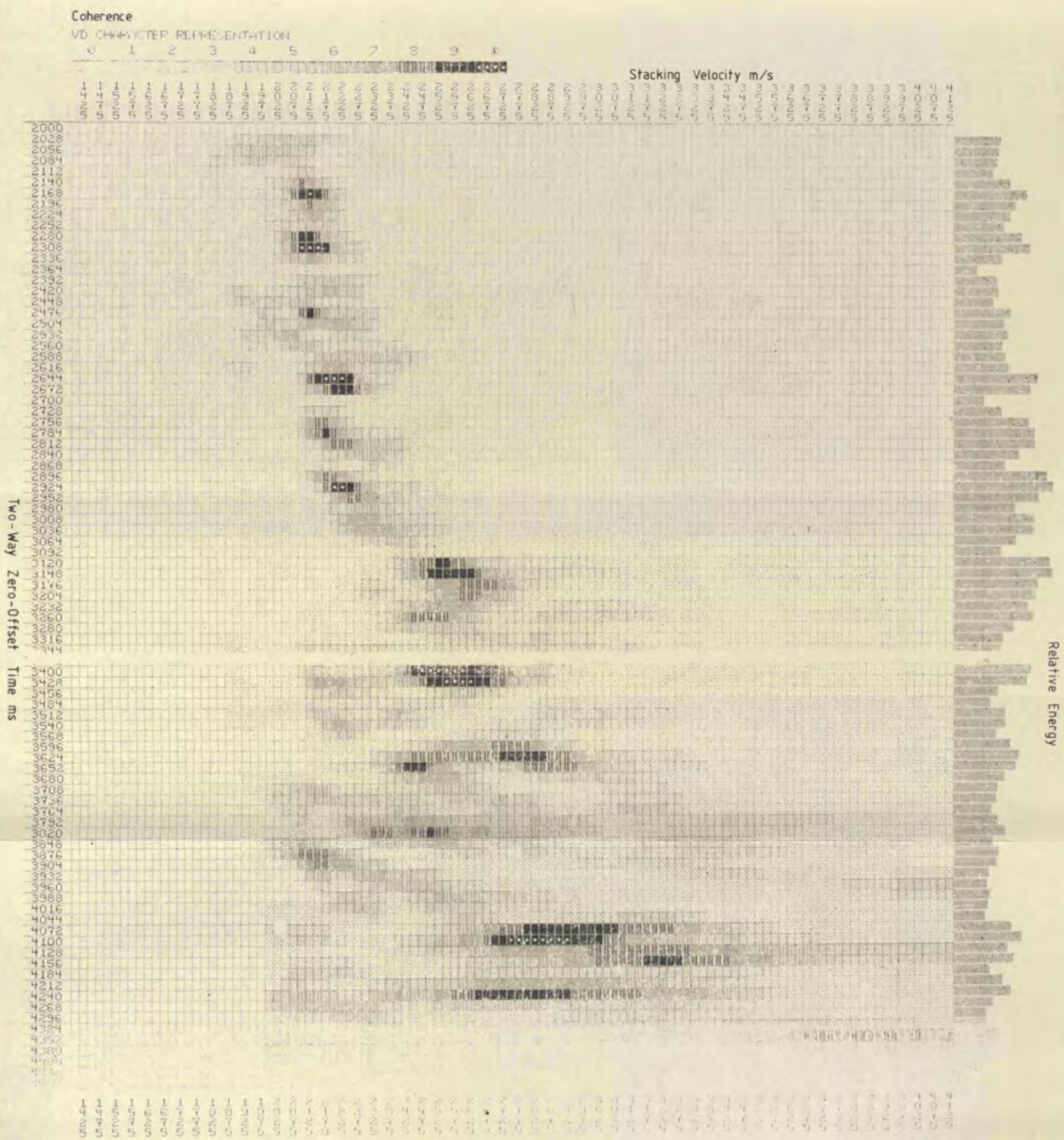

Figure 2.5 Velocity Analysis at Shot Point 108 on Line B-4

From the Data of Figure 2.4
Analysis and Display by VLAN

Figure 2.6 Stacked Section for Line A-103

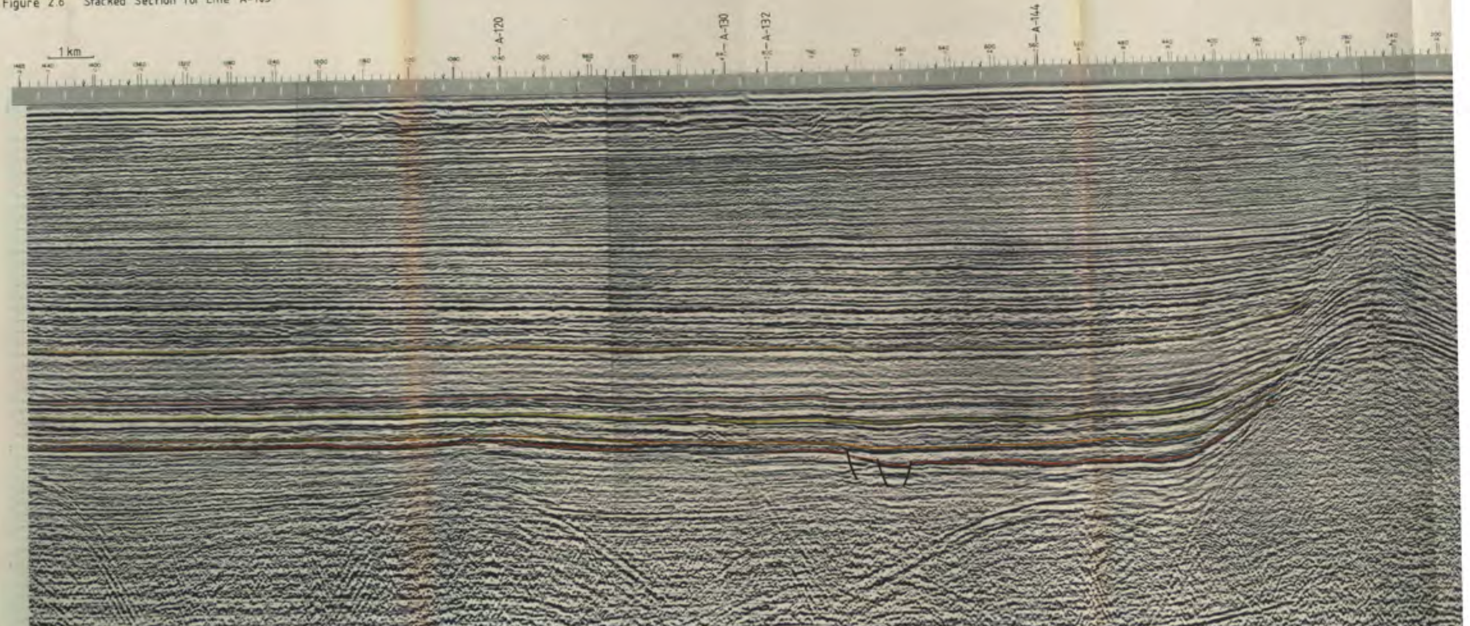

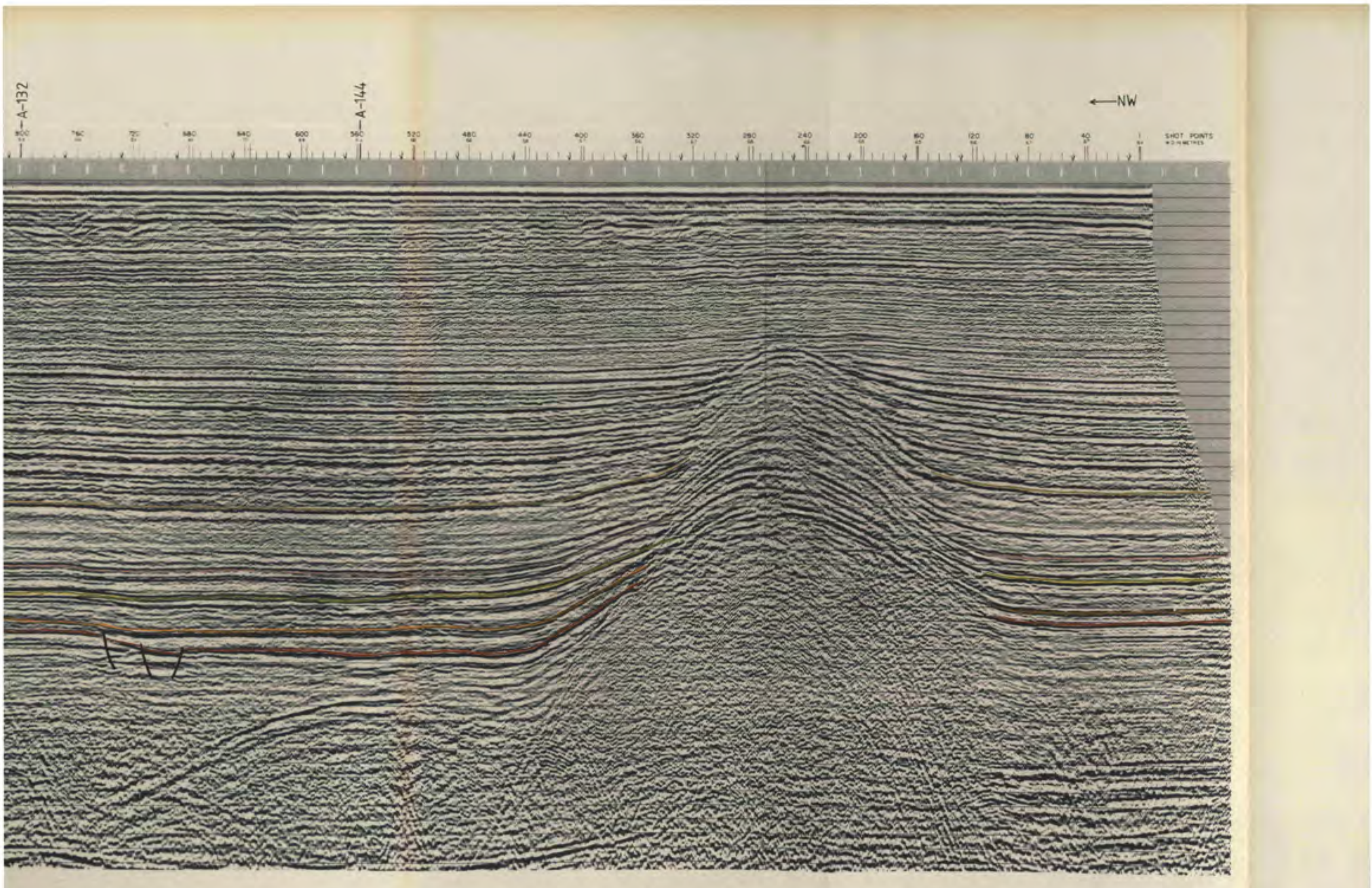
A-132
A-144
NW
800
760
720
680
640
600
560
520
480
440
400
360
320
280
240
200
160
120
80
40
1
SHOT POINTS

Figure 27 Stacked Section for Line A-111

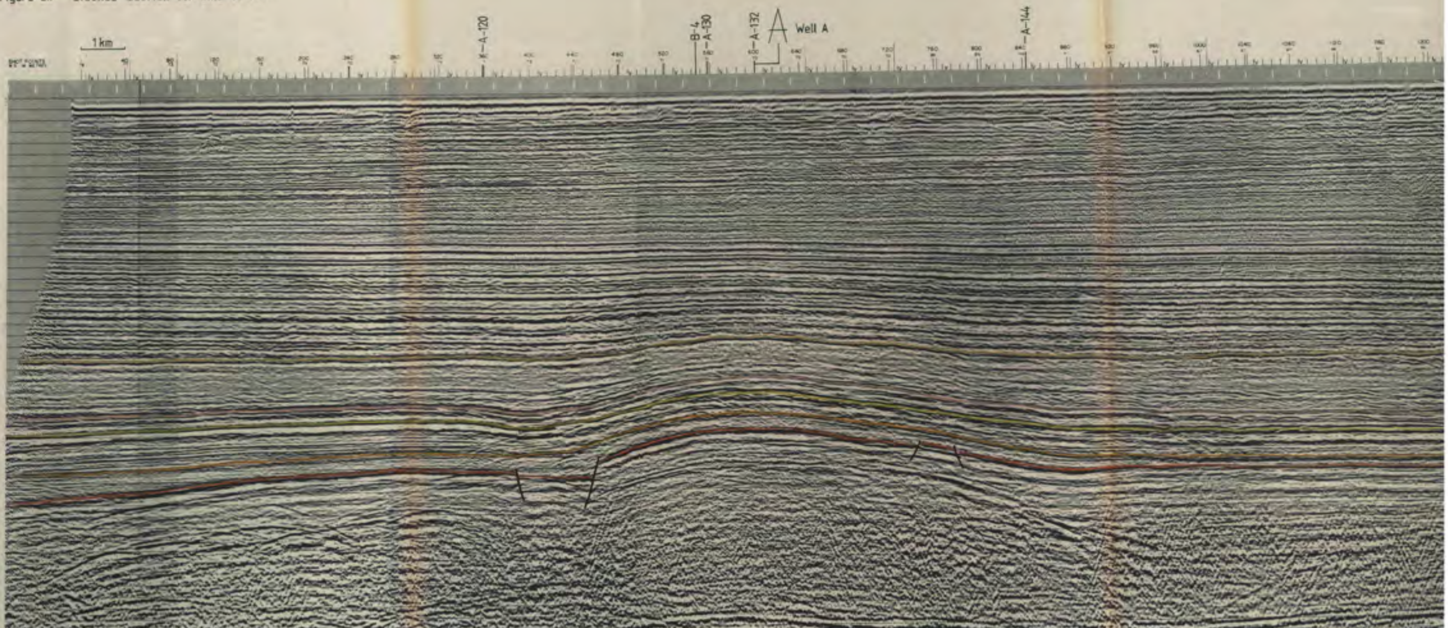

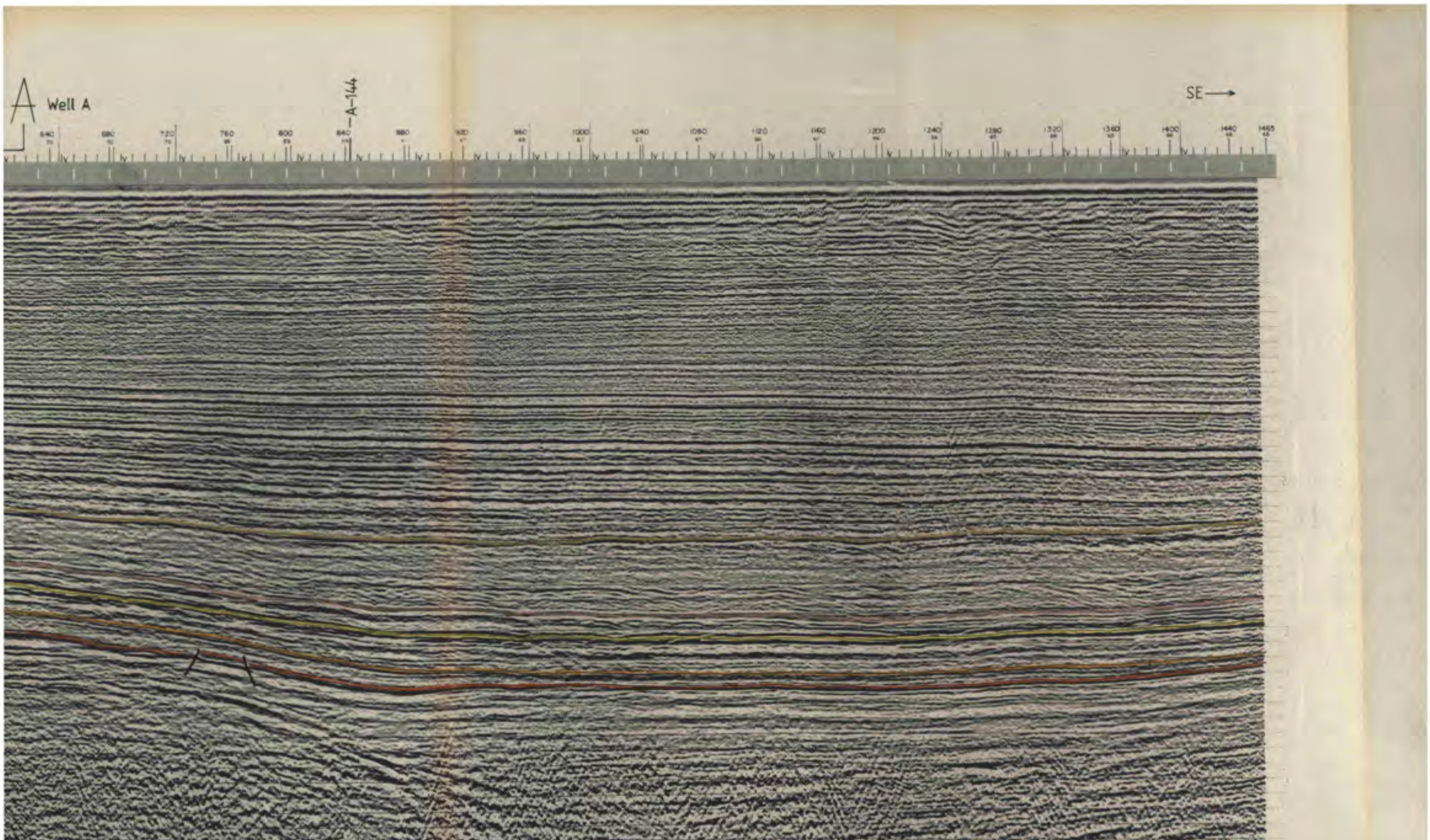
A
Well A
A-144
SE
640
680
720
760
800
840
880
920
960
1000
1040
1080
1120
1160
1200
1240
1280
1320
1360
1400
1440
1465

Figure 2.8 Stacked Section for Line A-115

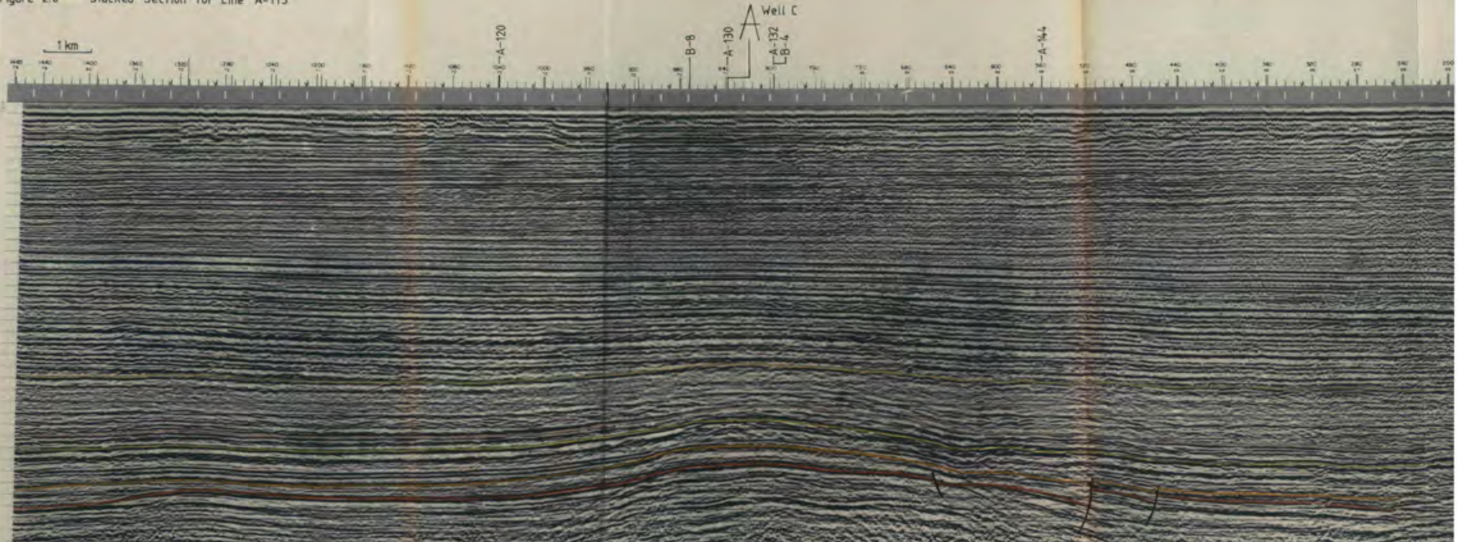

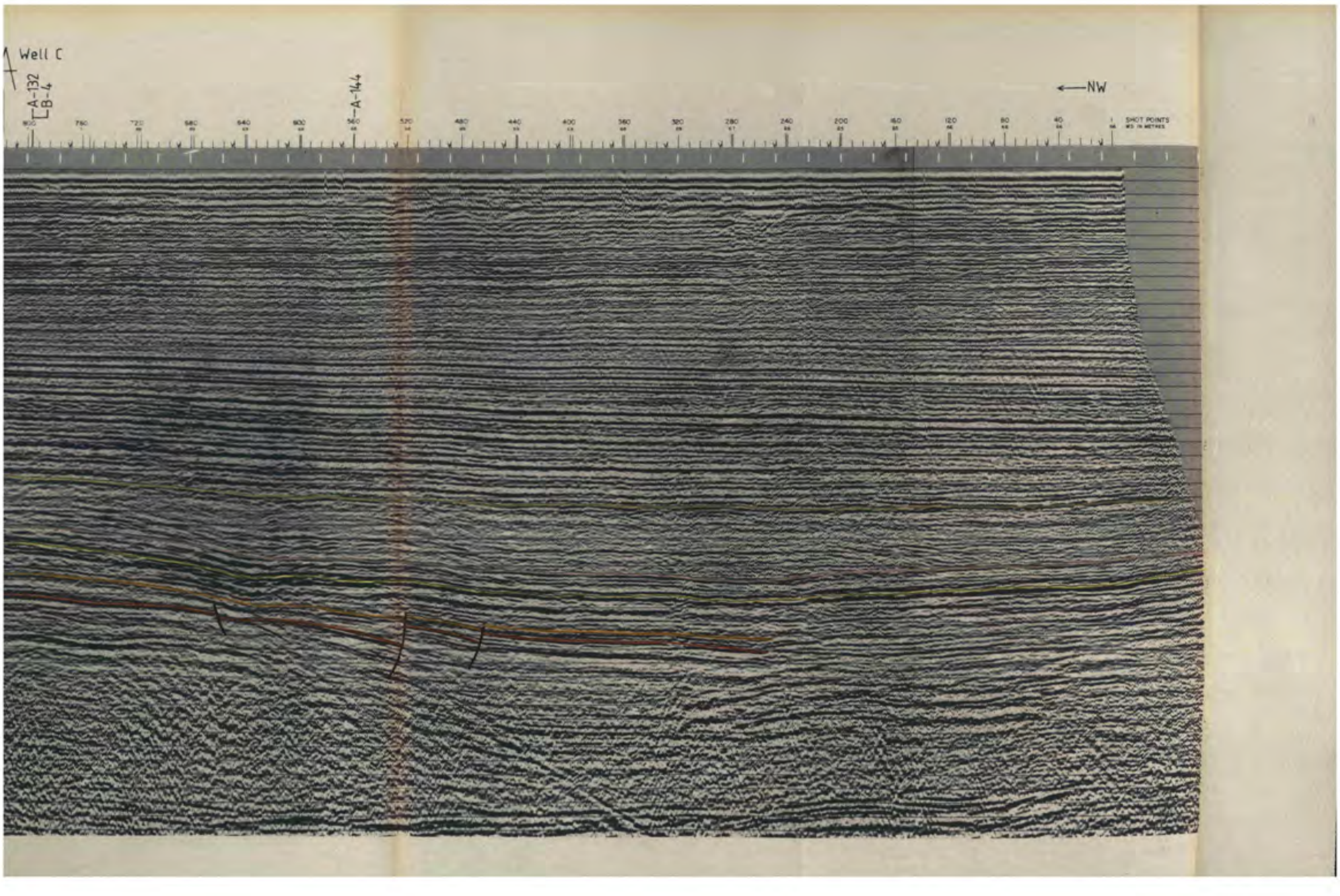
Well C
A-132
B-4
A-144
NW
SHOT POINTS

Figure 2.9 Stacked Section for Line A-123

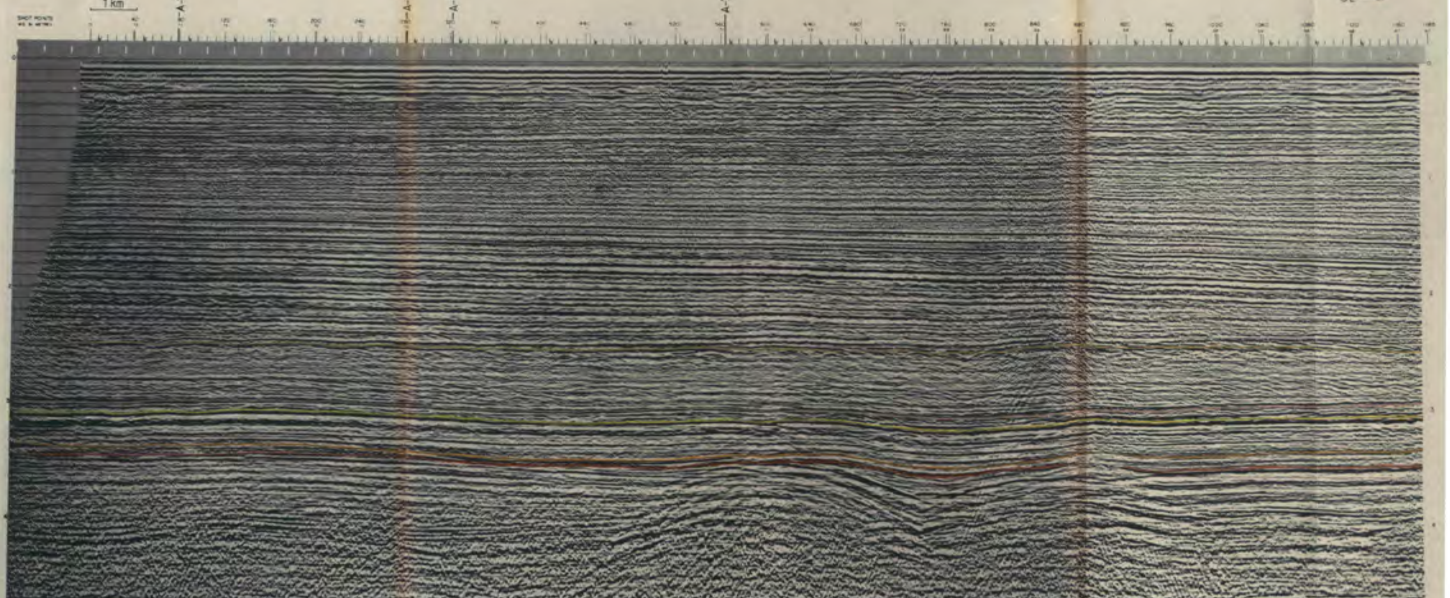

Figure 2.10 Stacked Section for Line A-120

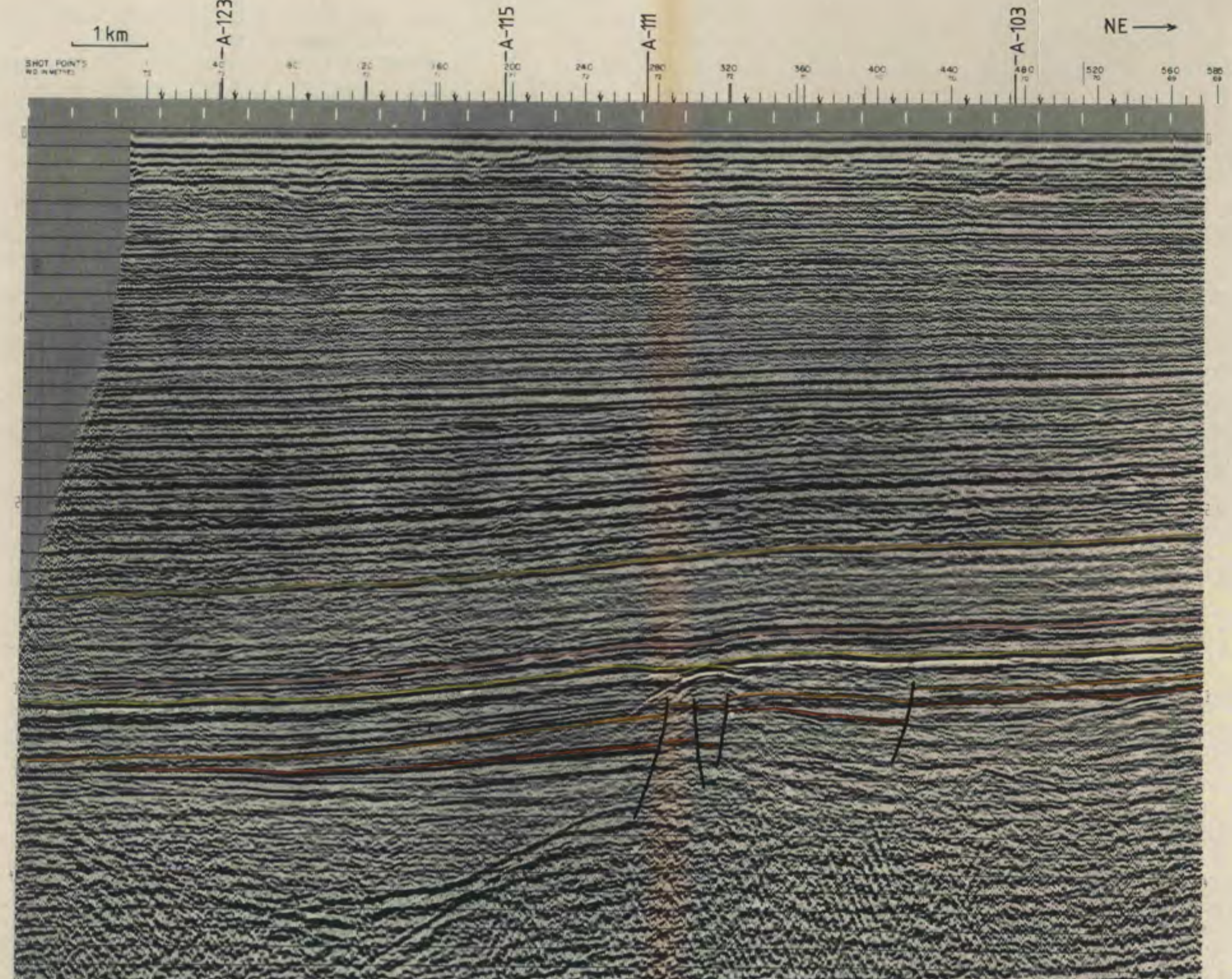

Figure 2.11 Stacked Section for Line A-130

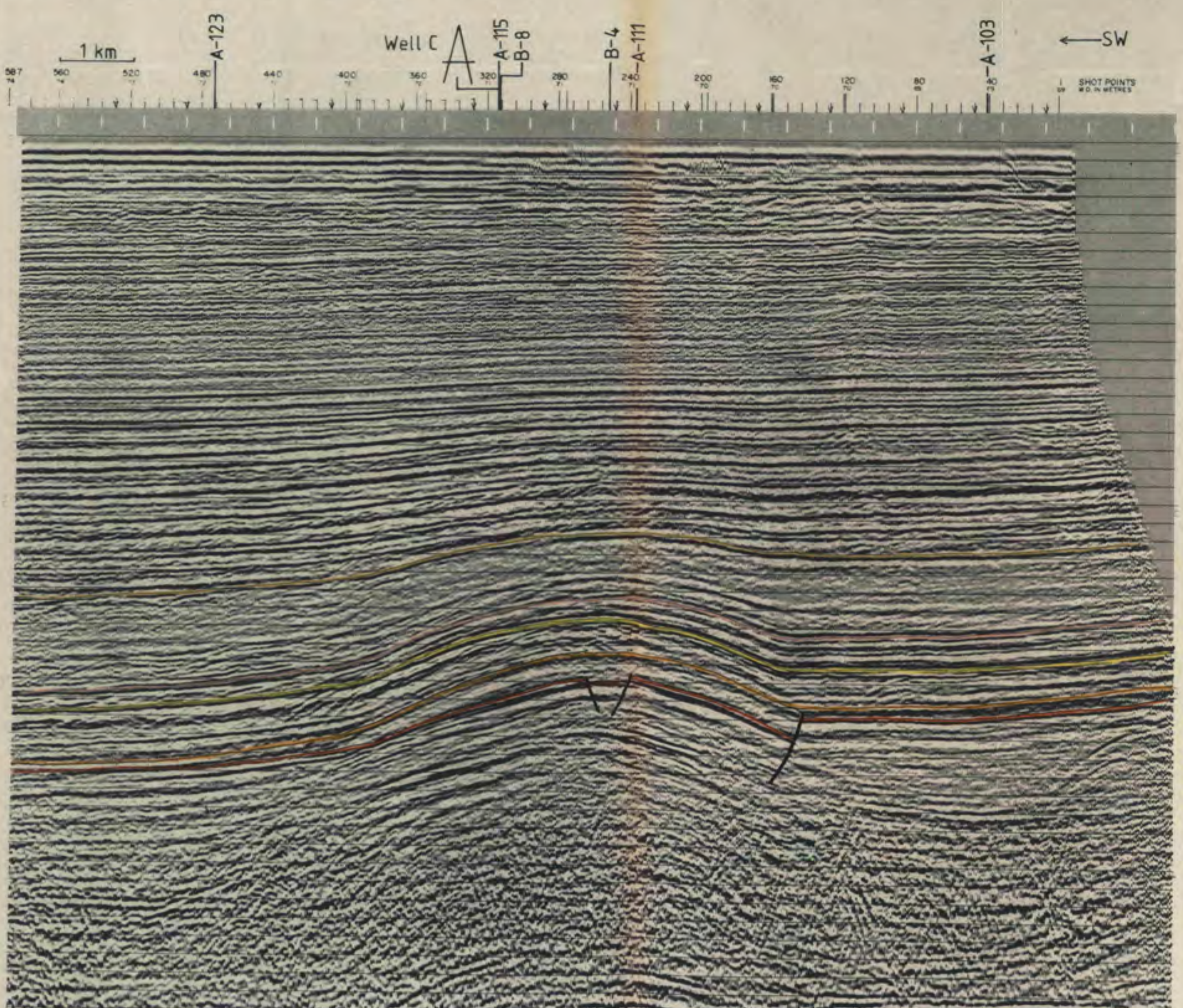

Figure 2.12 Stacked Section for Line A-132

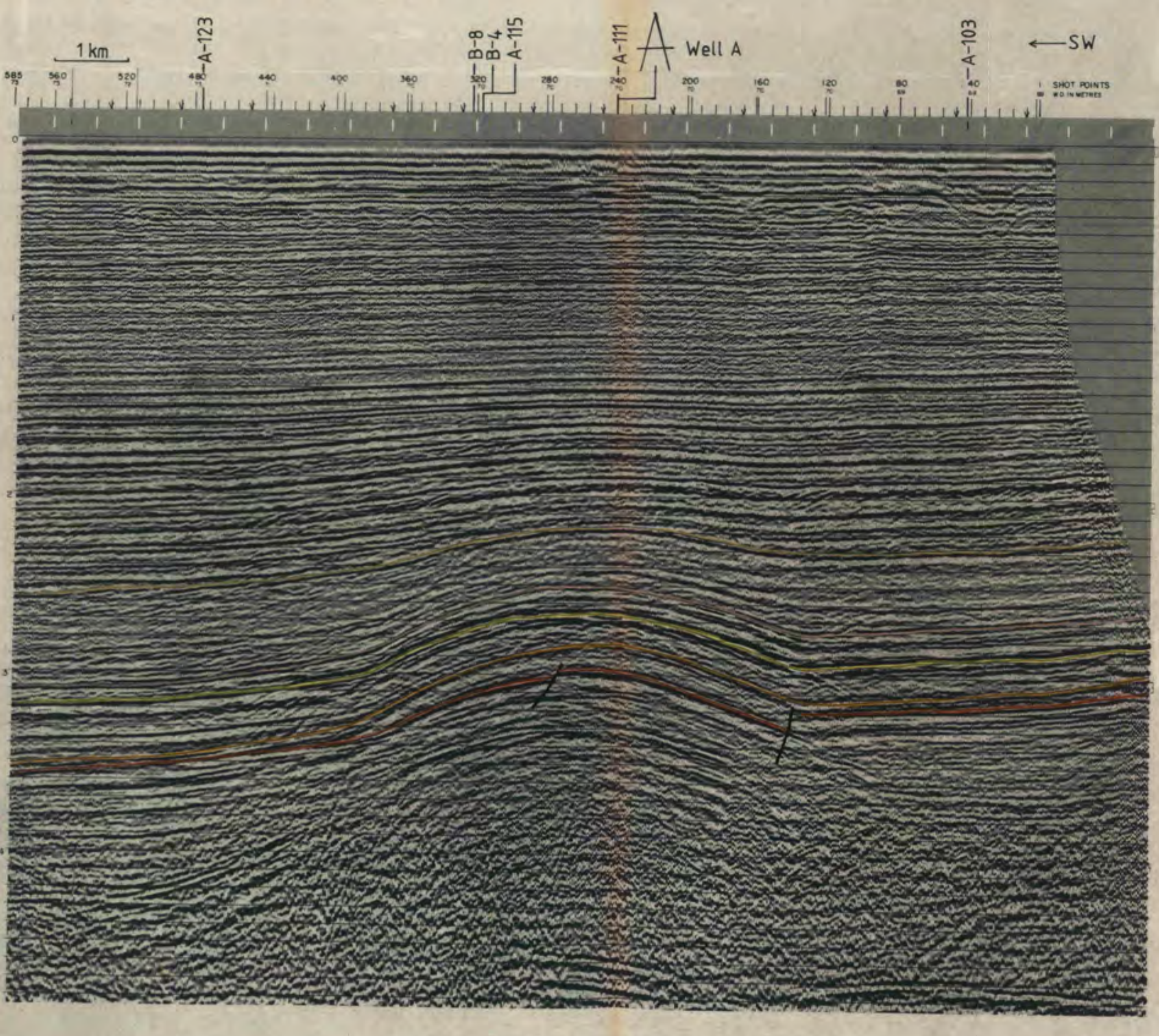

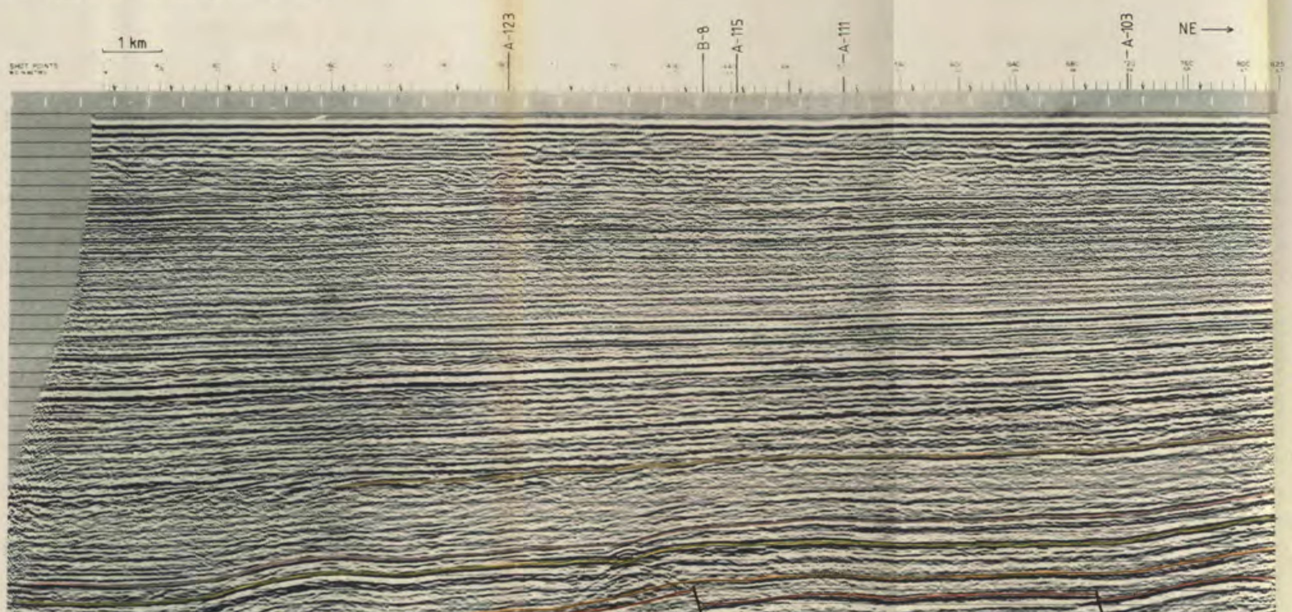

Figure 2.13 Stacked Section for Line A-144

Figure 2.14 Stacked Sections for Line B-4

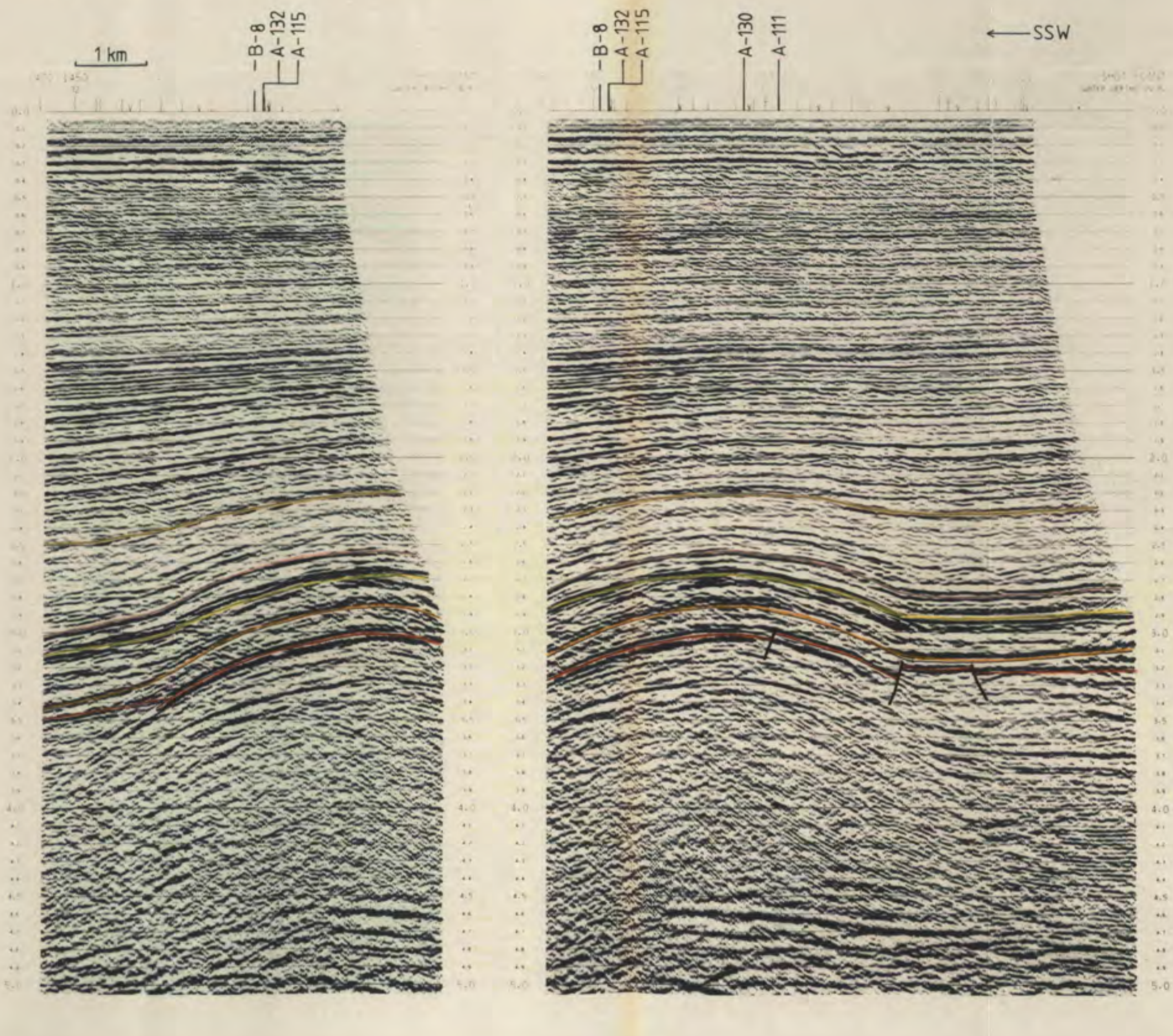

Figure 2.15 Stacked Section for Line B-8

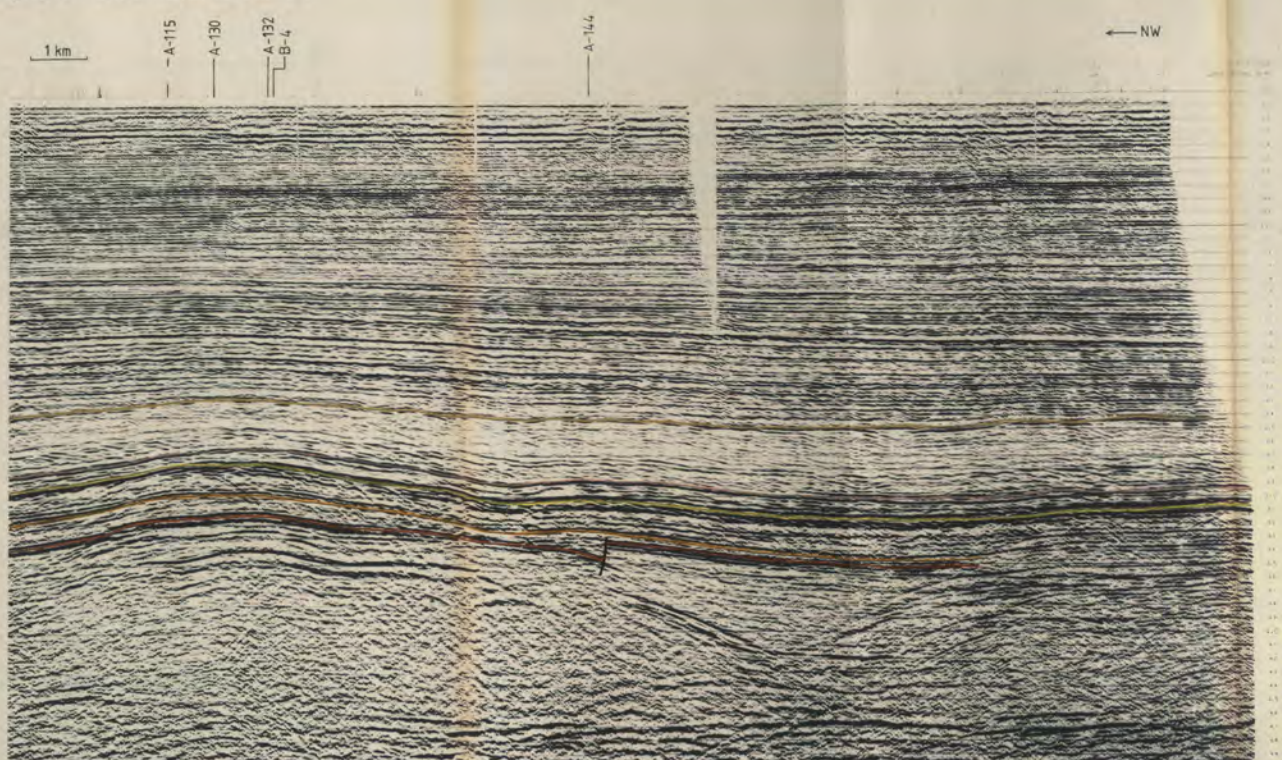

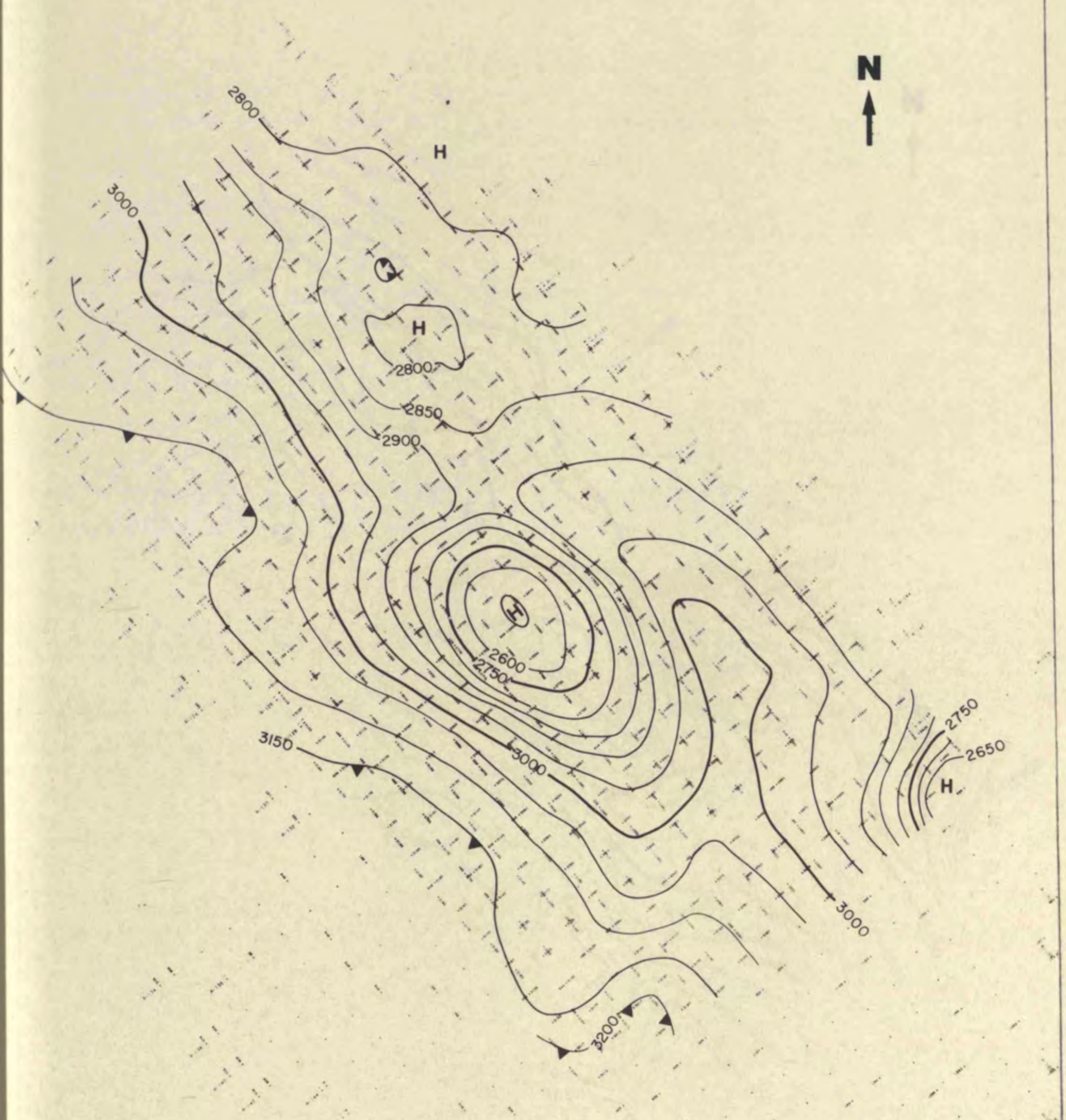

Figure 2.16

TWO-WAY TIMES TO THE YELLOW HORIZON (UNMIGRATED)

Contour Interval — 50 msecs

Figure 2.17

TWO-WAY TIMES TO THE RED HORIZON (UNMIGRATED)

Contour Interval - 50 msecs

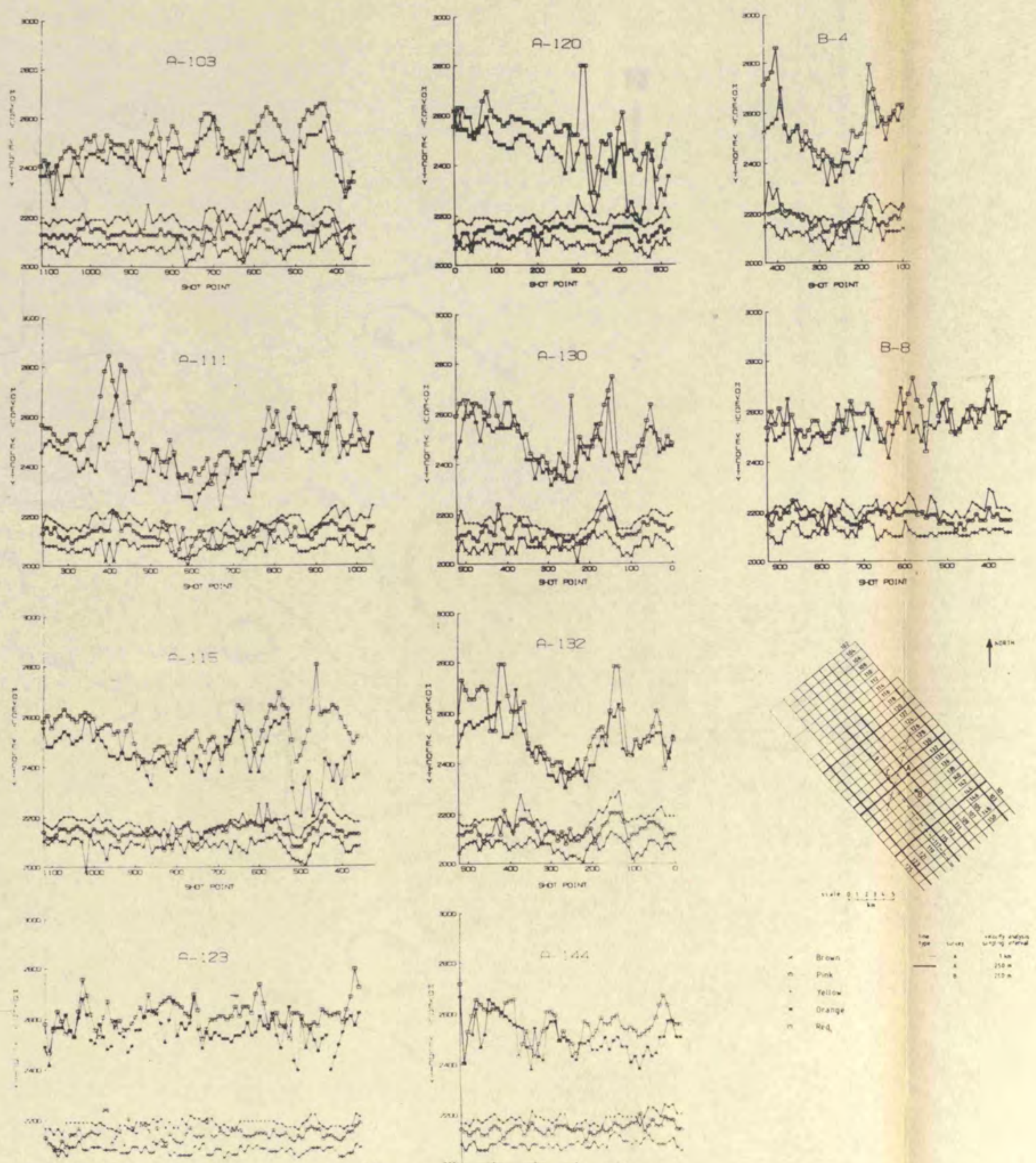

Figure 2.18 Moveout Velocity Profiles

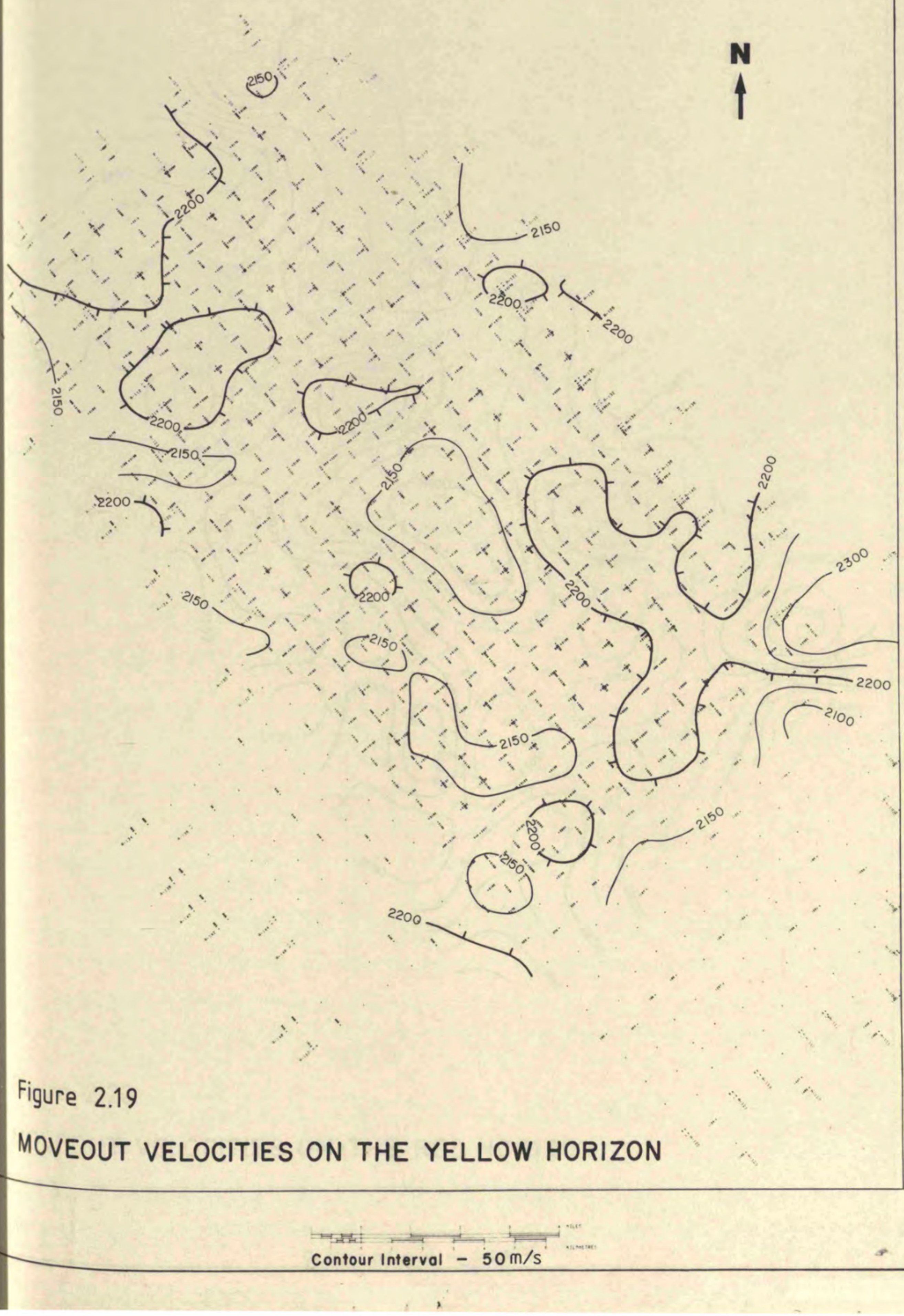

Figure 2.19

MOVEOUT VELOCITIES ON THE YELLOW HORIZON

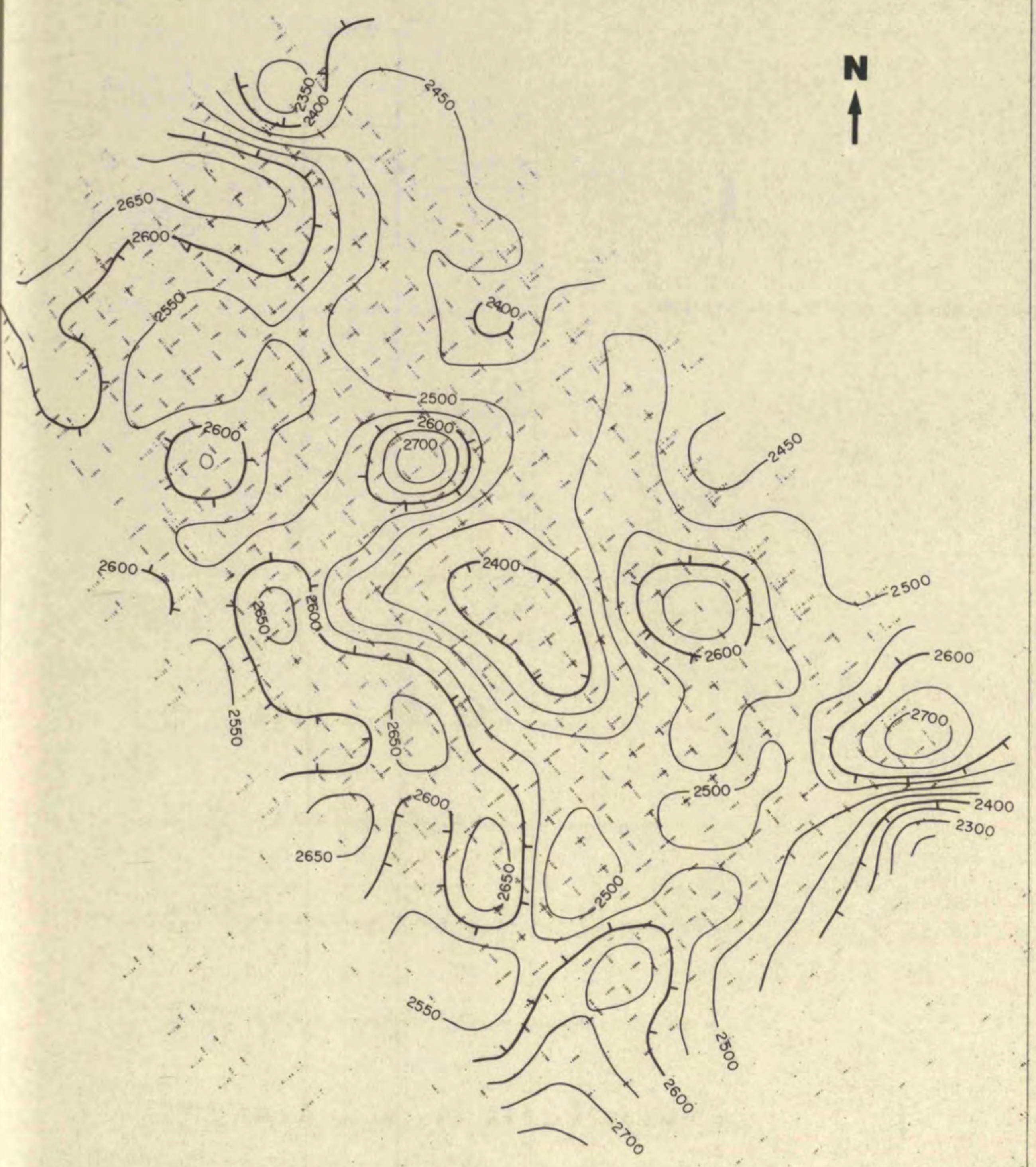

Figure 2.20

MOVEOUT VELOCITIES ON THE RED HORIZON

Contour Interval – 50 m/s

Figure 2.21 Synthetic Seismogram for Well A

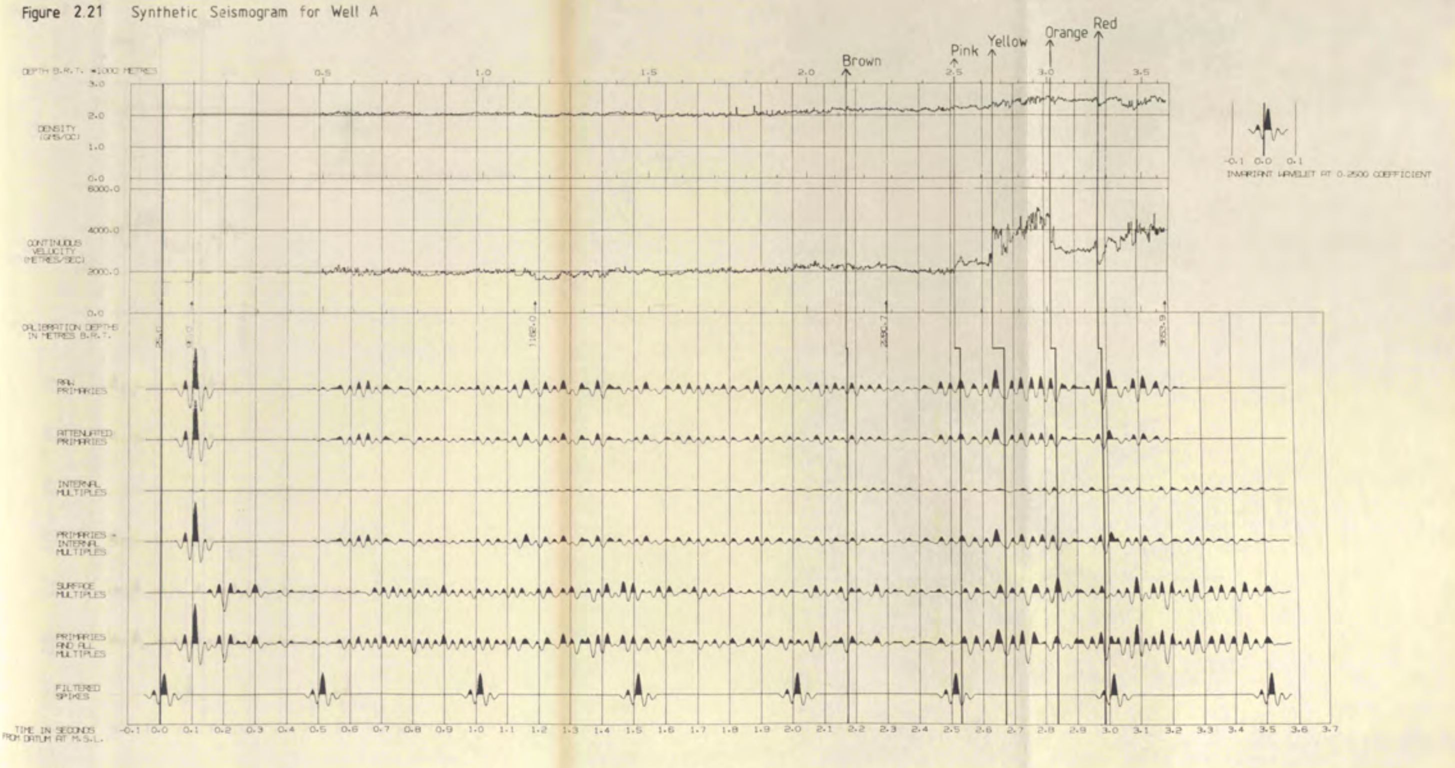

Figure 2.22 Synthetic Seismogram for Well B

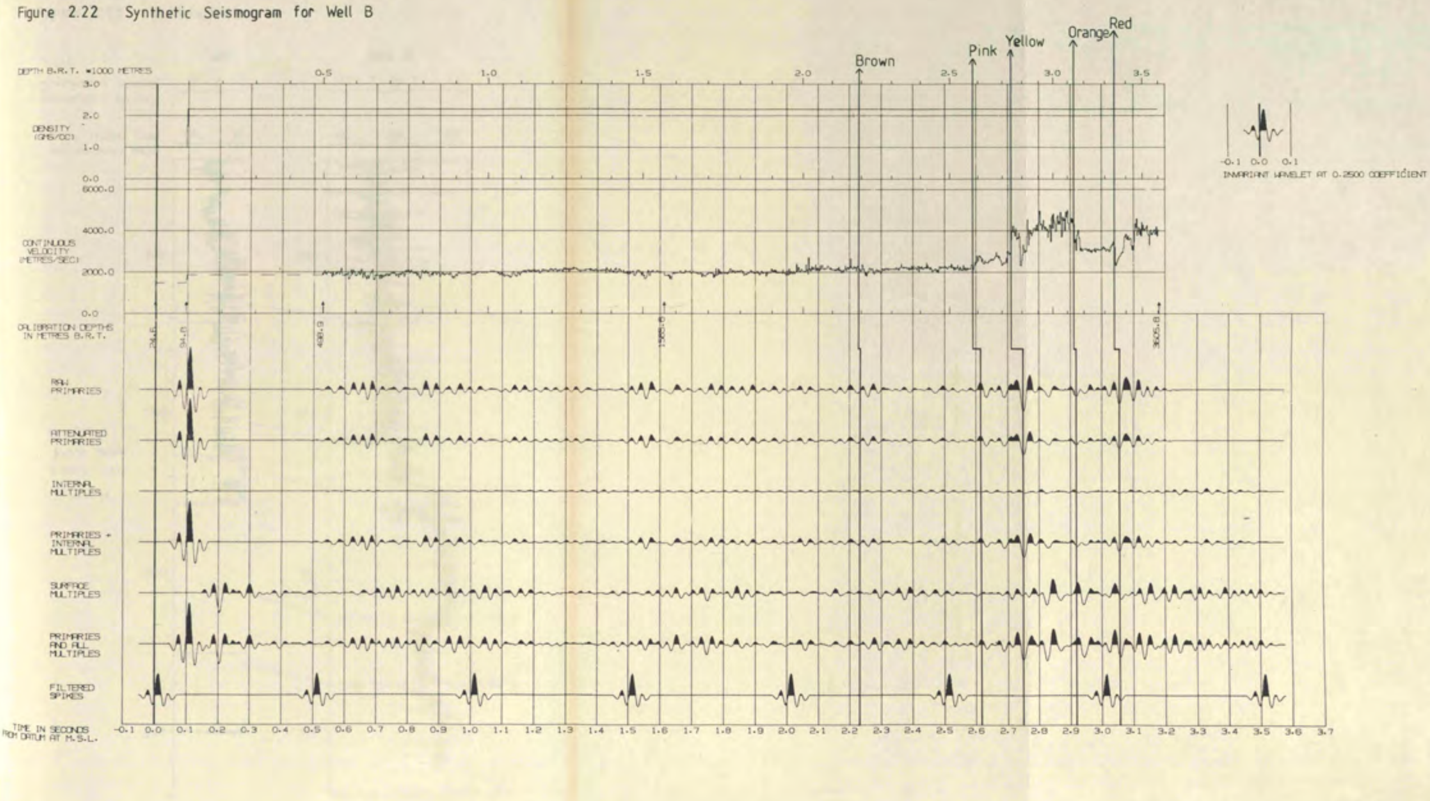

Figure 2.23 Correlation of Sonic Logs Scale 1:10 000

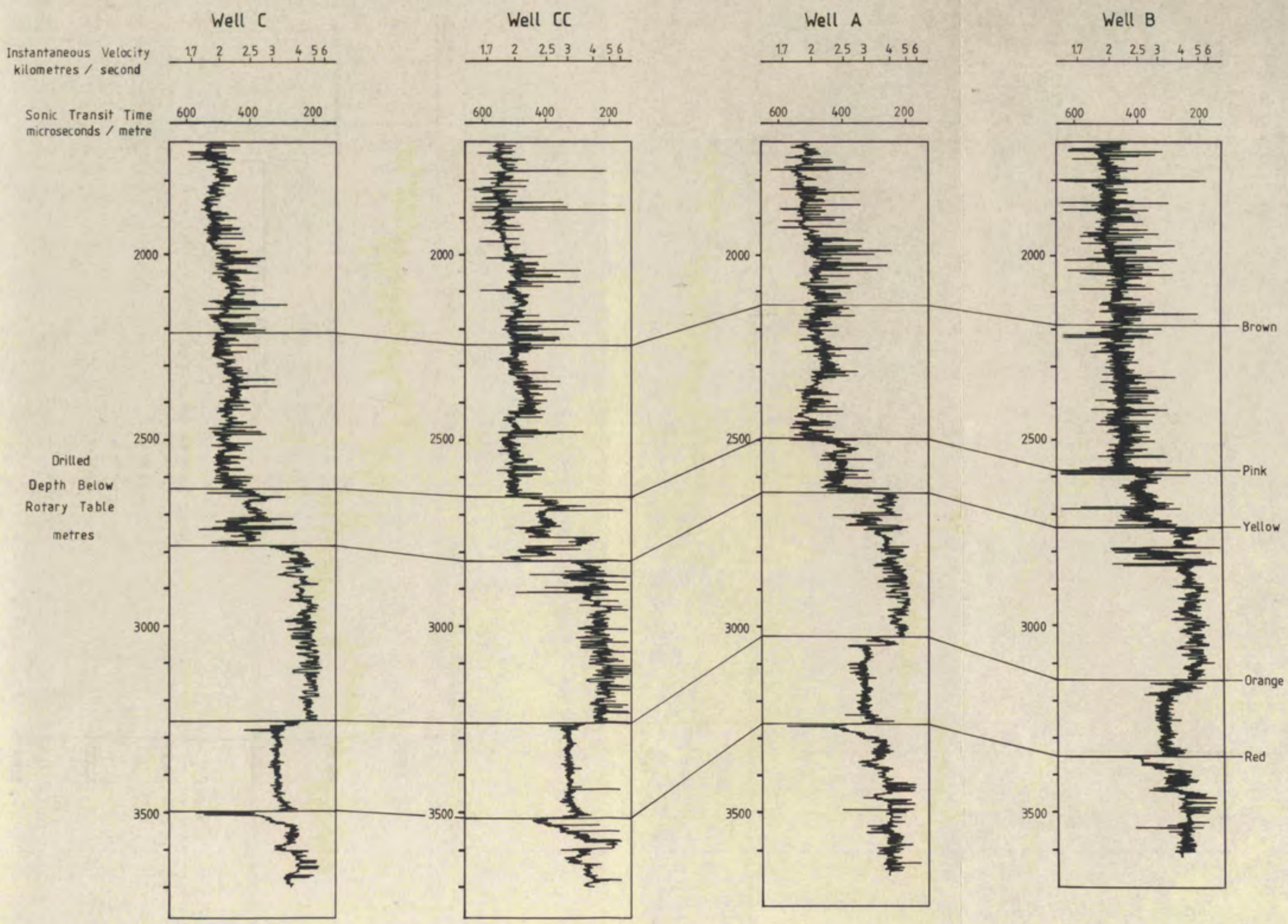

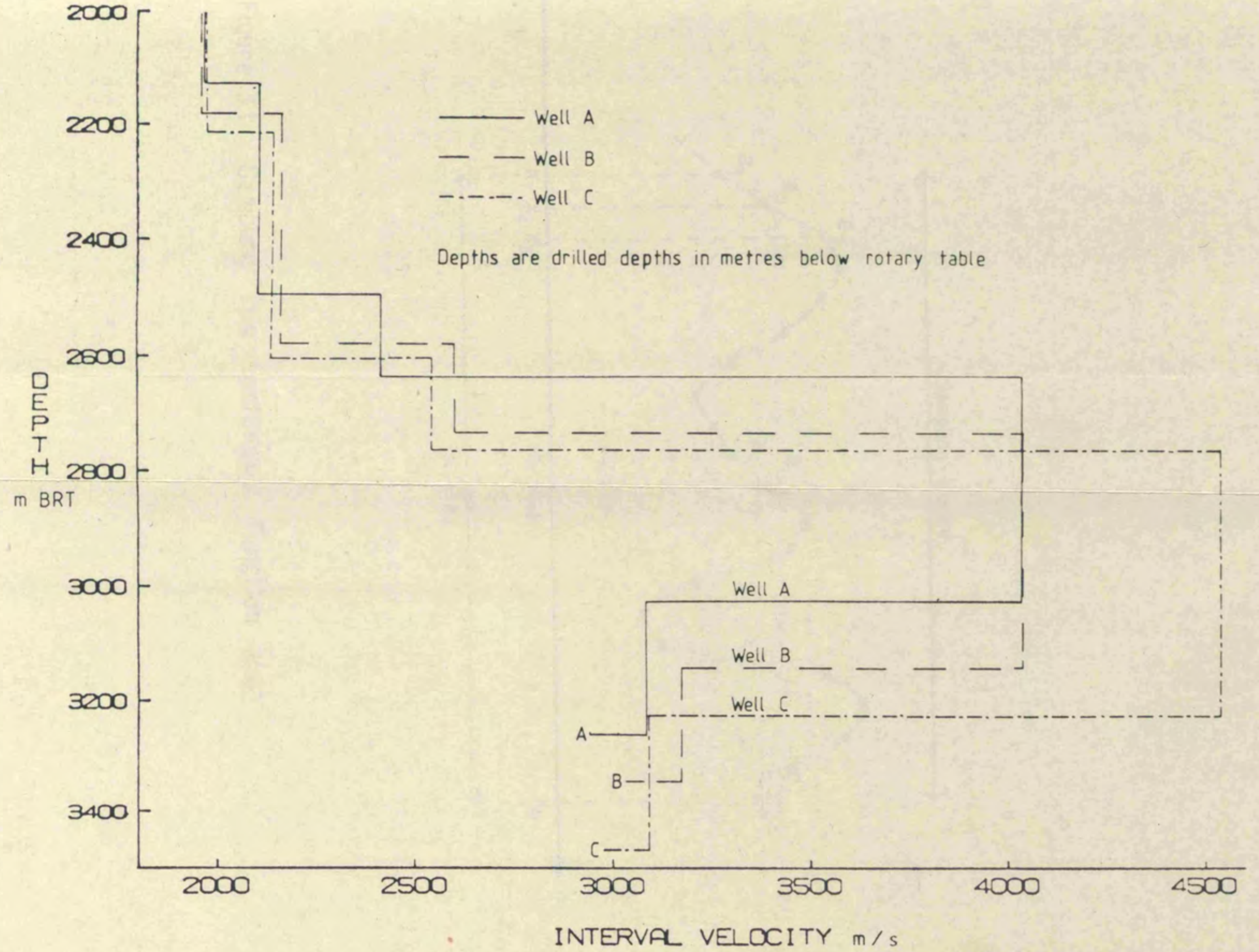

Figure 2.24 Gross Interval Velocity - Depth Functions for Wells A, B and C

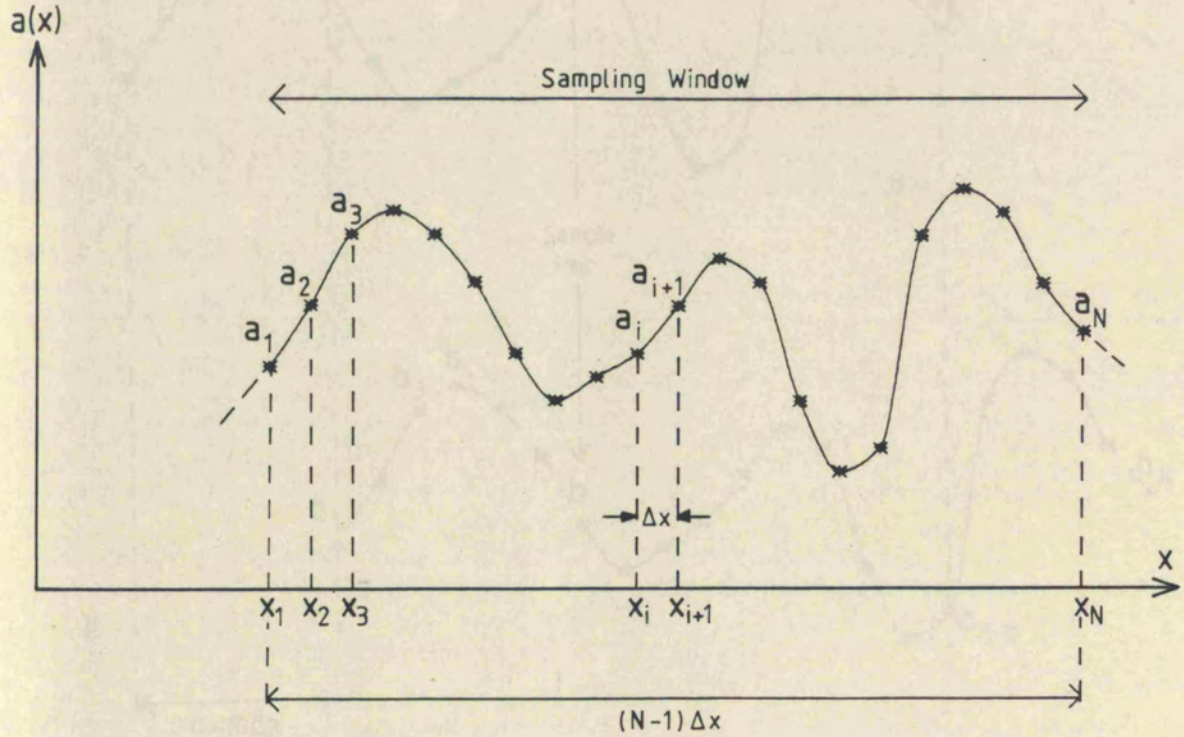

Figure 3.1 Sampling The Continuous Function a(x)

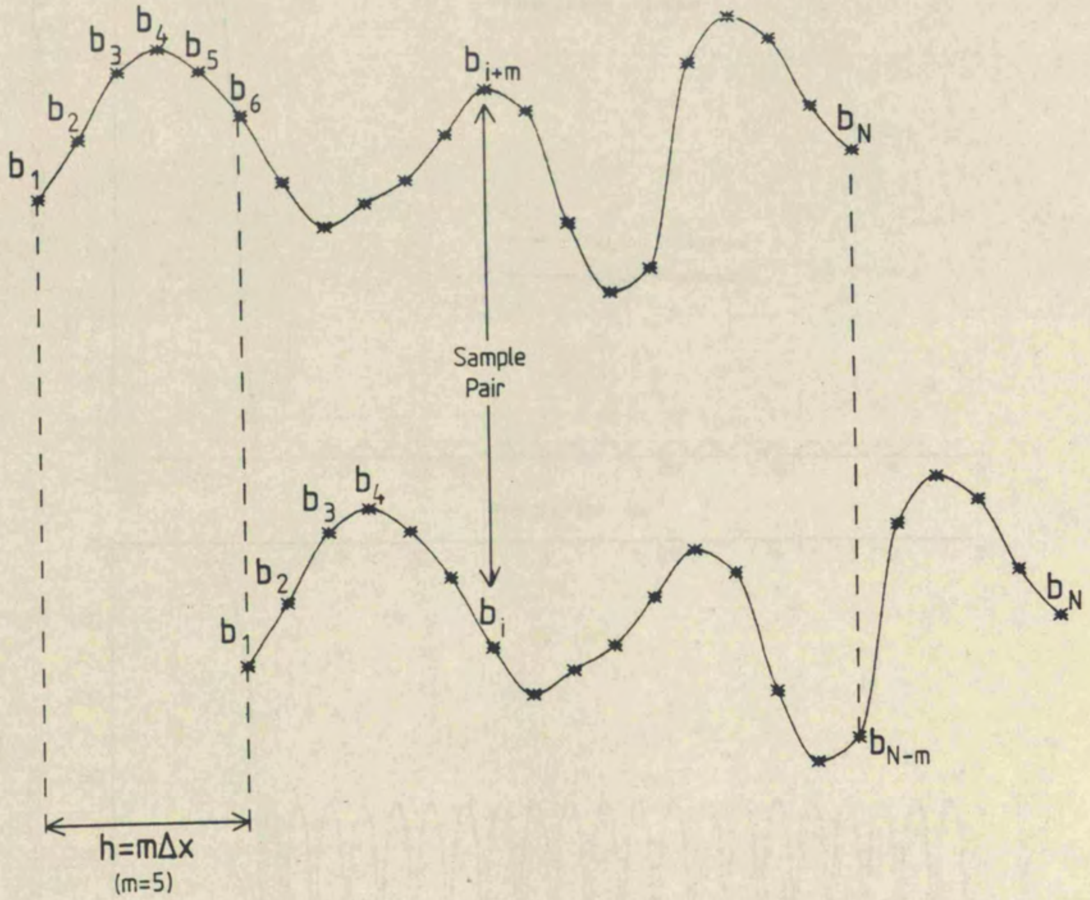

Figure 3.2 The Sampled Function b_i at Lag $m\Delta x$

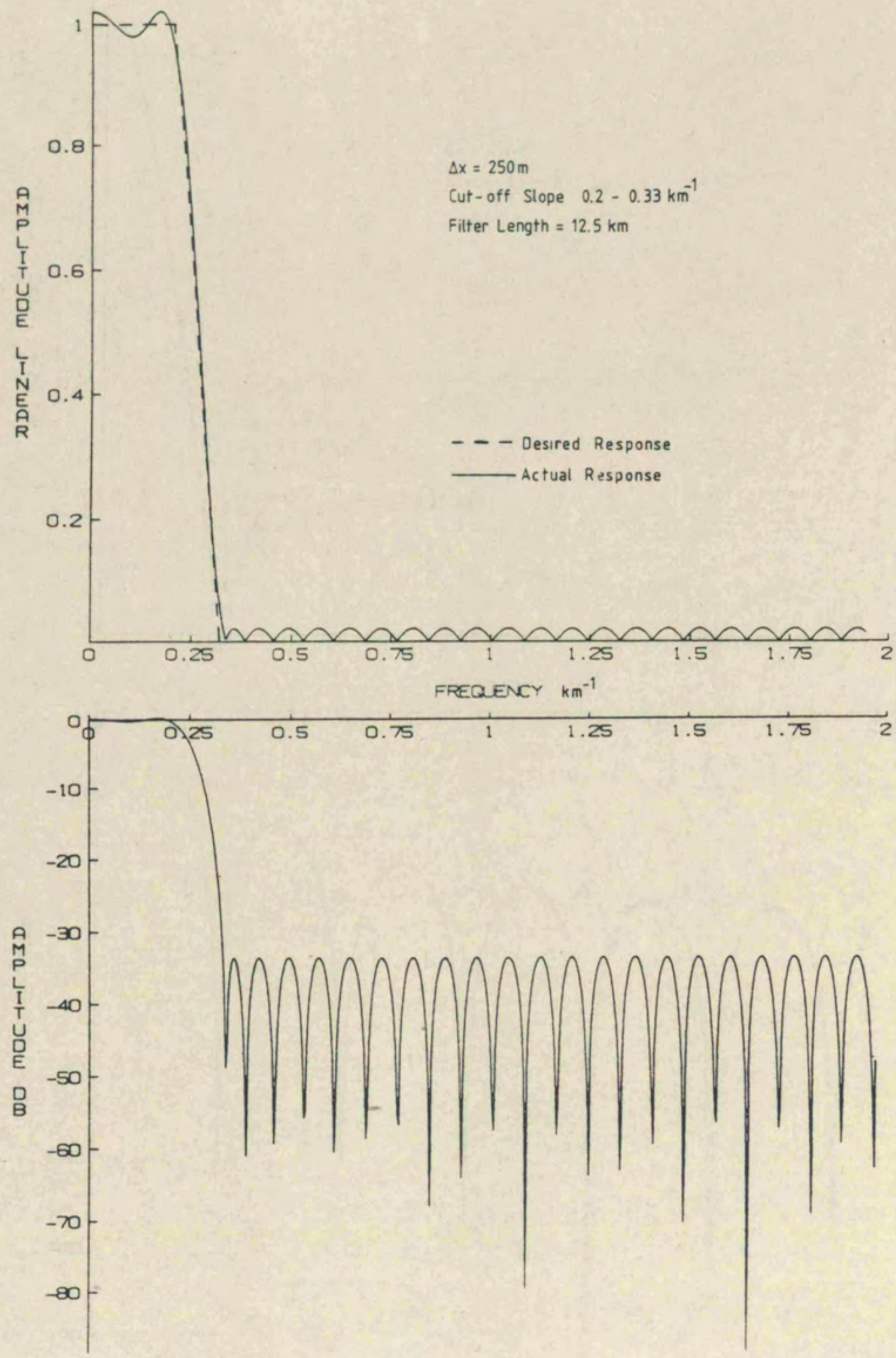

Figure 3.3 Frequency Response of a Typical Low-Pass Filter Designed by the Remez Exchange Algorithm

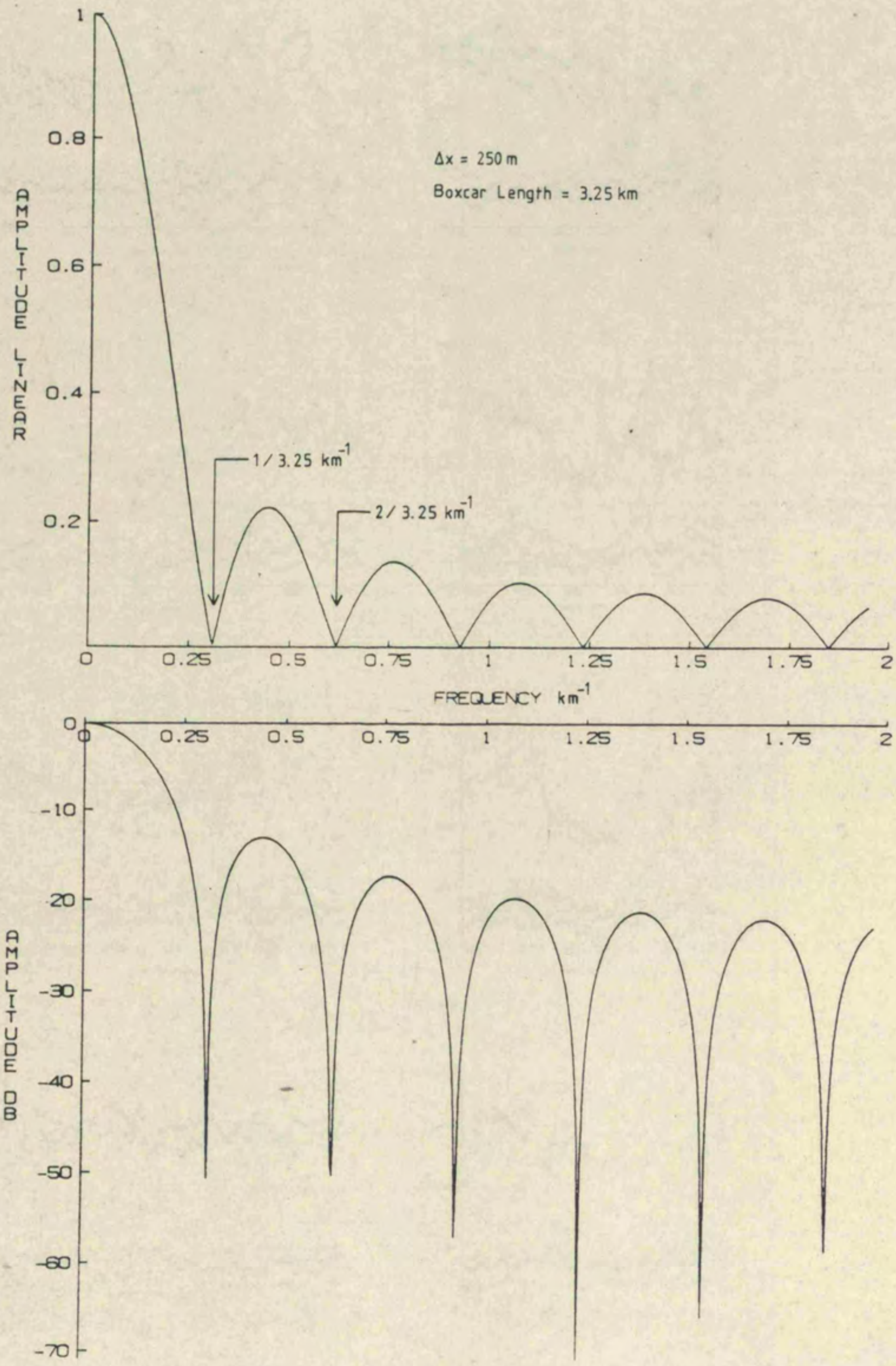

Figure 3.4 Frequency Response of a Typical Boxcar Moving Average

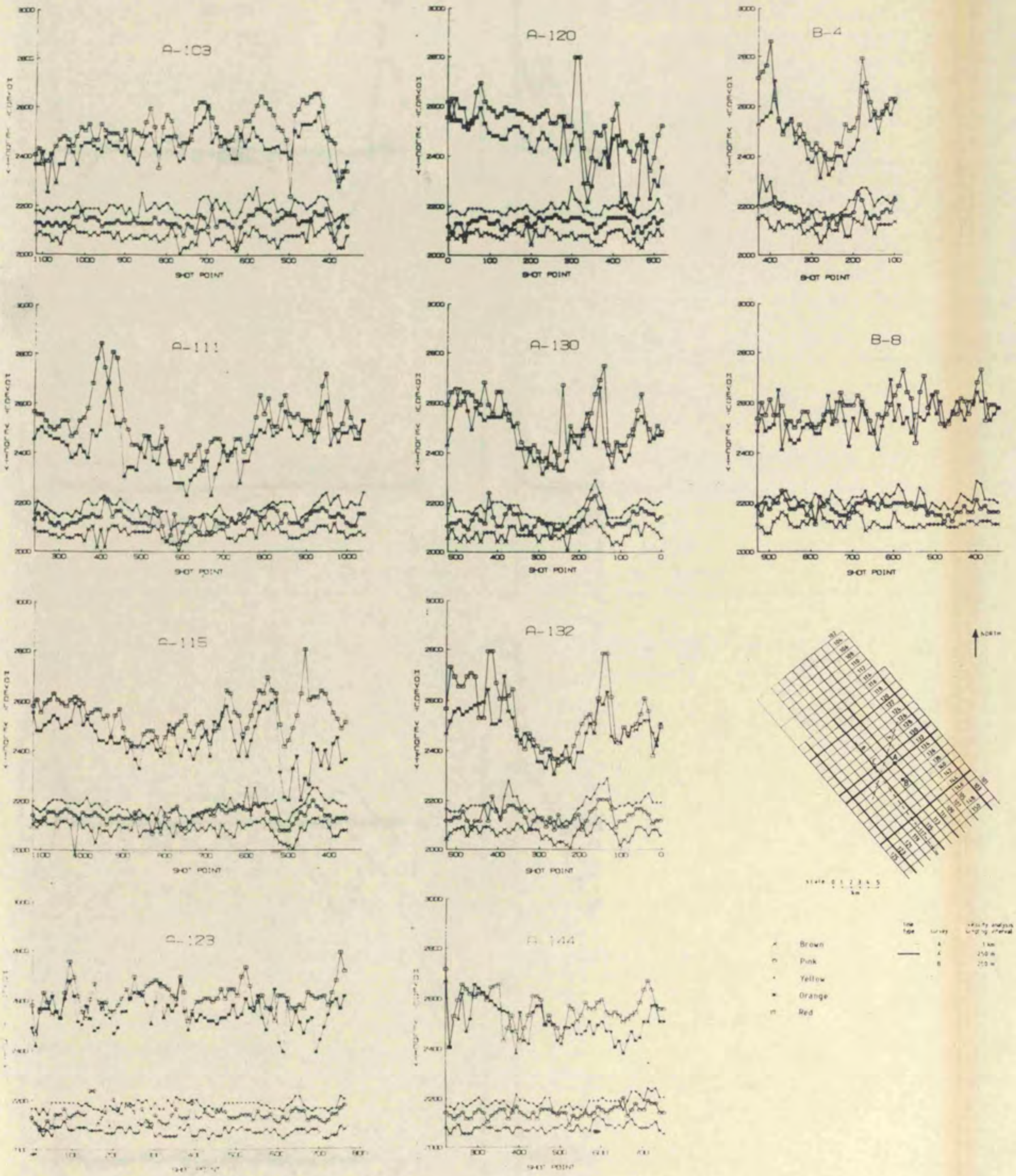

Figure 3.5 Raw Moveout Velocity Profiles (m/s)

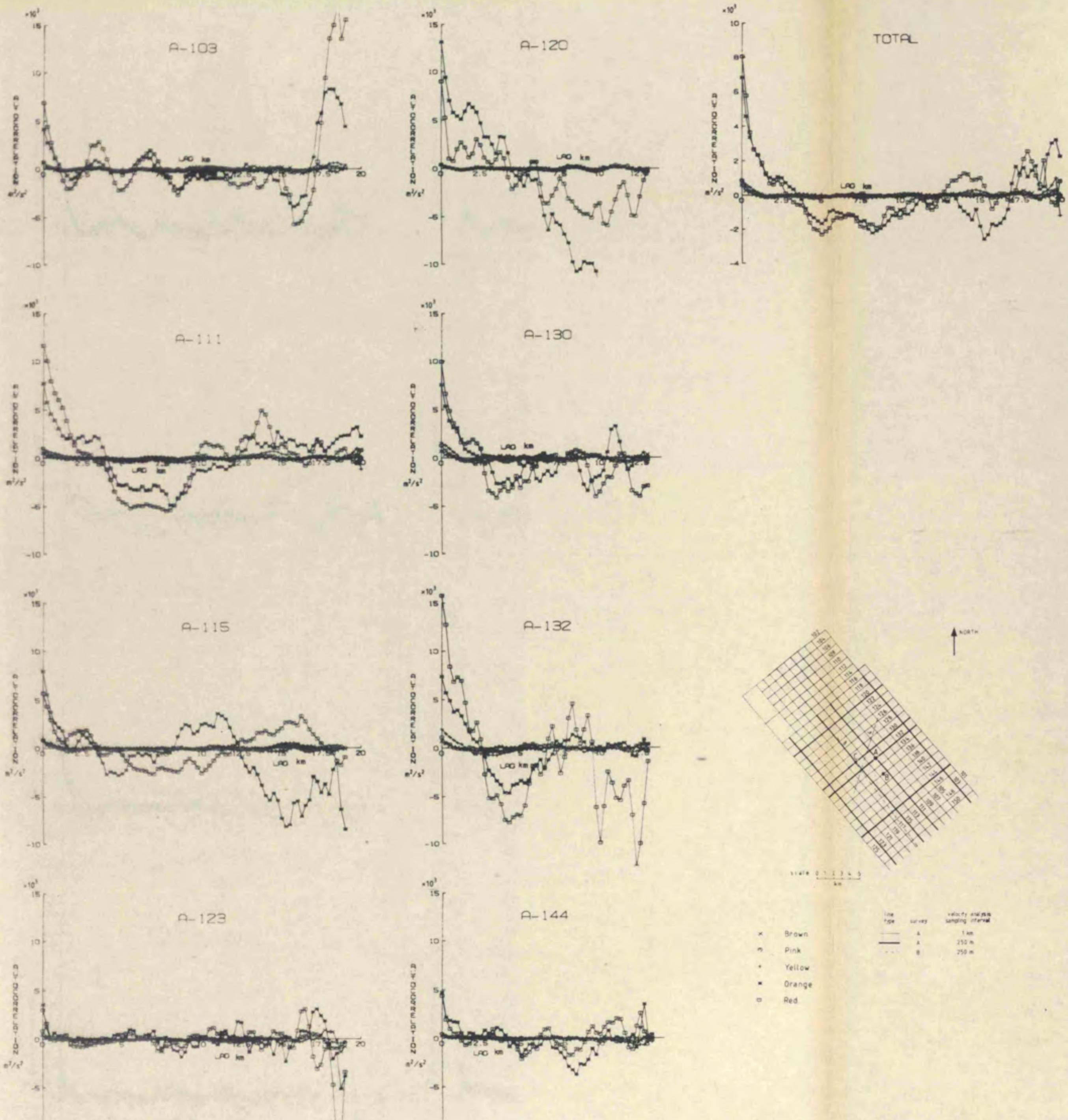

Figure 3.6 Autocorrelograms of the Brown, Pink, Yellow, Orange and Red Moveout Velocity Profiles

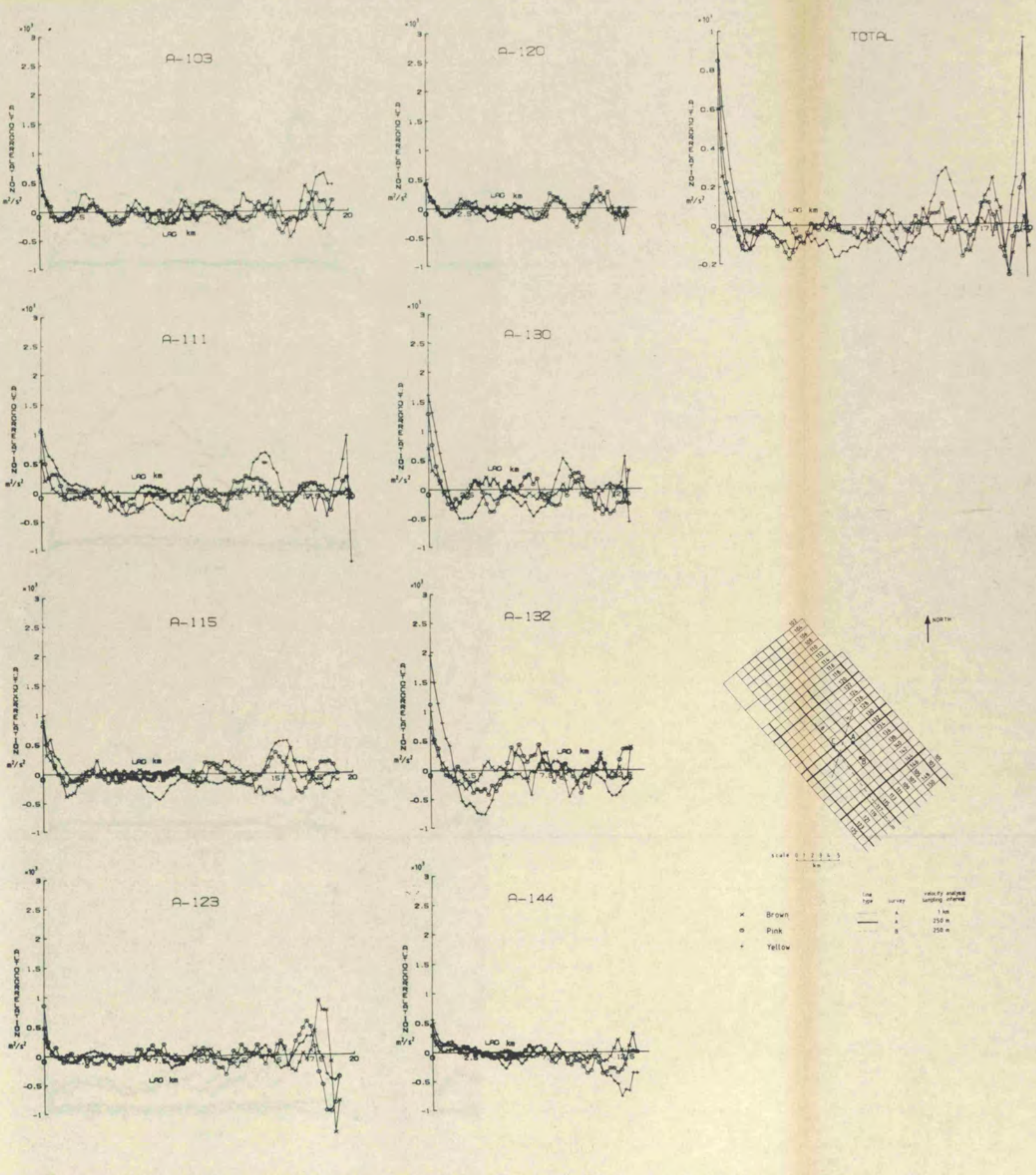

Figure 3.7 Autocorrelograms of the Brown, Pink and Yellow Moveout Velocity Profiles

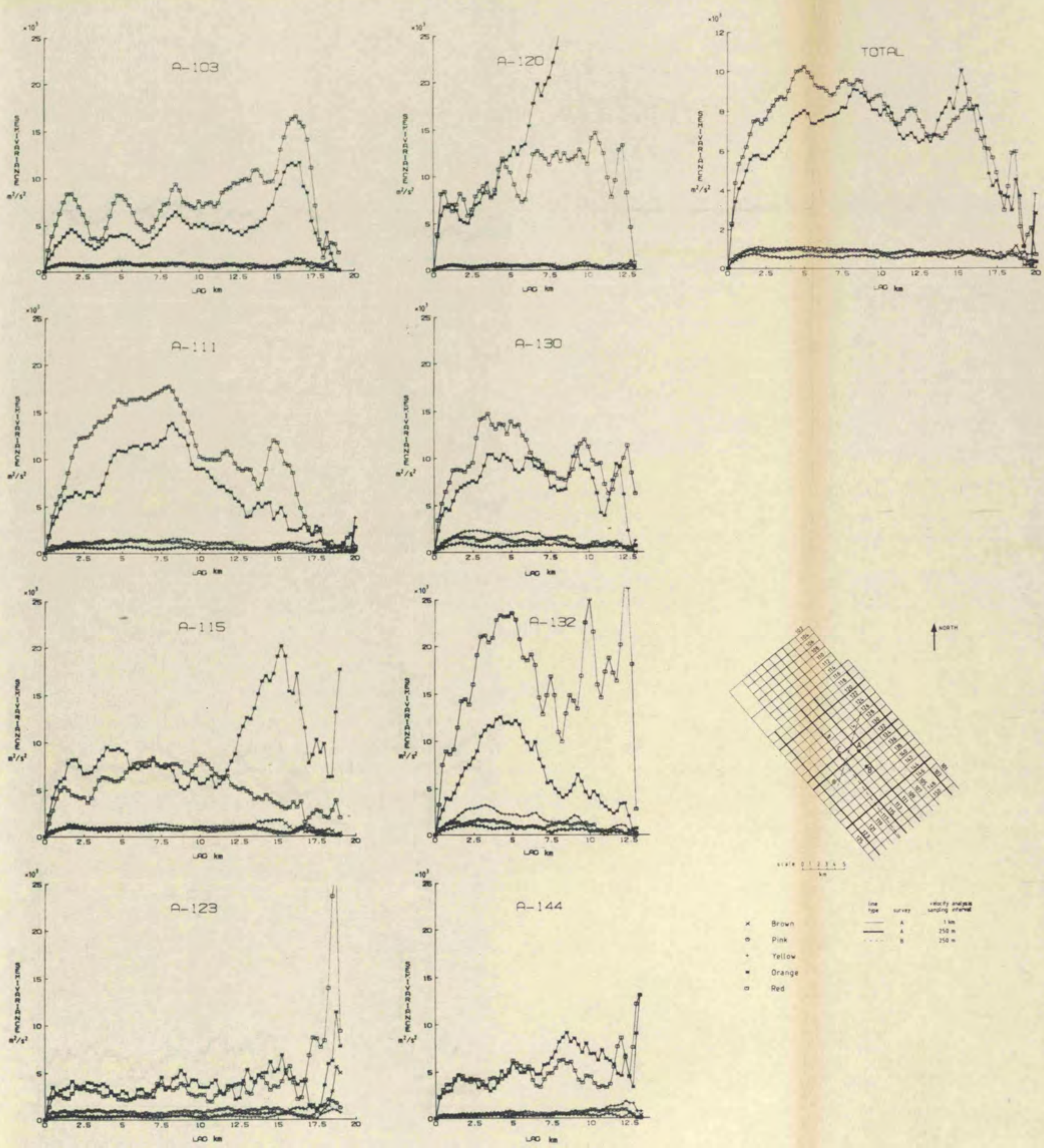

Figure 3.8 Semivariograms of the Brown, Pink, Yellow, Orange and Red Moveout Velocity Profiles

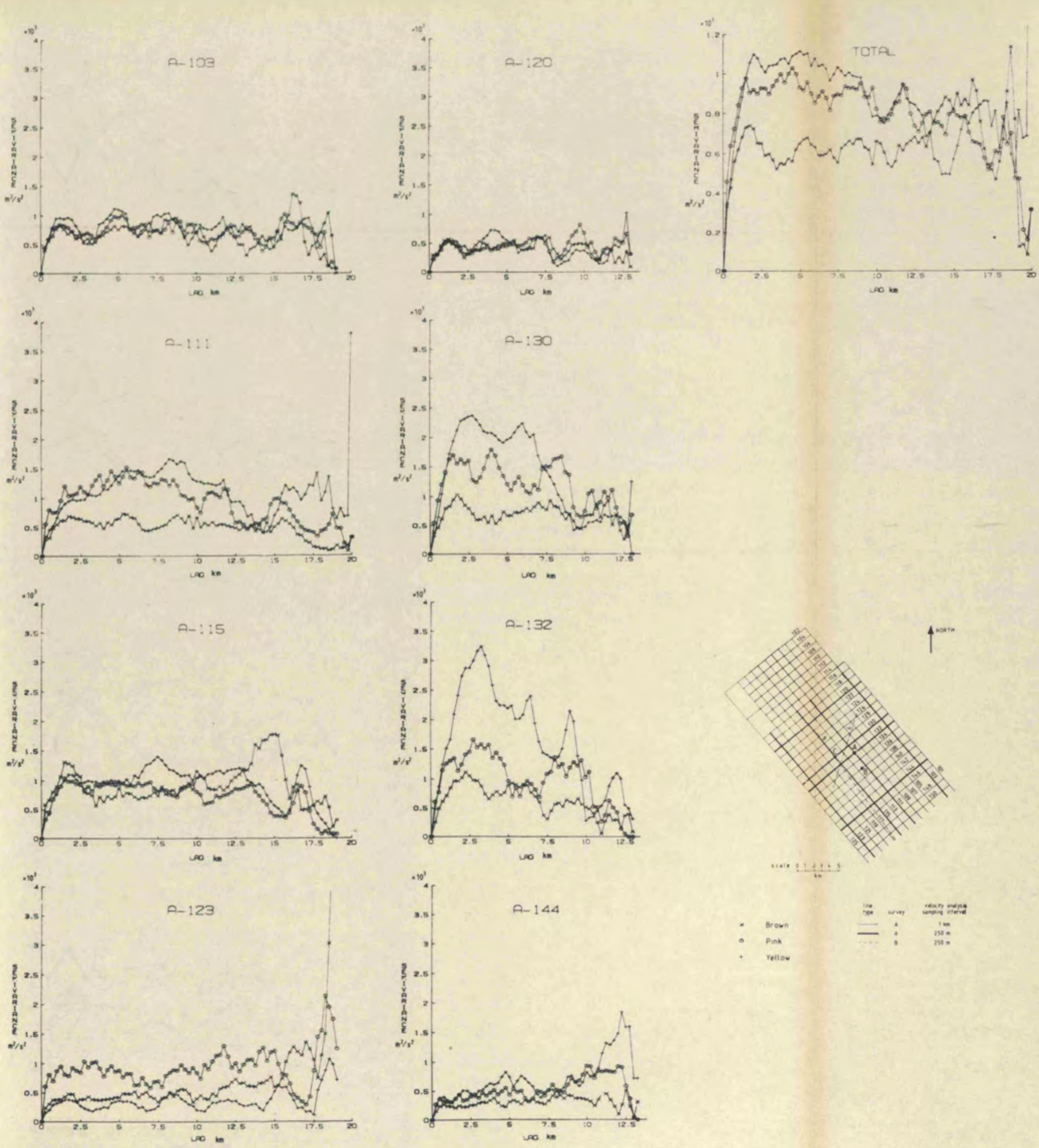

Figure 3.9 Semivariograms of the Brown, Pink and Yellow Moveout Velocity Profiles

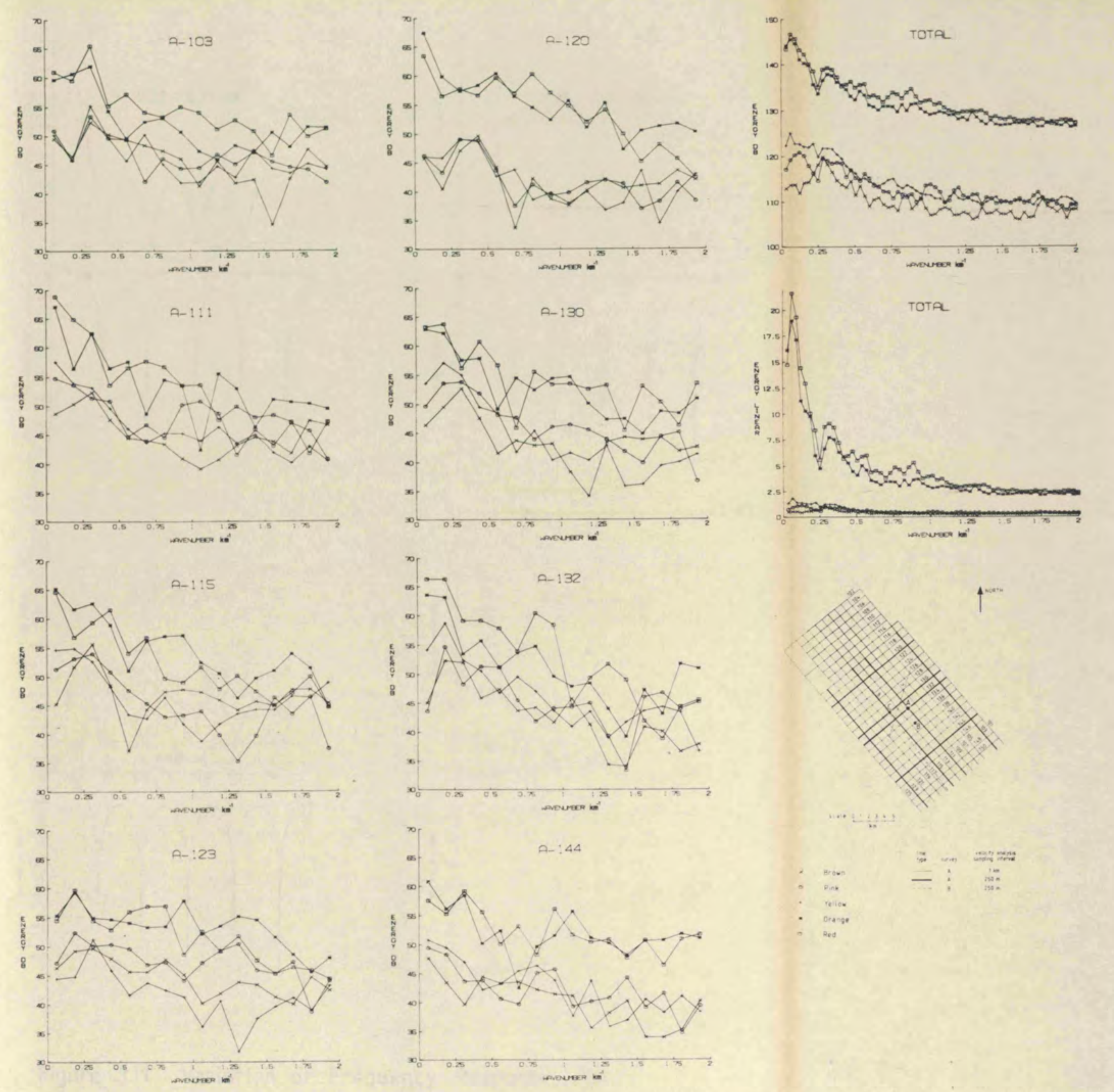

Figure 3.10 Energy Spectra of the Brown, Pink, Yellow, Orange and Red Moveout Velocity Profiles

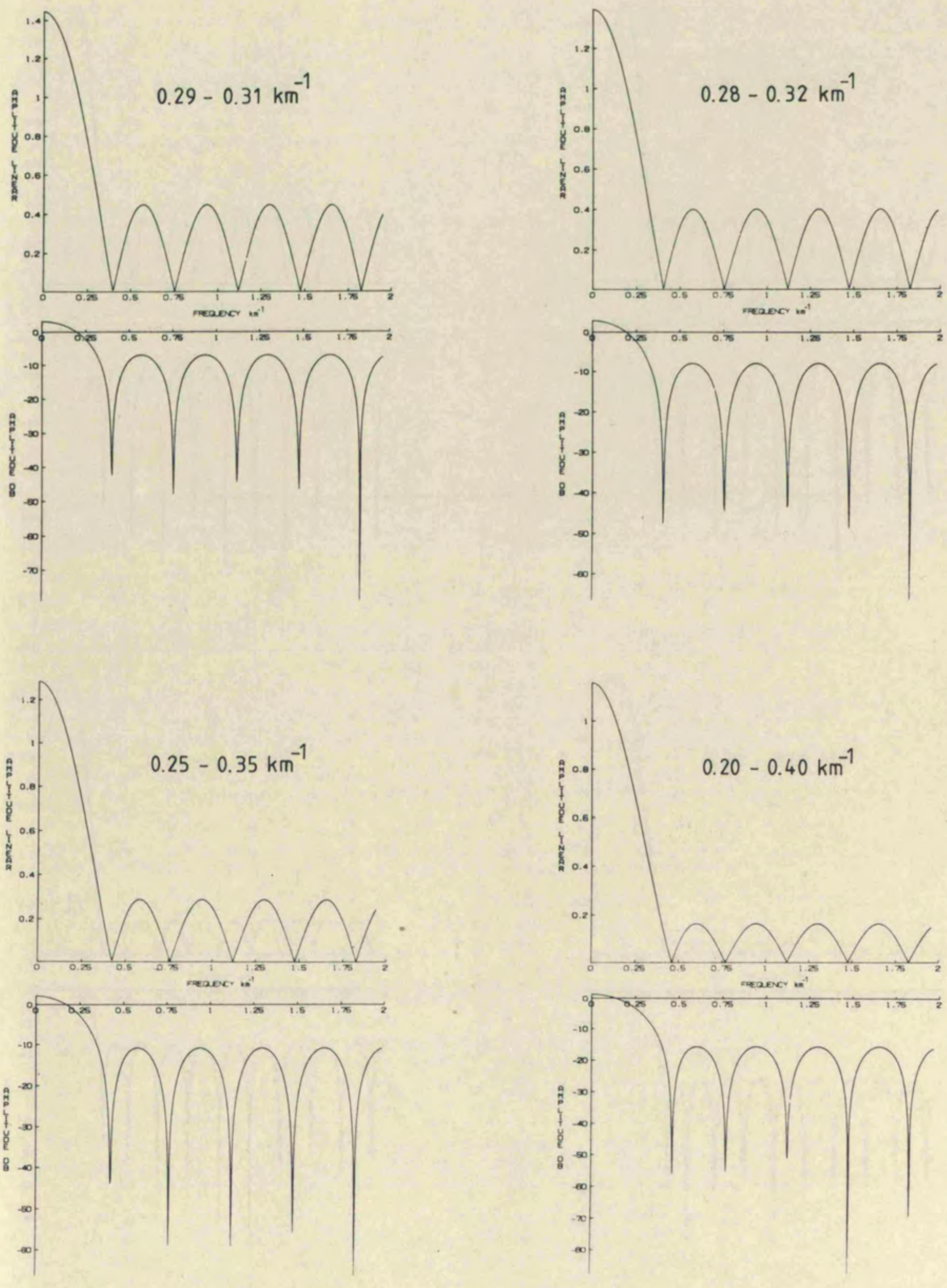

Figure 3.11 Variation of Frequency Response with Cut-off Slope for Low-pass Filters of Length 3 km

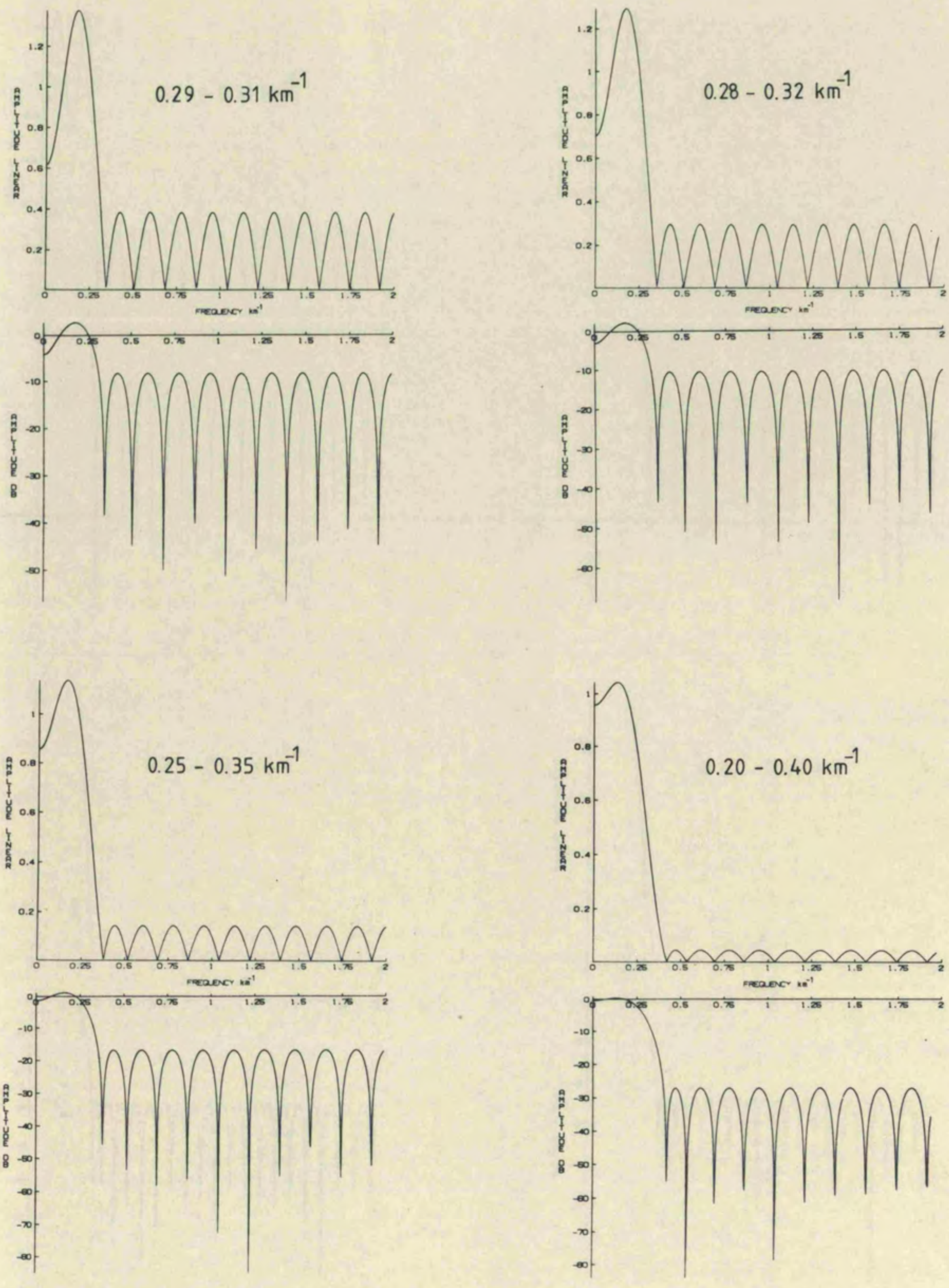

Figure 3.12 Variation of Frequency Response with Cut-off Slope for Low-pass Filters of Length 6 km

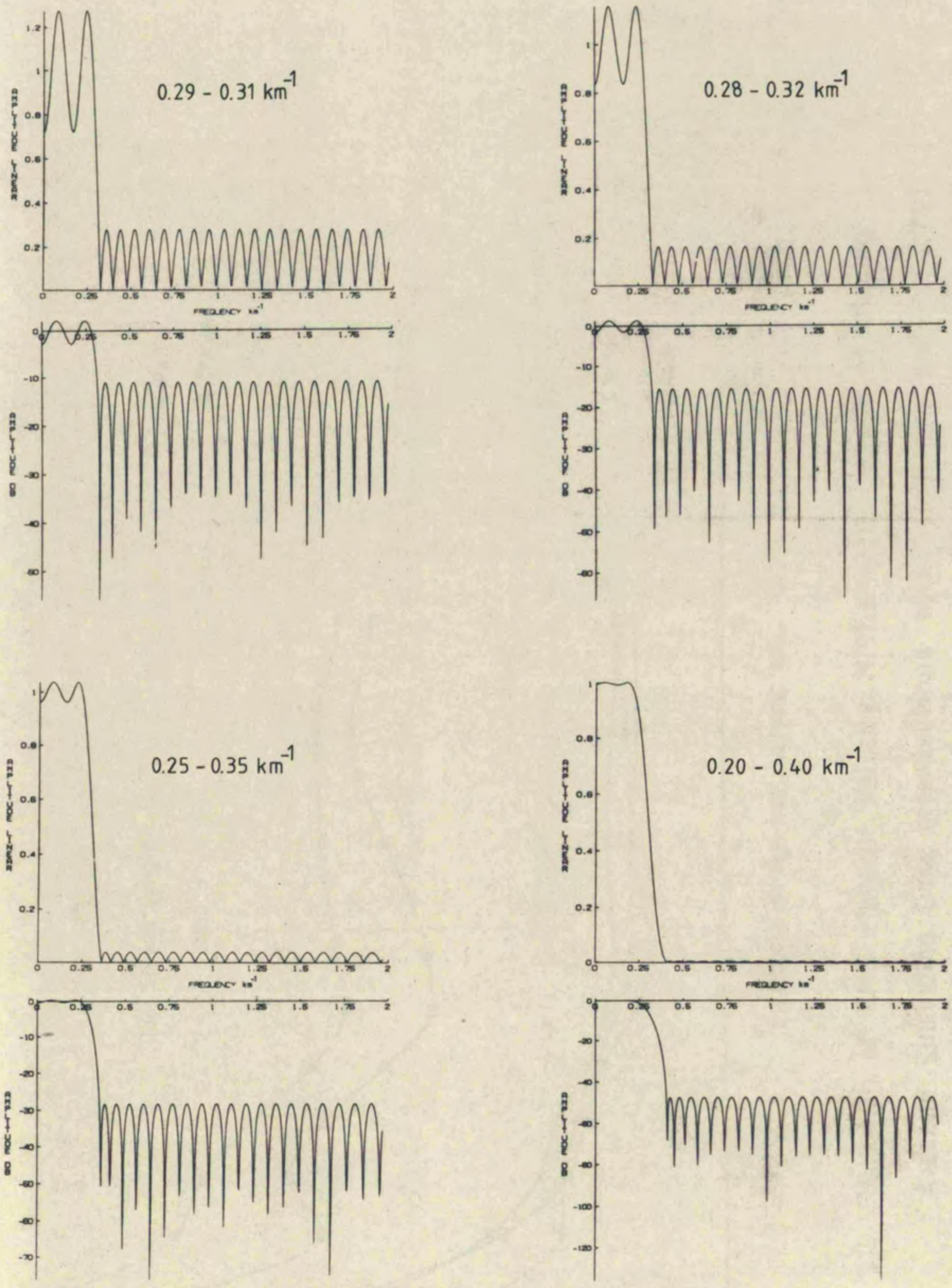

Figure 3.13 Variation of Frequency Response with Cut-off Slope for Low-pass Filters of Length 12 km

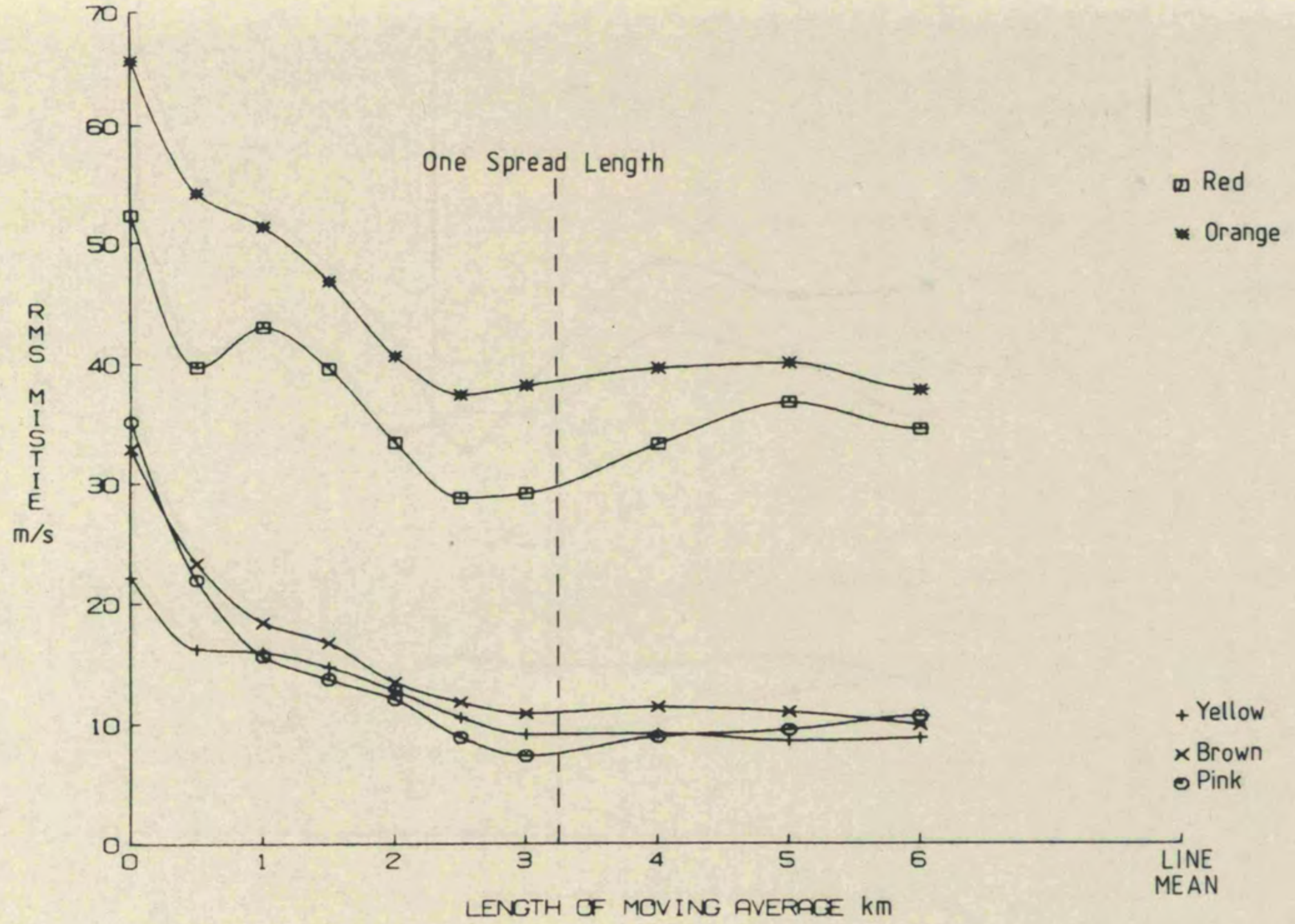

Figure 3.14 Variation of RMS Moveout Velocity Mistie with Length of Moving Average (Including Line Intersections with Smoothing End-effects)

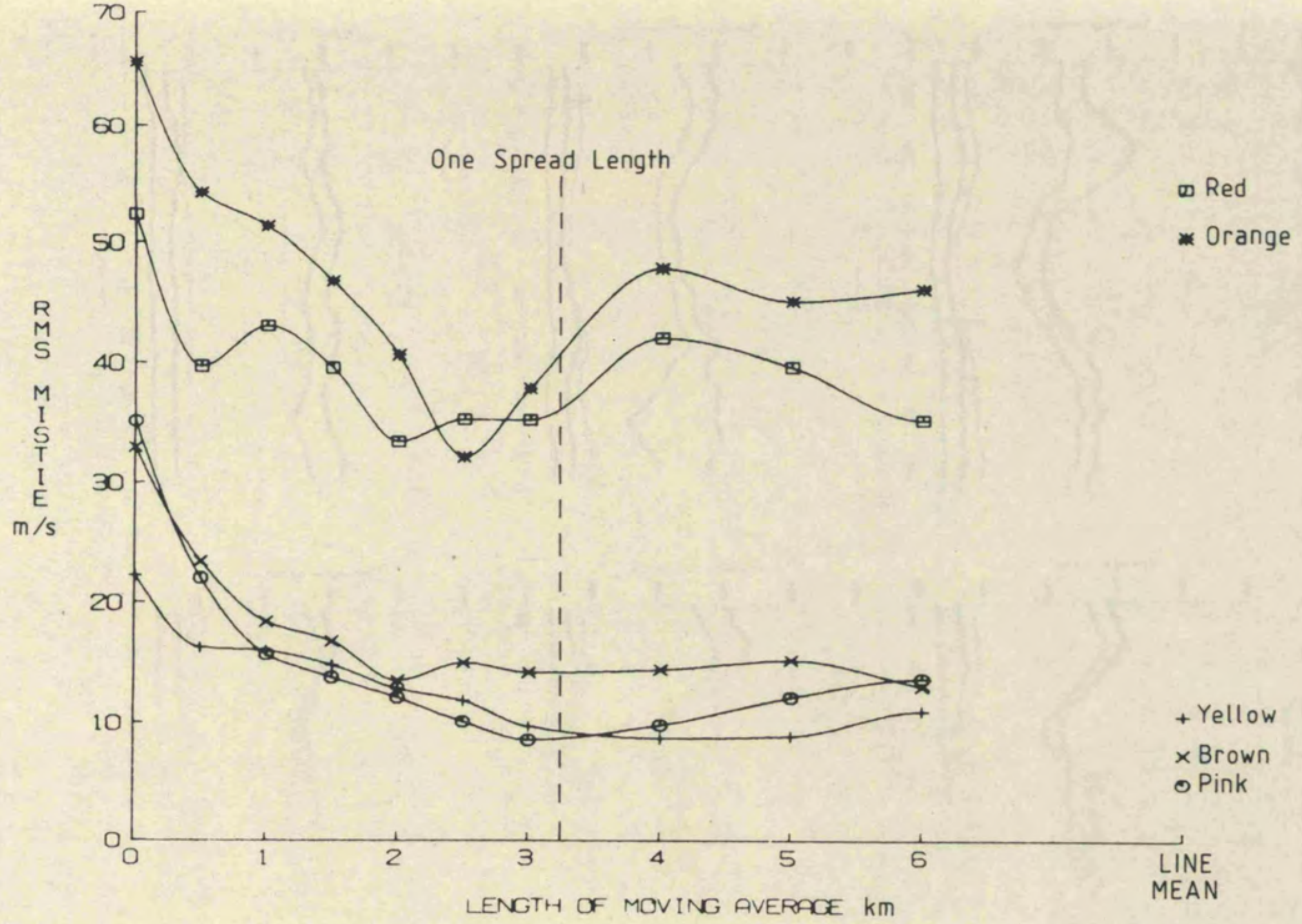

Figure 3.15 Variation of RMS Moveout Velocity Mistie with Length of Moving Average (Excluding Line Intersections with Smoothing End-effects)

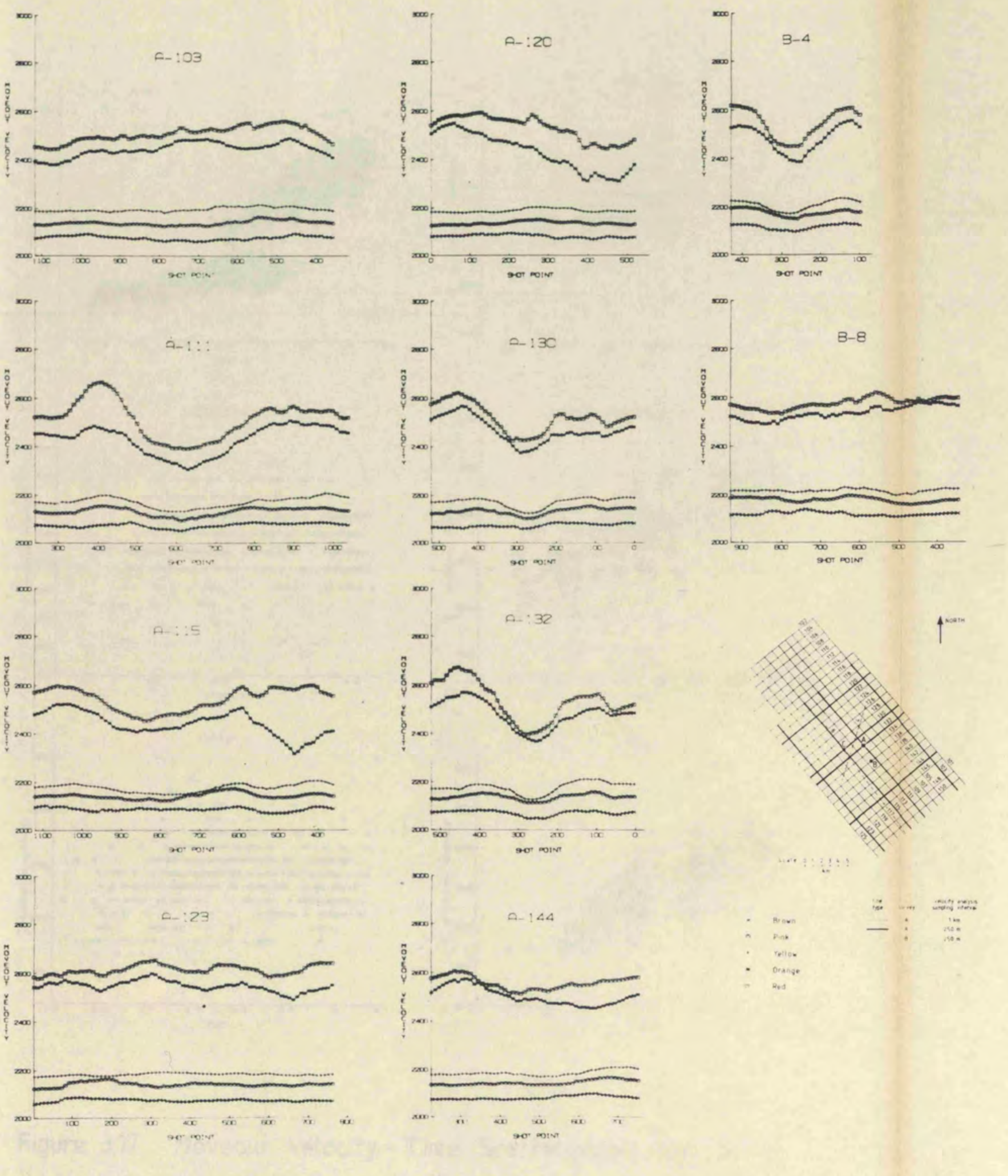

Figure 3.16 Smoothed Moveout Velocity Profiles (m/s)
(One Spread Length Boxcar Moving Average)

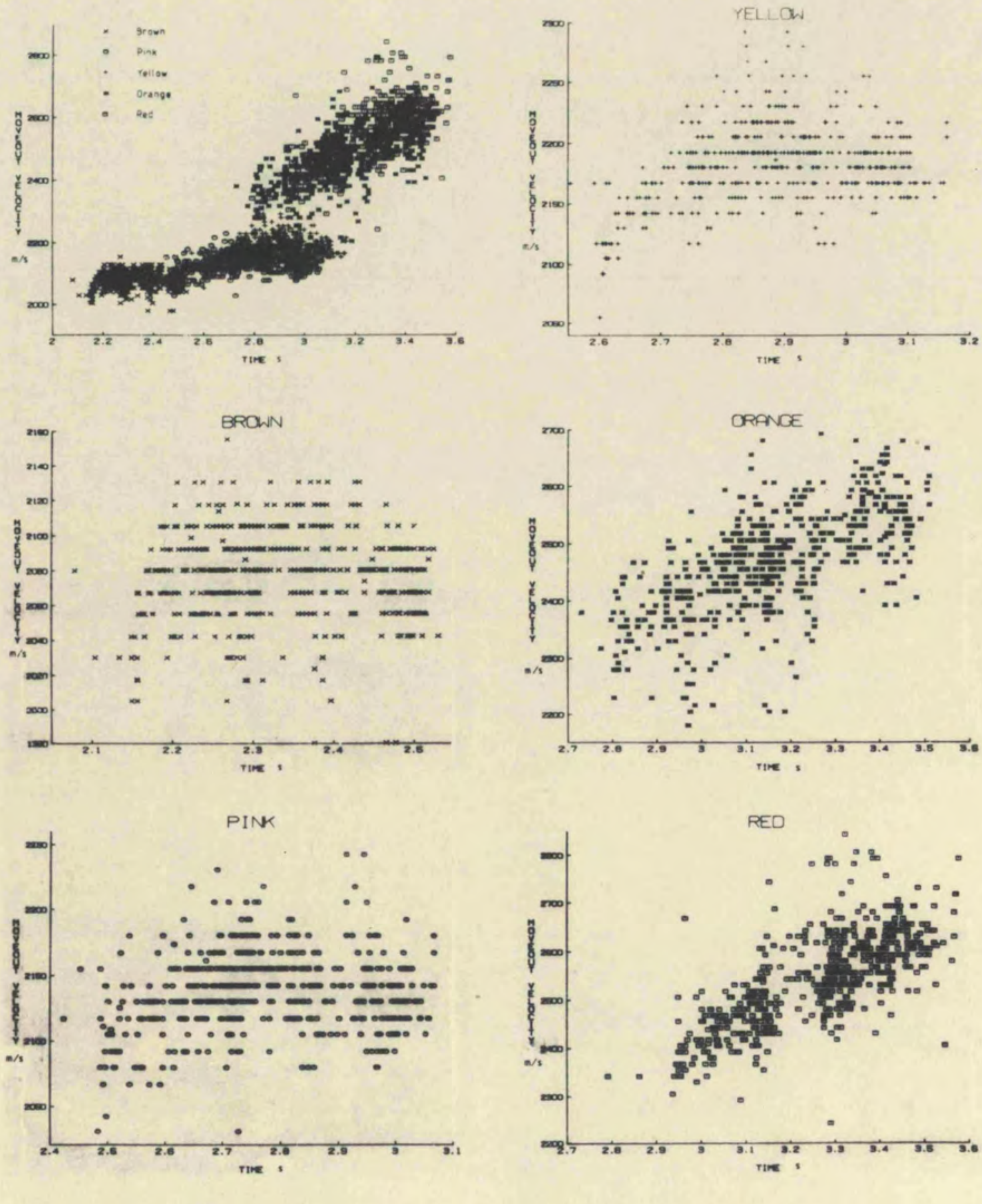

Figure 3.17 Moveout Velocity - Time Scattergrams for the Raw Moveout Velocity Profiles

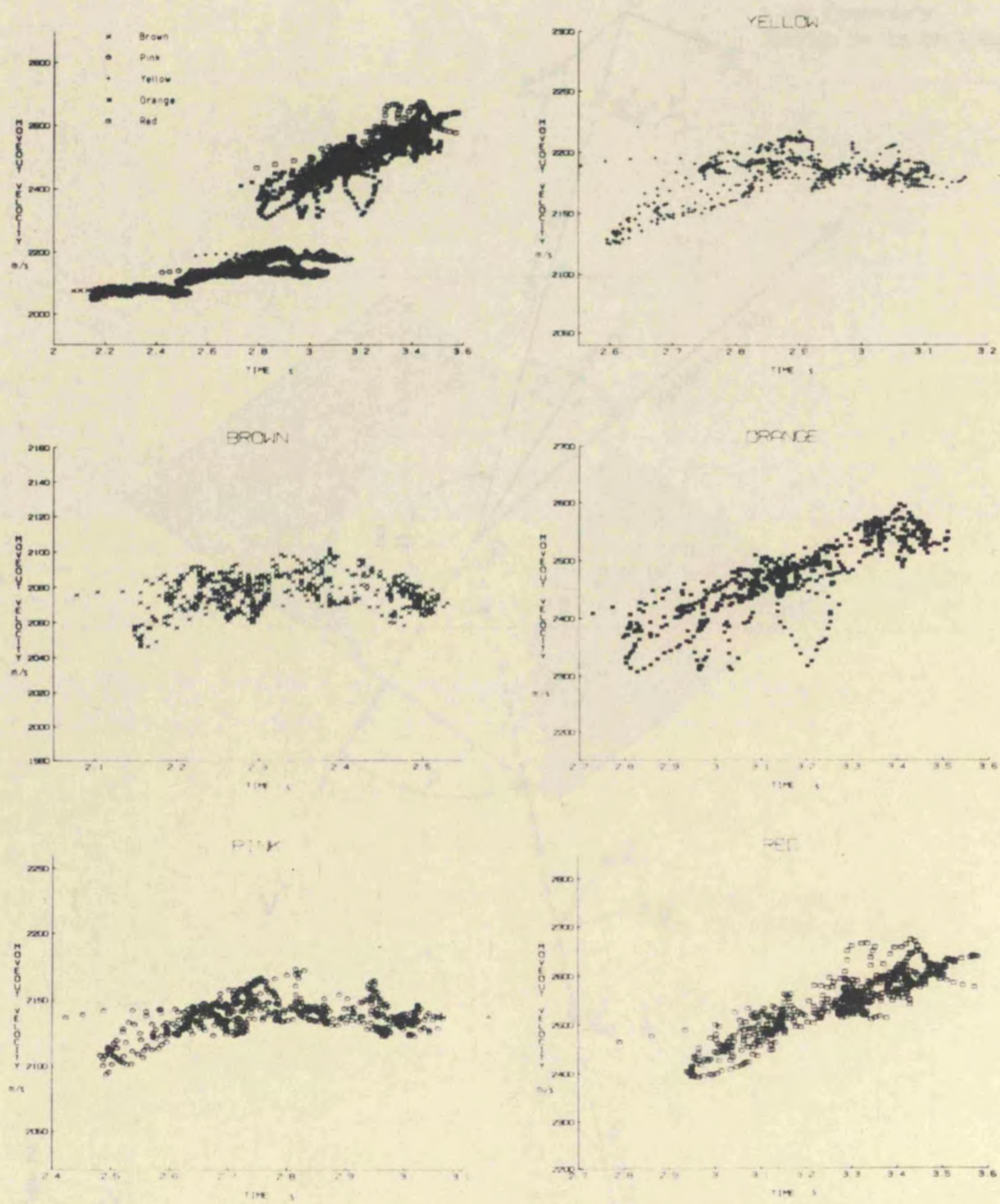

Figure 3.18 Moveout Velocity - Time Scattergrams for the Smoothed Moveout Velocity Profiles (One Spread Length Boxcar Moving Average)

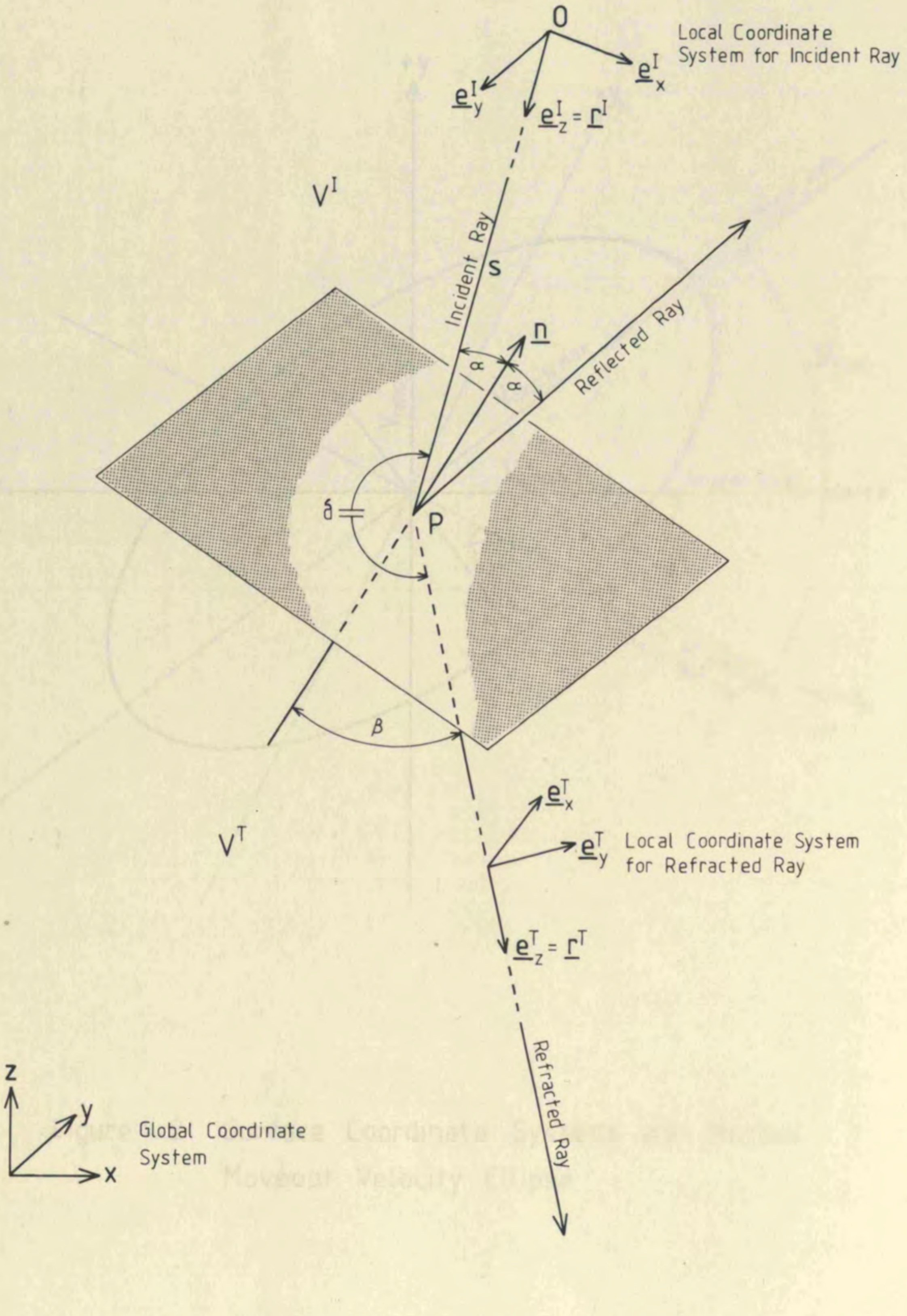

Figure 4.1 Raytracing Geometry at a 3D Plane Dipping Interface

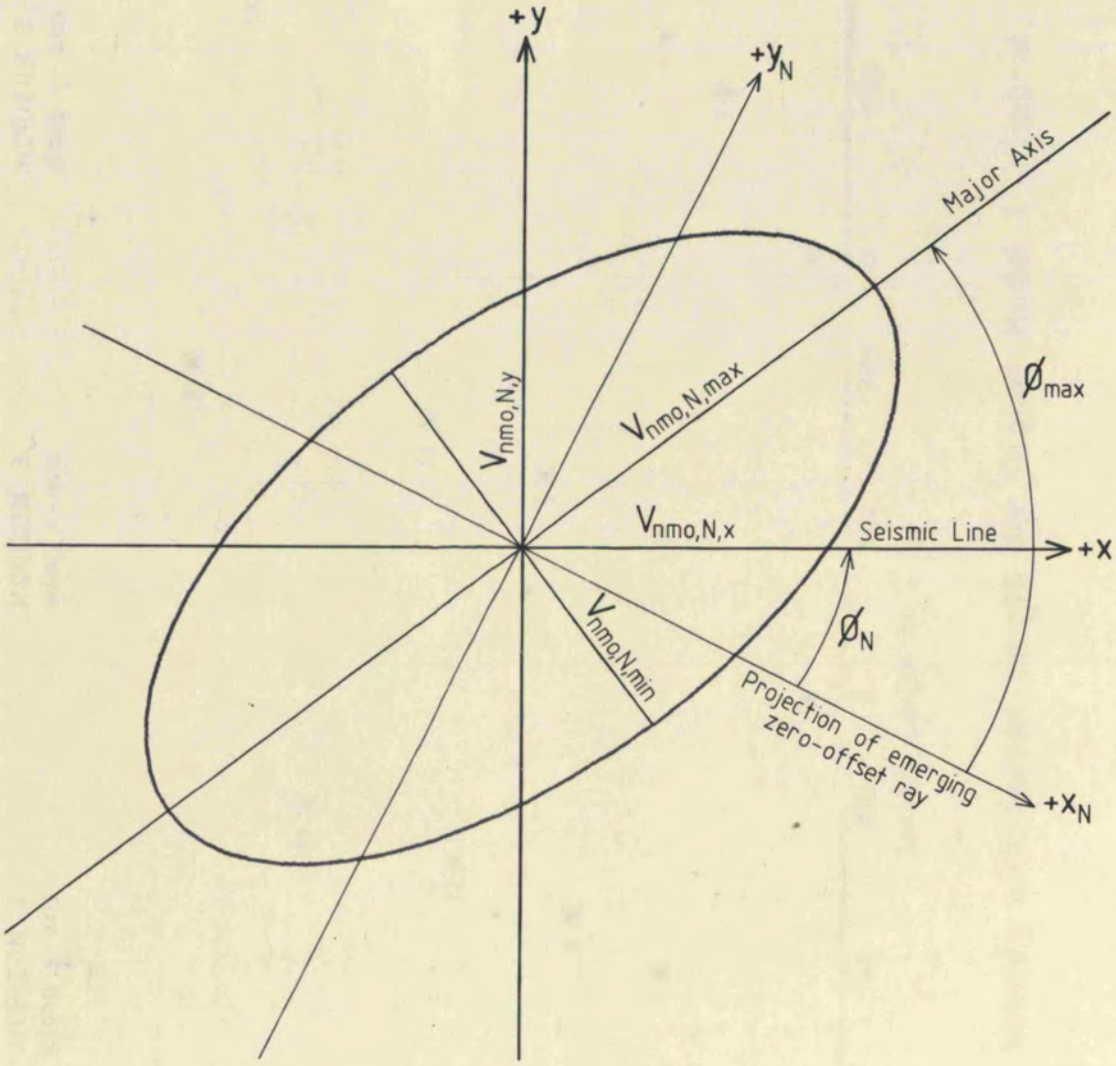

Figure 4.2 Surface Coordinate Systems and Normal Moveout Velocity Ellipse

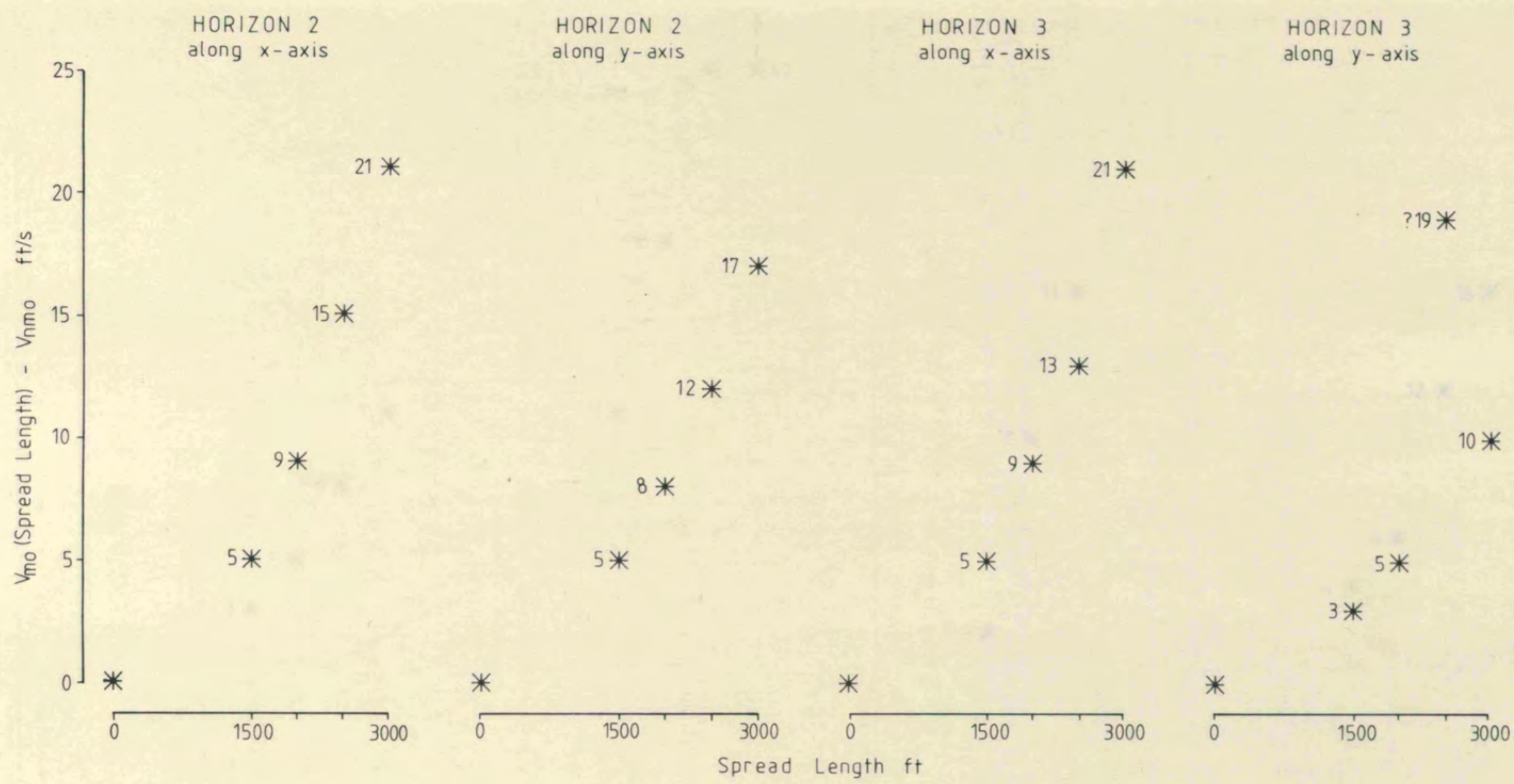

Figure 4.3 Variation of Moveout Velocity with Spread Length for Ground Model 1 (Hubral, 1976a; Table 1)

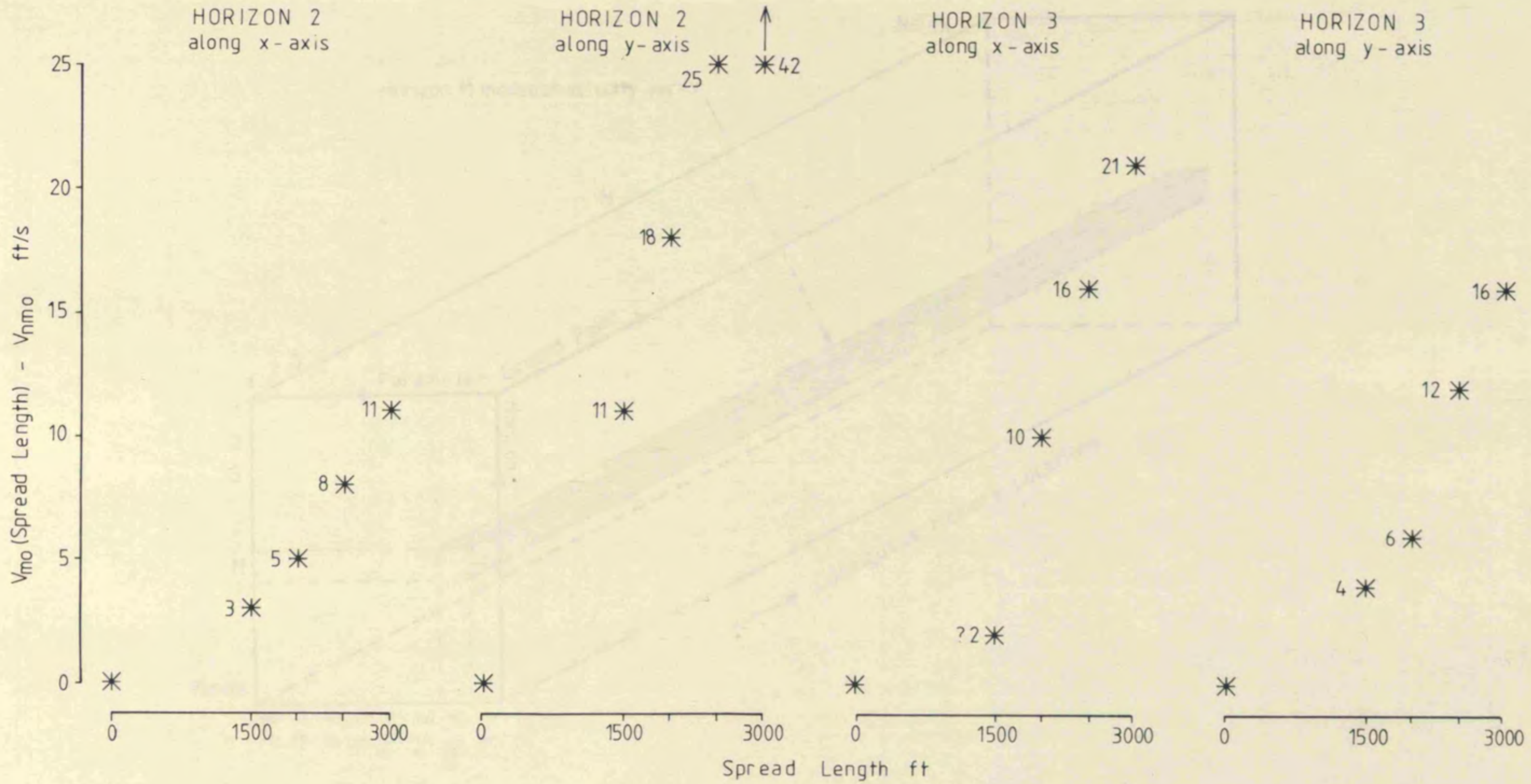

Figure 4.4 Variation of Moveout Velocity with Spread Length for Ground Model 2 (Hubral, 1976a; Table 2)

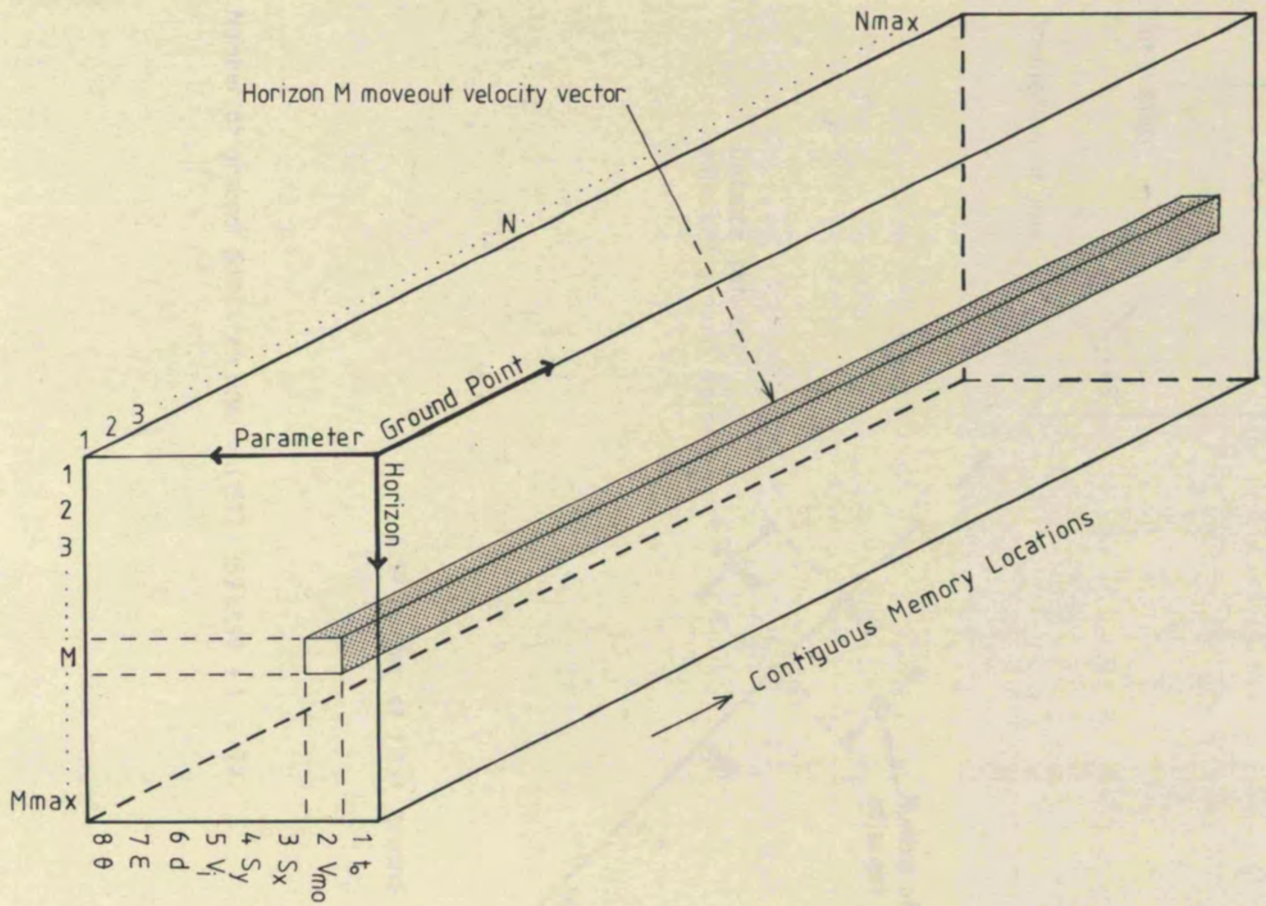

Figure 5.1 Schematic Configuration of the KRUNCH Matrix

This matrix accommodates data for up to Mmax horizons and Nmax ground points

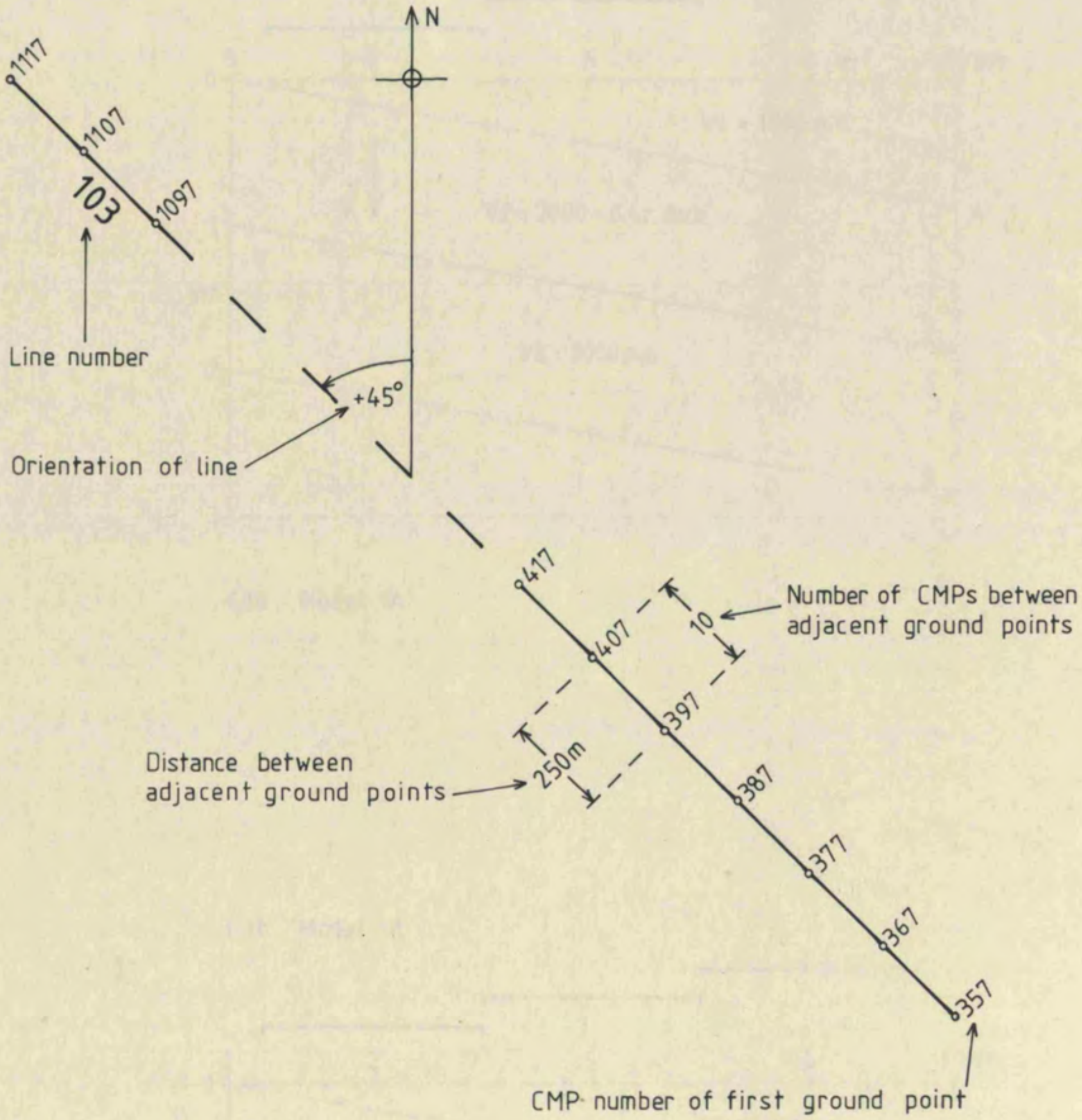

Number of ground points on line = (1117 - 357)/10 + 1 = 77

Figure 5.2 KRUNCH Definition of a Seismic Line in the LINDEF Instruction

The example shown is line A-103 from Chapter 2

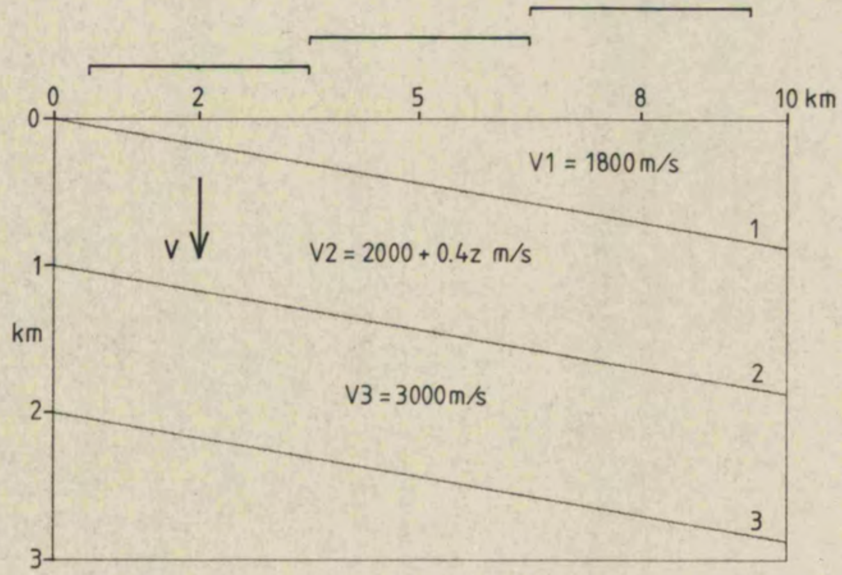

6.1a Model 1A

6.1b Model 1B

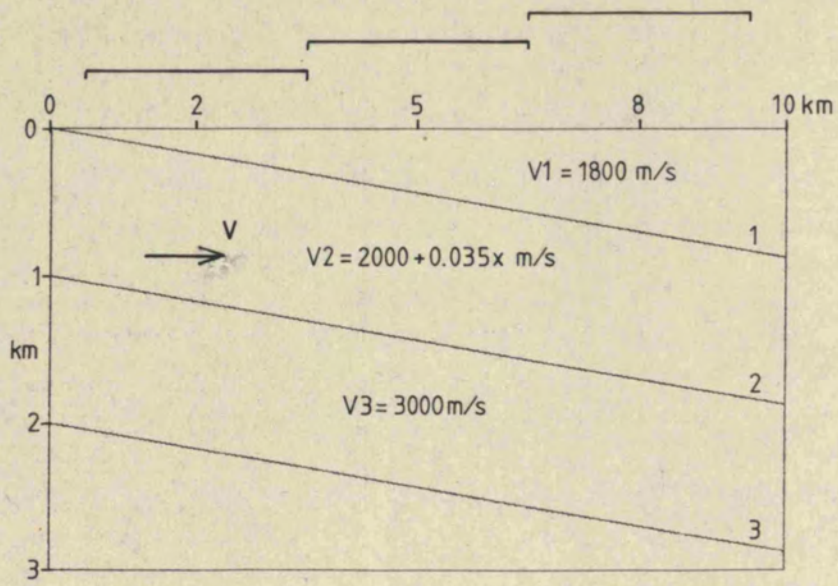

Figure 6.1 Model Definition and Selected CMP Locations for Models 1A and 1B

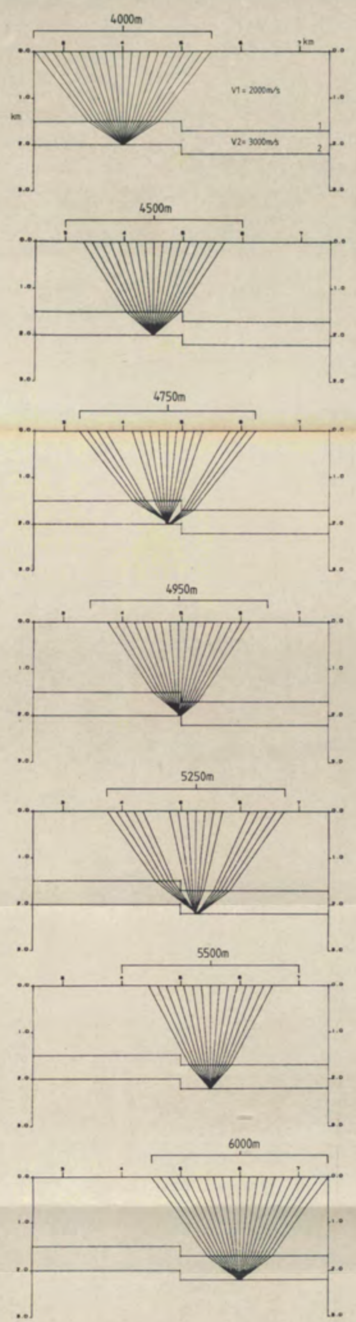

Figure 6.2 Model Definition and CMP Gather Raypaths for Selected CMP Locations over Model 2

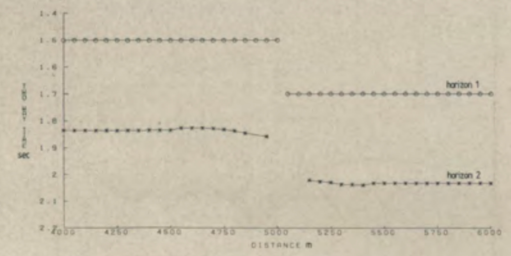

6.3a Two-way Times Modelled by CMP Gather Raytracing

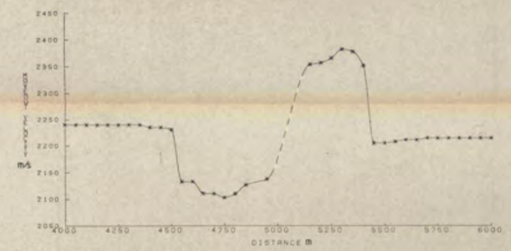

6.3b Moveout Velocities on Horizon 2 Modelled by CMP Gather Raytracing

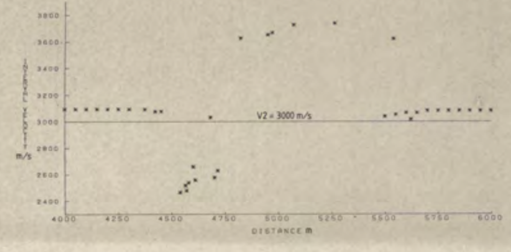

6.3c Interval Velocities in Layer 2 Derived by the Hubral Algorithm

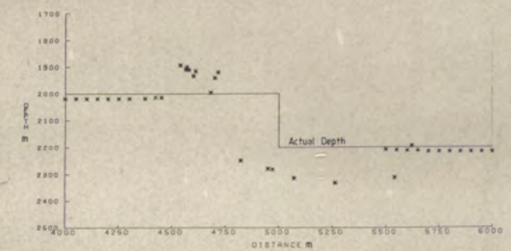

6.3d Depth Estimates for Horizon 2 using the Derived Interval Velocities

Figure 6.3 CMP Ray Modelling and Hubral Inversion over Model 2

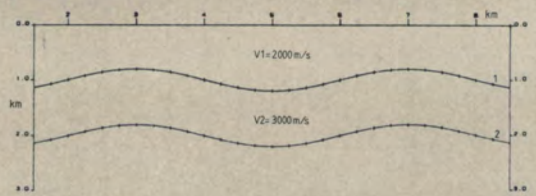

6.4a Model Definition

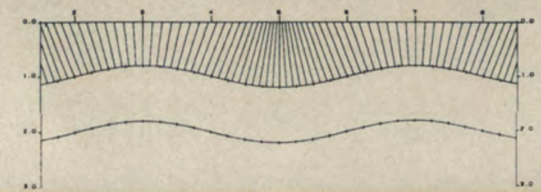
6.4b Zero-offset Rays to Horizon 1

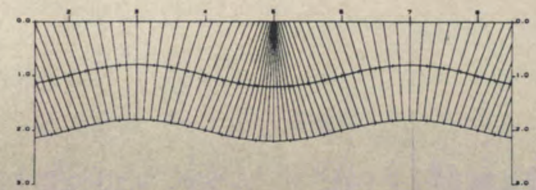
6.4c Zero-offset Rays to Horizon 2

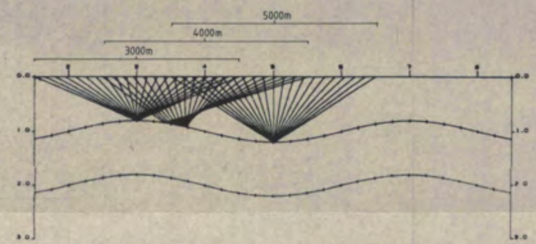

6.4d CMP Gather Raypaths to Horizon 1

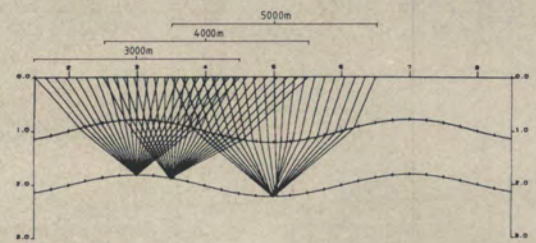

6.4e CMP Gather Raypaths to Horizon 2

Figure 6.4 Model Definition, Zero-offset Raypaths and CMP Gather Raypaths for Model 3

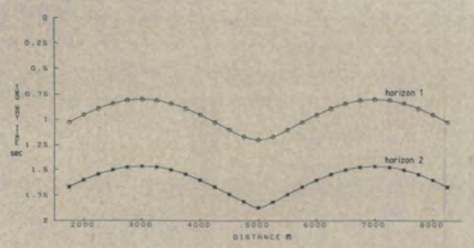

6.5a Two-way Times Modelled by CMP Gather Raytracing

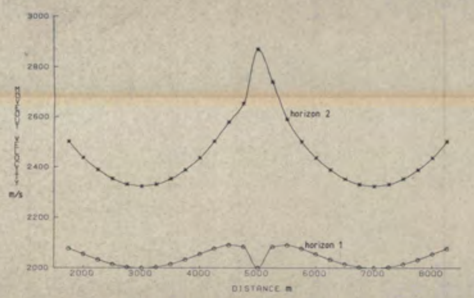

6.5b Moveout Velocities Modelled by CMP Gather Raytracing

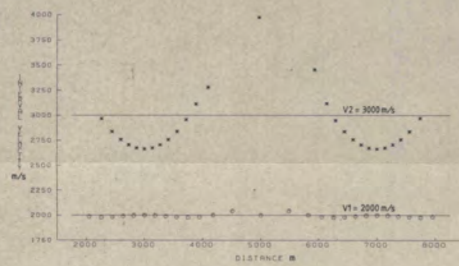

6.5c Interval Velocities Derived by the Hubral Algorithm

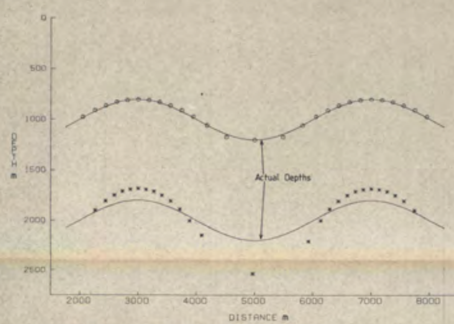

6.5d Depth Estimates using the Derived Interval Velocities

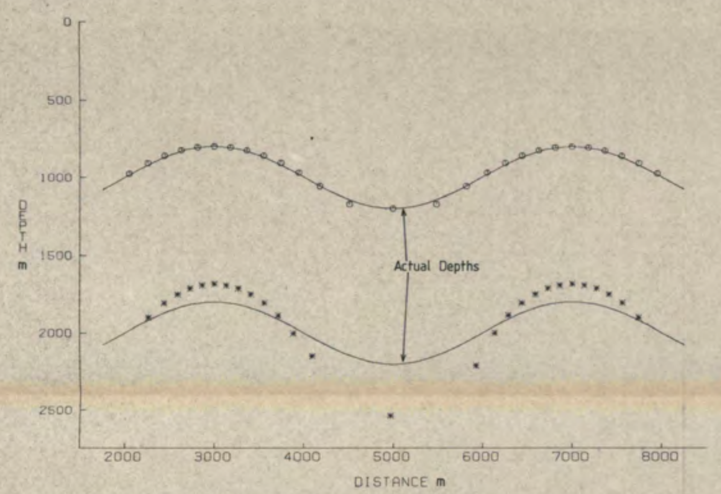

6.5d Depth Estimates using the Derived Interval Velocities

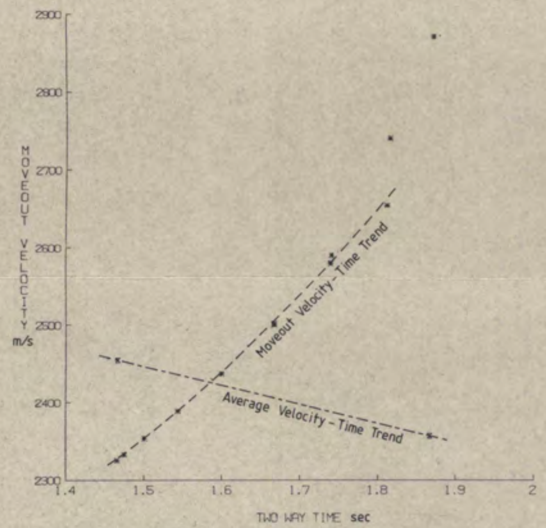

6.5e Velocity - Time Crossplot for Horizon 2

Figure 6.5 CMP Ray Modelling and Hubral Inversion over Model 3

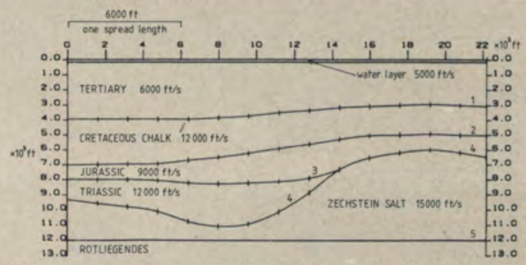

6.6a Model Definition

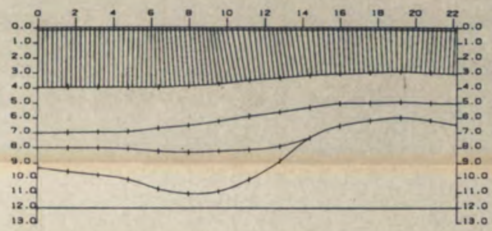

6.6b Zero-offset Raypaths to Horizon 1 (Top Cretaceous)

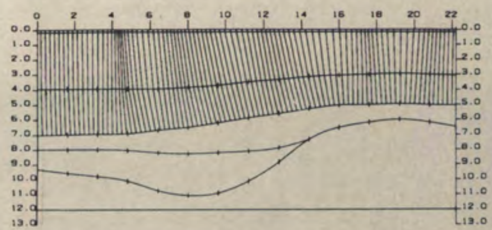

6.6c Zero-offset Raypaths to Horizon 2 (Top Jurassic)

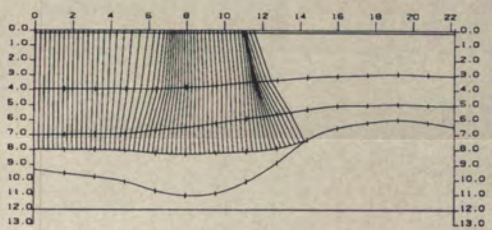

6.6d Zero-offset Raypaths to Horizon 3 (Top Triassic)

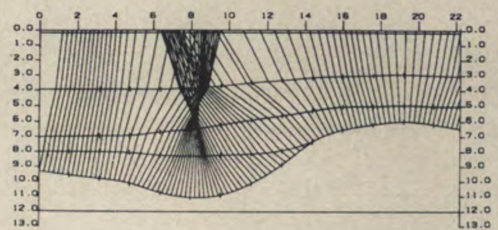

6.6e Zero-offset Raypaths to Horizon 4 (Top Zechstein)

6.6d Zero-offset Raypaths to Horizon 3 (Top Triassic)

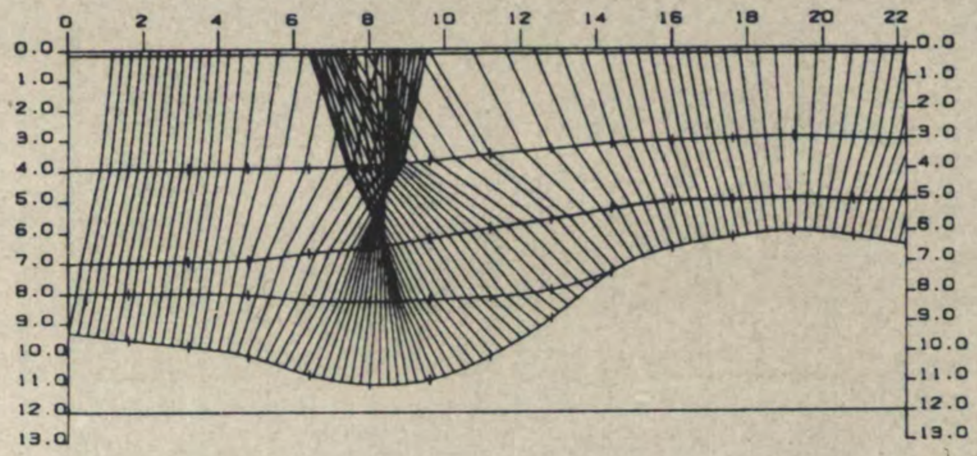

6.6e Zero-offset Raypaths to Horizon 4 (Top Zechstein)

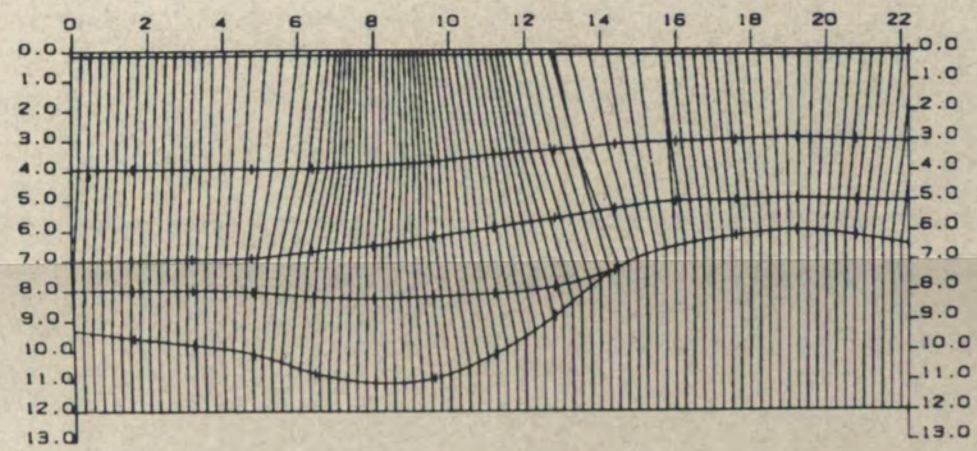

6.6f Zero-offset Raypaths to Horizon 5 (Top Rotliegendes)

Figure 6.6 Model Definition and Zero-offset Raypaths for Model 4

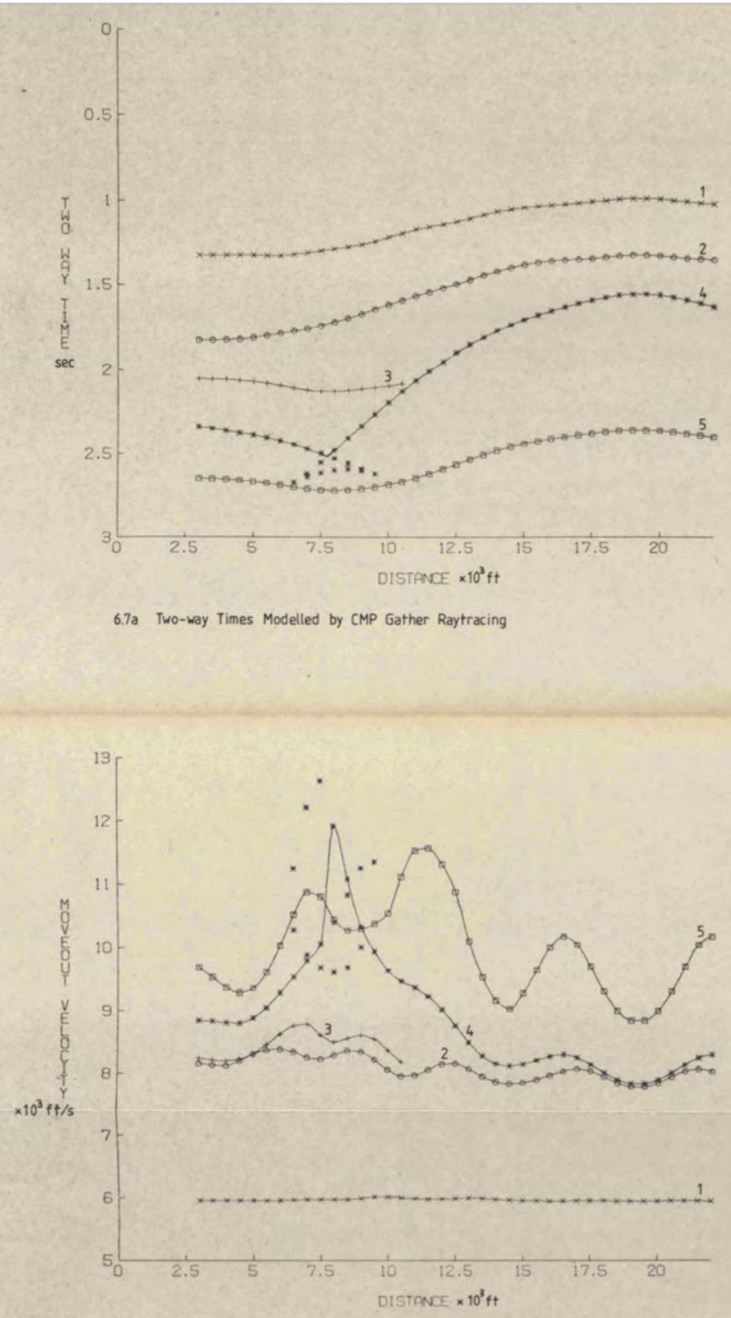

6.7a Two-way Times Modelled by CMP Gather Raytracing

6.7b Moveout Velocities Modelled by CMP Gather Raytracing

Figure 6.7 Results of CMP Gather Raytracing over Model 4

×	TERTIARY	6000 ft/s
⊙	CRETACEOUS	12000 ft/s
+ ⌘	JURASSIC	9000 ft/s
✳	TRIASSIC	12000 ft/s
⊡	ZECHSTEIN	15000 ft/s

Two symbols are used for the Jurassic in order to distinguish the Top Jurassic-Top Triassic and Top Jurassic-Top Zechstein intervals

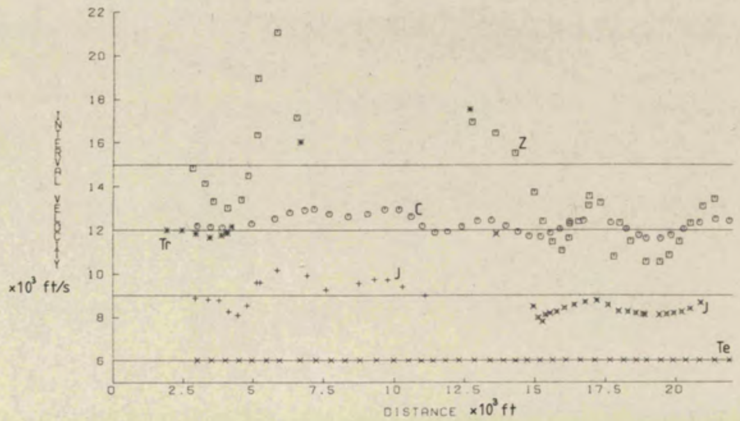

6.8a Direct Inversion using Raw Moveout Velocities (Raw Interval Velocities)

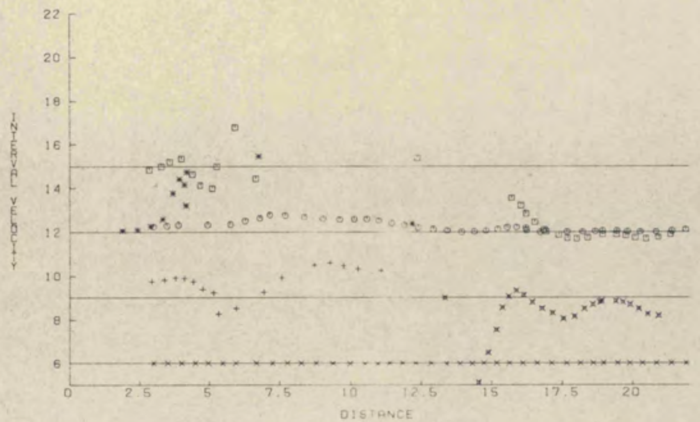

6.8b Direct Inversion using Smoothed Moveout Velocities (Raw Interval Velocities)

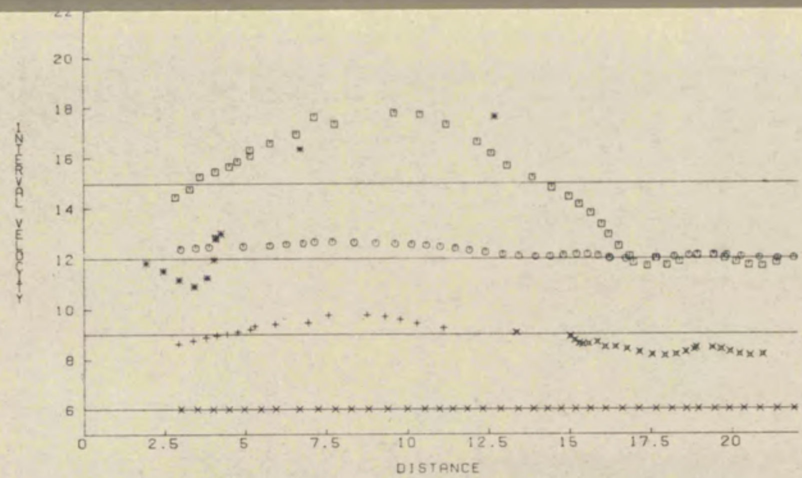

6.8c Layer-by-layer Inversion using Raw Moveout Velocities and Smoothed Interval Velocities

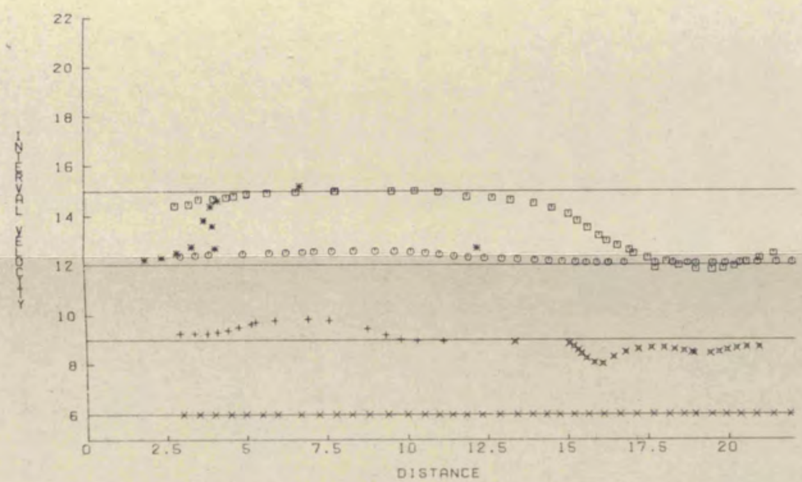

6.8d Layer-by-layer Inversion using Smoothed Moveout Velocities and Smoothed Interval Velocities

Figure 6.8 Interval Velocities Derived by the Hubral Algorithm over Model 4

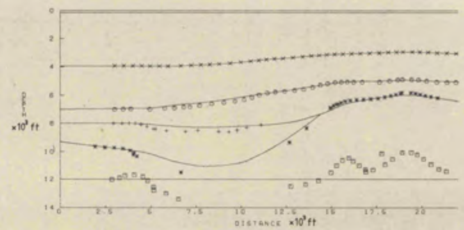

6.9a Direct Inversion using Raw Moveout Velocities (Raw Interval Velocities)

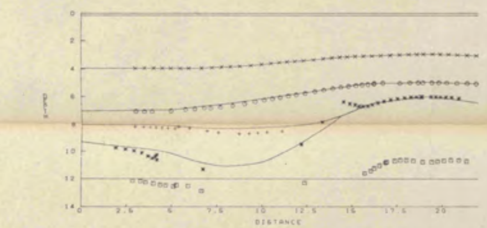

6.9b Direct Inversion using Smoothed Moveout Velocities (Raw Interval Velocities)

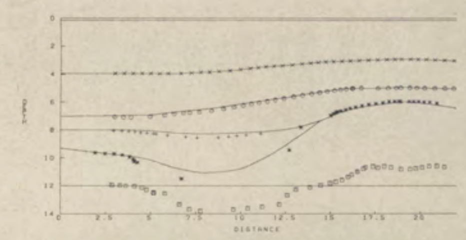

6.9c Layer-by-layer Inversion using Raw Moveout Velocities and Smoothed Interval Velocities

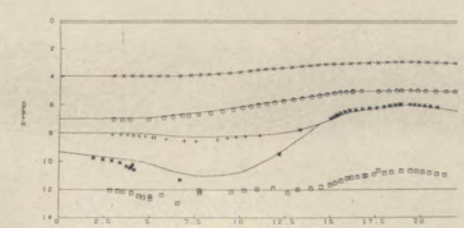

6.9d Layer-by-layer Inversion using Smoothed Moveout Velocities and Smoothed Interval Velocities

Figure 6.9 Depth Estimates using the Derived Interval Velocities over Model 4

A-103

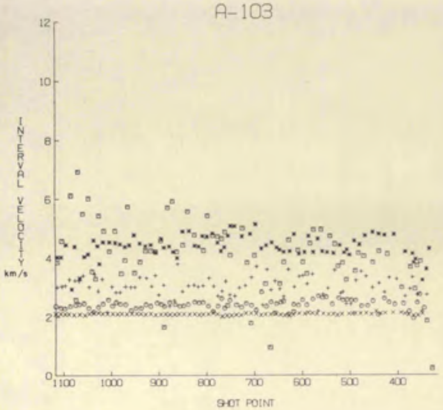

A-120

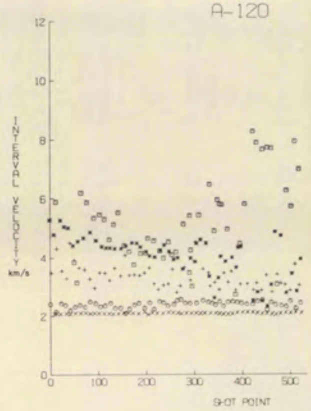

A-111

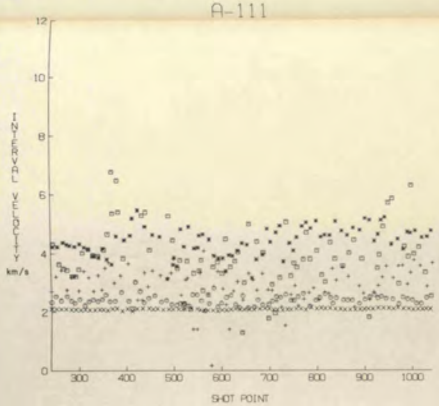

A-130

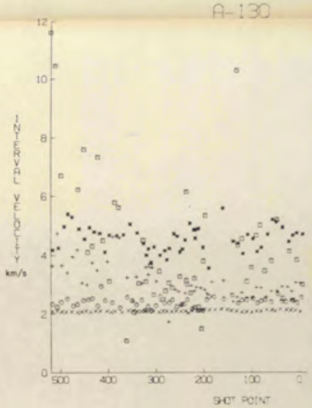

A-115

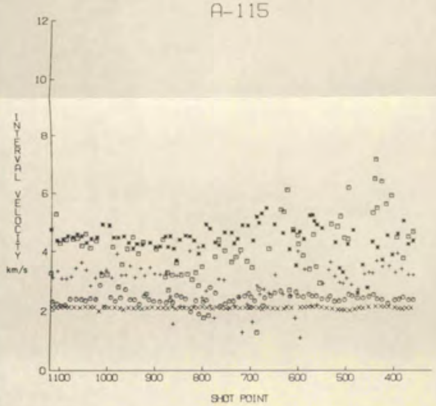

A-132

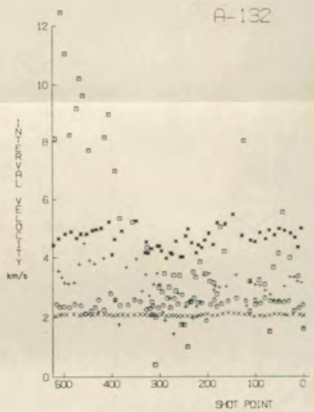

A-123

A-144

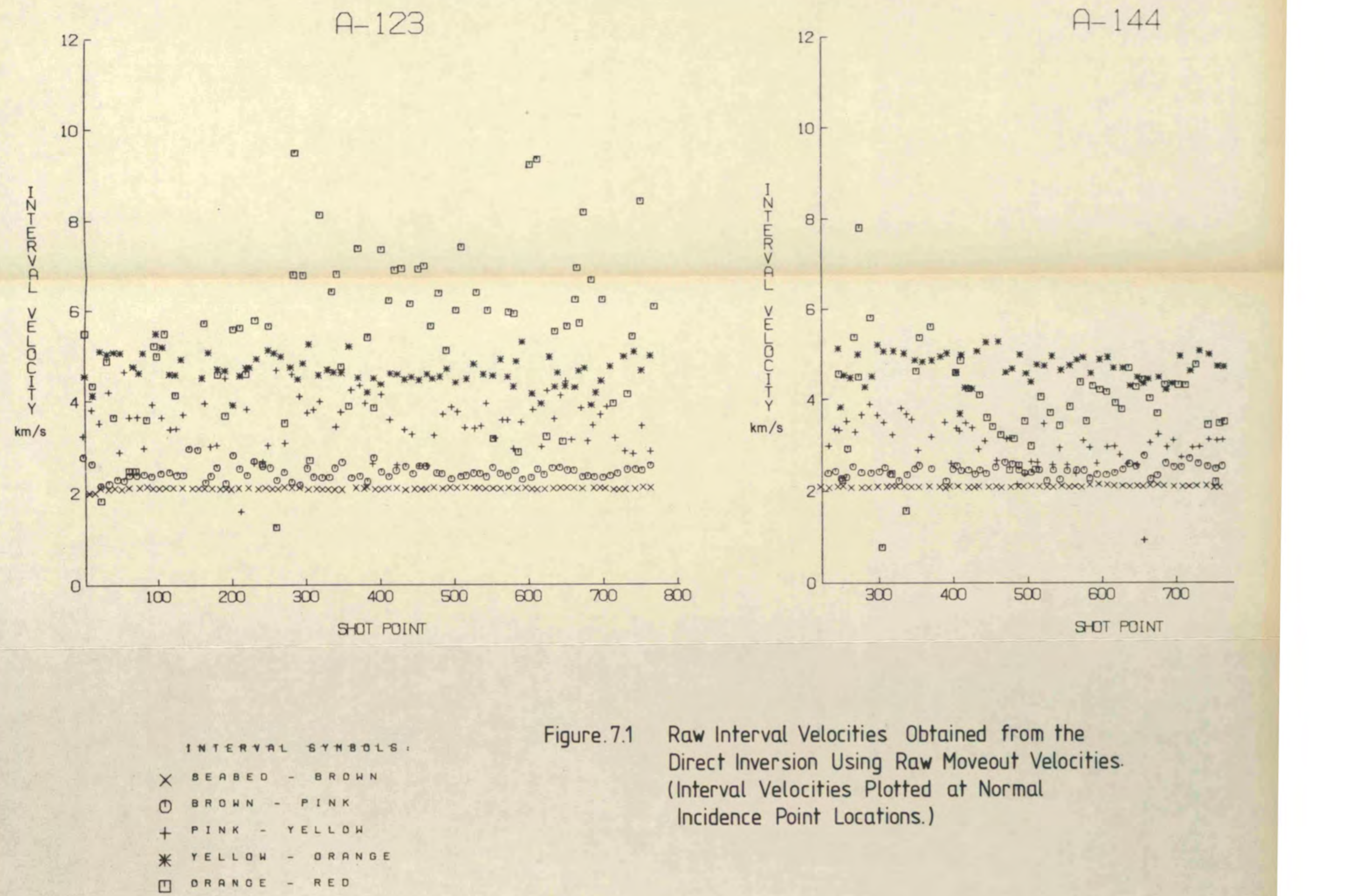

Figure. 7.1 Raw Interval Velocities Obtained from the Direct Inversion Using Raw Moveout Velocities. (Interval Velocities Plotted at Normal Incidence Point Locations.)

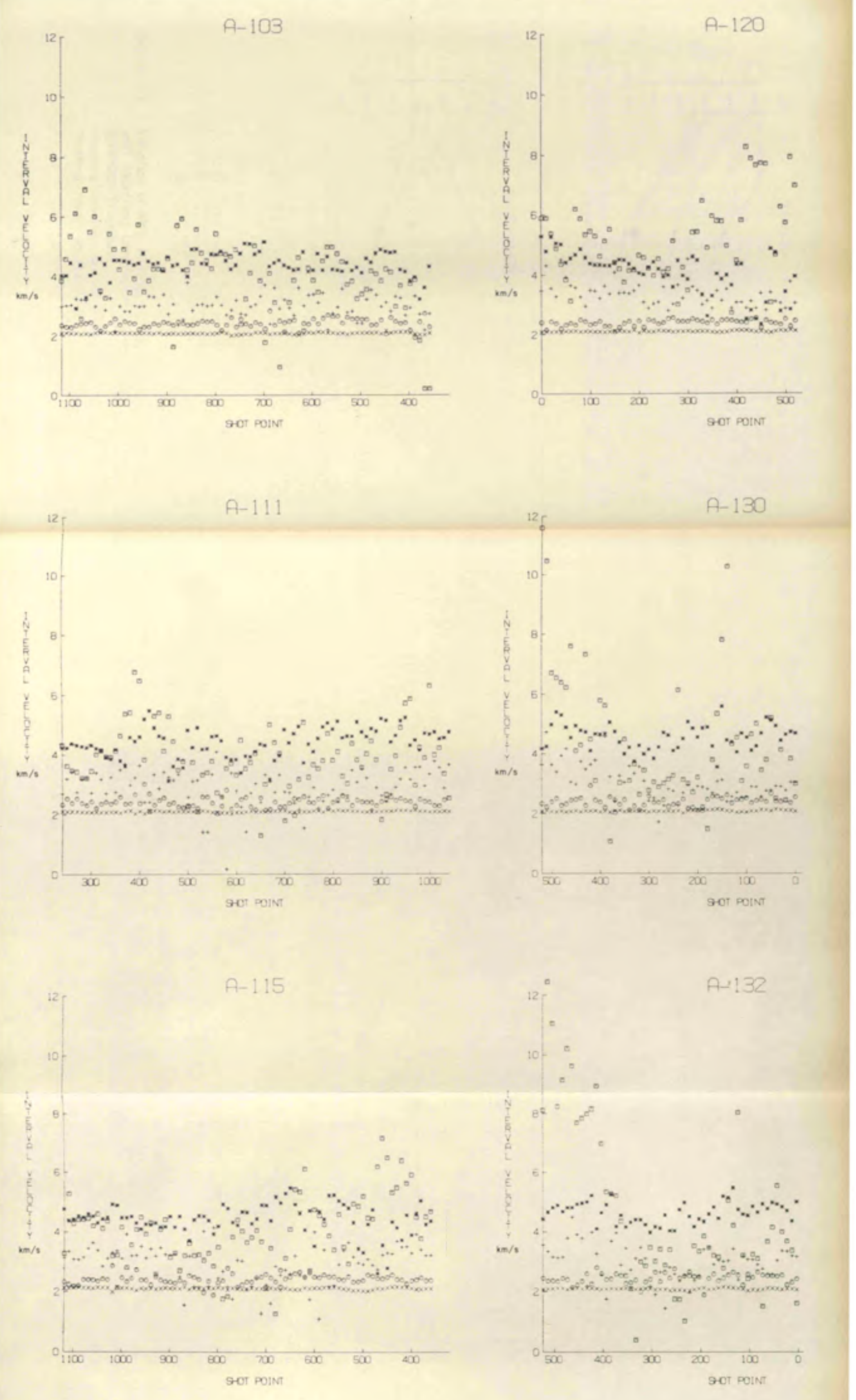
A-103
A-120
A-111
A-130
A-115
A-132
INTERVAL VELOCITY km/s
SHOT POINT

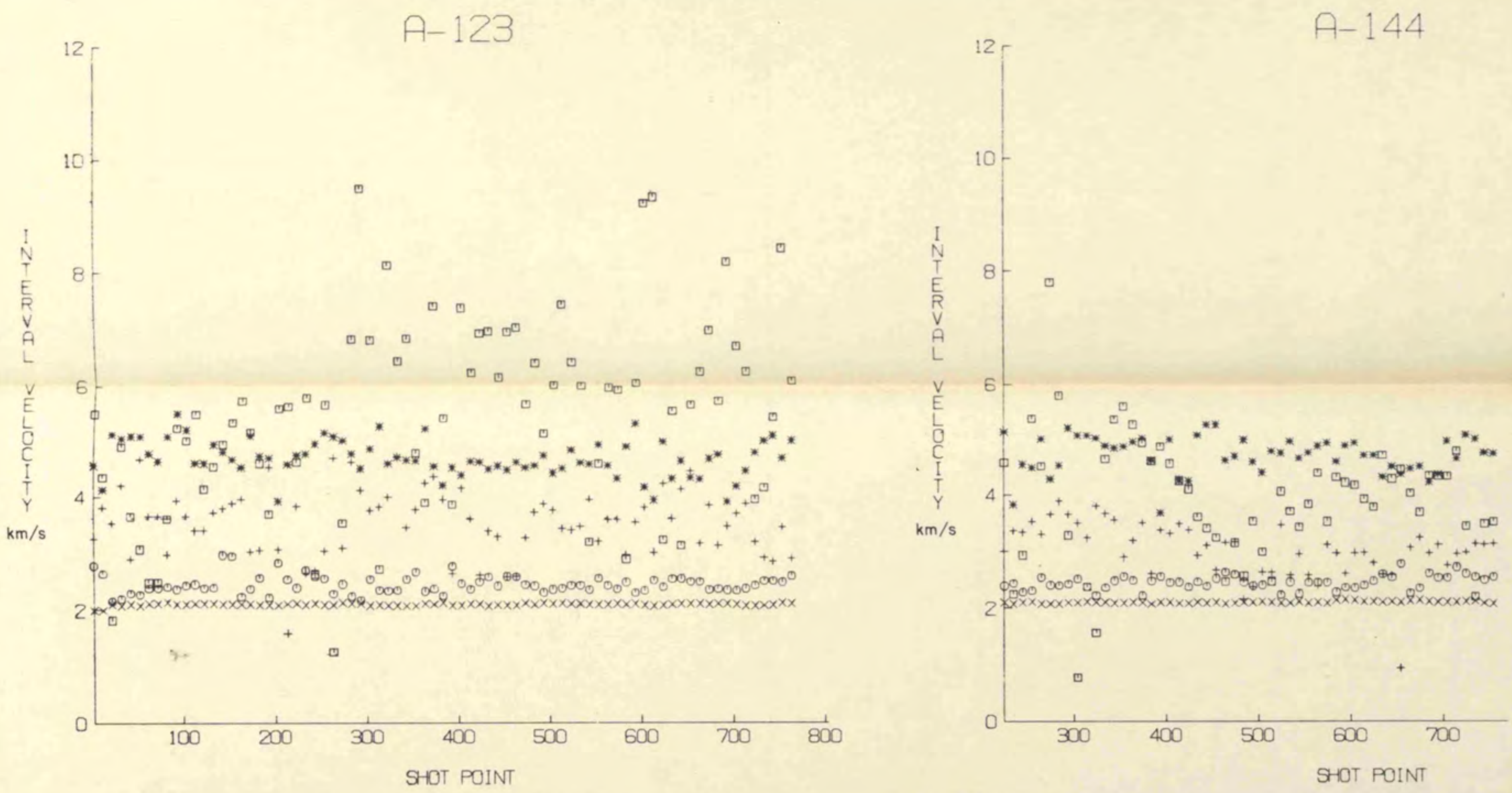

INTERVAL SYMBOLS:

× SEABED - BROWN
⊕ BROWN - PINK
+ PINK - YELLOW
✱ YELLOW - ORANGE
□ ORANGE - RED

Figure 7.2 Raw Interval Velocities Obtained from the Direct Inversion Using Raw Moveout Velocities (Interval Velocities Plotted at Ground Point Locations.)

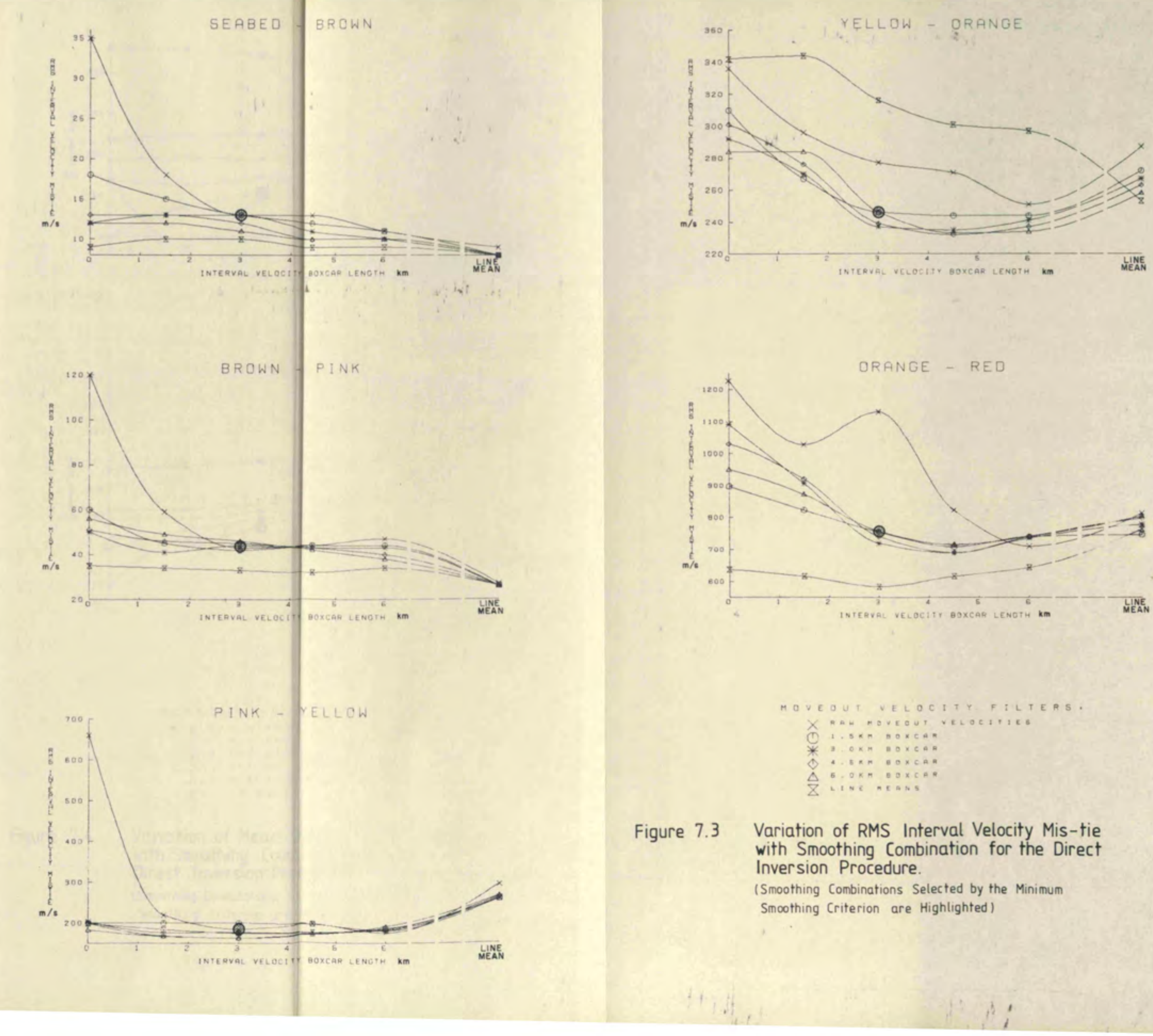

Figure 7.3 Variation of RMS Interval Velocity Mis-tie with Smoothing Combination for the Direct Inversion Procedure.

(Smoothing Combinations Selected by the Minimum Smoothing Criterion are Highlighted)

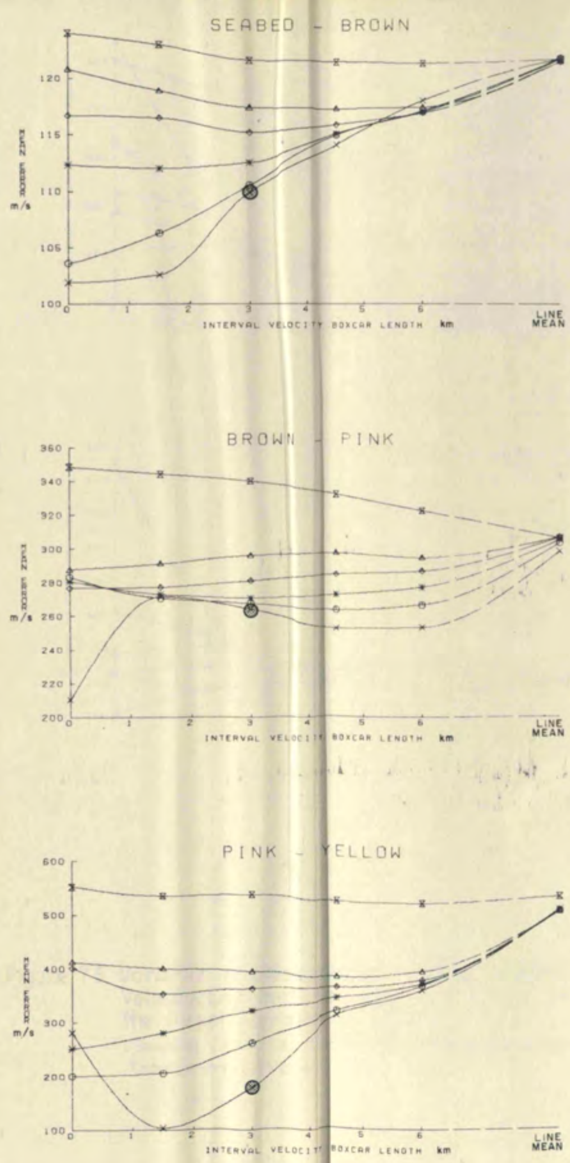

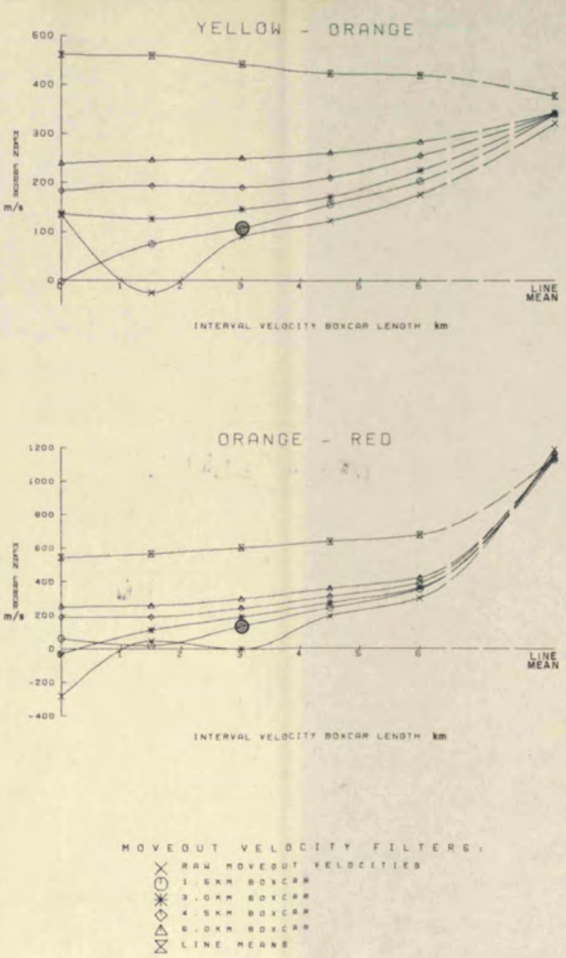

Figure 7.4 Variation of Mean Interval Velocity Error with Smoothing Combination for the Direct Inversion Procedure.

(Smoothing Combinations Selected by the Minimum Smoothing Criterion are Highlighted.)

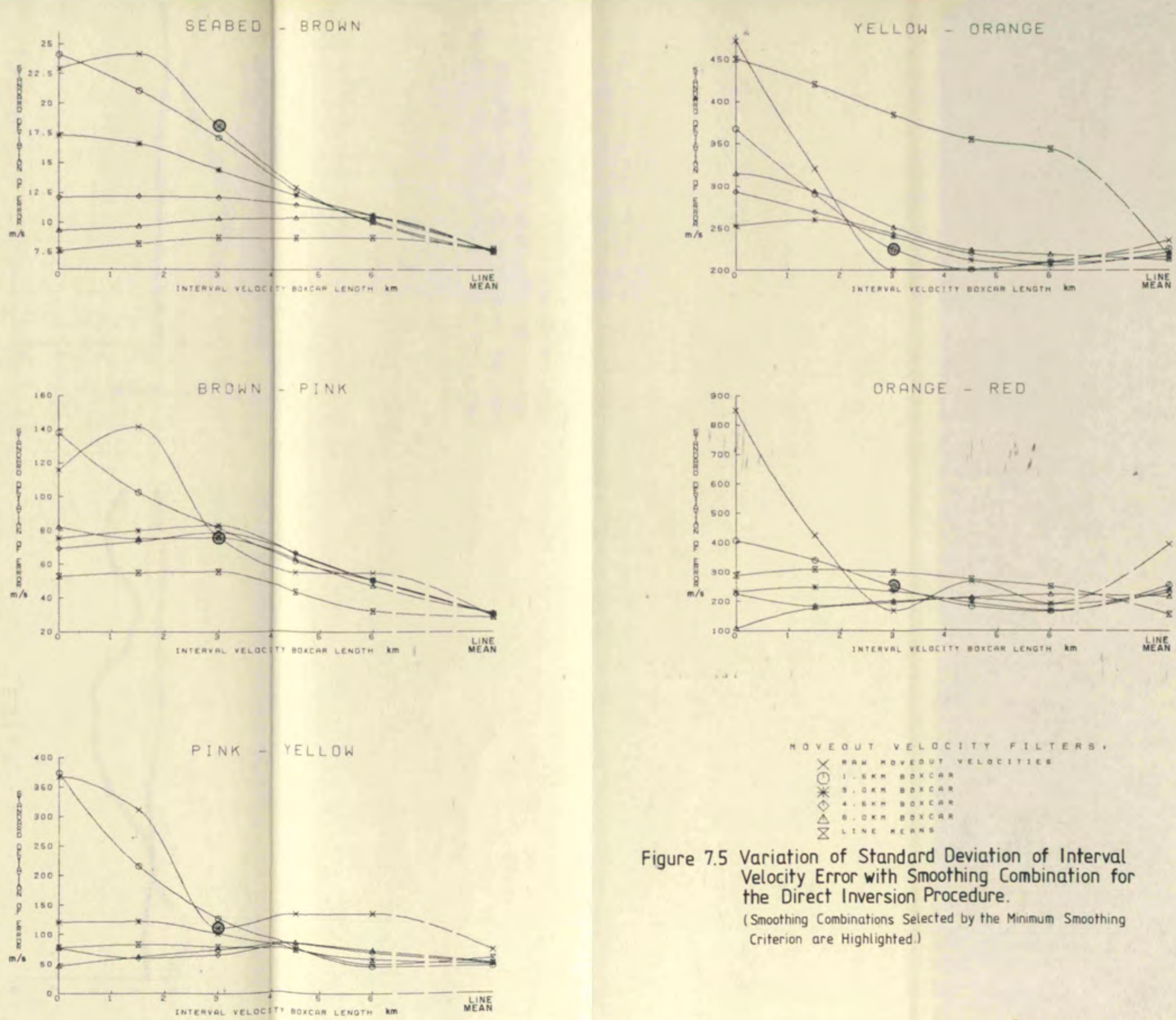

Figure 7.5 Variation of Standard Deviation of Interval Velocity Error with Smoothing Combination for the Direct Inversion Procedure.

(Smoothing Combinations Selected by the Minimum Smoothing Criterion are Highlighted.)

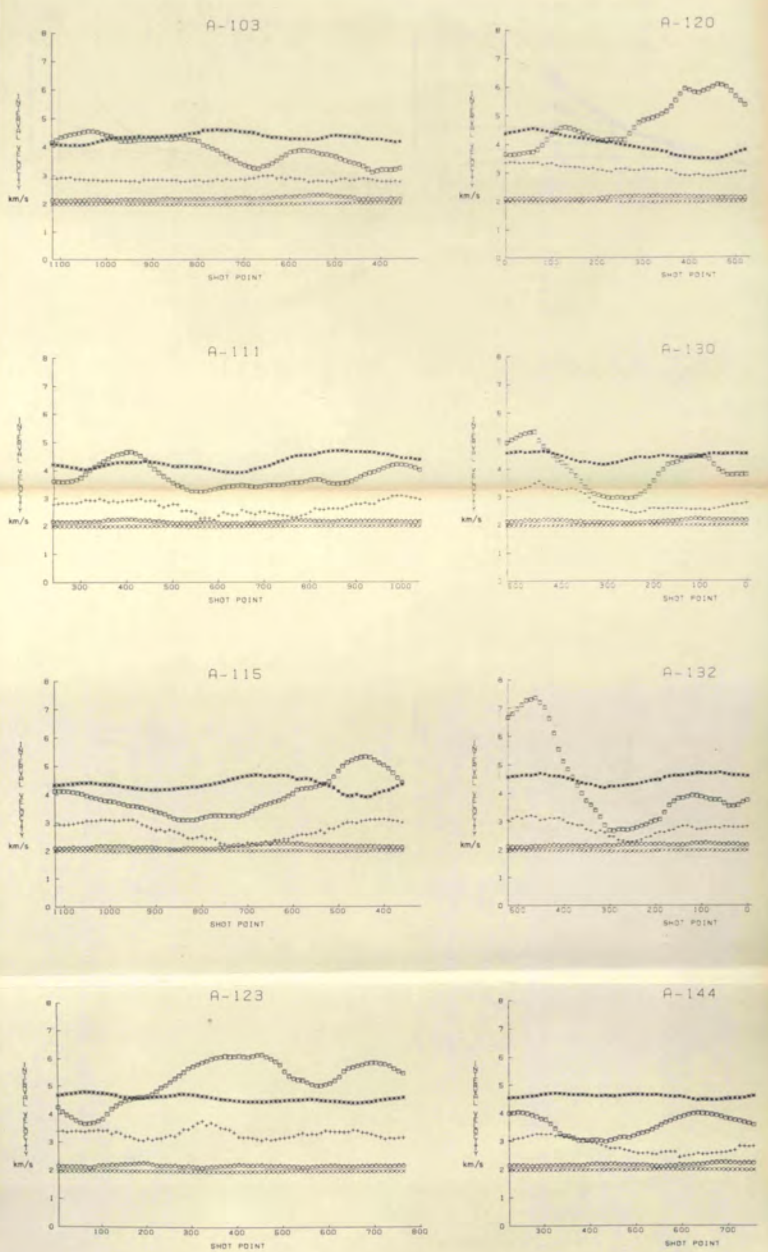

Figure 7.6 Interval Velocities Obtained Using the Selected Smoothing Combination for Direct Inversion. (Interval Velocities Plotted at Ground Point Locations.)

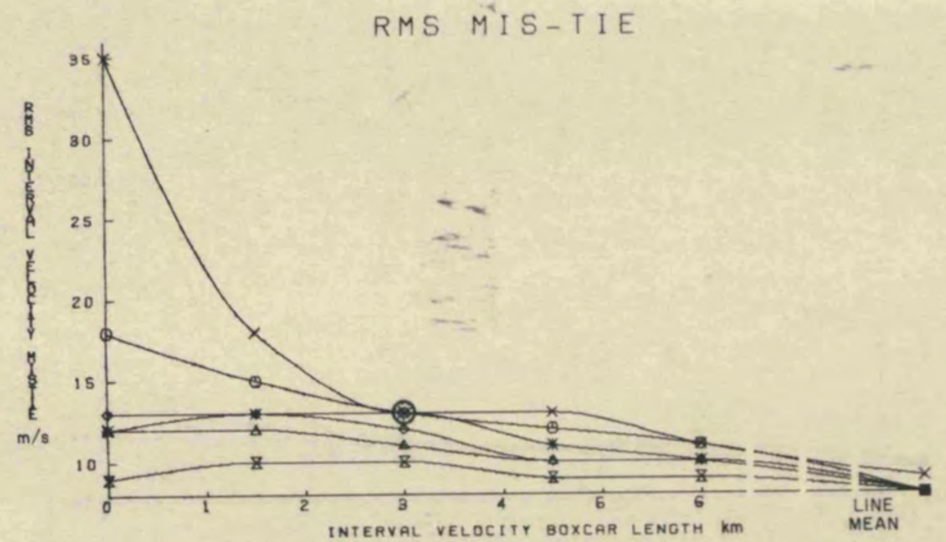

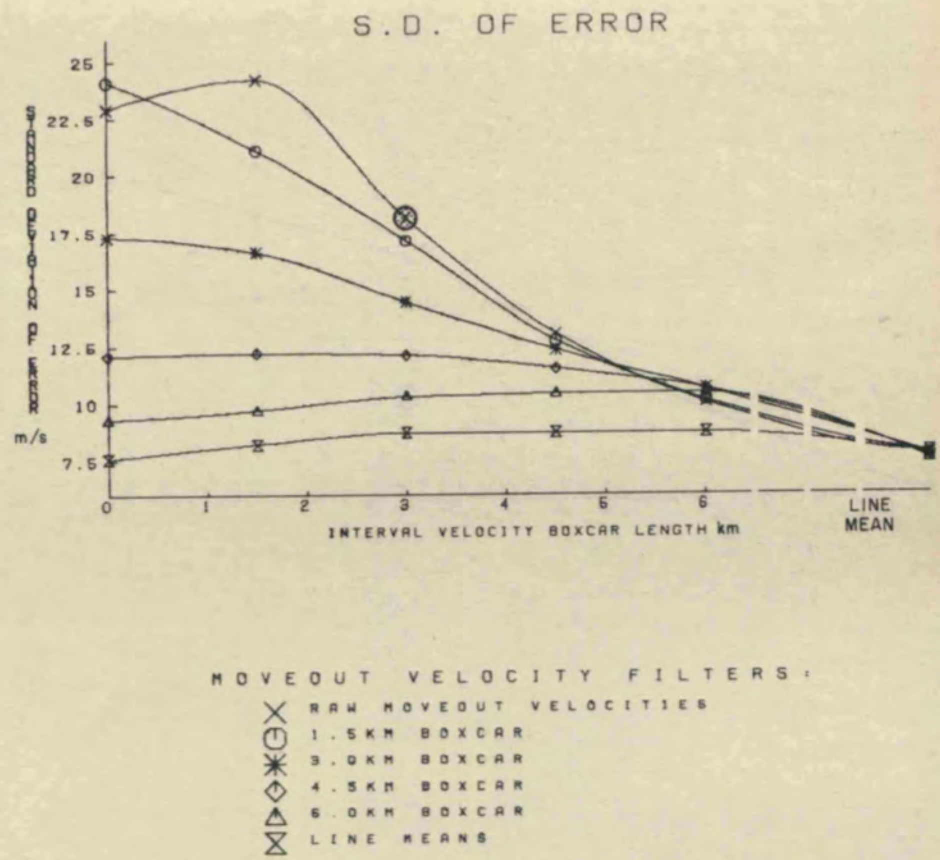

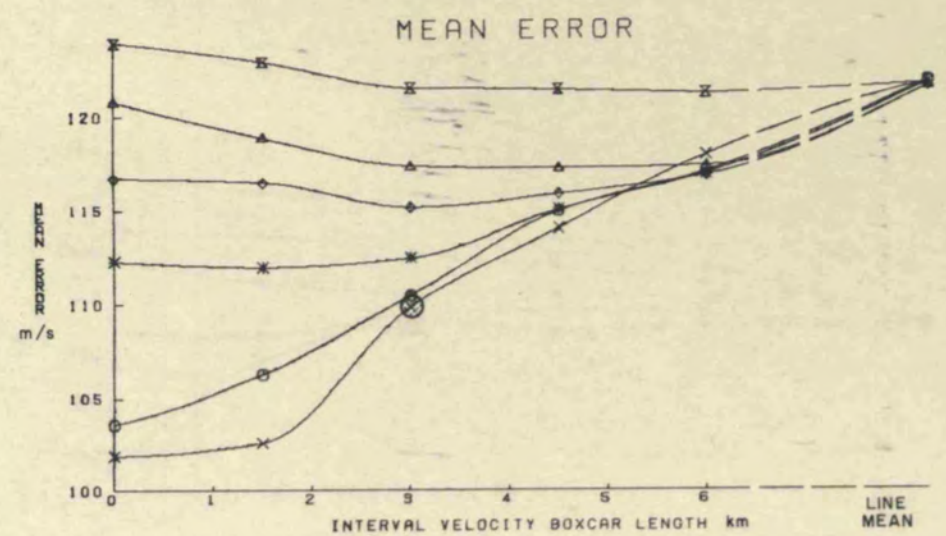

Figure 7.7 Interval Velocity Statistics for Layer-by-Layer Inversion in the Seabed-Brown Interval.
(Selected Smoothing Combination Highlighted.)

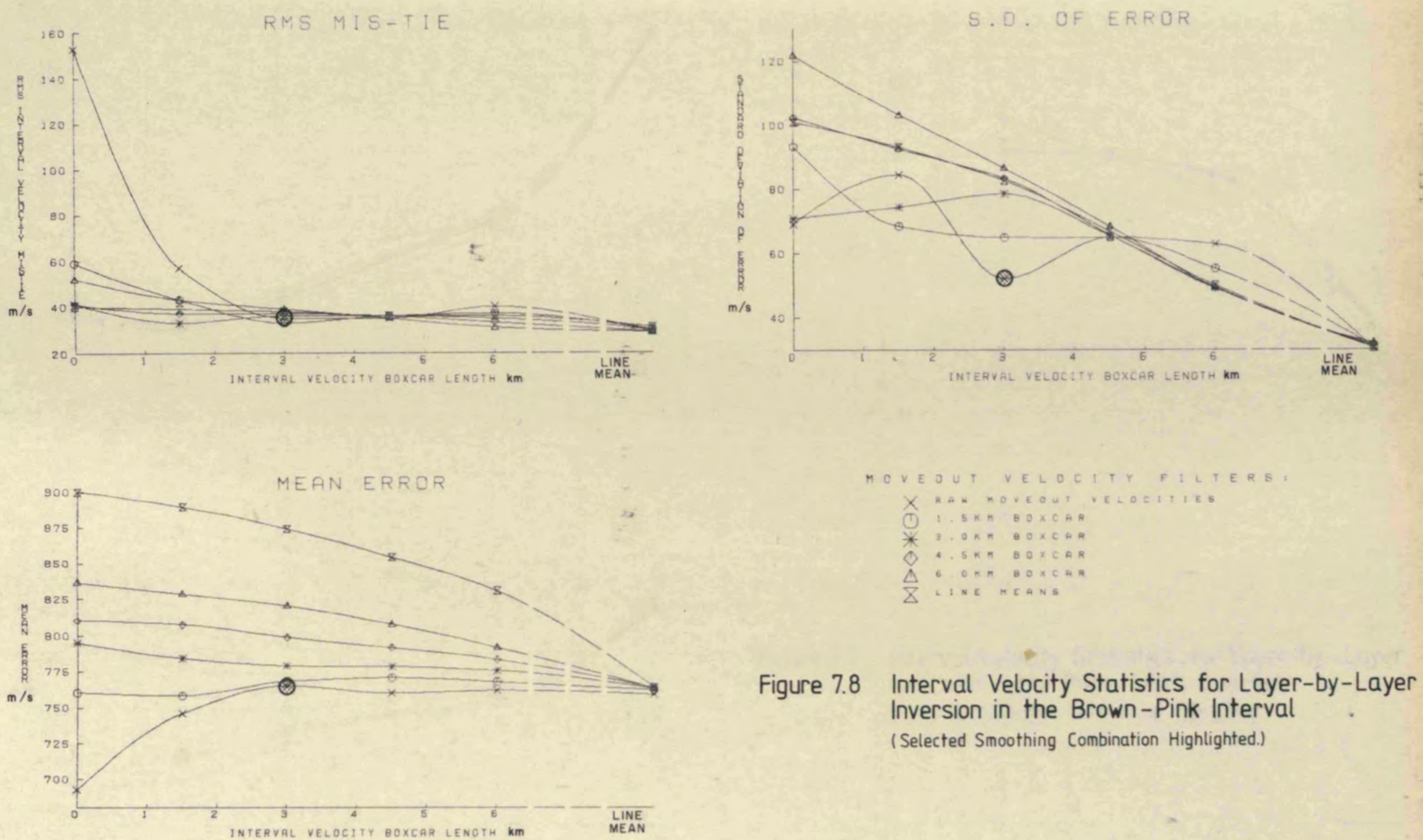

Figure 7.8 Interval Velocity Statistics for Layer-by-Layer Inversion in the Brown-Pink Interval

(Selected Smoothing Combination Highlighted.)

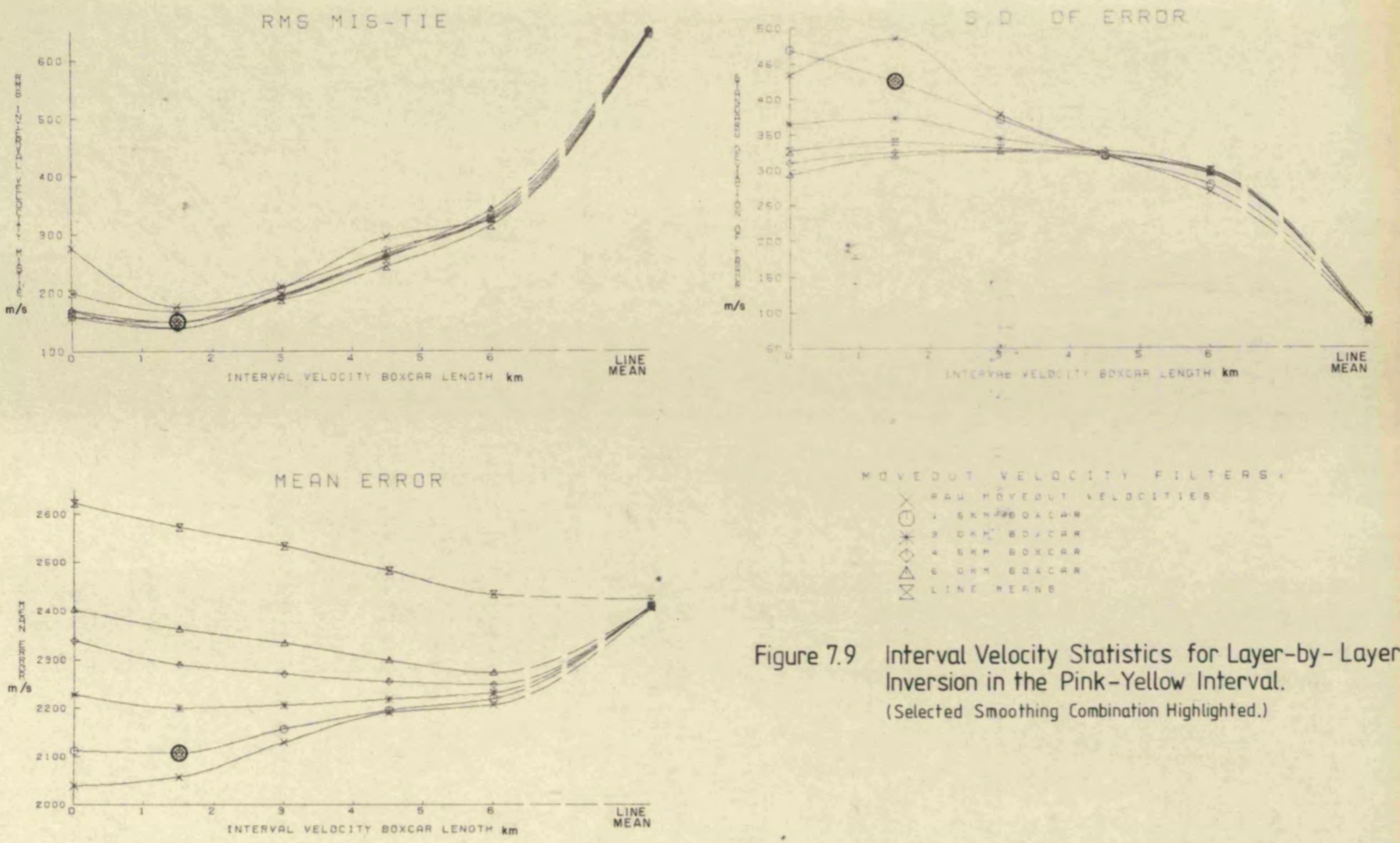

Figure 7.9 Interval Velocity Statistics for Layer-by-Layer Inversion in the Pink-Yellow Interval.
(Selected Smoothing Combination Highlighted.)

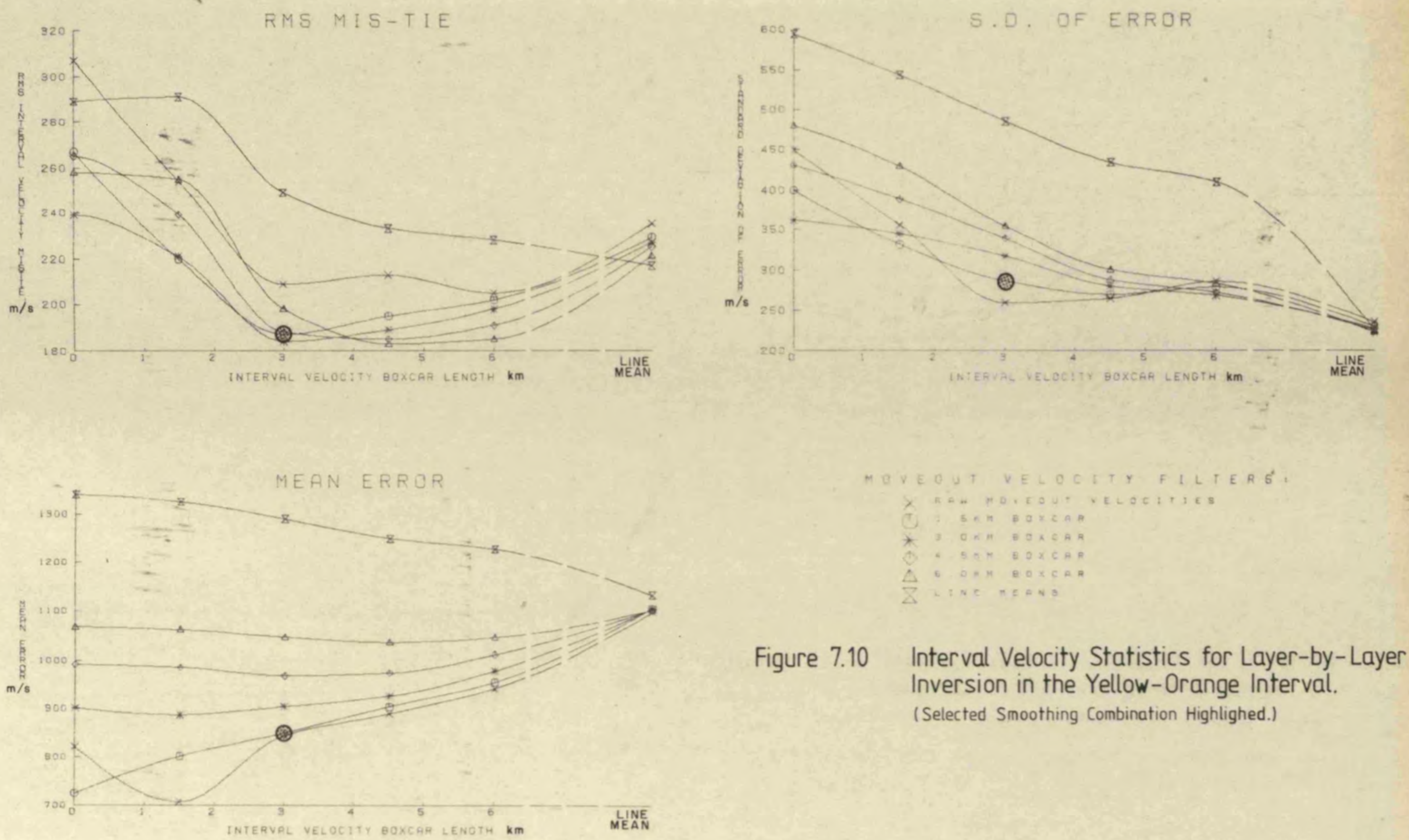

Figure 7.10 Interval Velocity Statistics for Layer-by-Layer Inversion in the Yellow-Orange Interval.
(Selected Smoothing Combination Highlighed.)

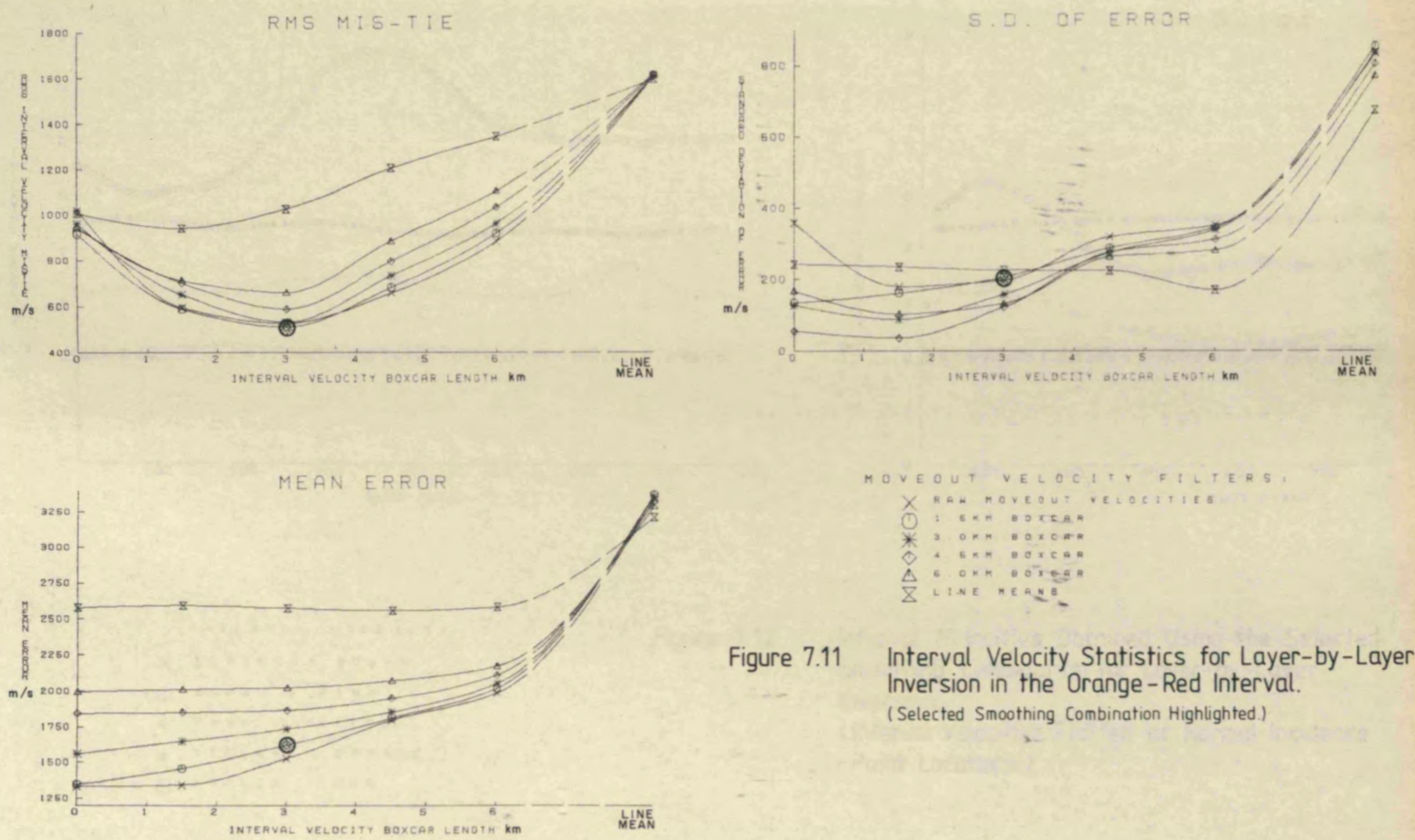

Figure 7.11 Interval Velocity Statistics for Layer-by-Layer Inversion in the Orange-Red Interval.

(Selected Smoothing Combination Highlighted.)

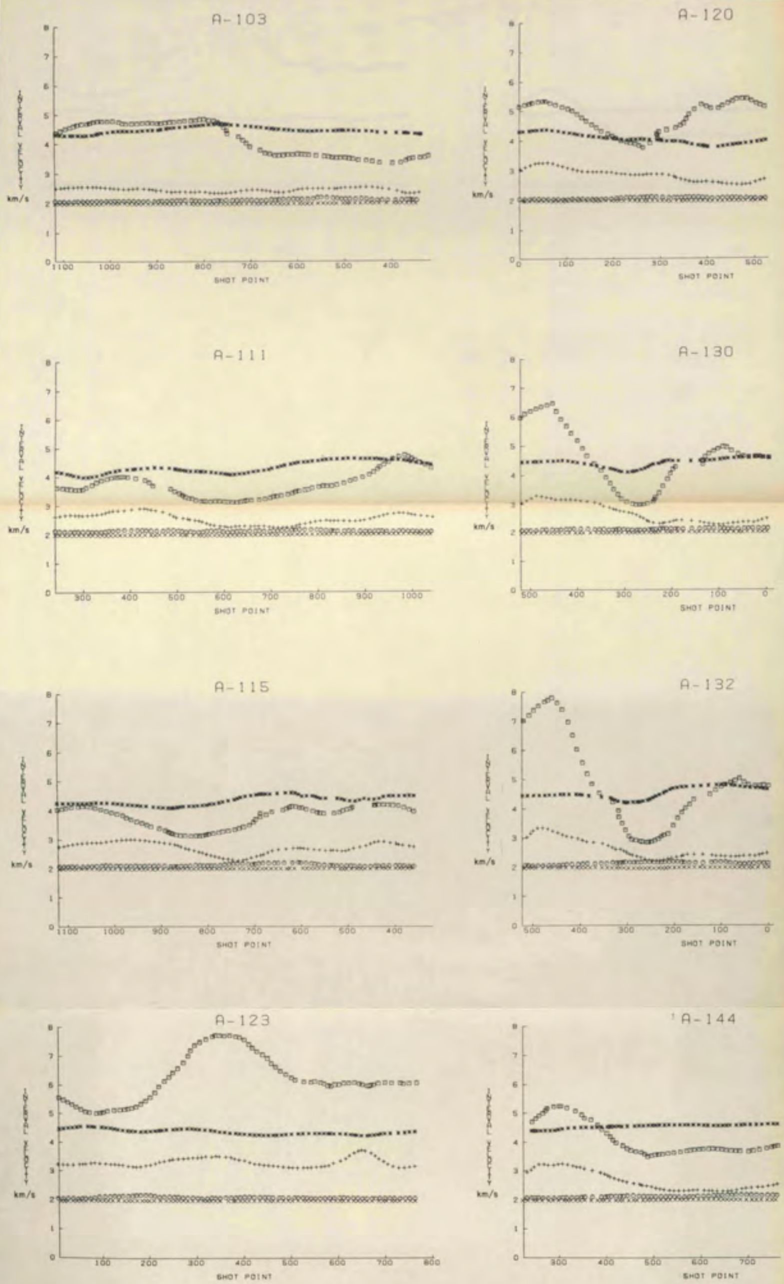

INTERVAL SYMBOLS:

- × SEABED - BROWN
- ⊙ BROWN - PINK
- + PINK - YELLOW
- ✱ YELLOW - ORANGE
- ⊡ ORANGE - RED

Figure 7.12 Interval Velocities Obtained Using the Selected Smoothing Combination for Layer-by-Layer Inversion.
(Interval Velocities Plotted at Normal Incidence Point Locations.)

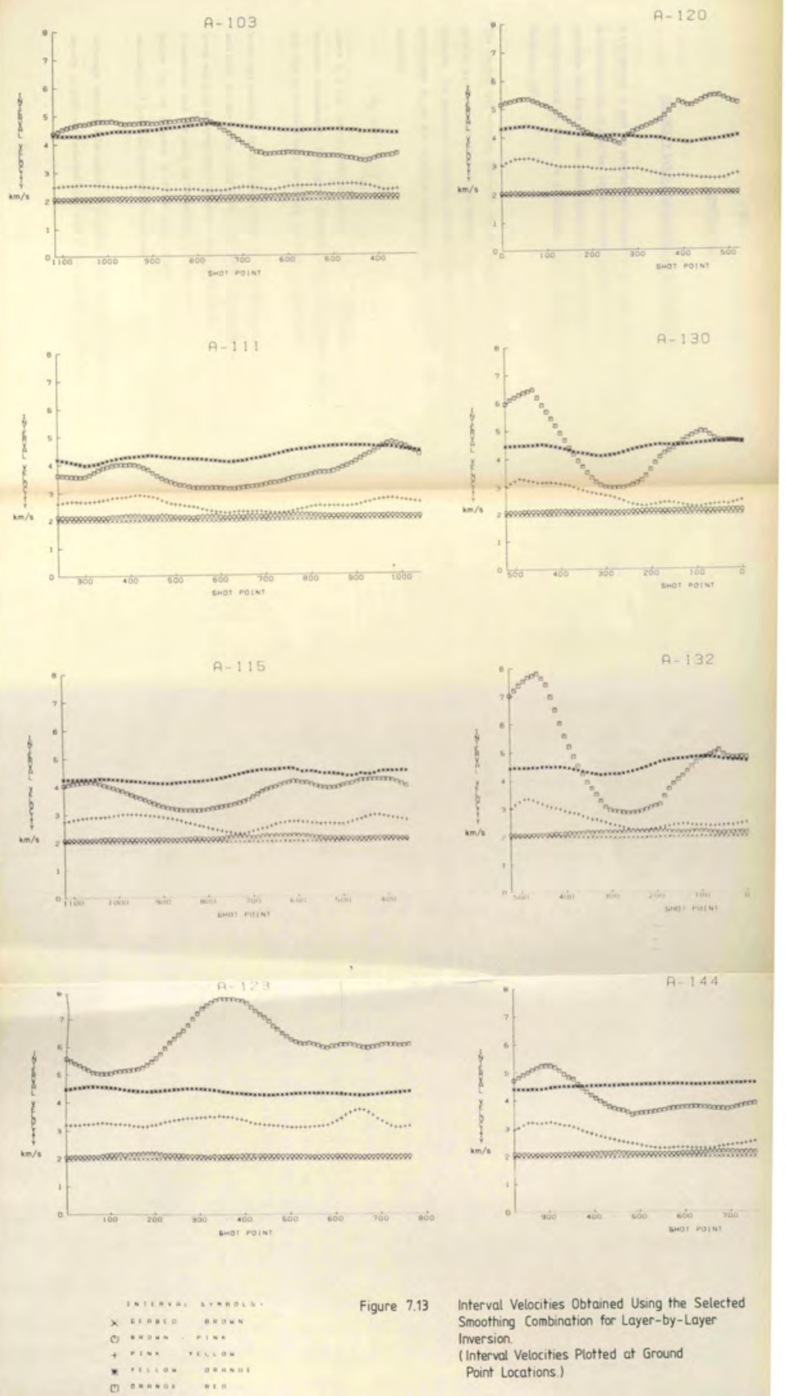

Figure 7.13 Interval Velocities Obtained Using the Selected Smoothing Combination for Layer-by-Layer Inversion.
(Interval Velocities Plotted at Ground Point Locations.)

APPENDIX 2A

VELOCITY LOGS AND SYNTHETIC SEISMOGRAMS

If the density ρ and the seismic wave velocity V of the subsurface are available as continuous (or, in practise, highly sampled) functions of depth, it is possible to calculate the form of the ideal, noise-free seismic reflection trace. Such a simulated trace is known as a 'synthetic seismogram' (Peterson et al, 1955; Dennison, 1960).

The density and velocity functions can be modelled by a series of thin plane parallel layers, in each of which the density ρ_j and seismic wave velocity V_j are uniform. For downward travelling normally incident plane waves, the reflection coefficient R_j of the interface separating layers j-1 and j is given by the equation:

$$R_j \quad = \quad \frac{I_j - I_{j-1}}{I_j + I_{j-1}} \tag{2A.1}$$

where I_j is the velocity-density product $\rho_j V_j$, usually referred to as the 'acoustic impedance'. The log of unattenuated primary reflection coefficients may thus be obtained from the density and velocity logs at a well.

Sonic logs provide a reliable measurement of local velocity variations down the well bore, but are liable to introduce errors if used to calculate integrated travel times and gross interval velocities over a large depth interval. For this reason it is essential that the sonic log be calibrated by the results of a checkshot survey before any use is made of it for either interval velocity estimation or the calculation of synthetic seismograms (see also Section 1.1.10).

Although velocity information is available from the sonic log in most wells, density is often not recorded over most of the well bore. In practise, this is of little significance, however, since the density often varies in sympathy with the velocity, and the density variation is usually small in comparison with the velocity variation. Coal and salt are two exceptions, with relatively low densities. In general, little error is incurred by the assumption that the density is constant, or that it varies as a simple empirical function of velocity.

With the calibrated velocity log and a measured or assumed density log, Equation (2A.1) can be used to obtain the log of reflection coefficients down the well. This log can include various combinations of primaries, internal multiples and surface multiples in order to highlight the different components of the seismogram. This procedure pertains strictly to the case of a vertical well in horizontal layers; the implied seismic raypaths do not follow the well bore if the layers are dipping or if the well is deviated from the vertical, and the logs may be calibrated incorrectly if a simpler model is assumed.

Finally, the log of reflection coefficients is convolved with a filter or 'wavelet' which represents the effects of the band-limited seismic source signature, the absorption of higher frequencies by the earth, the recording equipment, and the processing which is applied before the final section is displayed. The filter applied is the one which results in the best match between the filtered synthetic seismogram and the traces closest to the well on the seismic section. The procedure for finding such an 'optimum' filter is necessarily of a trial and error nature.

A log of reflection coefficients containing a single spike (or delta function) would cause the input wavelet to be reproduced exactly on the synthetic seismogram with a delay equivalent to the time of the spike. Such phenomena are not observed in practise because real velocity logs never contain perfect step discontinuities. However, any large isolated velocity discontinuity does produce a sharp peak in reflection coefficients which gives rise to a good replica of the wavelet in the primary synthetic seismogram. If the calibrated velocity log is displayed on the same time axis as the primary synthetic seismogram, recognition of the wavelet in the latter leads to immediate correlation with the causative velocity discontinuity. Reference to the geological composite log then allows the stratigraphic origin of the seismic reflection horizon to be identified.

In order that the reflected wavelet be recognised in the seismic trace, the following points are of interest:

- the amplitude and polarity of the reflected wavelet depend on the magnitude and sign of the reflection coefficient;
- significant interference may occur if the reflectors are closely spaced; and
- the most important part of the reflected wavelet is the first cycle or 'first break'; this cycle is diagnostic of the polarity of the reflection but is often difficult to recognise as the later cycles of the wavelet are generally of higher amplitude.

APPENDIX 4A

A 3D RAYTRACING SUBROUTINE: RAYTR3D

```
      SUBROUTINE RAYTR3D(PVS,EZI,EXI,AN,PERP,VRATIO,PVP,EZT,
     &                   EXT,RAYLEN,CALPHA,CBETA,DELTA,IER)
      IMPLICIT DOUBLE PRECISION (A-H),(O-Z)
      INTEGER IER
      DIMENSION PVS(3),EZI(3),EXI(3),AN(3),PVP(3),EZT(3),EXT(3)
C
C SUBROUTINE TO TRACE RAY IN 3D PLANE ISOVELOCITY LAYERED SPACE WITH
C SPECIFIED DIRECTION COSINES FROM SOURCE S THROUGH INTERSECTION WITH
C DIPPING PLANE AT P AND INTO NEXT LAYER.
C
C REFERENCES: (1) SHAH 1973 GEOPHYSICS 38 PP.600-604.
C             (2) HUBRAL AND KREY 1980 SEG MONOGRAPH ENTITLED
C                 'INTERVAL VELOCITIES FROM SEISMIC REFLECTION TIME
C                 MEASUREMENTS' PP.44-54.
C
C THE 'GLOBAL' COORDINATE SYSTEM IS RIGHT HANDED WITH Z AXIS POINTING
C VERTICALLY UPWARDS. THE NORMAL VECTOR DEFINING THE PLANE MUST
C POINT UPWARDS.
C
C THE 'LOCAL' COORDINATE SYSTEM HAS ITS Z AXIS POINTING ALONG THE
C LOCAL RAY DIRECTION AND ITS X AXIS LYING IN THE PLANE OF INCIDENCE
C AT P.
C
C ALL INPUT AND OUTPUT VECTORS ARE DEFINED IN THE GLOBAL SYSTEM.
C
C INPUT
C -----
C PVS    : POSITION VECTOR OF SOURCE S.
C EZI    : DIRECTION COSINES OF RAY LEAVING S.
C          NOTE THAT THIS IS ALSO THE UNIT VECTOR ALONG THE LOCAL
C          Z AXIS.
C EXI    : DIRECTION COSINES OF LOCAL X AXIS.
C          IF EXI IS INPUT AS A ZERO VECTOR, NEITHER THE ROTATION
C          ANGLE DELTA, OR THE OUTPUT ROTATED LOCAL X AXIS EXT ARE
C          COMPUTED.
C AN     : DIRECTION COSINES OF NORMAL TO PLANE.
C PERP   : DISTANCE MEASURED PERPENDICULARLY FROM PLANE TO ORIGIN.
C VRATIO : VELOCITY RATIO V TRANSMITTED / V INCIDENT.  IF VRATIO.LE.0
C         THE RAY IS NOT TRACED THROUGH THE PLANE.
C
C OUTPUT
C ------
C PVP    : POSITION VECTOR OF P, THE POINT OF INTERSECTION ON PLANE.
C EZT    : DIRECTION COSINES OF RAY TRANSMITTED AT P.
C          NOT COMPUTED IF VRATIO.LE.0
C EXT    : DIRECTION COSINES OF TRANSMITTED LOCAL X AXIS.
C          NOT COMPUTED IF EXI IS A ZERO VECTOR.
C RAYLEN : LENGTH OF RAYPATH IN TRANSIT FROM S TO P.
C CALPHA : COS(ANGLE OF INCIDENCE) = COS(ANGLE OF REFLECTION) AT P.
C CBETA  : COS(ANGLE OF REFRACTION) AT P. NOT COMPUTED IF VRATIO.LE.0
C DELTA  : 3D ROTATION ANGLE AT P (RADIANS).
C          DEFAULTS TO ZERO IF EXI IS A ZERO VECTOR.
C IER    : ERROR FLAG :
C         .EQ.0 ON NORMAL EXIT, OR
C         .EQ.1 IF ERROR IN INPUT DATA EG. PLANES INTERSECT BELOW S.
C         .EQ.2 IF RAY IS CRITICALLY REFRACTED AT P.
C         .EQ.3 IF ZERO RAY OR NORMAL VECTOR INPUT.
C
C GFA.251180
C
C---------------------------------------------------------------------
C
      PARAMETER ZERO=0D0,ONE=1D0,SMALL=1D-5
```

```
C
C  SET INITIAL DEFAULTS.
C
      IER=3
      DELTA=ZERO
C
C  SET INVARIANTS.
C
      S1=PVS(1)
      S2=PVS(2)
      S3=PVS(3)
C
C-----------------------------------------------------------------------
C
C  VALIDATE DIRECTION COSINES.
C
      EZI1=EZI(1)
      EZI2=EZI(2)
      EZI3=EZI(3)
      TEMP=SQRT(EZI1*EZI1+EZI2*EZI2+EZI3*EZI3)
      IF(ABS(TEMP-ONE).GT.SMALL)THEN
         CALL WARNING('RAYTR3D','INCIDENT RAY REQUIRES NORMALIZING')
         IF(TEMP.LE.SMALL)THEN
            RETURN
         ELSE
            EZI1=EZI1/TEMP
            EZI2=EZI2/TEMP
            EZI3=EZI3/TEMP
            ENDIF
         ENDIF
      A=AN(1)
      B=AN(2)
      C=AN(3)
      TEMP=SQRT(A*A+B*B+C*C)
      IF(ABS(TEMP-ONE).GT.SMALL)THEN
         CALL WARNING('RAYTR3D','INTERFACE NORMAL REQUIRES NORMALIZING')
         IF(TEMP.LE.SMALL)THEN
            RETURN
         ELSE
            A=A/TEMP
            B=B/TEMP
            C=C/TEMP
            ENDIF
         ENDIF
C
C  BOTH VECTORS NOW UNIT MAGNITUDE.
C
      IER=0
C
C-----------------------------------------------------------------------
C
C  COSINE OF ANGLE OF INCIDENCE FROM DOT PRODUCT N.EZI
C
      CALPHA=A*EZI1+B*EZI2+C*EZI3
      IF(CALPHA.GT.ONE)CALPHA=ONE
      IF(CALPHA.LT.-ONE)CALPHA=-ONE
C
C-----------------------------------------------------------------------
C
C  LENGTH OF RAYPATH FROM S TO P. SHAH EQNS.3A,3B
C
      RAYLEN=-(A*S1+B*S2+C*S3+PERP)/CALPHA
      IF(RAYLEN.LT.ZERO)THEN
```

```
            CALL WARNING('RAYTR3D','CROSSING OR BADLY DEFINED INTERFACES')
            IER=1
            RETURN
            ENDIF
C
C-----------------------------------------------------------------------
C
C  POSITION VECTOR OF P. SHAH EQN 3A
C
        PVP(1)=S1+EZI1*RAYLEN
        PVP(2)=S2+EZI2*RAYLEN
        PVP(3)=S3+EZI3*RAYLEN
C
C-----------------------------------------------------------------------
C
C  TRANSMITTED DIRECTION COSINES. SHAH EQN 9C
C  NB. ONLY COMPUTED IF VRATIO > 0.
C
        IF(VRATIO.GT.ZERO)THEN
           SALPHA=SQRT(ONE-CALPHA*CALPHA)
           SBETA=VRATIO*SALPHA
C
C  CHECK FOR CRITICAL REFRACTION ALONG INTERFACE.
C
           IF(SBETA.GT.ONE)THEN
              CALL WARNING('RAYTR3D',
     &                     'RAY REFRACTED CRITICALLY AT NEXT HORIZON')
              CBETA=ZERO
              IER=2
           ELSE
              CBETA=(CALPHA/ABS(CALPHA))*SQRT(ONE-SBETA*SBETA)
              VANG=VRATIO*CALPHA-CBETA
              EZT(1)=VRATIO*EZI1-VANG*A
              EZT(2)=VRATIO*EZI2-VANG*B
              EZT(3)=VRATIO*EZI3-VANG*C
              ENDIF
           ENDIF
C
C-----------------------------------------------------------------------
C
C  COMPUTE ROTATION ANGLE DELTA.
C  RETURN TO CALLING ROUTINE IF INPUT EX IS A ZERO VECTOR.
C
        EXI1=EXI(1)
        EXI2=EXI(2)
        EXI3=EXI(3)
        TEMP=SQRT(EXI1*EXI1+EXI2*EXI2+EXI3*EXI3)
        IF(TEMP.LE.SMALL)THEN
           RETURN
        ELSEIF(ABS(TEMP-ONE).GT.SMALL)THEN
           CALL WARNING('RAYTR3D','LOCAL EX VECTOR REQUIRES NORMALIZING')
           EXI1=EXI1/TEMP
           EXI2=EXI2/TEMP
           EXI3=EXI3/TEMP
           ENDIF
        EYI1=EZI2*EXI3 - EZI3*EXI2
        EYI2=EZI3*EXI1 - EZI1*EXI3
        EYI3=EZI1*EXI2 - EZI2*EXI1
        AA=EXI1*A + EXI2*B + EXI3*C
        BB=EYI1*A + EYI2*B + EYI3*C
        DELTA=ZERO
        IF(AA.NE.ZERO.OR.BB.NE.ZERO)DELTA=ATAN2(BB,AA)
C
```

```
C-----------------------------------------------------------------------
C
C  RETURN TO CALLING ROUTINE IF NO TRANSMISSION THROUGH PLANE, IN WHICH
C  CASE TRANSMITTED LOCAL EX AXIS CANNOT BE COMPUTED.
C
      IF(VRATIO.LE.ZERO.OR.SBETA.GT.ONE)RETURN
      SDELTA=SIN(DELTA)
      CDELTA=COS(DELTA)
C
C-----------------------------------------------------------------------
C
C  DERIVE NEXT EX AXIS VECTOR BY ROTATING OLD ONE THROUGH INTERFACE.
C  3D ROTATION BY ANGLE DELTA. HUBRAL EQN 4.27
C  NOTE EZ AXIS UNAFFECTED.
C
      EXR1=CDELTA*EXI1 + SDELTA*EYI1
      EXR2=CDELTA*EXI2 + SDELTA*EYI2
      EXR3=CDELTA*EXI3 + SDELTA*EYI3
C
C  SNELL REFRACTION CAUSES ROTATION BY ANGLE SIGMA=ALPHA - BETA.
C  HUBRAL EQN 4.28
C
      SSIGMA=SALPHA*CBETA - CALPHA*SBETA
      CSIGMA=CALPHA*CBETA + SALPHA*SBETA
      EXT(1)=CSIGMA*EXR1 - SSIGMA*EZI1
      EXT(2)=CSIGMA*EXR2 - SSIGMA*EZI2
      EXT(3)=CSIGMA*EXR3 - SSIGMA*EZI3
C
C  NOTE HERE THAT THE TRANSMITTED RAY (EZ AXIS) COULD ALTERNATIVELY
C  HAVE BEEN COMPUTED FROM THE FOLLOWING: (ALSO HUBRAL EQN 4.28)
C     EZT(1)=SSIGMA*EXR1+CSIGMA*EZI1
C     EZT(2)=SSIGMA*EXR2+CSIGMA*EZI2
C     EZT(3)=SSIGMA*EXR3+CSIGMA*EZI3
C
C-----------------------------------------------------------------------
C
C  RETURN TO CALLING ROUTINE.
C
      RETURN
      END
```

```
      SUBROUTINE WARNING(IDSUB,MESSAG)
      CHARACTER*(*) IDSUB,MESSAG
C
C  PRINTS WARNING MESSAGE RELATING TO ERROR CONDITION TO CURRENT
C  OUTPUT DEVICE.
C
C  INPUT
C  -----
C  IDSUB  : NAME OF MODULE IN WHICH ERROR OCCURED.
C  MESSAG : CHARACTER STRING INDICATING THE REASON FOR FAILURE.
C
C  GFA.151280
C
C-----------------------------------------------------------------------
C
      PRINT 1,'"'//IDSUB(1:NUCHAR(IDSUB))//'"',MESSAG
      RETURN
    1 FORMAT(' ***WARNING: ERROR HAS OCCURED IN MODULE ',A/
     +' ***',A)
      END
```

APPENDIX 4B

A 3D FORWARD MODELLING SUBROUTINE: HUBRALF

```
      SUBROUTINE HUBRALF(LFST,LAST,XORG,YORG,VINT,DEPTH,ETA,THETA,LUN,
     &                  T0,SX,SY,VNMOX,VNMOY,VMAJOR,VMINOR,SIGMA,XN,YN,
     &                  ZN,IER)
      IMPLICIT DOUBLE PRECISION (A-H),(O-Z)
      INTEGER LFST,LAST,LUN,IER
      REAL XORG,YORG,
     &     VINT(LAST),DEPTH(LAST),ETA(LAST),THETA(LAST),
     &     T0(LAST),VNMOX(LAST),VNMOY(LAST),SX(LAST),SY(LAST),
     &     VMAJOR(LAST),VMINOR(LAST),SIGMA(LAST),
     &     XN(LAST),YN(LAST),ZN(LAST)
      PARAMETER MXL=15
C
C PURPOSE
C -------
C RAY TRACES NORMAL INCIDENCE RAYS FROM SPECIFIED HORIZONS THROUGH
C ISOVELOCITY LAYERS WITH 3D PLANE INTERFACES OF ARBITRARY DIP AND
C STRIKE, RETURNING TWO-WAY TIME, TIME SLOPES, NORMAL MOVEOUT VELOCITY
C ELLIPSE PARAMETERS AND NORMAL INCIDENCE COORDINATES.
C REFERENCES: (1) HUBRAL 1976 GEOPHYSICAL PROSPECTING 24 PP. 478-491
C             (2) HUBRAL 1976 GEOPHYSICS 41 PP. 233-242
C             (3) HUBRAL AND KREY 1980 SEG MONOGRAPH ENTITLED
C                 'INTERVAL VELOCITIES FROM SEISMIC REFLECTION TIME
C                  MEASUREMENTS'.
C
C CONVENTIONS USED IN HUBRALF INCLUDE:
C   -RIGHT HANDED COORDINATE SYSTEM WITH +X ALONG PROFILE, +Z
C    VERTICALLY UP.
C   -INCREASING DEPTH IMPLIES POSITIVE DIP ANGLE.
C   -INCREASING TIME IMPLIES POSITIVE TIME SLOPE.
C   -ALL ANGLES INPUT AND USED IN RADIANS.
C
C INPUT
C -----
C LFST   : FIRST LAYER/HORIZON TO BE FORWARD MODELLED.
C LAST   : LAST  LAYER/HORIZON TO BE FORWARD MODELLED.
C XORG   : CARTESIAN X OF SURFACE ORIGIN.
C YORG   : CARTESIAN Y OF SURFACE ORIGIN.
C VINT   : INTERVAL VELOCITY OF EACH LAYER INDEXED AS VINT(I) = LAYER I
C          VELOCITY ETC.
C          NB. ALL OTHER INPUT/OUTPUT ARRAYS ARE INDEXED CF. VINT.
C DEPTH  : VERTICAL DEPTHS (BELOW ORIGIN) FOR EACH HORIZON.
C ETA    : MAXIMUM DIP ANGLE (RADIANS) FOR EACH HORIZON.
C THETA  : AZIMUTH (RADIANS) OF MAXIMUM DIP FOR EACH HORIZON IE. THE
C          AZIMUTH PERPENDICULAR TO STRIKE IN THE DIRECTION
C          OF DOWNWARD DIP. THIS ANGLE IS MEASURED AWAY FROM THE
C          PROFILE (+X) DIRECTION WITH ANTICLOCKWISE ANGLES (TOWARDS
C          +Y) POSITIVE.
C LUN    : LOGICAL UNIT NUMBER (INTEGER) OF PRINT FILE.
C          NB. LUN < 1 SUPPRESSES PRINTING.
C
C OUTPUT
C ------
C T0     : TWO-WAY NORMAL INCIDENCE TIMES FOR EACH HORIZON.
C SX     : TIME DIP DT/DX IN DIRECTION OF INCREASING X (ALONG PROFILE)
C          FOR EACH HORIZON.
C SY     : CROSS DIP DT/DY IN DIRECTION OF INCREASING Y (ACROSS
C          PROFILE) FOR EACH HORIZON.
C VNMOX  : NMO VELOCITY DERIVED (ALONG PROFILE) FOR EACH HORIZON.
C VNMOY  : NMO VELOCITY DERIVED (ACROSS PROFILE) FOR EACH HORIZON.
C VMAJOR : MAGNITUDE OF MAJOR AXIS OF NMO VELOCITY ELLIPSE FOR EACH
C          HORIZON.
C VMINOR : MAGNITUDE OF MINOR AXIS OF NMO VELOCITY ELLIPSE FOR EACH
C          HORIZON.
```

```
C  SIGMA  : ANGLE (RADIANS) BETWEEN NMO VELOCITY ELLIPSE MAJOR AXIS AND
C           PROFILE (+X) DIRECTION FOR EACH HORIZON.
C  XN     : CARTESIAN X OF NORMAL INCIDENCE POINT ON EACH HORIZON.
C  YN     : CARTESIAN Y OF NORMAL INCIDENCE POINT ON EACH HORIZON.
C  ZN     : CARTESIAN Z OF NORMAL INCIDENCE POINT ON EACH HORIZON.
C  IER    : ERROR FLAG:
C           .EQ.0 IF SUBROUTINE COMPLETED SUCCESSFULLY.
C           .EQ.N IF FORWARD MODEL FAILED AT HORIZON N.
C
C  COMMENTS
C  --------
C  THE FOLLOWING LIST INDICATES THE MINIMUM ARRAY SIZES THAT MUST
C  BE DECLARED IN THE CALLING ROUTINE:
C
C  VINT,DEPTH,ETA,THETA,T0,SIGMA,SX,SY,VNMOX,VNMOY,VMAJOR,VMINOR,SIGMA,
C  XN,YN,ZN:  DIMENSIONED AT LEAST (LAST).
C
C  THE FOLLOWING DATA ARE SET ON THE PARAMETER CARD ABOVE:
C
C  MXL    : THE MAXIMUM NUMBER OF LAYERS/HORIZONS ALLOWED IN THIS
C           VERSION.
C
C  GFA.251180
C
C-----------------------------------------------------------------------
C
      PARAMETER ZERO=0D0,HALF=0.5D0,ONE=1D0,SMALL=1D-5
      PARAMETER PI=3.141592653589793D0
      DIMENSION P1(2,2),P2(2,2),R(2,2),WK(2,2),EX(3)
      DIMENSION PATH(3,MXL+1),ANORM(3,MXL+1),RAY(3,MXL+1),PERP(MXL+1)
      LOGICAL ANNOT
C
C  SET DEFAULT ERROR FLAG TO OK.
C
      IER=0
C
C  SET INVARIANTS.
C
      ANNOT=LUN.GE.1
      PIBY2=PI*HALF
      RADDEG=180D0/PI
      V1=VINT(1)
C
C  PRINT HEADING.
C
      IF(ANNOT)WRITE(LUN,1000)LFST,LAST.XORG,YORG
C
C-----------------------------------------------------------------------
C
C  DERIVE DIRECTION COSINES OF NORMALS AND PERPENDICULAR DEPTHS TO EACH
C  INTERFACE.
C
      ANORM(1,1)=ZERO
      ANORM(2,1)=ZERO
      ANORM(3,1)=ONE
      PERP(1)=ZERO
      DO 10 I=1,LAST
         IP1=I+1
         SETA=SIN(ETA(I))
         CETA=SQRT(ONE-SETA*SETA)
         ANORM(1,IP1)=SETA*COS(THETA(I))
         ANORM(2,IP1)=SETA*SIN(THETA(I))
         ANORM(3,IP1)=CETA
```

```
            PERP(IP1)=DEPTH(I)*CETA
   10       CONTINUE
C
C-----------------------------------------------------------------------
C
C  FORWARD MODEL EACH HORIZON IN TURN.
C
        DO 20 N=LFST,LAST
        NM1=N-1
        NP1=N+1
C
C  DERIVE DIRECTION COSINES OF SURFACE DOWNGOING RAY WHICH IS INCIDENT
C  NORMALLY ON HORIZON N.
C
        IF(N.EQ.1)THEN
C
C  FIRST HORIZON: DIRECTION COSINES OF DOWNGOING RAY NORMAL TO
C  HORIZON 1 ARE THE REVERSE OF NORMAL VECTOR TO HORIZON 1.
C
            RAY(1,1)=-ANORM(1,2)
            RAY(2,1)=-ANORM(2,2)
            RAY(3,1)=-ANORM(3,2)
        ELSE
C
C  OTHERWISE TRACE RAY UPWARDS FROM NORMAL INCIDENCE ON HORIZON N.
C  SET RAY START POSITION AND DIRECTION ON HORIZON N.
C  SET EX VECTOR TO ZERO FOR EARLY EXITS FROM RAYTR3D.
C
            PATH(1,NP1)=XORG
            PATH(2,NP1)=YORG
            PATH(3,NP1)=-DEPTH(N)
            RAY(1,N)=ANORM(1,NP1)
            RAY(2,N)=ANORM(2,NP1)
            RAY(3,N)=ANORM(3,NP1)
            EX(1)=ZERO
            EX(2)=ZERO
            EX(3)=ZERO
C
C  RAY TRACE UPWARDS.
C
            DO 30 I=N,2,-1
               IM1=I-1
               IP1=I+1
               VRATIO=VINT(IM1)/VINT(I)
               CALL RAYTR3D(PATH(1,IP1),RAY(1,I),EX,ANORM(1,I),PERP(I),
     &                      VRATIO,PATH(1,I),RAY(1,IM1),EX,RLEN,CB,CA,
     &                      DELTA,IER)
               IF(IER.NE.0)THEN
                  CALL WARNING('HUBRALF','RAY TRACING UPWARDS FAILED')
                  IER=N
                  RETURN
                  ENDIF
   30          CONTINUE
C
C  DIRECTION COSINES OF DOWNGOING RAY NORMAL TO HORIZON N ARE REVERSE
C  OF THOSE OF UPGOING RAY IN LAYER 1.
C
            RAY(1,1)=-RAY(1,1)
            RAY(2,1)=-RAY(2,1)
            RAY(3,1)=-RAY(3,1)
            ENDIF
C
C-----------------------------------------------------------------------
```

```
C
C  INITIALISE FOR DOWNWARD RAY TRACING.
C
C  SET RAY START POSITION AT ORIGIN, TWO WAY TIME, RADIUS AND WORKSPACE
C  MATRICES.
C
      PATH(1,1)=XORG
      PATH(2,1)=YORG
      PATH(3,1)=ZERO
      TWT=ZERO
      R(1,1)=ZERO
      R(2,1)=ZERO
      R(1,2)=ZERO
      R(2,2)=ZERO
      P1(1,1)=ONE
      P1(2,1)=ZERO
      P1(1,2)=ZERO
      P1(2,2)=ONE
      P2(1,1)=ONE
      P2(2,1)=ZERO
      P2(1,2)=ZERO
      P2(2,2)=ONE
C
C  SET EX VECTOR.
C
      IF(N.EQ.1)THEN
C
C  NO ROTATION FOR FIRST HORIZON. SET EX TO A ZERO VECTOR FOR EARLY EXIT
C  FROM RAYTR3D.
C
         EX(1)=ZERO
         EX(2)=ZERO
         EX(3)=ZERO
      ELSE
C
C  OTHERWISE VEC = [RAY IN LAYER 1] CROSS [SURFACE NORMAL]
C             EX = [VEC] CROSS [RAY IN LAYER 1]
C
         RAY1=RAY(1,1)
         RAY2=RAY(2,1)
         RAY3=RAY(3,1)
         VEC1=RAY2*ANORM(3,1)-RAY3*ANORM(2,1)
         VEC2=RAY3*ANORM(1,1)-RAY1*ANORM(3,1)
         VEC3=RAY1*ANORM(2,1)-RAY2*ANORM(1,1)
         EX(1)=VEC2*RAY3-VEC3*RAY2
         EX(2)=VEC3*RAY1-VEC1*RAY3
         EX(3)=VEC1*RAY2-VEC2*RAY1
C
C  CHECK MAGNITUDE OF EX. IF APPROXIMATELY ZERO SET TO DEFAULT (1,0,0)
C  VECTOR. OTHERWISE NORMALISE TO UNIT MAGNITUDE.
C
         TEMP=SQRT(EX(1)*EX(1)+EX(2)*EX(2)+EX(3)*EX(3))
         IF(TEMP.GT.SMALL)THEN
            EX(1)=EX(1)/TEMP
            EX(2)=EX(2)/TEMP
            EX(3)=EX(3)/TEMP
         ELSE
            EX(1)=ONE
            EX(2)=ZERO
            EX(3)=ZERO
            ENDIF
         ENDIF
C
```

```
C  TRACE RAY FROM SURFACE DOWN TO HORIZON N.
C  DT(I) REFERS TO TWO-WAY TIME IN LAYER I CF. CONVENTION REF(2)
C  COMPUTE RADIUS MATRIX R. REF (1) EQN 26. NO DIVISION BY V1 IS MADE.
C
      DO 60 I=1,N
         VII=VINT(I)
         IP1=I+1
         IF(I.EQ.N)THEN
            VRATIO=ZERO
         ELSE
            VRATIO=VINT(IP1)/VII
            ENDIF
         CALL RAYTR3D(PATH(1,I),RAY(1,I),EX,ANORM(1,IP1),PERP(IP1),
     &                VRATIO,PATH(1,IP1),RAY(1,IP1),EX,RLEN,CA,CB,
     &                DELTA,IER)
         IF(IER.NE.0)THEN
            CALL WARNING('HUBRALF','RAY TRACING DOWNWARDS FAILED')
            IER=N
            RETURN
            ENDIF
C
C  SET LAYER TWO-WAY TRANSIT TIME AND UPDATE CUMULATIVE TWO-WAY TIME.
C
         DTI=(RLEN+RLEN)/VII
         TWT=TWT+DTI
C
C  UPDATE RADIUS OF CURVATURE MATRIX.
C
         CALL MATMLTD(P1,P2,WK)
         TEMP=VII*VII*DTI
         R(1,1)=R(1,1)+TEMP*WK(1,1)
         R(2,1)=R(2,1)+TEMP*WK(2,1)
         R(1,2)=R(1,2)+TEMP*WK(1,2)
         R(2,2)=R(2,2)+TEMP*WK(2,2)
         IF(I.LT.N)THEN
            CABYCB=CA/CB
            CD=COS(DELTA)
            SD=SIN(DELTA)
            WK(1,1)=CD*CABYCB
            WK(2,1)=SD*CABYCB
            WK(1,2)=-SD
            WK(2,2)=CD
            CALL MATMLTD(P1,WK,P1)
            TEMP=WK(1,2)
            WK(1,2)=WK(2,1)
            WK(2,1)=TEMP
            CALL MATMLTD(WK,P2,P2)
            ENDIF
   60    CONTINUE
C
C-----------------------------------------------------------------------
C
C  SET TWO-WAY TIME AND NORMAL INCIDENCE COORDINATES FOR THIS LAYER.
C
      T0(N)=TWT
      XN(N)=PATH(1,NP1)
      YN(N)=PATH(2,NP1)
      ZN(N)=PATH(3,NP1)
C
C  B0 IS THE ANGLE OF EMERGENCE TO VERTICAL.
C
      CB0=-RAY(3,1)
      C2B0=CB0*CB0
```

```
      SB0=SQRT(ONE-C2B0)
C
C  SET PARAMETERS DN, EN, FN IN REF(2). THESE WILL BE USED LATER ON IN
C  THE COMPUTATION OF VNMO.
C
      R11=R(1,1)*HALF
      R12=R(1,2)*HALF
      R22=R(2,2)*HALF
      DETR=R11*R22-R12*R12
      IF(DETR.EQ.ZERO)THEN
         CALL WARNING('HUBRALF','RADIUS MATRIX SINGULAR')
         IER=N
         RETURN
         ENDIF
      DN=C2B0*R22/DETR
      EN=CB0*R12/DETR
      FN=R11/DETR
C
C-----------------------------------------------------------------------
C
C  DERIVE TIME SLOPES. TSLOPE IS SMINUSPHIN IN REF(2). PHIN IS ANGLE
C  BETWEEN PROFILE (+X) AND PROJECTION OF EMERGING RAY ONTO SURFACE,
C  MEASURED AWAY FROM THE LATTER.
C
      TSLOPE=(SB0+SB0)/V1
      IF(ABS(RAY(2,1)).LT.SMALL.AND.ABS(RAY(1,1)).LT.SMALL)THEN
         PHIN=ZERO
      ELSE
         PHIN=ATAN2(RAY(2,1),-RAY(1,1))
         ENDIF
      CPHIN=COS(PHIN)
      SPHIN=SIN(PHIN)
      SX(N)=TSLOPE*CPHIN
      SY(N)=-TSLOPE*SPHIN
C
C-----------------------------------------------------------------------
C
C  DERIVE NMO VELOCITY ELLIPSE USING DN, EN, FN CALCULATED ABOVE.
C
C  PHIMAX IS A TURNING POINT IN THE VNMO(AZIMUTH) FUNCTION (IE. EITHER
C  A MAXIMUM VNMO OR MINIMUM VNMO AZIMUTH) MEASURED AWAY FROM THE RAY
C  EMERGE ANGLE PHIN.
C
      IF(EN.EQ.ZERO.AND.DN.EQ.FN)THEN
         PHIMAX=ZERO
      ELSE
         PHIMAX=HALF*ATAN2(EN+EN,DN-FN)
         ENDIF
      CPHIM=COS(PHIMAX)
      SPHIM=SIN(PHIMAX)
      C2PHIM=CPHIM*CPHIM
      S2PHIM=ONE-C2PHIM
      VMAX2=ONE/(TWT*(HALF*DN*C2PHIM+HALF*FN*S2PHIM+EN*CPHIM*SPHIM))
      VMIN2=ONE/(TWT*(HALF*DN*S2PHIM+HALF*FN*C2PHIM-EN*CPHIM*SPHIM))
      IF(VMAX2.LT.VMIN2)THEN
         PHIMAX=PHIMAX+PIBY2
         TEMP=VMIN2
         VMIN2=VMAX2
         VMAX2=TEMP
         ENDIF
      VMAJOR(N)=SQRT(VMAX2)
      VMINOR(N)=SQRT(VMIN2)
C
```

```
C  DERIVE NMO VELOCITY ALONG AND ACROSS PROFILE FROM THE ELLIPSE.
C
C  SIG IS THE ANGLE BETWEEN THE AZIMUTH OF MAXIMUM VNMO AND THE PROFILE,
C  MEASURED AWAY FROM THE LATTER.
C
      SIG=PHIMAX-PHIN
      IF(SIG.GE.PI)SIG=SIG-PI
      SIGMA(N)=SIG
      CSIG=COS(SIG)
      C2SIG=CSIG*CSIG
      S2SIG=ONE-C2SIG
      VNMOX(N)=SQRT(ONE/(C2SIG/VMAX2+S2SIG/VMIN2))
      VNMOY(N)=SQRT(ONE/(C2SIG/VMIN2+S2SIG/VMAX2))
C
C-----------------------------------------------------------------------
C
C  OUTPUT RESULTS FOR HORIZON N.
C
      IF(ANNOT)THEN
         WRITE(LUN,1010)N,VINT(N),ETA(N)*RADDEG,THETA(N)*RADDEG,
     &                  DEPTH(N),TWT,XN(N),YN(N),ZN(N),ACOS(CB0)*RADDEG,
     &                  -PHIN*RADDEG,SX(N),SY(N),VNMOX(N),VNMOY(N),
     &                  VMAJOR(N),VMINOR(N),SIG*RADDEG
         ENDIF
C
C  NEXT HORIZON.
C
   20 CONTINUE
C
C-----------------------------------------------------------------------
C
C  RETURN TO CALLING ROUTINE.
C
      RETURN
C
C-----------------------------------------------------------------------
C
C  FORMATS.
C
 1000 FORMAT(' HUBRAL 3D FORWARD MODEL FOR LAYERS ',I2,' THROUGH ',
     & I2,' SURFACE ORIGIN AT X=',F8.1,' Y=',F8.1,28X,'HUBRALF.251180'/
     &  1X,130(1H-)//
     &' HORI INTV   MAX-DIP  VERTICAL  2WAY NORMAL-INCIDENCE-POINT RAY
     &-EMERGE-ANG  TIME-SLOPE           NORMAL-MOVEOUT-VELOCITY'/
     &' -ZON  VEL  ANGLE AZIMT  DEPTH    TIME     XN      YN      ZN   TO
     &+Z   TO+X   DT/DX   DT/DY    VNMOX  VNMOY  MAJOR  MINOR  AXIS'/)
 1010 FORMAT(I3,F8.1,2F6.1,F8.1,F7.3,3F8.1,F5.1,F7.1,2(1X,E9.3),5F7.1)
      END
```

```
      SUBROUTINE MATMLTD(A,B,C)
      DOUBLE PRECISION A(2,2),B(2,2),C(2,2)
C
C  2*2 MATRIX MULTIPLICATION IN DOUBLE PRECISION.
C
C  INPUT
C  -----
C  A       : 2*2 MATRIX.
C  B       : 2*2 MATRIX.
C
C  OUTPUT
C  ------
C  C       : 2*2 MATRIX C= A * B.
C
C  GFA.211180
C
C-----------------------------------------------------------------------
C
      A11=A(1,1)
      A21=A(2,1)
      A12=A(1,2)
      A22=A(2,2)
      B11=B(1,1)
      B21=B(2,1)
      B12=B(1,2)
      B22=B(2,2)
      C(1,1)= A11*B11 + A12*B21
      C(2,1)= A21*B11 + A22*B21
      C(1,2)= A11*B12 + A12*B22
      C(2,2)= A21*B12 + A22*B22
      RETURN
      END
```

APPENDIX 4C

A 3D INVERSION SUBROUTINE: HUBRALI

```
      SUBROUTINE HUBRALI(LFST,LAST,MODE,XORG,YORG,VTOL,T0,VNMOX,SX,SY,
     &                    LUN,VINT,DEPTH,ETA,THETA,VNMOY,VMAJOR,VMINOR,
     &                    SIGMA,XN,YN,ZN,IER)
      IMPLICIT DOUBLE PRECISION (A-H),(O-Z)
      INTEGER LFST,LAST,MODE,LUN,IER
      REAL XORG,YORG,VTOL,
     &      T0(LAST),VNMOX(LAST),SX(LAST),SY(LAST),
     &      VINT(LAST),DEPTH(LAST),ETA(LAST),THETA(LAST),
     &      VNMOY(LAST),VMAJOR(LAST),VMINOR(LAST),SIGMA(LAST),
     &      XN(LAST),YN(LAST),ZN(LAST)
      PARAMETER MXL=15,MAXIT=20
      PARAMETER VNMIN=1D0,VNMAX=100000D0
C
C PURPOSE
C -------
C DERIVES INTERVAL VELOCITIES AND SUBSURFACE GEOMETRY FOR A MODEL WITH
C ISOVELOCITY LAYERS SEPARATED BY PLANE REFLECTING INTERFACES OF
C ARBITRARY DIP AND STRIKE IN 3D SPACE, GIVEN ZERO-OFFSET / NORMAL-
C INCIDENCE TWO-WAY TIMES, MOVEOUT VELOCITIES AND ORTHOGONAL TIME
C SLOPES ( VIZ. IN-LINE DT/DX AND CROSS-DIP DT/DY) AT EACH HORIZON.
C
C REFERENCES: (1) HUBRAL 1976 GEOPHYSICAL PROSPECTING 24 PP. 478-491
C             (2) HUBRAL 1976 GEOPHYSICS 41 PP. 233-242
C             (3) HUBRAL AND KREY 1980 SEG MONOGRAPH ENTITLED
C                 'INTERVAL VELOCITIES FROM SEISMIC REFLECTION TIME
C                 MEASUREMENTS'.
C             (4) SHAH 1973 GEOPHYSICS 38 PP. 600-604
C
C SUBROUTINE HUBRALI ALLOWS THE DIRECT INVERSION OF N LAYERS (MODE=0)
C OR THE GRADUAL (LAYER BY LAYER) INVERSION CONSISTING OF VELOCITY
C DERIVATION (MODE=1), RETURN TO CALLING ROUTINE TO PROCESS DERIVED VN,
C AND THEN RAY TRACING THROUGH THIS PROCESSED VELOCITY (VN) TO NEXT
C HORIZON (MODE=2).
C
C CONVENTIONS USED IN HUBRALI INCLUDE:
C   -RIGHT HANDED COORDINATE SYSTEM WITH +X ALONG PROFILE AND +Z
C    VERTICALLY UP.
C   -INCREASING DEPTH IMPLIES POSITIVE DIP ANGLE.
C   -INCREASING TIME IMPLIES POSITIVE TIME SLOPE.
C   -ALL ANGLES INPUT IN RADIANS.
C   -HORIZON NORMAL VECTORS POINT UPWARDS.
C
C INPUT
C -----
C LFST   : FIRST LAYER/HORIZON TO BE INVERTED/TRACED TO.
C LAST   : LAST  LAYER/HORIZON TO BE INVERTED/TRACED TO.
C MODE   : .EQ.0 => DERIVE VN AND REFLECTOR GEOMETRY FOR LAYERS
C          N=LFST,LAST.
C          .EQ.1 => DERIVE VN FOR LAYER N=LFST (=LAST). DO NOT
C          TRACE TO REFLECTOR N.
C          .EQ.2 => DERIVE REFLECTOR GEOMETRY AT HORIZON N=LFST
C          (=LAST). DO NOT DERIVE VN.
C XORG   : CARTESIAN X OF SURFACE ORIGIN.
C YORG   : CARTESIAN Y OF SURFACE ORIGIN.
C VTOL   : REQUIRED ACCURACY OF DERIVED INTERVAL VELOCITIES IN UNITS
C          OF VELOCITY.
C T0     : TWO-WAY ZERO-OFFSET (NORMAL INCIDENCE) TIMES FOR EACH
C          HORIZON INDEXED AS T0(I) = TWO-WAY TIME TO HORIZON I.
C          NB. ALL OTHER INPUT/OUTPUT ARRAYS ARE INDEXED CF. T0.
C VNMOX  : NMO VELOCITY OBSERVED (ALONG PROFILE) FOR EACH HORIZON.
C SX     : TIME DIP DT/DX IN DIRECTION OF INCREASING X (ALONG PROFILE)
C          FOR EACH HORIZON.
C SY     : CROSS DIP DT/DY IN DIRECTION OF INCREASING Y (ACROSS
```

```
C                PROFILE) FOR EACH HORIZON.
C   LUN    : LOGICAL UNIT NUMBER (INTEGER) OF PRINT FILE.
C            NB. LUN < 1 SUPPRESSES PRINTING.
C
C   OUTPUT
C   ------
C   VINT   : INTERVAL VELOCITY DERIVED FOR EACH LAYER TO AN ACCURACY
C            OF +/- VTOL.
C   DEPTH  : VERTICAL DEPTHS (BELOW ORIGIN) DERIVED FOR EACH HORIZON.
C   ETA    : MAXIMUM DIP ANGLE (RADIANS) DERIVED FOR EACH HORIZON.
C   THETA  : AZIMUTH (RADIANS) OF MAXIMUM DIP FDERIVED FOR EACH HORIZON
C            IE. THE AZIMUTH PERPENDICULAR TO STRIKE IN THE DIRECTION
C            OF DOWNWARD DIP. THIS ANGLE IS MEASURED AWAY FROM THE
C            PROFILE (+X) DIRECTION WITH ANTICLOCKWISE ANGLES (TOWARDS
C            +Y) POSITIVE.
C   VNMOY  : NMO VELOCITY DERIVED ACROSS PROFILE FOR EACH HORIZON.
C   VMAJOR : MAGNITUDE OF MAJOR AXIS OF NMO VELOCITY ELLIPSE FOR EACH
C            HORIZON.
C   VMINOR : MAGNITUDE OF MINOR AXIS OF NMO VELOCITY ELLIPSE FOR EACH
C            HORIZON.
C   SIGMA  : ANGLE (RADIANS) BETWEEN NMO VELOCITY ELLIPSE MAJOR AXIS AND
C            PROFILE (+X) DIRECTION FOR EACH HORIZON.
C   XN     : CARTESIAN X OF NORMAL INCIDENCE POINT ON EACH HORIZON.
C   YN     : CARTESIAN Y OF NORMAL INCIDENCE POINT ON EACH HORIZON.
C   ZN     : CARTESIAN Z OF NORMAL INCIDENCE POINT ON EACH HORIZON.
C   IER    : ERROR FLAG:
C            .EQ.0 IF SUBROUTINE COMPLETED SUCCESSFULLY.
C            .EQ.N IF INVERSION FAILED AT HORIZON N.
C
C   COMMENTS
C   --------
C   NOTE: FOR MODE=1 AND MODE=2 THE ARRAYS VINT, ETA, THETA, DEPTH MUST
C   CONTAIN DATA FOR LAYERS I=1,LFIRST-1 IN ORDER THAT RAY TRACING TO
C   HORIZON "N-1" BE POSSIBLE.
C
C   THE FOLLOWING LIST INDICATES THE MINIMUM ARRAY SIZES THAT MUST BE
C   DECLARED IN THE CALLING ROUTINE:
C
C   T0,VNMOX,SX,SY,VINT,DEPTH,ETA,THETA,VNMOY,VMAJOR,VMINOR,SIGMA,
C   XN,YN,ZN:      DIMENSIONED AT LEAST (LAST).
C
C   THE FOLLOWING DATA ARE SET ON THE PARAMETER CARDS ABOVE:
C
C   MXL    : THE MAXIMUM NUMBER OF LAYERS/HORIZONS ALLOWED IN THIS
C            VERSION.
C
C   MAXIT  : THE MAXIMUM NUMBER OF NEWTON RAPHSON ITERATIONS ALLOWED
C            TO FIND THE INTERVAL VELOCITY FOR ANY ONE LAYER.
C
C   VNMIN  : THE MINIMUM VALUE IN THE RANGE OF INTERVAL VELOCITY
C            SOLUTIONS ALLOWED IN THE ITERATION.
C   VNMAX  : THE MAXIMUM VALUE IN THE RANGE OF INTERVAL VELOCITY
C            SOLUTIONS ALLOWED IN THE ITERATION.
C            NB. ALL DERIVED VELOCITIES SHOULD LIE IN THE RANGE
C                      VNMIN .LE. VN .LE. VNMAX
C            THIS RESTRICTION IS IMPOSED IN ORDER TO PREVENT THE
C            NEWTON-RAPHSON ITERATION BLOWING UP TO GIVE SPURIOUS
C            RESULTS.
C
C   GFA.270181
C
C-----------------------------------------------------------------
C
```

```
      PARAMETER ZERO=0D0,HALF=0.5D0,ONE=1D0,SMALL=1D-5
      PARAMETER PI=3.141592653589793D0,RADDEG=180D0/PI,FACTOR=1.01D0
      DIMENSION P1(2,2),P2(2,2),U(2,2),UINV(2,2),WK(2,2),EX(3)
      DIMENSION A(2,2),B(2,2),C(2,2)
      DIMENSION PATH(3,MXL),ANORM(3,MXL+1),RAY(3,MXL),PERP(MXL+1)
      LOGICAL ANNOT
C
C  SET DEFAULT ERROR FLAG TO OK.
C
      IER=0
C
C  SET INVARIANTS.
C
      ANNOT=LUN.GE.1
      PIBY2=HALF*PI
      ANORM(1,1)=ZERO
      ANORM(2,1)=ZERO
      ANORM(3,1)=ONE
      PERP(1)=ZERO
      PATH(1,1)=XORG
      PATH(2,1)=YORG
      PATH(3,1)=ZERO
C
C  PRINT HEADING.
C
      IF(ANNOT)WRITE(LUN,1000)LFST,LAST,MODE,XORG,YORG,VTOL
C
C-----------------------------------------------------------------------
C
C  SET HORIZON GEOMETRY FOR UPPER LAYERS IF TOP PART OF MODEL COMPLETE.
C
      IF(LFST.GT.1)THEN
         DO 20 I=1,LFST-1
            IP1=I+1
            SETA=SIN(ETA(I))
            CETA=SQRT(ONE-SETA*SETA)
            ANORM(1,IP1)=SETA*COS(THETA(I))
            ANORM(2,IP1)=SETA*SIN(THETA(I))
            ANORM(3,IP1)=CETA
            PERP(IP1)=DEPTH(I)*CETA
   20       CONTINUE
         ENDIF
C
C-----------------------------------------------------------------------
C
C  SET VELOCITY IN FIRST INTERVAL IF REQUIRED.
C
      IF(LFST.EQ.1.AND.MODE.NE.2)THEN
         V1=ONE/SQRT((ONE/(VNMOX(1)*VNMOX(1)))+(HALF*HALF*SX(1)*SX(1)))
         VINT(1)=V1
      ELSE
         V1=VINT(1)
         ENDIF
C
C-----------------------------------------------------------------------
C
C  INVERT LAYERS LFST THROUGH LAST.
C
      DO 1 N=LFST,LAST
      NM1=N-1
      NP1=N+1
      TWT=T0(N)
      DTN=TWT
```

```
C
C-----------------------------------------------------------------------
C
C  DERIVE RAY EMERGE ANGLES.
C
C  PHIN IS THE ANGLE MEASURED FROM THE PROJECTION OF THE EMERGING
C  RAY ONTO THE SURFACE PLANE TO THE PROFILE (+X) WITH ANTICLOCKWISE
C  ROTATIONS POSITIVE.
C  TSLOPE IS SMINUSPHIN IN REF(2).
C  B0 IS THE ANGLE BETWEEN THE EMERGING RAY AND THE VERTICAL.
C
      IF(ABS(SX(N)).LT.SMALL.AND.ABS(SY(N)).LT.SMALL)THEN
         PHIN=ZERO
      ELSE
         PHIN=-ATAN2(SY(N),SX(N))
         ENDIF
      SPHIN=SIN(PHIN)
      CPHIN=COS(PHIN)
      TSLOPE=SX(N)*CPHIN-SY(N)*SPHIN
      SB0=ABS(HALF*V1*TSLOPE)
      CB0=SQRT(ONE-SB0*SB0)
C
C-----------------------------------------------------------------------
C
C  FOR FIRST LAYER SET RAY IN LAYER N=1 AND DN, EN, FN THEN JUMP.
C
      IF(N.EQ.1)THEN
         VN=V1
         EN=ZERO
         FN=ONE/(VN*VN*HALF*DTN)
         DN=FN*CB0*CB0
         IF(MODE.NE.1)THEN
            TX=-CPHIN*SB0
            TY=SPHIN*SB0
            TZ=-CB0
            ENDIF
         GOTO 3
         ENDIF
C
C-----------------------------------------------------------------------
C
C  LAYERS 2 THROUGH N. INITIALISE FOR DOWNWARD RAY TRACING.
C
C  SET RAY DIRECTION IN LAYER 1. REF(2) EQN 14.
C
      RAY(1,1)=-CPHIN*SB0
      RAY(2,1)=SPHIN*SB0
      RAY(3,1)=-CB0
      P1(1,1)=ONE
      P1(2,1)=ZERO
      P1(1,2)=ZERO
      P1(2,2)=ONE
      P2(1,1)=ONE
      P2(2,1)=ZERO
      P2(1,2)=ZERO
      P2(2,2)=ONE
      A(1,1)=ZERO
      A(2,1)=ZERO
      A(1,2)=ZERO
      A(2,2)=ZERO
C
C  SET EX VECTOR. VEC = [RAY IN LAYER 1] CROSS [SURFACE NORMAL]
C                 EX = [VEC] CROSS [RAY IN LAYER 1]
```

```
C
      RAY1=RAY(1,1)
      RAY2=RAY(2,1)
      RAY3=RAY(3,1)
      VEC1=RAY2*ANORM(3,1)-RAY3*ANORM(2,1)
      VEC2=RAY3*ANORM(1,1)-RAY1*ANORM(3,1)
      VEC3=RAY1*ANORM(2,1)-RAY2*ANORM(1,1)
      EX(1)=VEC2*RAY3-VEC3*RAY2
      EX(2)=VEC3*RAY1-VEC1*RAY3
      EX(3)=VEC1*RAY2- EC2*RAY1
C
C  CHECK MAGNITUDE OF EX. IF APPROXIMATELY ZERO SET TO DEFAULT (1,0,0)
C  VECTOR. OTHERWISE NORMALISE TO UNIT MAGNITUDE.
C
      TEMP=SQRT(EX(1)*EX(1)+EX(2)*EX(2)+EX(3)*EX(3))
      IF(TEMP.GT.SMALL)THEN
         EX(1)=EX(1)/TEMP
         EX(2)=EX(2)/TEMP
         EX(3)=EX(3)/TEMP
      ELSE
         EX(1)=ONE
         EX(2)=ZERO
         EX(3)=ZERO
         ENDIF
C
C---------------------------------------------------------------------
C
C  TRACE RAY FROM SURFACE ORIGIN (XORG,YORG,0.0) TO HORIZON N-1.
C
C  NB. BETA(N-1) IS UNDEFINED AT THIS STAGE.
C  DTI REFERS TO TWO-WAY TIME IN LAYER I CF.CONVENTION IN REF(2).
C
      DO 200 I=1,NM1
         IP1=I+1
         VII=VINT(I)
         IF(I.EQ.NM1)THEN
            VRATIO=ZERO
         ELSE
            VRATIO=VINT(IP1)/VII
            ENDIF
         CALL RAYTR3D(PATH(1,I),RAY(1,I),EX,ANORM(1,IP1),PERP(IP1),
     &                 VRATIO,PATH(1,IP1),RAY(1,IP1),EX,RLEN,CA,CB,
     &                 DELTA,IER)
         IF(IER.NE.0)THEN
            CALL WARNING('HUBRALI','RAY TRACING DOWNWARDS FAILED')
            IER=N
            RETURN
            ENDIF
C
C  SET TWO-WAY LAYER TRANSIT TIME AND UPDATE "TIME LEFT" VARIABLE.
C
         DTI=(RLEN+RLEN)/VII
         DTN=DTN-DTI
C
C  UPDATE A, P1, P2, U, UINV MATRICES DEFINING WAVEFRONT CURVATURE.
C
         IF(I.EQ.1)THEN
            WK(1,1)=ONE
            WK(2,1)=ZERO
            WK(1,2)=ZERO
            WK(2,2)=ONE
         ELSE
            CALL MATMLTD(P1,U,P1)
```

```
               CALL MATMLTD(UINV,P2,P2)
               CALL MATMLTD(P1,P2,WK)
               ENDIF
            TEMP=VII*VII*DTI
            A(1,1)=A(1,1)+TEMP*WK(1,1)
            A(2,1)=A(2,1)+TEMP*WK(2,1)
            A(1,2)=A(1,2)+TEMP*WK(1,2)
            A(2,2)=A(2,2)+TEMP*WK(2,2)
            CD=COS(DELTA)
            SD=-SIN(DELTA)
            U(1,2)=-SD
            U(2,2)=CD
            IF(I.LT.NM1)THEN
               CABYCB=CA/CB
               U(1,1)=CD*CABYCB
               U(2,1)=SD*CABYCB
            ELSE
               U(1,1)=CD
               U(2,1)=SD
               ENDIF
            UINV(1,1)=U(1,1)
            UINV(2,1)=U(1,2)
            UINV(1,2)=U(2,1)
            UINV(2,2)=U(2,2)
  200       CONTINUE
C
C---------------------------------------------------------------------
C
C  RAY HAS NOW BEEN TRACED TO INCIDENCE AT HORIZON N-1.
C
C  SET MATRICES A, B, C AND VARIABLES G1, G2 REQUIRED FOR INVERSION.
C  A, B AND C ARE COMPUTED FROM REF(2) EQN 17.
C  A RELATES TO TRANSFORMATIONS UP TO AND INCLUDING REFRACTION AT N-2.
C  B AND C RELATE SPECIFICALLY TO REFRACTION AT N-1.
C  NOTE THAT HERE VII IS VINT(N-1).
C
         A(1,1)=HALF*A(1,1)
         A(2,1)=HALF*A(2,1)
         A(1,2)=HALF*A(1,2)
         A(2,2)=HALF*A(2,2)
         CALL MATMLTD(P1,U,B)
         CALL MATMLTD(UINV,P2,C)
         G1=CA*CA
         G2=(ONE-G1)/(VII*VII)
C
C  SET INVARIANTS IN F(VN) EQN 10 REF(2).
C
         VNMOXN=VNMOX(N)
         TD=HALF*CPHIN*CPHIN
         TE=CPHIN*SPHIN
         TF=HALF*SPHIN*SPHIN
         TV=ONE/(VNMOXN*VNMOXN*TWT)
         T1=HALF*DTN
         H1=A(1,1)
         H2=B(1,2)*C(2,1)
         H3=B(1,1)*C(1,1)
         W1=A(2,2)
         W2=B(2,2)*C(2,2)
         W3=B(2,1)*C(1,2)
         Q1=A(1,2)
         Q2=B(1,2)*C(2,2)
         Q3=B(1,1)*C(1,2)
C
```

```
C  IF VN ITERATION IS NOT TO BE PERFORMED (MODE=2) COMPUTE H,W,Q,P
C  FUNCTIONS EQNS.18-20 REF(2) AND THEN JUMP OVER ITERATION SECTION.
C
      IF(MODE.EQ.2)THEN
         VN=VINT(N)
         V2=VN*VN
         T2=T1*V2
         T3=(G1*T2)/(ONE-G2*V2)
         H=H1+H2*T2+H3*T3
         W=W1+W2*T2+W3*T3
         Q=Q1+Q2*T2+Q3*T3
         P=H*W-Q*Q
         GOTO 32
         ENDIF
C
C-----------------------------------------------------------------------
C
C  DERIVE VN BY NEWTON-RAPHSON ITERATION. EQNS 15-20 REF(2).
C
C  USE TWO TRIAL VELOCITIES VA AND VB=1.01*VA.
C  THE DERIVATIVE D/DVN(F(VN)) IS GIVEN BY (F(VB)-F(VA))/(VB-VA).
C
C  TAKE THE FIRST ESTIMATE OF VN AS THE VN PREDICTED BY THE DIX FORMULA.
C  IF AN ERROR CONDITION ARISES, USE THE MOVEOUT VELOCITY AS THE FIRST
C  ESTIMATE.
C
C  ENSURE THAT ALL DIX ESTIMATES ARE IN THE RANGE VNMIN < VN < VNMAX.
C
      ARG=(VNMOXN*VNMOXN*TWT-VNMOX(NM1)*VNMOX(NM1)*T0(NM1))/
     &    (TWT-T0(NM1))
      IF(ARG.GE.VNMIN*VNMIN.AND.ARG.LE.VNMAX*VNMAX)THEN
         VN=SQRT(ARG)
      ELSE
         VN=VNMOXN
         ENDIF
C
C  ENTER ITERATION LOOP. A MAXIMUM MAXIT ITERATIONS IS ALLOWED.
C
      DO 80 NIT=1,MAXIT
         VA=VN
         VB=FACTOR*VA
         V2=VB*VB
         T2=T1*V2
         T3=(G1*T2)/(ONE-G2*V2)
         H=H1+H2*T2+H3*T3
         W=W1+W2*T2+W3*T3
         Q=Q1+Q2*T2+Q3*T3
         P=H*W-Q*Q
         FVB=((CB0*CB0*W*TD+H*TF-CB0*Q*TE)/P)-TV
         V2=VA*VA
         T2=T1*V2
         T3=(G1*T2)/(ONE-G2*V2)
         H=H1+H2*T2+H3*T3
         W=W1+W2*T2+W3*T3
         Q=Q1+Q2*T2+Q3*T3
         P=H*W-Q*Q
         FVA=((CB0*CB0*W*TD+H*TF-CB0*Q*TE)/P)-TV
         DBYDVN=(FVB-FVA)/(VB-VA)
         IF(DBYDVN.EQ.ZERO)THEN
            CALL WARNING('HUBRALI',
     &                   'ZERO SLOPE IN NEWTON-RAPHSON ITERATION')
            IER=N
            RETURN
```

```
            ENDIF
         VN=VA-(FVA/DBYDVN)
         IF(VN.LT.VNMIN.OR.VN.GT.VNMAX)THEN
            CALL WARNING('HUBRALI',
     &                   'NEWTON-RAPHSON ITERATION IS BLOWING UP TO '//
     &                   'GIVE INTERVAL VELOCITIES OUT OF BOUNDS')
            IER=N
            RETURN
            ENDIF
         IF(ABS(VN-VA).LT.VTOL)GOTO 82
   80    CONTINUE
      CALL WARNING('HUBRALI','NO CONVERGENCE ON NEWTON-RAPHSON '//
     &             'ITERATIONS')
      IER=N
      RETURN
C
C  ITERATION SUCCESSFUL.
C
   82 CONTINUE
      VINT(N)=VN
C
C-----------------------------------------------------------------------
C
C  SET PARAMETERS DN, EN, FN IN REF(2).
C
   32 CONTINUE
      DN=CB0*CB0*W/P
      EN=-CB0*Q/P
      FN=H/P
C
C-----------------------------------------------------------------------
C
C  COMPUTE NMO VELOCITY ELLIPSE.
C
C  PHIMAX IS A TURNING POINT IN THE VNMO(AZIMUTH) FUNCTION (IE. EITHER
C  A MAXIMUM VNMO OR MINIMUM VNMO) MEASURED AWAY FROM THE RAY EMERGE
C  ANGLE PHIN.
C
    3 CONTINUE
      IF(EN.EQ.ZERO.AND.DN.EQ.FN)THEN
         PHIMAX=ZERO
      ELSE
         PHIMAX=HALF*ATAN2(EN+EN,DN-FN)
         ENDIF
      CPHIM=COS(PHIMAX)
      SPHIM=SIN(PHIMAX)
      C2PHIM=CPHIM*CPHIM
      S2PHIM=ONE-C2PHIM
      VMAX2=ONE/(TWT*(HALF*DN*C2PHIM+HALF*FN*S2PHIM+EN*CPHIM*SPHIM))
      VMIN2=ONE/(TWT*(HALF*DN*S2PHIM+HALF*FN*C2PHIM-EN*CPHIM*SPHIM))
      IF(VMAX2.LT.VMIN2)THEN
         PHIMAX=PHIMAX+PIBY2
         TEMP=VMIN2
         VMIN2=VMAX2
         VMAX2=TEMP
         ENDIF
      VMAJOR(N)=SQRT(VMAX2)
      VMINOR(N)=SQRT(VMIN2)
C
C  COMPUTE VNMO ACROSS THE PROFILE FROM THE ELLIPSE EQUATION.
C
C  SIG IS THE ANGLE BEWEEN THE AZIMUTH OF MAXIMUM VNMO AND THE PROFILE,
C  MEASURED AWAY FROM THE LATTER.
```

```
C
      SIG=PHIMAX-PHIN
      IF(SIG.GE.PI)SIG=SIG-PI
      SIGMA(N)=SIG
      CSIG=COS(SIG)
      C2SIG=CSIG*CSIG
      VNMOY(N)=SQRT(ONE/(C2SIG/VMIN2+(ONE-C2SIG)/VMAX2))
C
C-----------------------------------------------------------------------
C
C  JUMP IF RAY TRACING TO NIP NOT TREQUIRED.
C
      IF(MODE.EQ.1)GOTO 40
C
C  TRANSMITTED RAY SEGMENT IN LAYER N. REF(4) EQN 9C.
C
      IF(N.GT.1)THEN
         VRATIO=VN/VII
         SB=VRATIO*SQRT(ONE-CA*CA)
C
C  CHECK RAY HAS NOT GONE CRITICAL ALONG INTERFACE N-1. THIS MAY HAPPEN
C  IF VINT(N-1) IS MUCH LOWER THAN VINT(N), AND MAY INDICATE SPURIOUS
C  INTERVAL VELOCITY VALUES.
C
         IF(SB.GT.ONE)THEN
            CALL WARNING('HUBRALI',
     &                   'RAY REFRACTED CRITICALLY ALONG HORIZON N-1')
            IER=N
            RETURN
            ENDIF
C
C  RAY TRANSMITTED INTO LAYER N.
C
         CB=(CA/ABS(CA))*SQRT(ONE-SB*SB)
         VAB=VRATIO*CA-CB
         TX=VRATIO*RAY(1,NM1)-VAB*ANORM(1,N)
         TY=VRATIO*RAY(2,NM1)-VAB*ANORM(2,N)
         TZ=VRATIO*RAY(3,NM1)-VAB*ANORM(3,N)
         ENDIF
C
C  DERIVE NORMAL INCIDENCE POINT COORDINATES.
C
      SN=VN*HALF*DTN
      XN(N)=PATH(1,N)+SN*TX
      YN(N)=PATH(2,N)+SN*TY
      ZN(N)=PATH(3,N)+SN*TZ
C
C  DERIVE PARAMETERS AT HORIZON N.
C
      ANORM(1,NP1)=-TX
      ANORM(2,NP1)=-TY
      ANORM(3,NP1)=-TZ
      ETA(N)=ACOS(-TZ)
      IF(ABS(TX).LT.SMALL.AND.ABS(TY).LT.SMALL)THEN
         THETA(N)=ZERO
      ELSE
         THETA(N)=ATAN2(-TY,-TX)
         ENDIF
      PERP(NP1)=TX*(XN(N)-XORG)+TY*(YN(N)-YORG)+TZ*ZN(N)
      DEPTH(N)=PERP(NP1)/(-TZ)
C
C-----------------------------------------------------------------------
C
```

```
C  OUTPUT DATA FOR HORIZON N.
C
   40 CONTINUE
      IF(ANNOT)THEN
         IF(MODE.EQ.1)THEN
            WRITE(LUN,1005)N,TWT,VNMOX(N),SX(N),SY(N),
     &                        ASIN(SB0)*RADDEG,-PHIN*RADDEG,VINT(N),
     &                        VNMOY(N),VMAJOR(N),VMINOR(N),SIG*RADDEG
         ELSE
            WRITE(LUN,1010)N,TWT,VNMOX(N),SX(N),SY(N),XN(N),YN(N),ZN(N),
     &                        ASIN(SB0)*RADDEG,-PHIN*RADDEG,VINT(N),
     &                        ETA(N)*RADDEG,THETA(N)*RADDEG,DEPTH(N),
     &                        VNMOY(N),VMAJOR(N),VMINOR(N),SIG*RADDEG
            ENDIF
         ENDIF
C
C  NEXT HORIZON.
C
    1 CONTINUE
C
C------------------------------------------------------------------------
C
C  RETURN TO CALLING ROUTINE.
C
      RETURN
C
C------------------------------------------------------------------------
C
C  FORMATS.
C
 1000 FORMAT(' HUBRAL 3D INVERSION FOR LAYERS ',I2,' THROUGH ',I2,
     &' IN MODE ',I1,'. SURFACE ORIGIN AT X=',F8.1,' Y=',F8.1,
     &21X,'HUBRALI.270181'/1X,130('-')//
     &' INTERVAL VELOCITIES DERIVED ACCURATE TO +/- ',G12.6,' UNITS'//
     &' HORI 2WAY  MOVEOUT   TIME-SLOPE     NORMAL-INCIDENCE-POINT RAY-E
     &MERGE-ANG  INTV    MAX-DIP  VERTICAL   NORMAL-MOVEOUT-VELOCITY'/
     &' -ZON TIME VELOCITY  DT/DX   DT/DY       XN       YN       ZN    TO+
     &Z   TO+X    VEL   ANGLE AZIMT  DEPTH    VNMOY  MAJOR  MINOR   AXIS'
     &/)
 1005 FORMAT(I3,F7.3,F7.1,2(1X,E9.3),24X,F5.1,F7.1,F8.1,20X,4F7.1)
 1010 FORMAT(I3,F7.3,F7.1,2(1X,E9.3),3F8.1,F5.1,F7.1,F8.1,2F6.1,F8.1,
     & 4F7.1)
      END
```

APPENDIX 5A

DOCUMENTATION FOR PROGRAM KRUNCH

APPENDIX 5A DOCUMENTATION FOR PROGRAM KRUNCH

KRUNCH is a regional seismic database system which allows the user to read in times, moveout velocities and time slopes, design filters, perform smoothing operations, derive interval velocities by local Hubral 3D inversions, plot graphs and calculate misties of parameters at line intersections.

PARAMETERS:

Each continuous seismic reflection on a CMP stacked seismic section can be characterized at a ground point by the following four parameters:

1. the two-way reflection time, assumed to be the two-way zero-offset time;
2. the moveout velocity, picked from a velocity analysis of the CMP gather centred at the ground point;
3. the time slope of the reflection on the stacked section, referred to here as the inline time slope; and
4. the time slope of the reflection measured in the direction perpendicular to that of the section, referred to here as the crossline time slope.

Program KRUNCH uses these four 'surface measurements' for each horizon in order to perform a Hubral 3D inversion at each ground point, thus deriving local limited depth models each consisting of uniform velocity layers separated by plane reflectors. Each plane reflector in the derived local depth model can then be characterized by a further four parameters:

5. the interval velocity of the layer immediately above it;
6. the vertical depth of the plane reflector below the ground point;
7. the maximum dip of the plane reflector; and
8. the azimuth of maximum dip of the plane reflector.

DATA STRUCTURE:

KRUNCH uses a 3D matrix which is stored in the computer as the 3D array ZAP(N,M,L) whose subscripts refer to:

(GROUND POINT, HORIZON, PARAMETER)

Each 'parameter value' can thus be indexed uniquely by ground point, horizon and parameter numbers. The parameter index takes the values 1 through 8 as defined above.

A contiguous string of parameter values at consecutive ground points for any horizon/parameter pair is called a 'horizon/parameter vector'.

The KRUNCH 3D matrix pertains to one seismic line only; the data stored for this line is termed the 'current data set'. Processing of further seismic lines is performed using the same matrix. Data handling is acheived through labelling the current data set and transferring it to and from direct access files. In this way many seismic lines can be processed in the same runstream using the array space required for just one line.

The KRUNCH data structure has two principal limitations:

- in order to avoid handling individual ground point location data the ground points are assumed to be equispaced; and
- each horizon must extend from the first ground point to the last.

The first limitation is not normally a problem as times and time slopes are available in continuous form from sections and maps, while moveout velocities are generally sampled at regular intervals in a detailed velocity study. The second limitation is likely to cause difficulty if a horizon terminates (eg. by onlap or subcrop) within the line. In this case a 'dummy' horizon can be generated immediately below the last valid horizon.

RUNNING KRUNCH:

KRUNCH can be used in either interactive or batch mode, and instructions can be processed in any order. A 'help' facility is provided by directing the required parts of this documentation file to the output device.

A KRUNCH instruction consists of a mnemonic and several data fields. The mnemonic selects the task while the data fields qualify how the task is to be performed. The KRUNCH instruction syntax is:

"MNEMONIC Field1,Field2,Field3, ... ,Field12"

where MNEMONIC is a character string and each data field may be character (C), integer (I), real (R) or omitted. Omitted fields other than trailing fields must be marked by a comma, to leave two consecutive commas.

A 'range' (of parameters, horizons or ground points) is a consecutive string specified by the lower and upper limits of the range e in the syntax LOWER:UPPER eg. 2:5 implies 2 through 5.

The current set of KRUNCH mnemonics, together with their minimum abbreviations, is documented below. The default action taken by KRUNCH when a data field is omitted is included in the documentation.

****

"CDTDX" ["CD"]

PURPOSE:

Calculates inline time slopes for specified horizons from two-way zero-offset times in the current data set.

COMMENTS:

The inline time slope of a horizon at ground point i is estimated using the formula:

$$dt/dx(i) = [\ t(i+1) - t(i-1)\ ] / 2Dx$$

where t(i) is the two-way zero-offset time to the horizon at ground point i, Dx is the distance between adjacent ground points as defined on LINDEF [F 6] and dt/dx(i) is the inline time slope at ground point i.

Zero-offset times must already exist in the current data set.

CDTDX is liable to introduce spurious dt/dx values if time discontinuities (ie. faults) exist within the CMP range [F 2]. It is preferable to run CDTDX separately on each side of the discontinuity.

OPTIONS:

F 1 C Range of horizons to be processed.
*Defaults to all horizons.

F 2 C Range of ground points to be processed specified in CMP numbers.
*Defaults to all ground points.

```
"CDTDX MF:ML,CMPF:CMPL"
       1---> 2------->
```

==

"CONST" ["CO"]

PURPOSE:

Scales or shifts parameter values in a specified horizon/parameter vector by a constant.

OPTIONS:

```
F 1 C  Range of parameters to be processed.
      *No default.
F 2 C  Range of horizons to be processed.
      *Defaults to all horizons.
F 3 C  Range of ground points to be processed specified in CMP numbers.
      *Defaults to all ground points.
F 4 C  [F 4] = 'A' => ADD [F 5] to all parameter values.
       [F 4] = 'M' => MULTIPLY all parameter values by [F 5].
      *No default.
F 5 R  Magnitude of scaling or shifting constant.
    C  If [F 4] = 'M': [F 5] = 'DTOR' = PI/180 (degrees to radians)
                       [F 5] = 'RTOD' = 180/PI (radians to degrees)
      *No default.
```

```
"CONST LF:LL,MF:ML,CMPF:CMPL,A/M,CONSTANT"
       1---> 2---> 3-------> 4-> 5------>
```

==

"CROSS"   ["CR"]

PURPOSE:

Defines locations where crossing lines intersect the current line in order to interpolate parameter values at line intersections for subsequent use in the calculation of misties in MISTIE.

COMMENTS:

Parameter values are linearly interpolated from data at ground points in the current line on either side of the intersection.

Total resultant time slopes at each intersection point on the current line can be calculated using the inline time slope, crossline time slope and line azimuth as defined by LINDEF [F 7]. This information can be used to check consistency of time slopes at line intersections.

OPTIONS:

```
F 1 I  Number of crossing lines.
       The following data are read from the NEXT LINE of the current
       input file in FORTRAN '*' (free) format:
         XLINE(1),CMP(1),XLINE(2),CMP(2), ... , XLINE(j),CMP(j)
       where XLINE(j) is the (integer) number of the jth crossing line
       (to match the [F 1] on its own LINDEF instruction) and CMP(j)
       is the (integer) CMP number on the CURRENT line where XLINE(j)
       intersects. j takes the values 1 through [F 1].
      *No default.
F 2 C  Range of parameters for which interpolations are to be made.
      *Defaults to all parameters.
F 3 C  Range of horizons for which interpolations are to be made.
      *Defaults to all horizons.
F 4 I  Logical unit number of file to which data is to be written, only
       used if the interpolations are to be saved for use other than
       for calculating misties during the current run.
      *Defaults to an internal file which is deleted at the end of the
       run.
F 5 C  [F 5] set => Calculate total resultant time slope and its
                    azimuth from inline and crossline time slopes at
                    each intersection point for horizons [F 3].
                    The parameter range [F 2] must include 3 and 4.
      *Defaults to no action.
```

```
"CROSS NLINES,LF:LL,MF:ML,UNIT,RESULTANT?"   2*[F 1] data on next line
       1----> 2---> 3---> 4--> 5-------->
```

==

"DREAD"   ["DR"]

PURPOSE:
Reads the new current data set into the KRUNCH matrix from a direct access file.

COMMENTS:
DREAD must follow a LINDEF instruction in order that the line be defined before the data is read.
The previous data set in the KRUNCH matrix is overwritten.

OPTIONS:
F 1 I Logical unit number of direct access file to be read.
*No default.
F 2 C Keyword of required data set, matching that assigned by DWRITE when the data set was originally written.
*Defaults to a list of all keywords in the header of file [F 1].

```
"DREAD UNIT,KEYWORD"
       1--> 2----->
```

==

"DUMMY"   ["DU"]

PURPOSE:
Generates a dummy horizon over a specified range of ground points.

COMMENTS:
This task is necessary to maintain integrity of the data structure if a horizon terminates within the line.
At each ground point the dummy horizon M is dz deeper and dt later than the valid horizon M-1 above, where:
$dz = 0.001$ distance units; and
$dt = 2 * dz$ / interval velocity in layer M-1
All other parameters are copied directly from horizon M-1 to dummy horizon M.
The interval velocity in layer M-1 must be known over the specified range of ground points. DUMMY must therefore be used either in a layer by layer inversion (after inversion to M-1) or by presetting the interval velocity in layer M-1 to an approximate value using CONST.

OPTIONS:
F 1 I Horizon to be generated. [F 1] must be > 1.
*No default.
F 2 C Range of ground points specified in CMP numbers for which the dummy horizon is to be generated.
*No default.

```
"DUMMY M,CMPF:CMPL"
       1 2------->
```

==

"DWRITE"   ["DW"]

PURPOSE:

Writes the current data set from the KRUNCH matrix to a direct access file.

COMMENTS:

The data set is assigned a user-specified 'keyword' by which it is identified for future addresses by DREAD.

The current data set remains in the KRUNCH matrix.

OPTIONS:

```
F 1 I  Logical unit number of direct access file.
      *No default.
F 2 C  Keyword used to define this data set on file [F 1] for all
       subsequent addresses by DREAD. Consists of up to ten
       non-blank characters.
       If the keyword [F 2] already exists in the header of file [F 1]
       the old data set can be overwritten in place and replaced on
       file by the current data set ONLY IF the overwrite flag [F 3] is
       also set (see below).
      *No default.
F 3 C  [F 3] = 'O' => allow overwriting if [F 2] already exists.
      *Defaults to no overwrite permission.
```

```
"DWRITE UNIT,KEYWORD,OVERWRITE?"
        1--> 2-----> 3-------->
```

==

"EDIT" ["E"]

PURPOSE:

Update or inspect a single parameter value in the current data set.

OPTIONS:

```
F 1 I  Parameter to be updated/inspected.
      *No default.
F 2 I  Horizon for which data is to be updated/inspected.
      *No default.
F 3 I  CMP number of ground point for which data is to be updated/
       inspected.
      *No default.
F 4 R  Parameter value to be entered for parameter [F 1] on horizon
       [F 2] at ground point with CMP number [F 3].
      *Defaults to listing the current value of parameter [F 1] on
       horizon [F 2] at ground point with CMP number [F 3].
```

```
"EDIT L,M,CMP,VALUE"
      1 2 3-> 4--->
```

==

"FDESN" ["FD"]

PURPOSE:

Designs a set of filter coefficients to become the current filter.

COMMENTS:

The filter may be one of three types:

- rectangular boxcar moving average filter;
- user-specified filter coefficients; or
- zero-phase bandpass/bandstop wavenumber filter.

If no LINDEF instructions have been processed earlier in the run, the sampling interval Dx (distance between adjacent ground

points) must be set by FDESN.
The previous filter is overwritten.

OPTIONS:

```
F 1 I  Determines the type of filter to be designed:
       [F 1] < 0 => Design rectangular boxcar moving average filter.
       [F 1] = 0 => Read user-specified filter coefficients.
       [F 1] > 0 => Design zero-phase bandpass/bandstop wavenumber
                    filter:
                1 =>  Bandpass filter;
                2 =>  Bandstop filter;
                3 =>  Highpass filter; or
                4 =>  Lowpass filter.
      *No default.
F 8 C  [F 8] set => Plot filter coefficients and wavenumber response of
                    filter.
      *Defaults to no plots.
F 9 R  Distance Dx between adjacent ground points. Dx should be
       specified in units which are consistent with depth and
       velocity units.
      *Defaults to that specified in [F 6] of the last LINDEF
       instruction.

IF [F 1] < 0  (Rectangular boxcar moving average filter):
F 2 I  Number of coefficients.
       FDESN assigns each of the [F 2] coefficients the weight 1/[F 2].
      *No default.

IF [F 1] = 0  (User-specified filter):
F 2 I  Number of coefficients.
       [F 2] coefficients will be read in FORTRAN '*' (free) format
       from the NEXT LINE of the current input file.
      *No default.

IF [F 1] > 0 (Zero-phase bandpass/bandstop filter):
F 2 R  [F 2] > 0 => Filter will have [F 2] coefficients.
       [F 2] < 0 => Filter is of length -[F 2] distance units.
                    The number of coefficients to be designed is:
                              -[F 2]/Dx + 1
                    where Dx is the sampling interval [F 6] of LINDEF.
      *No default.
F 7 R  Ratio (weighting of pass bands/weighting of stop bands).
       The amount of ripple in each band is inversely proportional to
       the band weighting.
      *Defaults to unity, ie. pass band ripple = stop band ripple.

IF [F 1] = 1  (Bandpass filter):
F 3 R  Highest wavenumber in first stop band.
F 4 R  Lowest wavenumber in pass band.
F 5 R  Highest wavenumber in pass band.
F 6 R  Lowest wavenumber in second stop band.
      *No defaults for [F 3],[F 4],[F 5] or [F 6].

IF [F 1] = 2  (Bandstop filter):
F 3 R  Highest wavenumber in first pass band.
F 4 R  Lowest wavenumber in stop band.
F 5 R  Highest wavenumber in stop band.
F 6 R  Lowest wavenumber in second pass band.
      *No defaults for [F 3],[F 4],[F 5] or [F 6].

IF [F 1] = 3  (Highpass filter):
F 3 R  Highest wavenumber in stop band.
F 4 R  Lowest wavenumber in pass band.
```

      *No defaults for [F 3] or [F 4].

```
IF [F 1] = 4  (Lowpass filter):
F 3 R  Highest wavenumber in pass band.
F 4 R  Lowest wavenumber in stop band.
     *No defaults for [F 3] or [F 4].

"FDESN TYPE,LENGTH,W1,W2,W3,W4,RATIO,PLOT,Dx"
       1--> 2----> 3> 4> 5> 6> 7---> 8--> 9>
```

==

"FILTER"   ["FI"]

PURPOSE:
   Filters specified horizon/parameter vectors with the current filter.

COMMENTS:
   The delay imposed by the convolution is removed by shifting the output vector back by one half of the filter length, which is valid for zero-phase filters. The filter should have an odd number of coefficients (such that the filter length is an even multiple of the sampling interval) to effect this shift correctly.
   A trend is removed from the vectors before filtering and added back afterwards. By default the DC component (zero wavenumber or arithmetic mean) is removed. If the moveout velocity is being filtered, however, the trend can be defined as a linear function of time. Real normal moveout velocity 'jumps' introduced by time discontinuities (faults) can thus be protected from the convolution. Application of the null (single zero) filter can be used to eliminate the residuals and leave the trend.
   Plots of the residuals and the raw/filtered data can be sent to the current print file.

OPTIONS:
```
F 1 I  Parameter to be filtered.
     *No default.
F 2 C  Range of horizons to be filtered.
     *Defaults to all horizons.
F 5 C  [F 5] includes 'R' => Plot residuals (raw data - filtered data)
                             for all horizons [F 2] on the same axes.
       [F 5] includes 'P' => Plot both raw and filtered data vectors on
                             the same axes individually for each of the
                             horizons [F 2].
     *Defaults to no plots.

IF [F 1] = 2  (Moveout velocity):
F 3 R  If both [F 3] and [F 4] are set to real numbers, a moveout
F 4 R  velocity trend defined by the linear equation:
          MOVEOUT VELOCITY  =  B0  +  B1 * TWO-WAY TIME
       where B0 = [F 3] and B1 = [F 4] is removed before the
       filtering and added back afterwards.
     *Defaults to removal of the mean.

"FILTER L,MF:ML,B0,B1,PLOTS?"
        1 2---> 3> 4> 5---->
```

==

"GRAPH"   ["G"]

PURPOSE:
   Plots graphs of specified horizon/parameter vectors.

COMMENTS:
Graphs are 101 characters wide and are annotated along the space axis with the ground point CMP numbers.

OPTIONS:
F 1 C Range of parameters to be plotted.
*Defaults to all parameters.
F 2 C Range of horizons for which data is to be plotted.
*Defaults to all horizons.
F 3 C Range of ground points for which data is to be plotted, specified by CMP numbers.
*Defaults to all ground points.
F 4 C Character string containing symbols to be used for plot; one symbol is associated with each horizon. The number of symbols in [F 4] should match the number of horizons specified in [F 2].
*Defaults to the last symbols specified in GRAPH or PSPEC. If no symbols have been defined earlier, ABCDEF... are used.
F 5 R Datum line (a constant parameter value) to be marked on plot by a line of dots.
*Defaults to zero.
F 6 R Minimum parameter value in plotting window.
*Defaults to the minimum value of the parameter in the horizon/ ground point range to be plotted.
F 7 R Maximum parameter value in plotting window.
*Defaults to the maximum value of the parameter in the horizon/ ground point range to be plotted.

```
"GRAPH LF:LL,MF:ML,CMPF:CMPL,SYMBOLS,DATUM,MIN,MAX"
       1---> 2---> 3-------> 4-----> 5---> 6-> 7->
```

==

"HELP" ["HE"]

PURPOSE:
Provides a help facility by directing the required part of this documentation file to the system output device.

OPTIONS:
F 1 C Name of mnemonic, which may be abbreviated to no less than two characters.
*Defaults to a listing of the current set of KRUNCH mnemonics, followed by a prompt for the required mnemonic.

```
"HELP MNEMONIC"
      1------>
```

==

"HFORWRD" ["HF"]

PURPOSE:
Performs Hubral 3D forward modelling for specified horizons over a range of ground points.

COMMENTS:
Two-way zero-offset times, normal moveout velocities, inline time slopes and crossline time slopes are calculated for each horizon at each ground point. A limited local ground model consisting of uniform velocity layers separated by 3D plane dipping reflectors is assumed.
Forward modelling may be impossible in some locations, in which case missing parameter values are interpolated from adjacent ground points

and warnings issued both to the current print file and the log file.

OPTIONS:

```
F 1 C  Range of horizons to be forward modelled.
      *Defaults to all horizons.
F 2 C  Range of ground points to be forward modelled, specified by
       CMP numbers.
      *Defaults to all ground points.
F 3 C  [F 3] set => Send output from Hubral 3D forward modelling
                    subroutine to the current print file.
      *Defaults to no print.

"HFORWRD MF:ML,CMPF:CMPL,PRINT?"
        1---> 2-------> 3---->
```

==

"HINVERT"   ["HI"]

PURPOSE:

Perform Hubral 3D inversion for specified horizons over a range of ground points.

COMMENTS:

Interval velocities, depths, maximum dips and azimuths of maximum dips are calculated for each horizon at each ground point. A limited local ground model consisting of uniform velocity layers separated by 3D plane dipping reflectors is assumed.

Either 'direct' or 'layer by layer' inversions can be performed.

Layer by layer inversions can be used in conjunction with pre-set interval velocities for conventional zero-offset raytrace migrations in the limited local ground models.

Inversion may be impossible in some locations, in which case missing parameter values are interpolated from adjacent ground points and warnings issued both to the current print file and to the log file.

OPTIONS:

```
F 1 C  Range of horizons to be inverted.
      *Defaults to all horizons.
F 2 C  Range of ground points to be inverted, specified by CMP numbers.
      *Defaults to all ground points.
F 3 I  Inversion mode flag:
       [F 3] = 0 => Direct inversion:
                    Invert all horizons in range [F 1] at each ground
                    point.
       [F 3] = 1 => Layer by layer inversion - Stage one:
                    [F 1] must contain ONLY ONE horizon.
                    Derive interval velocity in layer [F 1] at each
                    ground point; do not trace ray down to reflector
                    [F 1].
       [F 3] = 2 => Layer by layer inversion - Stage two:
                    [F 1] must contain ONLY ONE horizon.
                    Trace ray down through layers 1 to [F 1] to
                    reflector [F 1], thus deriving depths, dips and
                    azimuths of maximum dips at each ground point.
      *Defaults to [F 3] = 0 ie. direct inversion.
F 4 C  [F 4] set => Send output from Hubral 3D inversion subroutine to
                    the current print file.
      *Defaults to no print.
F 5 I  Logical unit number of formatted file to receive the following:
         - ground point CMP number;
         - horizon number;
         - normal incidence point coordinates (CMPXn,Xn,Yn,Zn); and
```

```
        - interval velocity
      for each horizon [F 1] in FORTRAN format '(2I10,5F10.2)'.
     *Defaults to no output of normal incidence point data.

"HINVERT MF:ML,CMPF:CMPL,INVMODE,PRINT?,UNIT"
        1---> 2-------> 3-----> 4----> 5-->
```

===

"INPUT"   ["I"]

PURPOSE:
   Reads a horizon/parameter vector into the KRUNCH matrix from a formatted file.

COMMENTS:
   This task is used in the creation of a data set from data on different files in varied formats. Parameter values for specified ground points are read from the required file in a user-specified FORTRAN format. The file can be rewound and card images skipped over as necessary.
   INPUT also allows a horizon/parameter vector in an existing data set to be overwritten.
   Any data read in with a value > MEGA are considered to indicate flagged missing data, which are then automatically linearly interpolated from the nearest unflagged data. The value of the constant MEGA is listed as part of the output from the VERSION instruction.

OPTION:

```
F 1 I  Parameter to be read.
      *No default.
F 2 I  Horizon for which data is to be read.
      *No default.
F 3 C  Range of ground points for which data is to be read, specified
       by CMP numbers.
      *Defaults to all ground points.
F 4 I  Logical unit number of formatted read file.
      *Defaults to the last unit specified by an INPUT instruction.
F 5 C  [F 5] set => Rewind unit [F 4] before read.
      *Defaults to no rewind.
F 6 I  [F 6] > 0 => Skip over [F 6] card images on unit [F 4] after
                    rewind and before read.
      *Defaults to no skip.
F 7 C  [F 7] set => Read first card image on unit [F 4] after rewind
                    and/or skip as a label which is written to the
                    current print file.
      *Defaults to no label read.
F 8 C  FORTRAN format to be used for read. Free format '*' is valid.
       The format MUST include parentheses cf. '(......)'.
       No commas should be included in the format, as they are confused
       with the data field separation commas. Formats including commas
       should be specified using semi-colons ';' instead - these are
       then decoded to commas internally.
       If the format has > 30 characters [F 8] must be set by any
       character other than '*' or '(' and the format is read from the
       NEXT LINE of the current input file.
      *Defaults to the last format specified by an INPUT instruction,
       or to '*' if no INPUT instructions have been processed.

"INPUT L,M,CMPF:CMPL,UNIT,REWIND?,NSKIP,LABEL?,FORMAT"
       1 2 3-------> 4--> 5-----> 6---> 7----> 8---->
```

===

"LINDEF" ["LI"]

PURPOSE:
Sets the invariants used to process the next current line.

COMMENTS:
This instruction must appear before processing commences, as it defines important constants which are required by many other tasks eg. number of ground points, number of horizons, distance between adjacent ground points etc.
A new LINDEF instruction is used to define each new line.

OPTIONS:
```
F 1 I  Line number. [F 1] is used to annotate printout and sort
        interpolated parameter values in MISTIE; it must be an integer
        number without a character prefix or suffix.
       *No default.
F 2 I  Number of ground points on the line, defining the length of all
        vectors in the current data set.
       *No default.
F 3 I  Number of horizons on the line to be processed.
       *No default.
F 4 I  CMP number of first ground point on the line.
       *No default.
F 5 I  Number of CMPs between adjacent ground points.
       *No default.
F 6 R  Distance Dx between adjacent ground points. Dx should be
        specified in units which are consistent with depth and velocity
        units.
       *No default.
F 7 R  Orientation of the line. The angle is measured in degrees
        between the direction of increasing CMP numbers and North, such
        that angles west of North are positive eg. NW = +45; SE = -135.
       *Defaults to [F 7] = 0 ie. North.
```

```
"LINDEF NUMBER,NGPS,NHORZ,CMPGP1,CMPGPINC,Dx,AZIMUTH"
        1----> 2--> 3---> 4----> 5------> 6> 7----->
```

==

"MACRO" ["MA"]

PURPOSE:
Creates a list of pre-set instructions which can subsequently be invoked repeatedly.

COMMENTS:
MACRO is used when a standard set of instructions is required for each seismic line in a runstream processing several lines.

OPTIONS:
```
F 1 I  [F 1] > 0 => Read instructions from the current input file and
                    write them into the current macro until [F 1]
                    instructions have been read or a blank line is
                    encountered, whichever is the sooner.
                    The instructions are not processed until the
                    current macro is invoked.
       [F 1] = 0 => Invoke the current macro.
       *Defaults to [F 1] = 0 ie. invoke macro.
```

```
"MACRO NLINES"
       1---->
```

```
==========================================================================

"MISTIE"     ["MI"]

PURPOSE:
   Calculates the mean and RMS misties of specified parameters over a
range of horizons from the parameter values interpolated at line
intersections by CROSS instructions.

COMMENTS:
   MISTIE must follow all CROSS instructions pertaining to this mistie
calculation.
   Interpolated data and individual misties are listed for each line
intersection.
   Correlations between misties on pairs of horizons can be calculated
and plotted.

OPTIONS:
F 1 C  Range of parameters for which misties are to be calculated.
      *Defaults to all parameters.
F 2 C  Range of horizons for which misties are to be calculated.
      *Defaults to all horizons.
F 3 C  Correlation processing:
       [F 3] includes 'C' => Calculate correlation coefficient for
                             misties on each horizon pair in the
                             range [F 2].
       [F 3] includes 'G' => Plot graph of mistie on lower horizon vs
                             mistie on upper horizon for any horizon
                             pair with a mistie correlation > 0.5.
      *Defaults to no correlation processing.

"MISTIE LF:LL,MF:ML,CORRELATIONS?"
        1---> 2---> 3----------->

==========================================================================

"OPENF"      ["OP"]

PURPOSE:
   Opens a file for subsequent read/write operations.

COMMENTS:
   Each file is assigned a FORTRAN logical unit number.
   Both formatted and direct access files may be opened.

OPTIONS:
F 1 C  Name of file to be opened (maximum 30 characters).
      *Defaults to a list of all files currently opened to the run,
       their assigned logical unit numbers and attributes.
F 2 I  Logical unit number to be assigned to file [F 1].
       [F 2] must be in the range 0 < [F 2] < 90.
      *No default.
F 3 C  File type:
       [F 3] = 'W'  => Open new formatted file with write access.
       [F 3] = 'D'  => Open old direct access file for read/write
                       operations.
       [F 3] = 'DW' => Open new direct access file for read/write
                       operations; initialise keyword header.
       [F 3] blank  => Open old formatted file with readonly access.
      *Defaults to [F 3] blank.

"OPENF FILENAME,UNIT,FILETYPE"
```

```
       1------> 2--> 3------>
```

===

"OUTPUT"   ["OU"]

PURPOSE:
   Writes specified horizon/parameter vectors from the KRUNCH matrix to a formatted file.

OPTIONS:

```
F 1 C  Range of parameters to be written.
      *Defaults to all parameters.
F 2 C  Range of horizons for which data is to be written.
      *Defaults to all horizons.
F 3 C  Range of ground points for which data is to be written,
       specified in CMP numbers.
      *Defaults to all ground points.
F 4 I  Logical unit number of formatted file to receive data.
      *Defaults to the current print file.
F 5 C  FORTRAN format to be used for write. Free format '*' is valid.
       The format MUST include parentheses cf. '(......)'.
       No commas should be included in the format, as they are confused
       with the data field separation commas. Formats including commas
       should be specified using semi-colons ';' instead - these are
       then decoded to commas internally.
       If the format has > 30 characters [F 5] must be set by any
       character other than '*' or '(' and the format is read from the
       NEXT LINE of the current input file.
      *Defaults to the last format specified by an OUTPUT instruction,
       or to '*' if no OUTPUT instructions have been processed.
F 6 C  [F 6] set => Write data parameter by parameter in tables where:
                   Column 1 is the ground point CMP number;
                   Column 2 is the data for the first horizon;
                   Column 3 is the data for the next horizon; etc.
       The format [F 5] must match precisely the INTEGER ground point
       CMP number and the number of columns of REAL parameter values.
       eg. if 4 horizons are to be written, '(I5,4F10.2)' is a valid
       format.
      *Defaults to write vector by vector.
```

```
"OUTPUT LF:LL,MF:ML,CMPF:CMPL,UNIT,FORMAT,TABLE?"
        1---> 2---> 3-------> 4--> 5----> 6---->
```

===

"PSPEC"   ["P"]

PURPOSE:
   Calculates and displays energy spectra for specified horizon/ parameter vectors.

COMMENTS:
   Options allow the length of the complex spectrum and degree of spectral smoothing to be specified. Energies can be transformed to dB if required.
   Plots are sent to the current print file.

OPTIONS:

```
F 1 I  Parameter for which energy spectra are to be calculated.
      *No default.
F 2 C  Range of horizons for which energy spectra are to be calculated;
       energy spectra for all horizon/parameter vectors are plotted on
```

```
        the same axes.
       *Defaults to all horizons.
F 3 C  Character string containing symbols to be used for plot; one
        symbol is associated with each horizon. The number of symbols
        in [F 3] should match the number of horizons specified in [F 2].
       *Defaults to the last symbols specified in PSPEC or GRAPH.
        If no symbols have been defined earlier, ABCDEF... are used.
F 4 I  Length of complex spectrum is 2 ** [F 4]
       *Defaults to [F 4] = 7  ( 2 ** 7 = 128 ).
F 5 I  [F 5] > 0 => Smooth energy spectra by averaging energy in
                    consecutive groups of [F 5] adjacent wavenumbers.
                    The number of wavenumbers remaining after
                    smoothing will be  ( 2 ** [F 4] ) / [F 5] as the DC
                    or zero wavenumber component is not plotted.
       *Defaults to no smoothing.
F 6 I  [F 6] = 0 => Plot energies.
       [F 6] = 4 => Plot 10log10 (energies) ie. transform to dB.
       *Defaults to [F 6] = 0.
F 7 R  Datum (a constant energy value) to be marked on plot by a
        line of dots.
       *Defaults to zero.
F 8 R  Minimum value in plotting window.
       *Defaults to the minimum energy over all the spectra to be
        plotted.
F 9 R  Maximum value in plotting window.
       *Defaults to the maximum energy over all the spectra to be
        plotted.

"PSPEC L,MF:ML,SYMBOLS,2**?,NSMOOTH,dB?,DATUM,MIN,MAX"
       1 2---> 3-----> 4--> 5-----> 6-> 7---> 8-> 9->

=======================================================================

"RESET"      ["R"]

PURPOSE:
   Resets the current input or print file.

COMMENTS:
   RESET allows both standard runstreams to be read from different
files and selected printout to be directed to different files.
   An input echo switch (which decodes the numeric and character
content of each instruction) and a page throw suppression switch
(to compress printout) can be toggled by RESET. Both switches are
set to 'off' at the start of the run.
   In addition, RESET allows a formatted file to be rewound.

OPTIONS:
F 1 I  Reset current input file to logical unit number [F 1].
    C  [F 1] = 'S' => Reset current input file to system input
                      channel.
      *Defaults to no change.
F 2 I  Reset current print file to logical unit number [F 2].
    C  [F 2] = 'S' => Reset current print file to system output
                      channel.
      *Defaults to no change.
F 3 C  [F 3] set => Toggle input echo switch.
      *Defaults to no toggle.
F 4 C  [F 4] set => Toglgle page throw suppression switch.
      *Defaults to no toggle.
F 5 I  Rewind logical unit number [F 5].
      *Defaults to no rewind.
```

```
"RESET INPUTUNIT,PRINTUNIT,ECHO,PAGETHROW,REWINDUNIT"
       1-------> 2-------> 3--> 4-------> 5-------->
```

==

"SELECT" ["SE"]

PURPOSE:
Resamples a new data set from within the current data set.

COMMENTS:
No interpolation is performed; the required ground points in the new data set must exist in the old data set and resampling must be made with an integer multiple of the old ground point spacing.
The old data set is overwritten in the KRUNCH matrix and the new resampled data set becomes the current data set.

OPTIONS:
F 1 C Range of ground points to be selected specified by CMP numbers. Both first and last ground points must exist within the old data set.
*Defaults to all ground points ie. no change.
F 2 I New ground point spacing, specified in CMPs. The new ground point spacing must be an integer multiple of the old ground point spacing.
*Defaults to the old ground point spacing ie. no change.

```
"SELECT CMPF:CMPL,CMPGPINC"
        1-------> 2------>
```

==

"SPLINE" ["SP"]

PURPOSE:
Designs a smooth curve and interpolates parameter values for a single horizon/parameter vector.

COMMENTS:
Parameter values are interpolated at each ground point from a smooth curve composed of a series of local cubic splines. The curve is constrained to pass through 'knots' which are either existing parameter values or new parameter values at specified CMP numbers.
This instruction must be run interactively.

OPTIONS:
F 1 I Parameter to be interpolated.
*No default.
F 2 I Horizon for which data is to be interpolated.
*No default.

```
"SPLINE L,M"
        1 2
```

==

"STOP" ["STOP"]

PURPOSE:
Stops the program.

COMMENTS:
A log of all instructions processed in the run is automatically

appended to the current print file.

All files currently opened to the run are closed.

There are no options.

"STOP"

==

"VERSION" ["V"]

PURPOSE:

Lists details of the current version of KRUNCH to the current print file.

COMMENTS:

VERSION lists the restrictions imposed by FORTRAN array sizes eg. maximum number of horizons and maximum number of ground points in the KRUNCH matrix, maximum length of the complex spectrum used in PSPEC, maximum number of files which can be opened to the run etc.

There are no options.

"VERSION"

****

APPENDIX 5B

KRUNCH INSTRUCTIONS FOR THE TASK SEQUENCES OF SECTION 5.4

APPENDIX 5B KRUNCH INSTRUCTIONS FOR THE TASK SEQUENCES OF SECTION 5.4

This appendix is included to show the KRUNCH instructions required to run the task sequences of Examples 1,2 and 3 of Section Section 5.4.

The sequences below use the three lines A-103, A-111 and A-130 from Chapter 2. For the purposes of this illustration, just two horizons are considered. Lines A-103 and A-111 are parallel and both intersect line A-130.

Example 1. INITIAL KRUNCH RUN:
To read in two-way times, moveout velocities and crossline time slopes from files 'TIME.DAT', 'VMO.DAT' and 'XLNSLOPE.DAT' respectively; calculate inline time slopes; plot graphs of each parameter (using symbols 'B' for the first horizon and 'P' for the second) and store the data sets on the new direct access file 'RAW.DAT':

```
OPENF TIME.DAT,10
OPENF VMO.DAT,11
OPENF XLNSLOPE.DAT,12
OPENF RAW.DAT,40,DW
LINDEF 103,77,2,357,10,250,45
INPUT 1,1,,10,R,,,(5X;F5.0)
INPUT 1,2,,10,R,,,(10X;F5.0)
INPUT 2,1,,11,R,,,(10X;F10.0)
INPUT 2,2,,11,R,,,(20X;F10.0)
INPUT 4,1,,12,R,,,(10X;F10.6)
INPUT 4,2,,12,R,,,(20X;F10.6)
CDTDX
GRAPH 1,,,BP,,2,4
GRAPH 2,,,,,2000,3000
GRAPH 3:4
DWRITE 40,A-103
LINDEF 111,81,2,240,10,250,-135
INPUT 1,1,,10,R,77,,(5X;F5.0)
INPUT 1,2,,10,R,77,,(10X;F5.0)
INPUT 2,1,,11,R,77,,(10X;F10.0)
INPUT 2,2,,11,R,77,,(20X;F10.0)
INPUT 4,1,,12,R,77,,(10X;F10.6)
INPUT 4,2,,12,R,77,,(20X;F10.6)
CDTDX
GRAPH 1,,,,,2,4
GRAPH 2,,,,,2000,3000
GRAPH 3:4
DWRITE 40,A-111
LINDEF 130,53,2,0,10,250,135
INPUT 1,1,,10,R,158,,(5X;F5.0)
INPUT 1,2,,10,R,158,,(10X;F5.0)
INPUT 2,1,,11,R,158,,(10X;F10.0)
INPUT 2,2,,11,R,158,,(20X;F10.0)
INPUT 4,1,,12,R,158,,(10X;F10.6)
INPUT 4,2,,12,R,158,,(20X;F10.6)
CDTDX
GRAPH 1,,,,,2,4
GRAPH 2,,,,,2000,3000
GRAPH 3:4
DWRITE 40,A-103
STOP
```

Example 2. SMOOTHING MOVEOUT VELOCITIES AND CALCULATION OF MISTIES
To design a trial smoothing filter (in this case a 5-point boxcar moving average); read in data sets from file 'RAW.DAT'; filter moveout velocities and interpolate filtered moveout velocities at line intersections. Moveout velocity misties are calculated at the end of the run:

```
OPENF RAW.DAT,40,D
FDESN -1,5,,,,,,,250
LINDEF 103,77,2,357,10,250,45
DREAD 40,A-103
FILTER 2
CROSS 1,2
130,838
LINDEF 111,81,2,240,10,250,-135
DREAD 40,A-111
FILTER 2
CROSS 1,2
130,558
LINDEF 130,53,2,0,10,250,135
DREAD 40,A-130
FILTER 2
CROSS 2,2
103,41,111,237
MISTIE 2
STOP
```

Example 3. HUBRAL 3D INVERSION:
To design the 'optimum' smoothing filter (designated here to be a 13-point boxcar moving average); read in data sets from file 'RAW.DAT'; filter moveout velocities; perform a 'direct' Hubral 3D inversion at each ground point; plot derived interval velocities and write updated data sets to the new direct access file 'INVERT.DAT'. Note that in this case the repeated sequence is performed by the MACRO instruction for each line:

```
OPENF RAW.DAT,40,D
OPENF INVERT.DAT,41,DW
FDESN -1,13,,,,,,,250
MACRO 3
FILTER 2
HINVERT ,,,P
GRAPH 5,,,BP
LINDEF 103,77,2,357,10,250,45
DREAD 40,A-103
MACRO
DWRITE 41,A-103
LINDEF 111,81,2,240,10,250,-135
DREAD 40,A-111
MACRO
DWRITE 41,A-111
LINDEF 130,53,2,0,10,250,135
DREAD 40,A-130
MACRO
DWRITE 41,A-130
STOP
```

REFERENCES

Al-Chalabi, M. 1973 Series Approximation in Velocity and Traveltime Computations; Geophysical Prospecting v.21 p.783-795.

Al-Chalabi, M. 1974 An Analysis of Stacking, RMS, Average, and Interval Velocities over a Horizontally Layered Ground; Geophysical Prospecting v.22 p.458-475.

Al-Chalabi, M. 1979 Velocity Determination from Seismic Reflection Data, in Developments in Geophysical Exploration Methods - 1, edited by A.A. Fitch; Applied Science Publishers Ltd., London.

Banik, N.C. 1984 Velocity Anisotropy of Shales and Depth Estimation in the North Sea Basin; Geophysics v.49 p.1411-1419.

Bath, M. 1974 Spectral Analysis in Geophysics; Developments in Solid Earth Geophysics Number 7, Elsevier, 563 pp.

Bendat, J.S. and Piersol, A.G. 1971 Random Data; Wiley-Interscience, 407 pp.

Birch, F. (ed.) 1942 Handbook of Physical Constants; Geol. Soc. America Special Paper 36.

Blackburn, G. 1980 Errors in Stacking Velocity - True Velocity Conversion over Complex Geologic Situations; Geophysics v.45 p.1465-1488.

Clark, I. 1979 Practical Geostatistics; Applied Science Publishers, 129 pp.

Cressman, K.S. 1968 How Velocity Layering and Steep Dip Affect CDP; Geophysics v.33 p.399-411.

Davis, J.C. 1973 Statistics and Data Analysis in Geology; John Wiley and Sons, 550 pp.

Dennison, A.T. 1960 An Introduction to Synthetic Seismogram Techniques; Geophysical Prospecting v.8 p.231-241.

Dinstel, W.L. 1971 Velocity Spectra and Diffraction Patterns; Geophysics v.36 p.415-417.

Dix, C.H. 1955 Seismic Velocities from Surface Measurements; Geophysics v.20 p.68-86.

Dupal, L., Gartner, J. and Vivet, B. 1977 Seismic Applications of Well Logs; presented at 'Problems of Radioactive Wastes in Nuclear Technology' conference, Essen, Germany, October 1977.

Everett, J.E.	1974	Obtaining Interval Velocities from Stacking Velocities when Dipping Horizons are Included; Geophysical Prospecting v.22 p.122-142.
Goetz, J.F., Dupal, L. and Bowler, J.	1979	An Investigation into Discrepancies Between Sonic Log and Seismic Check Shot Velocities; Australian Petroleum Exploration Association Journal v.19 p.131-141.
Hubral, P.	1976a	Interval Velocities from Surface Measurements in the 3D Plane Layer Case; Geophysics v.41 p.233-242.
Hubral, P.	1976b	CDP Ray Modelling in the Presence of 3D Plane Isovelocity Layers of Varying Dip and Strike; Geophysical Prospecting v.24 p.478-491.
Hubral, P.	1980a	Computation of the Normal Moveout Velocity in 3D Laterally Inhomogeneous Media with Curved Interfaces; Geophysical Prospecting, v.28 p.221-239.
Hubral, P.	1980b	Wavefront Curvatures in 3D Laterally Inhomogeneous Media with Curved Interfaces; Geophysics v.45 p.905-913.
Hubral, P. and Krey, Th.	1980	Interval Velocities from Seismic Reflection Time Measurements; Society of Exploration Geophysicists, Tulsa, 203 pp.
Levin, F.K.	1971	Apparent Velocity from Dipping Interface Reflections; Geophysics v.36 p.510-516.
Mayne, W.H.	1962	Common Reflection Point Horizontal Data Stacking Technique; Geophysics v.27 p.927-938.
Montalbetti, J.F.	1971	Computer Determination of Seismic Velocities - a Review; Journal of the Canadian Society of Exploration Geophysicists, v.7 p.32-45.
O'Brien, P.N.S. and Lucas, A.L.	1971	Velocity Dispersion of Seismic Waves; Geophysical Prospecting v.19 p.1-26.
Peterson, R.A., Fillipone, W.R. and Coker, F.B.	1955	The Synthesis of Seismograms from Well Log Data; Geophysics v.20 p.516-538.
Prakla Seismos	1978	Determination and Presentation of Velocities Derived from Seismic Data; Prakla Seismos Information No. 14.
Rabiner, L.R. and Gold, B.	1975	Theory and Application of Digital Signal Processing; Prentice-Hall, 762 pp.

Robinson, E.A.	1967	Multichannel Time Series Analysis with Digital Computer Programs, Holden-Day, 298 pp.
Schneider, W.A.	1971	Developments in Seismic Data Processing and Analysis (1968-1970); Geophysics v.36 p.1043-1073.
Shah, P.M.	1973a	Ray Tracing in Three Dimensions; Geophysics v.38 p.600-604.
Shah, P.M.	1973b	Use of Wavefront Curvature to Relate Seismic Data with Subsurface Parameters; Geophysics v.38 p.812-825.
Sherriff, R.E.	1973	Encyclopedic Dictionary of Exploration Geophysics; Society of Exploration Geophysicists, Tulsa, 266 pp.
Sherriff, R.E.	1977	Limitations on Resolution of Seismic Reflections and Geologic Detail Derivable from them, in Seismic Stratigraphy - Applications to Hydrocarbon Exploration, edited by C.E. Payton; American Association of Petroleum Geologists.
Slotnick, M.M.	1959	Lessons in Seismic Computing, A Memorial to the Author; Society of Exploration Geophysicists, Tulsa, 268 pp.
Taner, M.T., Cook, E.E. and Neidell, N.S.	1970	Limitations of the Reflection Seismic Method; Lessons from Computer Simulations; Geophysics v.35 p.551-573.
Taner, M.T. and Koehler, F.	1969	Velocity Spectra - Digital Computer Derivation and Applications of Velocity Functions; Geophysics v.34 p.859-881.
Woods, J.P.	1975	A Seismic Model Using Sound Waves in Air; Geophysics v.40 p.593-607.